

School of Medicine

Division of Medical Sciences and Graduate Entry Medicine

Metabolic regulation and consequences of an altered microenvironment in cancer cell lines

Ujjal Bose

A thesis submitted for the degree of Doctor of Philosophy at the University of Nottingham

January 2019

Student ID Number - 4181919

Surname or family name (block letters) - BOSE

Other names (in full) - UJJAL

I declare that the thesis is the result of my own work which has been mainly undertaken during my period of registration for this degree at The University of Nottingham. I have complied with the word limit for my degree (as stated in the Quality Manual: http://www.nottingham.ac.uk/academicservicesiqualitymanual/researchdegree_proqrammes/indexoage-research-degree-regulations.aspx)

Ujjal Bose



Signature

Acknowledgement

I would like to express my deepest appreciation to all those who provided me the possibility to complete this report. I am immensely grateful to my supervisor Professor Raheela N Khan, who's been ever encouraging and untiringly supportive towards my work in every possible way. I am moved, impressed and overwhelmed by her humility and strength of character that has helped me mirror the same towards the challenges in my research. I am also indebted to her for selecting a galaxy of supervisors from different disciplines, who are as great human beings as herself. A special gratitude to my supervisor Dr Cristina Tufarelli, whose contribution in stimulating suggestions and encouragement, helped me to coordinate my project especially in writing this report. I am thankful to my supervisor; Dr Cyril Rauch who has always shown great interest in refining my work and paving the way ahead not only for my research but also helped me to establish valuable contacts. My supervisor, Dr Cinzia Allegrucci, has been always been very supportive and has always given me the correct advice especially when it came to devise the research questions for my work. Furthermore, I would also like to acknowledge with much appreciation the crucial role of the technical staff of Clinical Science laboratory, who gave the training and permission to use all required equipment and the necessary advice on different aspects in the lab. Special thanks go to my fellow PGR students, who helped me to culture science through lively and competitive discussions. Last but not least, many thanks go to Manipal Academy of Highe Education for investing full effort in guiding me to aim towards achieving the goal. I have to appreciate the guidance given by other scientific experts that has improved my presentation skills to the present day.

Dissemination of research work

Posters presented and conference proceedings:

Bose U, Allegrucci C, Rauch C, Tufarelli C, Khan R. (2013) Evaluation of the role of pH in cancer cell proliferation. Proc 37th IUPS. Birmingham, UK. Available at: http://www.physoc.org/proceedings/abstract/Proc 37th IUPSPCD201.

Bose U, C Tufarelli, Rauch C, Bali A, Allegruci C, Khan RN. Evaluation of the role of pH in cancer cell proliferation. Satellite Meeting for the 37th Congress of the IUPS. H^+SSS: H^+Ion Sensing, Signalling and Servo-Control (27th July 2013). Department of Physiology, Anatomy and Genetics, University of Oxford, UK.

Bose U, Khan RN, Rauch C, Tufarelli C. Extracellular pH modulates expression of *LCT13* to silence metastasis suppressor *TFPI-2* in cancer. Genes and Cancer 2015 31st meeting (13-15 April) Robinson College, University of Cambridge, Cambridge, UK.

Bose U, Rauch C, Allegruci C, C Tufarelli, Khan RN. Role of extracellular pH and pH sensitive potassium channels in cancer cell metabolism and viability. *Genes and Cancer 2015* 31st meeting (13-15 April) Robinson College, University of Cambridge, Cambridge, UK.

Bose U, C Tufarelli, Rauch C, Bali A, Allegruci C, Khan RN. Acidic microenvironment and potassium gradient alters intrinsic pH buffering to favour aggressive behaviour in ovarian cancer cell. *Royal College of Obstetrics and Gynaecology. Annual Academic Meeting* (3-5 March 2016), London, UK.

Bose U, McBride M, Raut J, Gell C, White O B, Allegrucci C, Rauch C, Bali A, Tufarelli C, Khan RN. (2016) Regulation and distribution of intracellular pH defines the role of a dynamic microenvironment in cancer cells, in *Proc Physiol Soc 37*. Available at: http://www.physoc.org/proceedings/abstract/Proc Physiol Soc 37PCB221.

McBride M, Bose U, Bali A, Khan R. (2016) The role of Na^+ in establishing the membrane potential in cancer cells, in *Proc Physiol Soc 37*. Available at: http://www.physoc.org/proceedings/abstract/Proc Physiol Soc 37PCB109.

Oral Presentation:

Bose U, Rauch C, Allegrucci C, Tufarelli C and Khan RN (2014). Evaluation of the role of pH in cancer cell proliferation. *Front. Pharmacol. Conference Abstract: 4th Annual Meeting of the International Society of Proton Dynamics in Cancer.* Available at: http://www.frontiersin.org/Journal/FullText.aspx?f=62&name=pharmacology&ART_DOI=10.3389/conf.fphar.2014.61.00009.

Publication:

Ofinran O, Bose U, Hay D, A Summi, Tufarelli C and Khan RN. 2016. Selection of suitable reference genes for gene expression studies in normal human ovarian tissues, borderline ovarian tumours and ovarian cancer. MOLECULAR MEDICINE REPORTS. 14: pp 5725-5731.

Abstract

Tumours are commonly associated with a shift in cellular metabolism to establish an acidic microenvironment that is further exacerbated by hypoxia. Such changes in extracellular pH (pH_e) and oxygen tension (PO_2) alter ion homeostasis effecting cancer hallmarks. High intracellular potassium (K^+) is a key determinant of membrane potential driving cellular function including proliferation and migration. Cancer cells overexpress several K^+ channel subtypes, modulated by metabolic factors including pH_e. We hypothesise that acidic and hypoxic microenvironment affects cancer cell behaviour mediated, in part, by K^+ transport involving K^+ channels. We aimed to develop and test the effects of a normal microenvironment (pH_e 7.4; PO_2 0.21 atm) and modified (low pH_e 6.3; low PO_2 0.029 atm) culture conditions on K^+ channel gene expression (by qPCR) and their contributions to cell proliferation in the SK-OV-3, MCF-7 and OE-19 cancer cell lines. Altered pH_e predominantly affected gene expression of pH-sensitive (*KCNK9* (TASK-3); *KCNK17* (TALK-2)) and voltage-gated (*KCNH1* (eag); *KCNH2* (HERG)) K^+ channels in SK-OV-3 cells. TASK-3 channel expression was upregulated in low pH_e & PO_2 compared with normal pH_e & PO_2 ($P < 0.05$). mRNA expression for *KCNH1* and *KCNH2* was decreased in low pH_e compared with normal pH_e & PO_2 for all three cell lines tested. Cell proliferation of SK-OV-3 cells was inhibited by the TASK-3 blocker methanandamide and the HERG blocker, E4031, most significantly in low pH_e & PO_2.

Live-cell imaging methods deploying pH-sensitive (BCECF-AM, carboxy-SNARF-AM, pH nanosensor) fluorophores and the K^+-sensitive (nigericin) ionophore were also developed and optimised in order to study the cellular responses of cancer cells following acid loading using the ammonium pre-pulse method. Values for the Intrinsic

Buffering Capacity (β_I), steady state pH_i recovery and net acid extrusion (NAE) of SK-OV-3 and MCF-7 cells in response to altered pH_e & PO_2 were derived. Results demonstrated that SK-OV-3 cells had lower buffering capacity in acidic pH_e than MCF-7 cells. In altered pH_e & PO_2, $NaHCO_3$-dependent (extrinsic) buffering promoted recovery of pH_i from acute acidification ($P < 0.001$) in both SK-OV-3 and MCF-7 cells. Low pH_e & PO_2 culture conditions significantly enhanced β_I as reflected through increased NAE of cancer cells. Finally, altered K^+ flux under low pH_e & PO_2 appeared to involve TASK-3 channels as shown by inhibition with methanandamide in SK-OV-3 and MCF-7 cells. Cancer cell behaviour is modified by an acidic, low oxygen microenvironment, in part involving the TASK-3 channel. These inferences are based on culture methodology developed in this study that will emerge as pivotal for future investigations of the role of these channels in response to the cancer environment.

Contents

ABSTRACT ..... **VI**

CHAPTER 1. INTRODUCTION **1**

1.1 CANCER - A CONTINUING CHALLENGE 1

1.1.1 Cancer as a metabolic disease and the 'Hallmarks of Cancer' *2*

1.2 METABOLIC CONSEQUENCES AND PH HOMEOSTASIS DECIDE DIFFERENT FATES FOR NORMAL AND CANCER CELLS 5

1.2.1 Cellular metabolism in normal cells *5*

1.2.2 Cellular metabolism in cancer cells *8*

1.2.3 Altered pH and oxygen tension has profound influence on cancer cell metabolism *11*

1.2.4 pH homeostasis and its role in tumour hallmarks- proliferation, migration and invasion *14*

1.2.5 Principle of pH regulation in biological processes *19*

1.3 FUNCTIONAL CORRELATION OF K^+ AND H^+ CONCENTRATION IN CANCER 22

1.4 EXPRESSION DISTRIBUTION AND ROLE OF POTASSIUM CHANNELS IN CANCER 24

1.4.1 Evidence of K^+ channels in normal and cancer cell proliferation *30*

1.4.2 Role of K^+ channels in cancer *34*

1.4.3 Role of pH_e sensitive Ion Channels (K^+ channels) in cancer *35*

1.4.4 Oncogenic potential of KCNK9 (TASK-3 coding gene) is due to physiological function *37*

1.5 TOOLS TO EVALUATE PH REGULATORY POTENTIAL 40

1.5.1 Ammonium pre-pulse technique – modifying pH *40*

1.5.2 Fluorescence and live-cell imaging to evaluate pH of cancer cells.....44

1.5.3 Selection of pH sensing and pH sensitive dyes/probes as pH indicator.....45

1.6 PROJECT RATIONALE AND AIMS.....48

1.6.1 Working hypothesis.....50

1.6.2 Aims of the work 50

CHAPTER 2. MATERIALS AND METHODS 51

2.1 CELL LINES USED FOR THE STUDY.....51

2.2 COMPUTER SOFTWARE AND DATABASES USED FOR THE STUDY 52

2.3 CULTURING AND MAINTENANCE OF ADHERENT CELL LINES.....53

2.3.1 Recovery of cells from liquid nitrogen 53

2.3.2 Subculture of adherent cells.....53

2.3.3 Cryopreservation of cells in Liquid nitrogen 57

2.4 ESTABLISHING A STANDARD CELL CULTURE BASED MODEL TO STABILISE THE pH_E 57

2.4.1 Methods to determine the buffer concentration to establish specific pH_e model.....57

2.4.2 Preparation of MEM medium without $NaHCO_3$ 58

2.4.3 Strategies to validate the buffer concentration to establish extracellular pHe model ...58

2.5 VIABILITY AND PROLIFERATION ASSAYS 61

2.5.1 Proliferation assay with MTS and resazurine dyes.....61

2.6 ASSESSING THE MIGRATORY AND INVASIVE POTENTIAL OF THE TUMOUR CELLS IN ALTERED MICROENVIRONMENT.....65

2.6.1 Scratch wound migration assay 65

2.6.2 PCF membrane assay 67

2.7 DETERMINATION OF pH_i IN CELLS 71

2.7.1 Experimental design and plans for live-cell observations over long-term sessions 71

2.7.2 The use of pH-sensing fluorescent dyes/probes with monolayer cells: Delivery of fluorescent dyes/probes within the cells 73

2.7.3 Image acquisition with Wide-Field microscopy 74

2.7.4 Data collection from Fluroskan microplate reader 75

2.7.5 Ratiometric analysis of RFU signals from pH sensing dyes 76

2.8. *IN VITRO* CALIBRATION AND OPTIMISATION OF FLUORESCENT DYES/PROBE 78

2.8.1 In situ calibration of pH nanosensors, BCECF-AM and cSNARF-1-AM 78

2.9. CONSTRUCTION OF CALIBRATION CURVE 80

2.10. OPTIMISATION OF MITO TRACKER DYE 81

2.11 DATA ANALYSIS 83

2.11.1 Intracellular acidification by 'Ammonium Pre-pulse manoeuvre' 83

2.11.2 Visualizing mitochondrial distribution in cancer cells cultured in altered pH_e 87

2.11.3 Functional association between potassium and pH_i regulation in cancer cells 89

2.12 IDENTIFICATION OF CHANNELS PROTEIN EXPRESSION 92

2.12.1 Immunofluorescence experiments 92

2.12.2 Confocal imaging of pH sensitive TASK-3 and TALK-2 protein in cancer cells 93

2.12.3 Signal collection: Z POSITIONING and continuous image acquisition 95

2.13.1 Extraction and quantification of total RNA 96

2.13.2 Assessing the integrity of the extracted RNA 97

2.13.3 Sample preparation 97

2.13.4 Synthesis of cDNA by Reverse Transcription PCR *98*

2.13.5 Quantitative (real-time) Polymerase Chain Reaction *98*

2.14 STATISTICAL ANALYSIS 101

CHAPTER 3. EXPRESSION OF PH SENSITIVE K^+ CHANNELS IN CANCER CELLS CULTURED IN ALTERED MICROENVIRONMENTS 102

3.1 INTRODUCTION 102

3.1.1 Aims *103*

3.2 RESULTS 104

3.2.1 Development of a cell culture system to study established cancer cell lines under 4 different pH_e and PO_2 conditions *104*

3.2.2 Expression of potassium channel genes KCNK9, KCNK17, KCNH1 and KCNH2 at the mRNA level by quantitative RT-PCR in cell lines under different culture conditions *106*

3.2.3 Expression and localisaton of TASK-3 and TALK-2 potassium channel proteins by immunofluorescence in cell lines under different culture conditions *112*

3.3 DISCUSSION 115

CHAPTER 4. ROLE OF PH_E/PO_2 AND PH REGULATION IN CANCER CELL PROGRESSION 119

4.1 INTRODUCTION 119

4.1.1 Aims *120*

4.2 RESULTS 121

4.2.1 Evaluate the viability and proliferation of cancer cells in altered pH_e and PO_2 ..... *121*

4.2.2 Determine the proliferation of SK-OV-3 cells in the presence and absence of the inhibitors of TASK-3 and HERG potassium channels *124*

4.2.3 Determine the pH_i during proliferation in the presence and absence of the inhibitors of TASK-3, HERG and H^+/K^+ATPase *125*

4.2.4 Determination of the migratory and invasive potential of cancer cells and their pH_i post migration in altered pH_e/PO_2 ..... *129*

4.3 DISCUSSION 136

4.3.1 Implications of using culture conditions with altered pH_e and PO_2 to target cell proliferation *136*

4.3.2 Influence of pH_i regulation in cancer cell proliferation *140*

4.3.3 Further implication of altered microenvironment on cell proliferation *142*

4.3.4 Migration and Invasion potential of cancer are influenced by pH_e *147*

4.3.5 Influence of pH_e on migratory potential of cancer cells *149*

CHAPTER 5. THE EFFECT OF PH ON ACID BUFFERING AND EXTRUSION. 159

5.1 INTRODUCTION 159

5.1.1. Aims *161*

5.2 RESULTS: 162

5.2.1 Time course of pH_i regulation from acute acid overload under altered pH_e/PO_2 ..... *162*

5.2.2 Determination of β_I of cancer cell lines in HEPES buffered media under altered pH_e/PO_2 ..... *166*

5.2.3 Estimation of the 'Rate of recovery' of cancer cells from acute acid loading in HEPES buffered medium under altered pH_e/PO_2 ..... *168*

5.2.4 Derivation of NAE of cancer cells from HEPES and $NaHCO_3$ buffered medium with altered pH_e and PO_2 169

5.2.5 Mapping the distribution of pH_i oscillations in localised areas within cancer cells 171

5.2.6 Identifying associations between intracellular zones of pH oscillations with the spatial distribution of mitochondria in test cancer cell lines under altered pH_e/PO_2 175

5.3 DISCUSSION 179

5.3.1 Measurement of β_I defines pH regulation in cancer cells in altered pH_e/PO_2 182

5.3.2 NAE in cancer cells is influenced by recovery of pH_i in altered microenvironment 185

5.3.3 Detecting differentially distributed pH_i pockets in cancer cells 189

5.3.4 Association between mitochondrial distribution and pH_i pockets in cancer cells 190

CHAPTER 6. ROLE OF K^+ AND TASK-3 CHANNEL IN PH HOMEOSTASIS IN CANCER CELLS 193

6.1 INTRODUCTION 193

6.1.1 Aims 195

6.2 RESULTS 196

6.2.1 ESTIMATION OF $[K^+]_I$ IN SKOV AND MCF-7 CELLS 196

6.2.2 TIME COURSE OF pH_I RECOVERY FROM AMMONIUM PRE-PULSE MANOEUVRE IN ALTERED pH_E, PO_2 AND $[K^+]_E$ CANCER CELL 199

6.2.3 DETERMINATION OF K^+ DEPENDENCE OF pH_I MAINTENANCE FOLLOWING ACUTE ACIDIFICATION 200

6.2.4 TIME COURSE TRACE OF pH_I RECOVERY AMMONIUM PRE-PULSE MANOEUVRE IN ALTERED pH_E/PO_2 IN THE PRESENCE OF METHANANDAMIDE (TASK-3 CHANNEL INHIBITOR) 201

6.2.5 THE NAE IN CANCER CELLS IN THE PRESENCE OF METHANANDAMIDE 203

6.3 DISCUSSION 206

6.3.1 ESTIMATION OF $[K^+]_I$ IN CANCER CELL LINES 206

6.3.2 DETERMINATION OF $[K^+]_E$ DEPENDENCE OF CANCER CELLS TO MAINTAIN pH_I FOLLOWING ACUTE ACIDIFICATION 207

6.3.3 DETERMINATION OF THE ROLE OF TASK-3 CHANNEL IN pH_I RECOVERY FROM AMMONIUM PRE-PULSE MANOEUVRE IN ALTERED pH_E, PO_2 209

CHAPTER 7. GENERAL DISCUSSION 215

7.1 GENERAL CONSIDERATION 215

7.2 ROLE OF pH REGULATION IN IMPORTANT CANCER HALLMARKS 221

7.3 ROLE OF pH BUFFERING IN REGULATING pH_I RESTORATION IN CANCER CELLS 224

7.4 FUTURE RESEARCH 231

7.5 CONCLUDING REMARKS 233

REFERENCES 234

APPENDICES 258

List of Figures

Figure 1.1: The Hallmarks of cancer 4

Figure 1.2: Energy generation in mammalian cells 8

Figure 1.3: Glucose metabolism in differentiated normal cells 10

Figure 1.4: Glucose metabolism in cancer cells 10

Figure 1.5: Major pH regulators in a cancer cell 15

Figure 1.6: Microenvironment pH and intracellular pH regulation in cancer migration 18

Figure 1.7: Ion transport in human renal cells 24

Figure 1.8: Classification of K^+ ion channels 26

Figure 1.9: Classification of two pore domain K^+ channel coding genes 29

Figure 1.10: Role of K^+ channels in cell proliferation 32

Figure 1.11: Principle of the 'ammonium pre-pulse' technique 43

Figure 1.12: Microscope configuration for live cell imaging 45

Figure 2.1: Scheme of PCF membrane migration assay..... 69

Figure 2.2: Calibration of pH sensor dyes/probes 81

Figure 2.3: Etoposide induced apoptosis of cancer cells 82

Figure 2.4: Depletion in Mito Tracker Deep Red dye signal intensity following apoptosis of cancer cells 82

Figure 3.1: The different culture conditions in MEM, maintain the pH_e over long period with SK-OV-3 cells in culture 105

Figure 3.2: Expression of five reference genes was tested in the MCF-7 cell lines under the different culture conditions to select the most appropriate for quantitative analysis 107

Figure 3.3: Expression of five reference genes was tested in the OE-19 cell lines under the different culture conditions to select the most appropriate for quantitative analysis 107

Figure 3.4: Expression of five reference genes was tested in the SK-OV-3 cell lines under the different culture conditions to select the most appropriate for quantitative analysis. 108

Figure 3.5: Relative expression of KCNK9 and KCNK17 in cancer cells in altered pH_e & PO_2. 110

Figure 3.6: Relative expression of KCNH1 and KCNH2 genes in cancer cells in altered pH_e and PO_2. 111

Figure 3.7: Expression of TASK-3 proteins in SK-OV-3 and MCF-7 vells in altered pH_e/PO_2 113

Figure 3.8: Expression of TASK-3 proteins in SK-OV-3 in low pH_e & normal PO_2 ...114

Figure 3.9: Expression of TALK-2 proteins in SK-OV-3 cells under normal pH_e & PO_2..... 114

Figure 4.1: Percent change in growth of cancer cells in altered pH_e/PO_2 122

Figure 4.2: Percent change in growth of cancer cells in altered pH_e/PO_2 122

Figure 4.3: Effect of K^+ channel inhibitors on cancer cell proliferation 125

Figure 4.4: Correlation between proliferation and pH_i of cancer cells..... 128

Figure 4.5: Scratch wound migration assay of SK-OV-3 cells 131

Figure 4.6: Scratch wound migration assay of MCF-7 cells..... 132

Figure 4.7: Effect of altered pH_e/PO_2 on migration (scratch wound assay) in cancer cells 133

Figure 4.8: PCF membrane migration assay in cancer cell lines 135

Figure 5.1: pH_i regulation by the $NaHCO_3$ -independent component of cancer cells in altered pH_e and PO_2..... 164

Figure 5.2: pH_i regulation by the $NaHCO_3$-dependent component of cancer cells in altered pH_e and PO_2. 166

Figure 5.3: β_I of SK-OV-3, MCF-7 and MCF-10A cells in altered pH_e/PO_2 in HEPES buffered medium 167

Figure 5.4: pH_i recovery rates of SK-OV-3, MCF-7 and MCF-10A cells in altered pH_e/PO_2 in HEPES and $NaHCO_3$ buffered medium..... 169

Figure 5.5: NAE of SK-OV-3 and MCF-7 cells in altered pH_e/PO_2 170

Figure 5.6: Representative processed image of a SK-OV-3 cell cultured in normal pH_e/PO_2 172

Figure 5.7: Processed image of a cluster of monolayer of SK-OV-3 cells 174

Figure 5.8: Processed image of a cluster of monolayer of MCF-10A cells..... 174

Figure 5.9: Mapping mitochondrial localisation against pH distribution in MCF-7 cells in normal pH_e & PO_2 176

Figure 5.10: Mapping mitochondrial localisation against pH distribution in MCF-7 cells..... 177

Figure 5.11: Mapping mitochondrial localisation against pH distribution in SK-OV-3 cells..... 178

Figure 5.12: Mapping mitochondrial localisation against pH distribution in MCF-10A cells 178

Figure 6.1: Interrelationship between extracellular and intracellular pH values of SK-OV-3 and MCF-7 cells treated with nigericin in altered $[K^+]_e$ 198

Figure 6.2: pH_i regulation of cancer cells in variable $[K^+]_e$ with altered pH_e/PO_2 199

Figure 6.3: Dependence of pH_i recovery (from intracellular acidification) on $[K^+]_e$ 201

Figure 6.4: TASK-3 effects pH_i regulation following ammonium pre-pulse in SK-OV-3 and MCF-7 cells in altered pH_e/PO_2 203

Figure 6.5: Differential effects of methanandamide (TASK-3 inhibitor) on NAE in cancer cells in altered pH_e/PO_2 205

Figure 7.1: Schematic representation of metabolic consequences of altered pH_e/PO_2 in cancer cells 230

List of Tables

Table 1.1: Expression of KCNK genes across different cancers.....33

Table 2.1. Cell line subculture profile layout.....56

Table 4.1: Effect of pH_e and PO_2 on relative doubling time of proliferating cancer cells..... 123

Table 5.1: pH_i recovery rate (pH/min) of cancer cells maintained in altered pH_e and PO_2.....168

Table 5.2: NAE (mM/min) of cancer cells maintained in altered pH_e and PO_2... 170

Table 6.1: Intracellular free potassium ion concentration of cancer cells.....196

List of Abbreviations

Acetyl-CoA……Acetyl-Coenzyme A

ACTB…… β-actin

ADP…….. Adenosine diphosphate

Akt……Ak Protein Kinase B

ANOVA……Analysis of Variance

APP……..Ammonium pre-pulse

ATCC……American Type Culture Collection

ATF4……. Activating transcription factor 4

ATP…… Adenosine-5-triphosphate

B2M…… β-2-microglobin

BCA……Bi-Chonconic Acid

BCECF……Bis (carboxyethyl)- carboxyfluorescein

BK……Big-conductance K^+ channel

BSA……..Bovine Serum Albumin

CA……..Carbonic Anhydrase

cDNA……complementary Deoxy-ribo Nucleic Acid

CGM……...Complete Growth Medium

CHOP……CCAAT-enhancer-binding protein homologous protein

CSHS……..Charcoal Stripped Horse Serum

CT……. Cycle Threshold

DAPI……Diamidino-2-phenylindole dihydrochloride

DMEM…… Dulbecco's Minimum Essential Medium

DMSO…… Dimethyl Sulfoxide

DRG…… Dorsal Root Ganglion

Eag……..Ether-a-go go

ECACC…… European Collection of Authenticated Cell Cultures

ECM……..Extra Cellular Matrix

EDTA……Ethylene Di-Amine Tetra-Acetate

EGF……..Epidermal Growth Factor

EtBr……Ethidium Bromide

ETS……..Electron Transport System

FADH2…… Flavin Adenine Dinucleotide (reduced)

FBS……Foetal Bovine Serum

FITC…… Fluorescien isothiocyanate

G-6-P……Glucose-6-phosphate

GAPDH…… Glyceraldehyde-3-Phosphate Dehydrogenase

HEPES…… Hydroxyethyl piperazineethanesulfonic acid

HERG……Human-Ether-a-go goRelated Gene

Hg…… Hydrorgyrum

HGNC…… Human Genome Nomenclature Committee

HIF…… Hypoxia-inducible factor

HK……..Hexokinase

HPRT……..Hypoxanthine Phosphoribosyl Transferase

IARC…… International Agency for Research in Cancer

IL…… Interleukins

IMM…… Immersion Medium

IRE……Iron-Responsive Elements

IUPHAR……The International Union of Basic and Clinical Pharmacology

JNK…… c-Jun N-terminal kinase

KCC…… KCl cotransporter

LAMP3……. lysosomal associated membrane protein 3

LOX……...Lysyl 6-oxidase

MCT……Mono Corboxylate Transporter

MEM…… Minimum Essential Medium

MET…….. Mesenchymal-Epithelial Transition

MMP……...Matrix Metallo-Potein

MRI……...Magnetic Resonance Imaging

Myc……Myelocytomatosis oncogene

NAD…… Nicotinamide adenine dinucleotide

NADH…… Nicotinamide adenine dinucleotide (reduced)

NHE……...Sodium Hydrogen Exchanger

NK……Natural Killer

NTC……No Template Control

OD……...Optical Density

OXPHOS……...Oxidative Phosphorylation

p53……Tumour protein 53

PBS……Phosphate Buffered Saline

PCF……Polycarbonate Thin-Film

PCO_2……Partial pressure of Carbon dioxide

PCR……Polymerase Chain Reaction

PERK…….. PRKR-Like Endoplasmic Reticulum Kinase

PFA……Para- Formaldehyde

PFK……Phospho fructokinase

PMT……Photo Multiplier Tube

PTEN……Phosphatase and tensin homolog

Raf……Rapidly Activated Fibrosarcoma

Ras…….. Rat sarcoma (viral oncogene homolog)

RFU……Relative Fluorescence Unit

ROI……Region of Interest

ROMK……. Renal Outer Medullary Potassium channel

rpm……Rotation per minute

RPMI 1640…… Roswell Park Memorial Institute medium 1640

RT……Reverse Transcriptase

SAR……Structure Activity Relationship

SCR……Single Channel Recording

siRNA …… Small Interfering Ribonucleic Acid

cSNARF……Carboxy Semi Naphthorhodafluor

TALK……Twik-related Alkali Sensitive Potassium channel

TASK……Twik-related Acid Sensitive Potassium channel

TNF……..Tumour Necrosis Factor

TEA……Tetra-Ethyl Ammonium

TMD……..Trans Membrane Domain

TWIK……Tandem of P domains in a Weak Inwardly rectifying K^+

V-ATPase……Vacuolar-Adenosine-5- Triphosphate-ase

VEGF……. Vascular endothelial growth factor

VEGF……Vascular Endothelial Growth Factor

WHO……World Health Organisation

XBP……X-box binding protein

YWHAZ……. Tyrosine 3-Monooxygenase /Tryptophan 5-Monooxygenase Activation Protein, Zeta Polypeptide

Chapter 1. Introduction

1.1 Cancer - a continuing challenge

The last quarter century of scientific advancement has seen unparalleled progress in cancer research. During this time, several theories have been espoused aimed at understanding and improving diagnosis and treatment of this insidious disease. Despite these strenuous efforts, cancer remains a conundrum and currently an enduring challenge. In this context, the World Cancer Report, published by the International Agency for Research in Cancer (IARC) of the World Health Organisation (WHO) suggests that new cancer cases are estimated to rise from 14 million annually in 2012 to 22 million by 2032 (WHO IARC, 2014). This critical situation demands novel research and unique strategies to be developed that would provide a holistic approach towards cancer therapy in order to ultimately improve quality of life and survival rates (Andresen, Jensen and Jorgensen, 2005; Luo, Solimini and Elledge, 2009; Tennant, Durán and Gottlieb, 2010).

Attempts to treat cancer by interfering with classical metabolic pathways has long been a challenge, partly due to the fact that cancer cell metabolism is very different to that of normal cells (Chiche, Brahimi-Horn and Pouyssegur, 2010). The extracellular acidic stress in which tumour cells evolve and adapt is a consequence of poor blood perfusion, low oxygen availability, increased metabolism of glucose and production of metabolic acids (Griffiths, 1991; Ozkan and Mutharasan, 2002; Cooper, 2003; Schonichen *et al.*, 2013). In recent years, research into the role of membrane ion channels in cancer (Semenza *et al.*, 2001; Sontheimer, 2008; Reshkin, Greco and Cardone, 2014) has gathered pace. As integral components of

the cell membranes, ion channels are able to sense and transduce signals generated by changes in, for example, pH and oxygen tension in the immediate vicinity of a cell, linking rapid electrolyte transport across the plasma membrane to cellular function. Several independent studies report upregulation of ion channel expression across a range of cancer types (Lastraioli, Iorio and Arcangeli, 2015; Litan and Langhans, 2015). Furthermore, important hallmark processes (viz., cell proliferation, cell migration, cell volume control, apoptosis etc) are also closely regulated by ion channel activity in cancer cells. Multiple studies have established a relationship between ion channels and tumour growth (Arcangeli *et al.*, 2009; Pardo and Stühmer, 2014; Litan and Langhans, 2015). These observations have led to the work described in this thesis directed at understanding the interactions between metabolic factors and ion transport with a focus on potassium (K^+) flux and K^+ channels in cancer, given their transforming potential, ectopic expression in tumours (Pei *et al.*, 2003; Camacho, 2006; Innamaa *et al.*, 2013) and clinical relevance. Within this context, it is first necessary to review key facets of cancer metabolism presented in the following sections.

1.1.1 Cancer as a metabolic disease and the 'Hallmarks of Cancer'

Cancers arise from a combination of metabolic, genetic and cellular transformations with tumour cells committed to uncontrolled proliferation. In cancer research, the period between 1950-1990 focused upon identifying genetic aberrations, mutational events and altered gene expression in tumourigenesis and became known as the 'oncogene revolution' (Vogt, 2010; Berger, Saunders and Mak, 2016; Cairns and Mak, 2016). Collectively, these research efforts brought to

light modification of multiple signalling pathways in tumour cells arising from an array of mutational events (Cairns and Mak, 2016). From the theories proposed for oncogenesis, progression and metastasis a seminal piece collated evidence to generate a unified theory known as the 'hallmarks of cancer' defining six key attributes with the capacity to promote survival, proliferation and adaptation of tumours resulting in a unique microenvironment (Hanahan and Weinberg, 2000, 2011).

Today, the essence of the hallmarks of cancer remains quintessential in explaining and understanding oncogenic processes and now incorporates new emerging hallmarks, for example, reprogramming energy metabolism and evading immune destruction (Figure 1.1) (Solimini, Luo and Elledge, 2007; Hanahan and Weinberg, 2011).

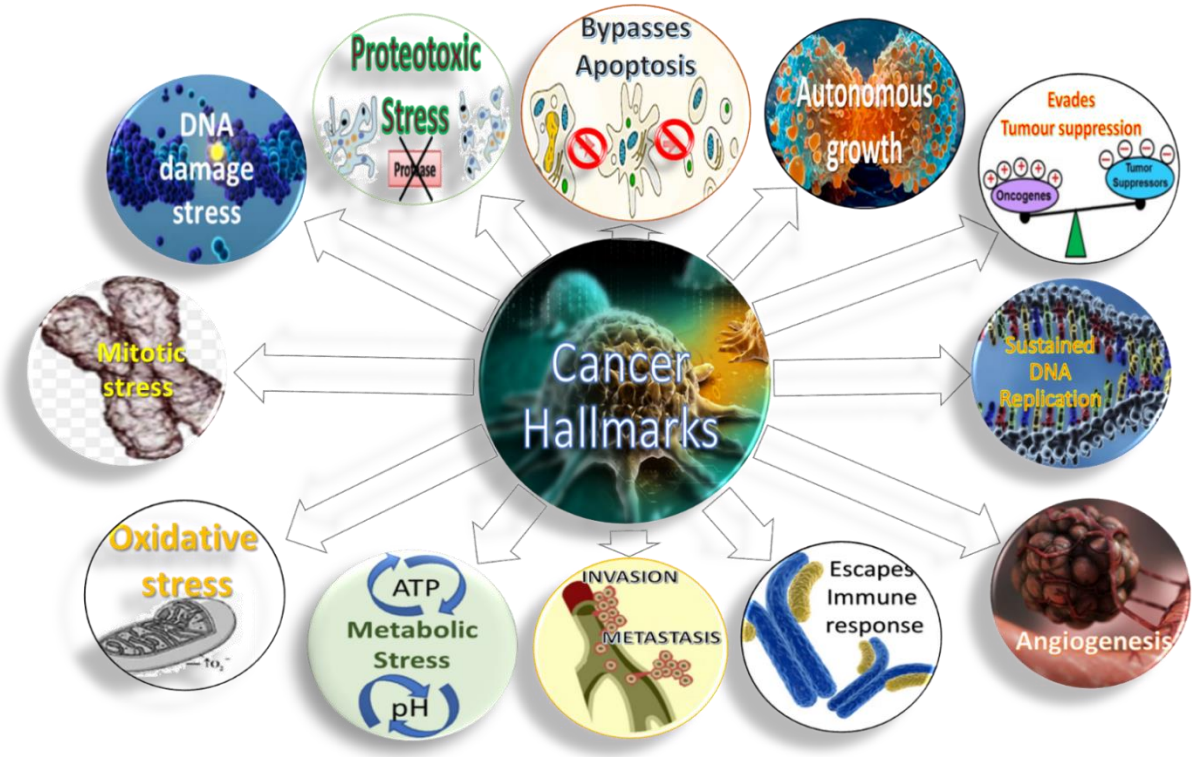

Figure 1.1: The Hallmarks of cancer
Schematic representation of the hallmarks that cancer cells exhibit to sustain tumour progression. Adapted from (Solimini, Luo and Elledge, 2007; Hanahan and Weinberg, 2011).

These newer hallmarks reflect hypotheses focusing on fundamental differences in core metabolic pathways initially described many years ago that lost their importance (Cairns, Harris and Mak, 2011) only to be revived (Weinhouse, 1976; Vander Heiden, Cantley and Thompson, 2009). Specifically, the 'Warburg hypothesis' (Section 1.2.2.1; Figure 1.4) describes how cancer cells are capable of "fermenting" glucose into lactate even in an oxygen rich environment to support mitochondrial oxidative phosphorylation. This shift in energy metabolism from that observed in normal cells is largely coordinated by proteins that again overtly modulate the core hallmarks of cancer (Solaini, Sgarbi and Baracca, 2011; Pavlova and Thompson, 2016). Hence, the alterations in intracellular and extracellular metabolites assisting 'neoplastic metabolic reprogramming' has helped 'metabolic

interactions of microenvironment' to gain position among additional hallmark of cancer metabolism (Pavlova and Thompson, 2016) and as potential therapeutic targets. Thus, this thesis is focussed on understanding the principles governing neoplastic metabolic reprogramming through experimentally established in vitro culture model designed to mimic the tumour microenvironment and therefore test the effects of altered pH_e and reduced oxygen tension. In order to identify the gaps in understanding cancer metabolism and appreciate the benefits that altered metabolism as emerging hallmarks of cancer confers on cancer cells, it is worthwhile considering the comparison with energy management and metabolism in normal healthy cells.

1.2 Metabolic consequences and pH homeostasis decide different fates for normal and cancer cells

1.2.1 Cellular metabolism in normal cells

The theory of metabolic alterations specifically as fallouts of genetic changes in cancer cells has gained major patronage with appropriation of metabolic pathways directed to meet a tumour's specific nutritional and growth requirements (Nagarajan, Malvi and Wajapeyee, 2016) contributing to tumour initiation and metastatic dissemination (Rotin *et al.*, 1989; Martinez-Zaguilan *et al.*, 1996; Pouyssegur, Franchi and Pages, 2001; McCarty and Whitaker, 2010).

Physiological processes in normal cells are carried out using glucose efficiently which generates large stores of energy currency in the form of adenosine-5-triphosphate (ATP). In contrast, although transformed cells have higher proliferation rates, they adapt to metabolic changes that result in inefficient ATP

synthesis (Vander Heiden, Cantley and Thompson, 2009; Solaini, Sgarbi and Baracca, 2011). The breakdown of glucose to ATP occurs with the help of oxygen. This takes place within the mitochondrion, which via Complex IV of the Electron Transport System (ETS), recruits an oxygen-dependent process termed oxidative phosphorylation or OXPHOS (Figure 1.2) (Chiche, Brahimi-Horn and Pouyssegur, 2010). Thus ETS couples the oxidation of the reduced form of nicotinamide adenine dinucleotide (NADH) and flavin adenine dinucleotide (FADH2) with the phosphorylation of adenosine-5-diphosphate (ADP) to form ATP (Lodish *et al.*, 2000).

Glycolysis (which takes place in the cytosol and does not require oxygen) can also be recruited independently by cells to break down glucose to produce ATP. This process of ATP synthesis by the cell also results in the consumption of NAD^+, which can in turn be regenerated by the conversion of pyruvate to lactate, the end products of glycolysis (Nelson and Cox, 2013).

A strict control of the intracellular pH (pH_i) for cells is essential for accessing the subsequent reactions of glycolysis absolutely necessary for ATP production. Indeed, several studies have pointed to a nucleophilic substitution reaction that is highly dependent on the increased pH_i, to drive the transfer of the phosphoryl group from ATP (Gerweck, Gillette and Dewey, 1974) thus, proving the importance of pH_i maintenance for the initiation of glycolysis and consequently for ATP synthesis (Wohlhueter and Plagemann, 1981; Spriet, 1991).

The production of ATP through OXPHOS when oxygen levels are adequate and is over ten times more efficient than glycolysis in generating ATP (Dixon, 1937; Vander Heiden, Cantley and Thompson, 2009; Nelson and Cox, 2013). However, it was postulated that the generation of ATP through glycolysis is preferred over OXPHOS in normal differentiated cells when oxygen levels are decreased by induction of the 'Pasteur effect' (Figure 1.3). This phenomenon was first observed during utilisation of glucose by yeasts, which is much more rapid in the absence than in the presence of oxygen (Racker, 1974; Vander Heiden, Cantley and Thompson, 2009; Nelson and Cox, 2013). In transformed cells this method of energy synthesis is modified to promote pathological progression.

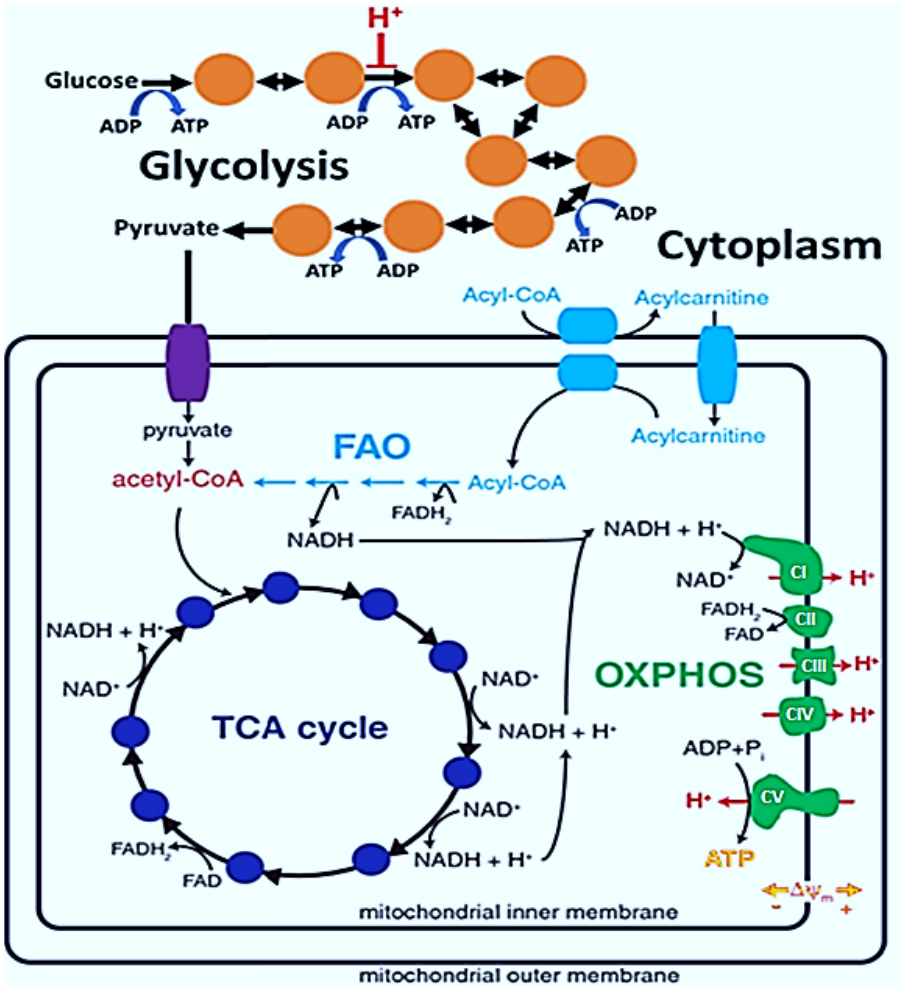

Figure 1.2: Energy generation in mammalian cells

Glucose breakdown through glycolysis (brown) and the TCA cycle (dark blue) generates reduced NADH and $FADH_2$. Electrons derived from NADH and $FADH_2$ are utilized by the five OXPHOS complexes (green CI-CV) to generate ATP. Complex I (CI), complex III (CIII) and complex IV (CIV) pump electrons out of the mitochondrial matrix to generate a membrane potential ($\Delta\psi m$) that drives the synthesis of ATP by complex V (CV). Cytosolic acidification (H^+, red) inhibits the glycolytic enzyme 'Phosphofructokinase'. Recreated and adaptated from (Nsiah-Sefaa and McKenzie, 2016)

1.2.2 Cellular metabolism in cancer cells

Around the turn of the 20th century, it was recognised that cancer cells have a unique metabolic pattern in terms of generating ATP via a highly inefficient process of utilizing glucose (Warburg, Wind and Negelein, 1927; Vander Heiden, Cantley and Thompson, 2009; Chiche, Brahimi-Horn and Pouyssegur, 2010). The consequences of this Warburg effect (Figure 1.4) has been implicated in irreversible resistance to cancer chemotherapy (Tannock, 1982; Chaplin, Durand

and Olive, 1985; Vander Heiden, Cantley and Thompson, 2009; Patlolla *et al.*, 2012) and as a measure of poor prognosis in cancer patients (Christ, 2009; Zhu, Lee and Shim, 2011). Interestingly, it is now known that genetic alterations in the tumour suppressor genes p53 (Matoba *et al.*, 2006) and PTEN (Xu *et al.*, 2015) as well as oncogenes such as Ras (Blum *et al.*, 2005), Myc (Shim *et al.*, 1997; Osthus *et al.*, 2000) and Akt (Rathmell *et al.*, 2003; Elstrom *et al.*, 2004; Plas and Thompson, 2005) enable them to function by altering tumour metabolism. Eventually, these strategies contribute to cellular tumorigenic properties and also exert two important changes on tumour fate. Firstly, deregulated uptake of glucose for bioenergetic resources and influx of glutamine for the N_2 and C supply are carried out by recruiting the Warburg effect (Section 1.2.2.1, Figure 1.4) or by employing *c-myc* respectively (Wise *et al.*, 2008; Wang *et al.*, 2011). Secondly, reciprocal metabolic interactions of the cancer cells with the microenvironment helps the emergence of a more aggressive state by imposing a selective pressure (Pavlova and Thompson, 2016). To this end, accumulation of metabolic acid (e.g. lactic acid) is coupled to the co-transport of H^+ and the surplus of CO_2 generated in mitochondrial decarboxylation reactions acidifies the cellular microenvironment (Walenta *et al.*, 1997; Brizel *et al.*, 2001; Stock and Schwab, 2009)

1.2.2.1 A consequence of the "Warburg effect"

Aerobic glycolysis although biochemically less efficient than OXPHOS (2 M of ATP compared to 32 M ATP produced for every mole of glucose) leads to the fast growth of tumour cells accompanied by high rates of glucose consumption

(Gerweck, Gillette and Dewey, 1974; Dang, 2012). This behaviour of cancer cells is well known as 'glucose addiction' of the developing tumour (Granja et al. 2015).

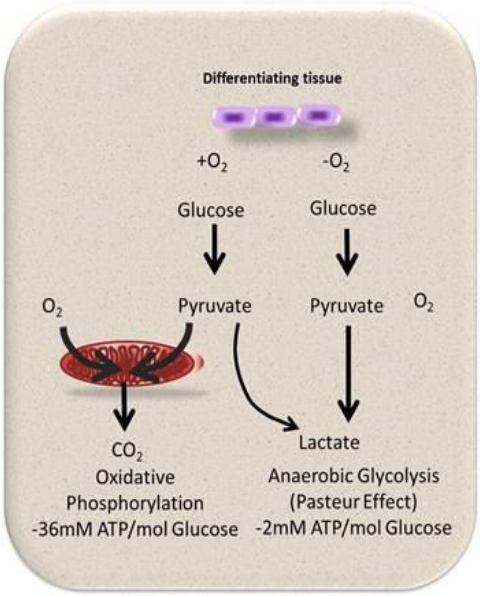

Figure 1.3: Glucose metabolism in differentiated normal cells
Diagram describing the biochemical pathways of glucose metabolism in the presence (OXPHOS) and absence (‘**Pasteur Effect’)** of O_2 in normal differentiated cells.
Recreated and adaptated from (Vander Heiden, Cantley and Thompson, 2009).

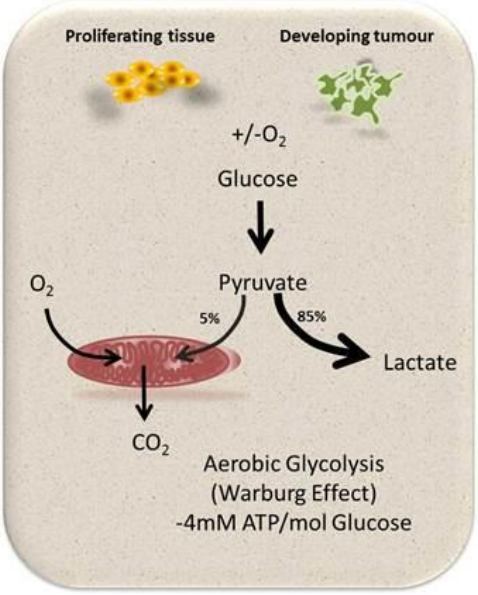

Figure 1.4: Glucose metabolism in cancer cells
Diagram describing the biochemical pathway of glucose metabolism in presence/absence of O_2 (`**Warburg Effect**’) in cancer cells.
Recreated and adaptated from (Vander Heiden, Cantley and Thompson, 2009).

With the increase in tumour size and associated depletion of oxygen and nutrients, proton concentrations near blood vessels are higher compared to those near the necrotic tumour periphery. This proton gradient is inversely related to the oxygen gradient (Chiche, Brahimi-Horn and Pouyssegur, 2010). The finding that cancer cells maintain an acidic extracellular environment leads us to a consideration of tumour-specific pH as a microenvironmental factor that influences cellular metabolic events to establish the malignant phenotype.

Hence, the gap that exists regarding the understanding of the role of modified micrenvironment in the vicinity of the cancer cell, needs to be identified and investigated. In the present study, we aim to address these lacunae in the existing literature by systematically testing the interaction of pH and oxygen tension in the tumour microenvironment mimicking experimental conditions. In this context the following section describes how these two components of the tumour microenviroent influence the cancer metabolism and tumour hallmarks.

1.2.3 Altered pH and oxygen tension has profound influence on cancer cell metabolism

1.2.3.1 Role of pH maintainence in cancer cells

Human physiology is strictly dependent on maintenance of acid-base homeostasis in response to changes in hydrogen ion concentrations [H^+]. These are measured as pH which can be either acid (pH 1 to 6.9), neutral (pH 7.0 to 7.4) or alkaline (pH above 7.4) (Arun Bahl, BS Bahl and Tuli, 2005). Since most of the human body uses water as a solvent, pH values have prominent effects spanning tissue and cell physiology, biochemistry and ultimately wellbeing and morbidity (Vaupel, Kallinowski and Okunieff, 1989). Unlike what is observed under physiological conditions, cancer cells have been shown to efficiently maintain an alkaline intracellular region (Griffiths, 1991; Stubbs *et al.*, 2000) even in the presence of high extracellular proton availability. This has led to extracellular acidity, earning the status of a cancer hallmark (Figure 1.1) (Tannock and Rotin, 1989; Vaupel, Kallinowski and Okunieff, 1989; Gillies, Liu and Bhujwalla, 1994; Hanahan and Weinberg, 2000, 2011). This unique proton gradient is almost exclusively observed

across cell membranes of solid tumours in contrast to normal tissues (Reshkin, Greco and Cardone, 2014). Additionally, the mechanistic metabolic adaptation, associated with inefficient glucose breakdown has also been attributed to a gradient of low O_2 tension existing in solid tumours. Hypoxia brings about changes in cell biology (Harris, 2002) enabling adaptive changes in cancer metabolism promoting a shift from normal glucose breakdown to glycolytic metabolism (Section 1.2.2) (Warburg, Wind and Negelein, 1927; Chiche, Brahimi-Horn and Pouyssegur, 2010). The poor prognosis and increased metastatic staging in solid tumours is also associated with low O_2 tension (Hockel *et al.*, 2001)

Recent techniques using nuclear magnetic resonance 31P spectroscopy for investigation into the pH_i and extracellular pH (pH_e) of tumours have confirmed the capacity of tumour cells to acidify the extracellular environment and to maintain a rather neutral/alkaline pH_i (Griffiths *et al.*, 1981; Wike-Hooley, Haveman and Reinhold, 1984; Griffiths, 1991).

1.2.3.2 Role of oxygen tension in cancer and pH regulation

Several intracellular processes are also triggered by low oxygen tension that promotes acidosis (Rotin *et al.*, 1989; Kizaka-Kondoh *et al.*, 2003). These processes include activation of oncogenic mediators and hence shifting from OXPHOS to aerobic breakdown of glucose (Kunz and Ibrahim, 2003). An improper vasculature often associated with impaired organisation and compromised perfusion in tumours results in a decreased delivery of nutrients and oxygen owing to the reduced blood supply in the vicinity of the proliferating tumour mass resulting in

the creation of a hypoxic tumour microenvironment. This decrease in oxygen partial pressure in the tumour microenvironment is realised by the cell through the activation of specific oncogenes (*Ras, Raf, PI3K, Akt, mTOR, Myc etc*) facilitated by the activation, and stabilisation of HIF-1α and its subsequent dimerization with its 'β' subunit (Hammond and Giaccia, 2005; Shafee *et al.*, 2009). The array of genes activated through the above mentioned dimerization involves those concerned with decreased respiration, promoting active erythropoiesis, triggering the activation of VEGF to promote neo-angiogenesis (Semenza *et al.*, 1994; Zimna and Kurpisz, 2015). These genes also bring about the related processes accompanying aerobic glycolytic metabolism and strict control of pH_i and pH_e favouring cell survival through autophagy and initiating invasion through active migration of disintegrated cells from the central tumour mass (Martinez-Zaguilan *et al.*, 1996; Lu *et al.*, 2010; Masson and Ratcliffe, 2014).

Tumour hypoxia has been observed in several solid tumours; cancers of the breast, uterine cervix, vulva, head & neck, prostate, rectum, pancreas, lung, brain tumours, soft tissue sarcomas, non-Hodgkin's lymphomas, malignant melanomas, metastatic liver tumours and renal cell cancer (Vaupel, Thews and Hoeckel, 2001; Vaupel and Höckel, 2002; Vaupel, Mayer and Hockel, 2004; Vaupel and Mayer, 2005). Hypoxia has been correlated with several factors related to tumour progression and is considered as the most pervasive microenvironmental oxidative stress with immense influence on malignant progression (Semenza, 2003). Hypoxia has emerged as the single largest factor in the repeated failure of chemotherapeutic agents in treating several types of adult malignancies (Kunz and

Ibrahim, 2003). Novel strategies are being considered after validating their efficiency in both normoxic and physiologically attributable low oxygen conditions to potentiate existing chemotherapeutic agents for cancer cell lines (Anbalagan *et al.*, 2015). These confounding factors make hypoxia an important physiological phenomenon that should be considered seriously when evaluating cancer prognostics and chemotherapeutic regimens (Lundgren, Holm and Landberg, 2007; Le and Courter, 2008).

Therefore, in the present study, major emphasis was laid on conceptualizing and designing of an experimental prototype that could be used as culture models to test the role of pH_e and oxygen tension in different cancer cell types. This formed an overarching aim for the present study as described in section 1.6.2

1.2.4 pH homeostasis and its role in tumour hallmarks- proliferation, migration and invasion

Identification of gaps in the undersatanding of the influence of metabolic reorganiosation on tumour hallmarks is very essential in cancer research. The following section highlights the interaction between pH regulation and oxygen tension to modulate proliferation and migration in cancer.

1.2.4.1 pH regulation - an indispensable strategy in adverse conditions

The strict control of pH (Figure 1.5) also governs many dynamic processes involved in cell proliferation and migration (Tannock and Rotin, 1989; Martinez-Zaguilan *et al.*, 1996; Pouyssegur, Franchi and Pages, 2001; McCarty and Whitaker, 2010). Malignant cells with high proliferation rate (squamous cell carcinoma, sarcoma,

non-Hodgkin's lymphoma, breast cancer etc) have been reported to harbour a relatively alkaline pH_i, that ranges between 7.2 - 7.6 (Griffiths, 1991) compared to a rather low pH_e, which lies between or in the range 6.3 - 6.7 (Lindner and Raghavan, 2009) or as low as 5.6 in squamous cell carcinoma (Arnold *et al.*, 1990). This contrasts with most normal eukaryotic cells where pH_i ranges between 7.0 - 7.4 (Madshus, 1988; Xu, Cui and Puett, 2014) and pH_e is tightly controlled between 7.1 - 7.2 (Damaghi, Wojtkowiak and Gillies, 2013).

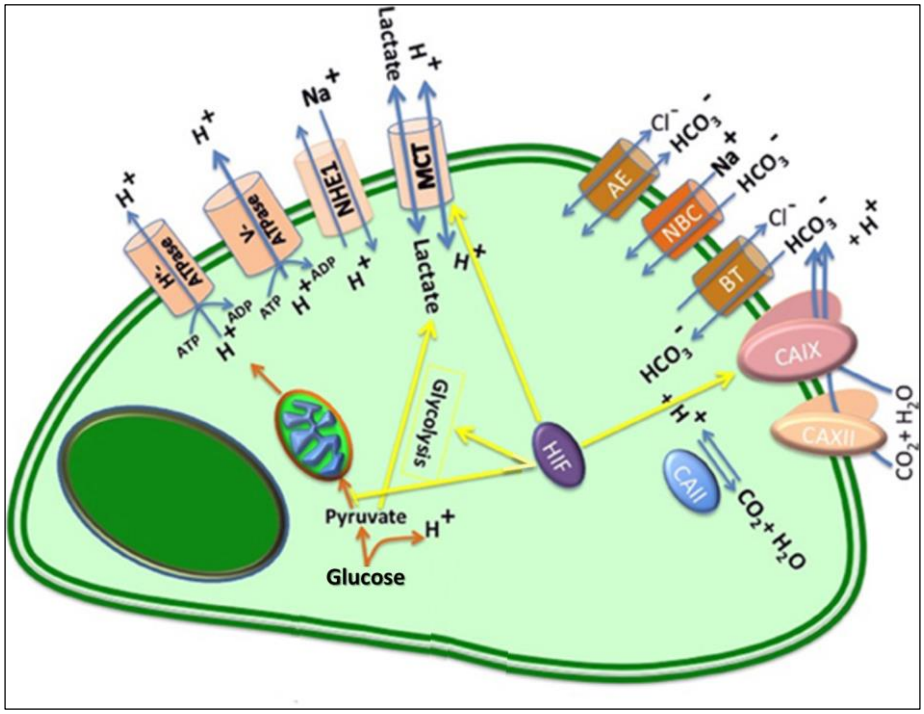

Figure 1.5: Major pH regulators in a cancer cell
After glucose uptake, glycolytic process in cancers produce protons (H^+), which cause acidification of the extracellular space. The above figure represents main proteins that regulate intracellular and extracellular pH in tumors, including: monocarboxylate transporters (MCTs); the plasma membrane proton pump vacuolar ATPase (V-ATPase); Na^+/H^+ exchangers (NHEs); anion exchangers (AEs); carbonic anhydrases (CAII, CAIX, and CA XII); Na^+/HCO_3^- co-transporters (NBCs), and HCO_3^- transporters (BTs). Modified with permission from (Damaghi, Wojtkowiak and Gillies, $^+$2013) Appendix 1I.1.

In addition, a relatively stable gradient of protons owing to glucose breakdown (Wike-Hooley, Haveman and Reinhold, 1984; Schonichen *et al.*, 2013) which is outspread from the microvasculature towards the tumour microenvironment is established and plays a major role in active tissue necrosis to support the rapidly proliferating tumour (Chiche, Brahimi-Horn and Pouyssegur, 2010).

The lower the oxygen level in cancer cells, the more protons (H^+) accumulate (Fukumura *et al.*, 2001; Chiche, Brahimi-Horn and Pouyssegur, 2010). For example, in lymphoma and leukaemic cells, PI3K/Akt/mTOR pathway is constitutively active, increasing the expression of nutrient transporters (glucose, amino acids) (Xu *et al.*, 2005). This activates and increases the expression of glycolytic enzymes (via Hypoxia Inducible Factor-1α) the supplies the energy demand of the rapidly proliferating tumour (Pouyssegur, Dayan and Mazure, 2006). Thus, Akt activation explains shift in metabolism to adapt the 'Warburg effect' (Rathmell *et al.*, 2003; Elstrom *et al.*, 2004; Plas and Thompson, 2005) leading to acidosis of the tumour microenvironment. Ras and Myc oncogenes also increase glycolytic enzyme activation leading to acid production (Tannock and Rotin, 1989). Thus $[H^+]$ within solid tumours is a consequence of oncogene activation, loss of tumour suppressor activity, adaptation to hypoxia and the ability of tumour cells to extrude acids.

The large metabolic acid loads deposited by elevated tumour metabolism, emerging from increased proliferation rate, emphasize the need for a pH_i regulatory system that remains functional even at hypoxic tissue regions. The ability of rapidly growing tumours to maintain a neutral pH_i is necessary for cancer progression since maintenance of pH_i near neutrality can sustain glycolysis even in

the presence of facultative anaerobiosis (Warburg, Wind and Negelein, 1927; Warburg, 1961; Chiche, Brahimi-Horn and Pouyssegur, 2010; Granja *et al.*, 2015). Intracellular neutralisation can also suppress OXPHOS by inducing hexokinase (HK) mediated mitochondrial activity repression. A high pH_i disrupts $[H^+]$, prevents pyruvate and inorganic phosphate transport into the mitochondrial matrix and blocks the synthesis of ATP from ADP (Alfarouk *et al.*, 2014). Intracellular alkalinisation activates glycolysis by directly increasing the activity of certain key glycolytic enzymes. These enzymes are extremely sensitive to small changes in pH in the physiological range (Nelson and Cox, 2013).

1.2.4.2 Role of pH in tumour migration and invasion

Tissue invasion and metastasis collectively represent one of the few novel capabilities adopted through transformation, considered a key hallmark of cancer (Hanahan and Weinberg, 2000). Extracellular tumour acidosis plays a vital role in promoting invasion, often aided by the proteolytic activity of matrix m-etalloproteinases (MMP) resulting in rapid degradation of the extracellular matrix (Figure 1.6) (Martinez-Zaguilan *et al.*, 1996; Glunde *et al.*, 2003). Furthermore, in-vitro studies reveal that a low pH_e not only activates MMP-9 but also potentiates migration and invasiveness in human melanoma models (Suzuki *et al.*, 2014). Interestingly, the metastatic potential of a tumour is closely associated with the interaction of membrane-type 1 matrix metalloproteinase (MT1-MMP) and NHE-1 (key pH requlatory protein) (Klein *et al.*, 2000; Lucien *et al.*, 2011). In addition, a fall in the pH_e reinforces the cytolytic property of cytotoxic T lymphocytes (Fischer *et al.*, 2007) and also hinders the function of natural killer (NK) cells resulting in a

decreased immunosurveillance status (Lardner, 2001) which would understandably prevent inflammatory responses following tissue invasion. Increased nodal metastatic ability of a tumour is associated with increased intracellular pH regulatory activity of the carbonic anhydrase, CA IX, through a stimulus from acidic pH_e (Chambard and Pouyssegur, 1986; Bose, Dort and Brockton, 2013).

An increase in pH_e elicits differential response in certain breast cancer cells in relation to their endocrine resistance and enhances their invasive potential reiterating the crucial influence of pH_e on oestrogen responsive cells (Khajah *et al.*, 2013). Studies have shown how pH_i is regulated differentially in response to a pH_e gradient existing across the migration axis of cancer cells (Figure 1.6) aiding dissemination of the tumour mass (Koltai, 2016).

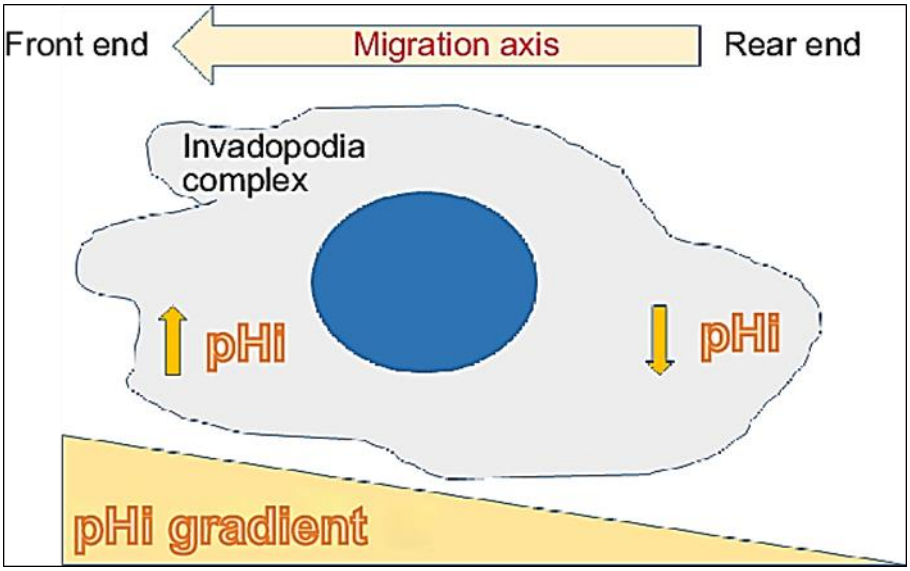

Figure 1.6*:* Microenvironment pH and intracellular pH regulation in cancer migration
Acid extrusion mechanisms establish an acidic extracellular microenvironment and a slightly alkaline cytosol. Acidic microenvironment contributes to the activation of catalytic enzymes that degenerate extracellular matrix. Cells migrating through the dissolved matrix, exhibit a pH_i gradient along the migration axis. Recreated and adapted from (Koltai, 2016).

Hence, in the present study, we focussed on using developed culture models mimicking tumour microenvironment to evaluate the change in proliferation and migratory potential of cancer cell types. Under the overarching aim of the study, this would serve as an important objective to investigate the dependence and influence of altered pH_e and oxygen tension on these hallmarks of cancer as described in section 1.6.2.

Furthermore, the regulation of pH is known to work under framework of different physical laws. The following section describes how these principles are applicable to regulate pH homeostasis in biological systems

1.2.5 Principle of pH regulation in biological processes

The eukaryotic cell with either physiological or pathophysiological inclination, functions with strict control over a narrow range of pH (Madshus, 1988). However, biomolecules involved in cellular functions dissociate into solutions over a wide range of pH. The unique behaviour of these solutes including proteins, carbohydrates and nucleic acids are ascribed to their multiple K_a (association constant) values associated with discrete sites with high affinity towards protons (Nelson and Cox, 2013).

From the perspective of proton dynamics, within the normal or cancer cell environment, the respective protonatable site reflecting through a low pK_a value remains unprotonated in an acidic solution (Swietach *et al.*, 2014). In contrast, an ambient alkaline pH results in complete titration of the protonatable site of a solute with high pK_a (Arun Bahl, BS Bahl and Tuli, 2005).

Furthermore, from the perspective of the whole cell, the numbers of protonated and unprotonated sites are balanced for a solute which reflects a pK_a close to the ambient pH and provide the necessary buffering capacity in the event of an impending pH challenge.

The idea explained above is well represented by the Henderson Hasselbalch's equation (Arun Bahl, BS Bahl and Tuli, 2005):

$pH = pK_a + \log[A^-]/HA]$

where: $[A^-]$ = molar concentration of a conjugate base

[HA] = molar concentration of an undissociated weak acid.

In response to the metabolic reactions in cancer or under normal physiological conditions affecting the pH_i/pH_e, there is a shift in the balance between the protonated or unprotonated entities accordingly. This shift is reflective of the metabolic alterations driving the complex biochemical and physiological processes in viable cells (Hammoudi *et al.*, 2011; Jang, Kim and Lee, 2013). The instability of pH_e buffering (through extrinsic CO_2-HCO_3 buffering and intrinsic pH regulatory proteins) over extensive cellular processes, due to the extrusion of other organic acids and lactate dehydrogenase activity, (Fis*cher et al*, 2007; Sauvant *et al*, 2008) varies between cells. The intrinsic buffering capacity (denoted β_I), stabilisation of steady state pH_i and net acid extrusion (NAE) collectively dictate the pH handling potential for cancer cells in response to acute changes in pH_i. In non-malignant cells, e.g. renal glomerular cells determination of β_I, and NAE has demonstrated

their importance in acid handling and pH buffering as has been observed in certain cancer-derived cell lines (Boyarsky *et al.*, 1988a; Hulikova, Vaughan-Jones and Swietach, 2011)

The existing literature exposes a gap in the understanding on how pH handling capacity of cancer cells are affected when the altered pH_e and oxygen tension interact in the tumour microenvironment. The present study focusses on utilising the developed culture models to evaluate the pH handling capacity of different cancer cell types by simultaneous alterations in pH and oxygen tension of microenvironment. This forms the basis of quantifying β_I, pH_i recovery and NAE using novel experimental tools and imaging techniques as discussed later (section 1.5 and 1.6.2)

The regulation in cancer cells involves multiple proteins and complex buffering systems. The following section discusses the properties and functions of these pH regulatiory mechanisms

1.2.5.1 pH regulatory mechanisms

Multiple membrane-associated pH regulatory systems, expressed constitutively in different mammalian cell types, are actively involved in maintaining the pH_i. The most extensively studied of these are:

(a) Those that promote and initiate cytosolic alkalinisation by allowing influx of negatively charged ions like HCO_3^- into the cytosol, working either as:

(i) Co-transporters of Na^+/HCO_3^- (Gorbatenko *et al.*, 2014)

(ii) Anion Exchangers for Cl^-/ HCO_3^- (Romero, Chang and Mount, 2010)

(b) The family of plasma and cellular enzymes known as the 'carbonic anhydrases' (CAs). These systems play a pivotal role in the control and restoration of the physiological pH (Swietach *et al.*, 2010; Zatovicova *et al.*, 2010).

(c) The ligand-activated H^+ pumps that expel two H^+ in exchange of energy (the vacuolar-type H^+K^+-ATPase V-ATPase) that depends on ATP to bind as a ligand (Martinez-Zaguilan *et al.*, 1993; Fais *et al.*, 2007)

The family of growth factor-activated ion exchangers that exchange sodium with proton (NHEs) (Alain E. Lagarde *et al.*, 1988; Loo *et al.*, 2012; Amith and Fliegel, 2013). (d) Bidirectional Monocarboxylic acid Transporters of lactic acid (MCT) (Fischer *et al*., 2007; Stock and Schwab, 2009; Le Floch *et al*., 2011).

The main systems are highlighted here for information only and did not form part of the present study. However, a little understood mechanism of pH-regulation in cancer is that of an ionic nature involving ion channels such as K^+ channels. In the section below, the relationship between K^+ and H^+ is described followed by K^+ channel classification and their involvement in cancer.

1.3 Functional correlation of K^+ and H^+ concentration in cancer

K^+ is the most abundant ion inside cells. Its unequal distribution across the cell membrane is a key determinant of the cell resting membrane potential but K^+ fluxes and concentrations also influence cellular metabolism.

Effects of acid-base status on internal K^+ distribution: Acidaemia associated with metabolic acidosis results in an overall movement of K^+ from within the cancer cells into the extracellular space (Aickin and Thomas, 1977). In contrast, a net cellular uptake of K^+ is observed in the event of metabolic alkalosis and associated alkalaemia (Aickin and Thomas, 1977). Cellular Na^+ and K^+ balance is indirectly affected by intracellular pH homeostasis in muscle cells (Juel, 2008). The level of intracellular pH and HCO_3^- is an important factor modifying the effect of extracellular pH on K^+ distribution (Juel, 2008). The mechanism of K^+ transport in renal cells is also known to be affected directly by low pH and indirectly through the effect of pH on multiple ion (Na^+, Cl^-, HCO_3^- etc.) transporters (Figure 1.7) but has not been studied in cancer cells. A low extracellular K^+ concentration $[K^+]_e$ relative to its intracellular levels is associated with cellular uptake of acid (Grinstein, Cohen and Rothstein, 1984; Grinstein and Dixon, 1989; Balkay *et al.*, 1997). In addition, the ratio of the intracellular to extracellular concentration of K^+ was shown to be directly proportional to the fall in the intracellular to extracellular proton ratio (Adler and Fraley, 1977).

Thus, present study investigates the dependence of cancer cells' acid extruding and pH handling capacities on the distribution or availability of free potassium. The indicators of pH handling capacities were evaluated in the presence of the developed culture models together serving as yet another relevant objective for the thesis.

Differentiated normal mammalian cells have also been shown to extrude protons in exchange for K^+ to maintain ionic balance (Aronson and Giebisch, 2011). Recognising the relationship between K^+ concentrations and metabolism, another significant consideration is the role of K^+ transport, mediated by K^+-selective channels in cancer.

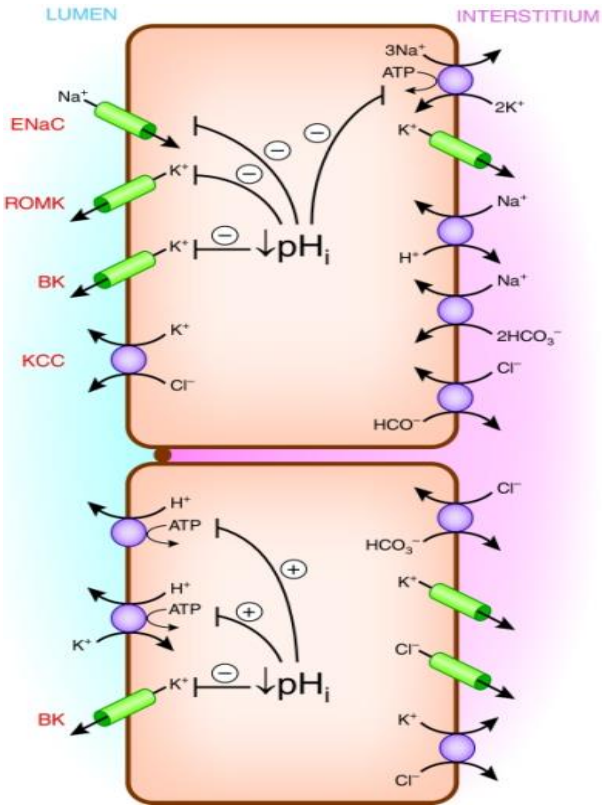

Figure 1.7 Ion transport in human renal cells
Low pH affects K^+ transport in the renal cells. The inhibitory or stimulatory effect of pH on multiple ion (Na^+, Cl^-, HCO_3^- etc.) also directly or indirectly affect K^+ transport in renal cells. The ion transporters are represented based on their expression on the luminal or the basolateral membrane of the renal cell. ENaC= Epithelial sodium channel; ROMK = Renal outer medullary potassium channel; BK = BK channel; KCC = KCl cotransporter. Represented with permission from (Aronson and Giebisch, 2011) Appendix 1I.2.

1.4 Expression distribution and role of potassium channels in cancer

Potassium transport and homeostasis in animal cells is mediated through a large array of membrane ion channels that make crucial contributions to cell

proliferation, migration, apoptosis and differentiation beyond their known role as regulators of membrane potential in excitable cells (Hatten and Roussel, 2011). In recent years, the expression of a plethora of K^+ channel subtypes have been shown to be linked to cancer (Camacho, 2006; Le Guennec *et al.*, 2007; Pardo and Stühmer, 2014) and they are therefore potentially attractive therapeutic targets. Understanding the role of K^+ channels in cancer metabolism may unveil new pathways to translation for novel cancer treatments (Fischer *et al.*, 2007; Stock and Schwab, 2009; Le Floch *et al.*, 2011).

The discovery of ion channels in malignant brain tumours and glioblastomas paved the way to unravel their role in other tumours (Sontheimer, 2008). Ion channel expression has been found to be altered in multiple malignancies. These include K^+ channels in breast, colon, and prostate cancer (Comes *et al.*, 2013), Na^+ channels in cervical and non-small cell lung cancers (Fraser *et al.*, 2014), Cl^- channels in colorectal cancer (Bustin, Li and Dorudi, 2001) and $Ca2^+$ in some oesophageal, breast cancer cell lines and glioma cells (Ding *et al.*, 2010).

Potassium channels comprise the largest ion channel family in the human genome comprising approximately 80 different gene products (Pardo and Stühmer, 2014). These channels represent the most structurally and functionally diverse group of ion channels and are potential targets for individualised/targeted cancer therapy (Huang and Jan, 2014).

The K^+ channel family is classified into three groups based on the number of domains that traverse the cell membrane (Zhong *et al.*, 2013) (Figure 1.8a). These

transmembrane domains (TMD) are associated with the functionality of the different types of member channels. In increasing order, the first group, comprising of two TMDs, are represented by the inward rectifying (Kir) channels. The second group, consisting of four TMDs (resulting in two pore formation; K2P), include the 'leak' K^+ channels. The final group includes K^+ channels that are voltage gated (Kv) and calcium activated (KCa). This third group is identified by their characteristic six or seven TMDs (Lee and Cui, 2010; Kuang, Purhonen and Hebert, 2015). Each group is divided into several families and subfamilies.

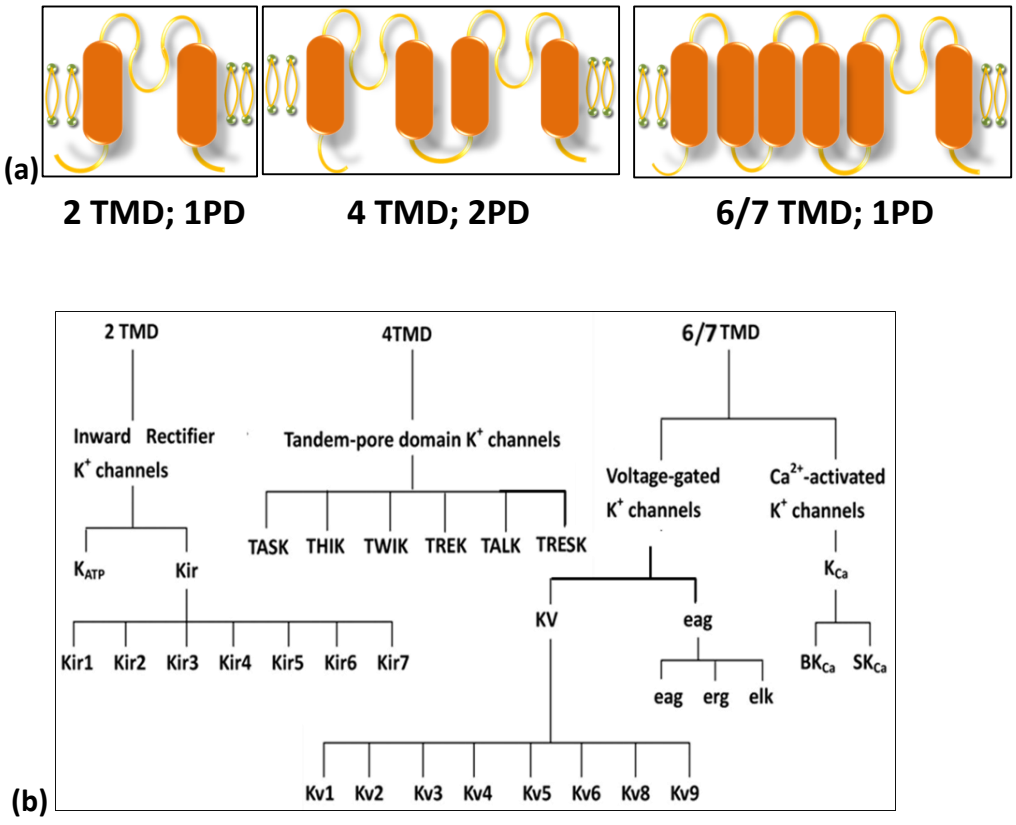

Figure 1.8 Classification of K^+ ion channels
(a) Structural classification – Three major K^+ channel gene families have been broadly characterised: Voltage-gated (K_v) channels have six (or seven) transmembrane segments (TMD) and one pore domain; inwardly rectifying (K_{ir}) channels present two TMDs and one pore domain. The weakly rectifying channels are predicted to have four TMDs and two pore domains (K_2P), each one resembling two K_{ir} channels arranged in tandem. *KCNK* channels are believed to form as dimers. **(b) Classification of K^+ channel families -** Four functional families of K^+ channels (K_{ir}, K_2P, K_v and K_{Ca}) are classified into three structural groups based on membrane topography prediction (Transmembrane Domain, TMD) viz., 2TMD, 4TMD and 6/7TMD. Modified from (Zhong et al., 2013).

Certain members of the second group (4TMD) are of interest in this thesis owing to their unique functional association with pH_i or pH_e. Referred to as TASK, TREK and TALK channels (Bayliss, Sirois and Talley, 2003), they may be prominently modulated by specific factors (e.g., fatty acids e,g, arachidonic acid, mechanical stimuli, acidic/alkaline pH_e etc; (Fink *et al*., 1998). This weakly rectifying channel family has been designated by the Human Genome Nomenclature Committee (HGNC) as *KCNK* channels, and by the International Union of Basic and Clinical Pharmacology (IUPHAR) (Alexander *et al.*, 2017) as K_2P where each one of the two pore domains, formed of four TMDs, resemble two K_{ir} channels positioned in tandem. There are currently six members in this 4TMD family (Figure 1.8b) (Chen *et al.*, 2014). The HGNC and IUPHAR nomenclature is followed by a number denoting the order of discovery of the genes coding for a channel (Figure 1.9). The popularly used naming scheme uses acronyms based on salient physiological or pharmacological properties listed here:

The HGNC and IUPHAR nomenclature is followed by a number denoting the order of discovery of the genes coding for a channel (Figure 1.9). The popularly used naming scheme uses acronyms based on salient physiological or pharmacological properties listed here:

1. TWIK - TWIK (Tandem of P domains in a Weak Inwardly rectifying K^+) channels (Goldstein *et al*., 2005).

2. TREK- (TWIK-related K^+) channels – modulated by fatty acids, heat and acidic pH_i and by tretch (Lesage *et al*., 2000; Kim *et al*., 2001; Honore *et al*., 2002; Sandoz *et al.*, 2009).

3. TALK - Alkaline-activated TALK (TWIK-related alkaline pH_e activated K^+) channels (Girard *et al*., 2001; Goldstein *et al*., 2005).

4. TASK - (TWIK-related acid-sensitive K^+) channels (Bang, Kim and Kim, 2000).

5. THIK - Halothane-inhibited THIK (tandem pore domain halothane-inhibited K^+) channels (Bayliss, Sirois and Talley, 2003; Blin *et al*., 2014).

6. TRESK - Endogenous arachidonic acid-inhibited TRESK (TWIK related spinal cord K^+ channels (Sano *et al*., 2003; Chen *et al*., 2014).

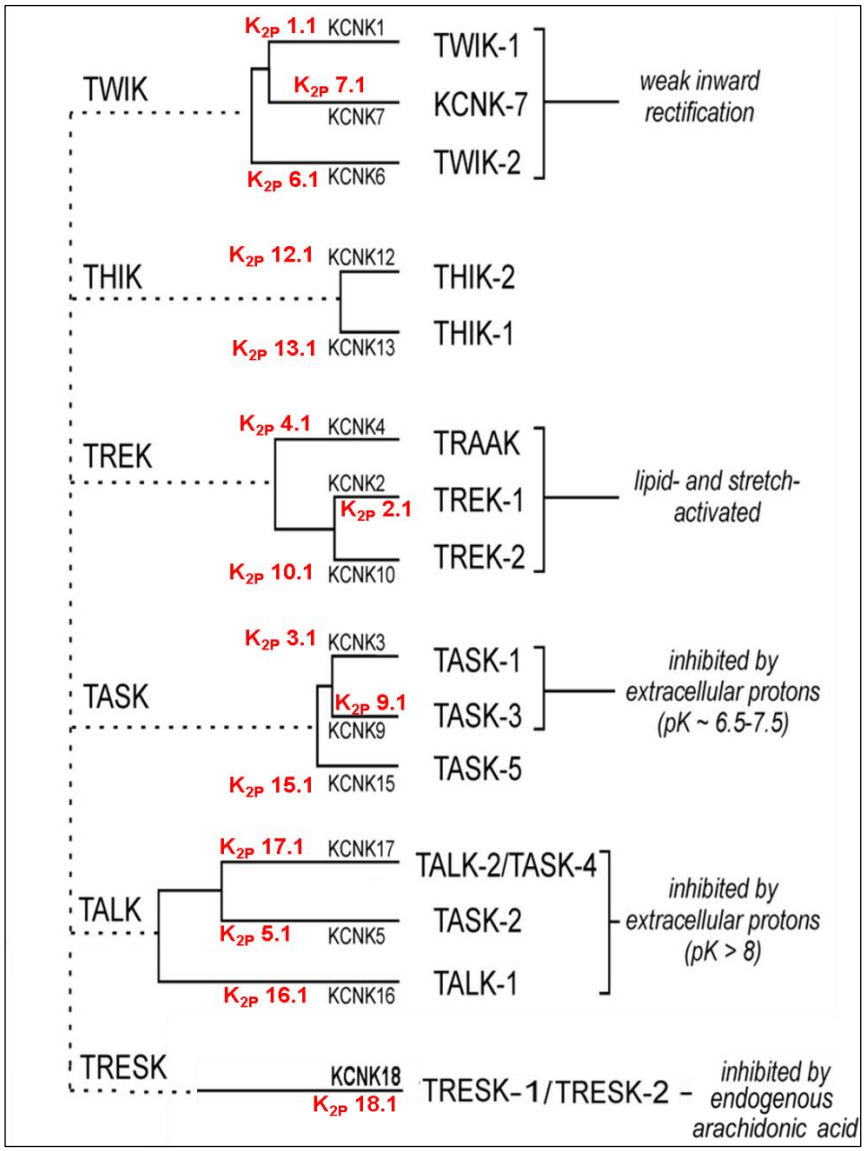

Figure 1.9 Classification of two pore domain K^+ channel coding genes
Adapted from (Bayliss, Sirois and Talley, 2003).

The fifteen known human two-pore-domain K^+ channel genes are classified in a phylogenetic tree, and placed into six subgroups as described by (Chen *et al.*, 2014). The naming convention of the genes coding for the K^+ channels by Human Genome Nomenclature Committee (HGNC) and International Union of Basic and Clinical Pharmacology (IUPHAR), *KCNK* and K2P (in red) respectively are denoted adjacent to their conventional/popular family names (Figure 1.9). The K^+-selective

channels have a crucial role in setting the membrane potential which in most cancer cells is depolarized (Yang and Brackenbury, 2013). Adding to this conundrum is the fact that K^+ fluxes occur through a variety of channels that manifest as voltage-gated or pH-sensitive proteins (Reyes *et al.*, 1998; Le Guennec *et al.*, 2007; Chen *et al.*, 2014; Kuang, Purhonen and Hebert, 2015). Our group has previously reported that blocking potassium channels in ovarian cancer cells inhibits cell proliferation (Asher *et al.*, 2011). Moreover, we also showed that expression of TASK-3 but not TREK-2 is associated with poorer survival. These lines of evidence suggest an interaction between these membrane proteins and the local environment emphasising the need to identify the nature of these interactions. Although, evidence indicates that Na^+ channels are widely involved with pH homeostasis in cancer cells (Bourguignon *et al.*, 2004; Lin *et al.*, 2011; Lucien *et al.*, 2011), the less studied relationship between pH regulation and K^+ balance across the cell membrane is thought to be of great importance (Adler and Fraley, 1977).

1.4.1 Evidence of K^+ channels in normal and cancer cell proliferation

As discussed earlier, cell proliferation is subject to very tight regulation through several interdependent cellular mechanisms. As early as the last quarter of the previous century, increasing evidence suggested that K^+ channels were key players that contribute towards the regulation of lymphocyte proliferation (Cahalan *et al.*, 1985). Channel blockers such as 4-aminopyridine, quinidine, and tetraethylammonium (TEA) were shown to inhibit proliferation in normal cells including lymphocytes, brown fat cells and Schwann cells (Wonderlin and Strobl,

1996) whereas significant inhibition of proliferation in cancer cells was observed in the presence of the nonspecific K^+ channel blockers. Although the underlying molecular mechanisms are poorly understood, inhibition of K^+ channels was shown to block the initiation of the G1 phase of the cell cycle, preventing progression of cell division (Wonderlin and Strobl, 1996; Schlichter and Khanna, 2002; S*chwab et al*., 2012).

The association between regulation of membrane potential by K^+ channels with their participation in cell proliferation is well understood in cancer cells. The constitutively depolarised cancer cells need to be transiently hyperpolarised during transition to the G1 phase of cell cycle and is centred on K^+ flux (Arcangeli *et al*., 1995) through K^+ channel inhibition (Wonderlin and Strobl, 1996). Apart from modulation of pH_i control, K^+ channel mediated variation in membrane potential majorly affects cell proliferation. Other key elements that contribute to cell proliferation are influx of Ca^+ and Na^+-dependent nutrient transport (Pardo, 2004).

Although the relevance of cell size checkpoint in this context is still controversial, maintenance of cell volume is also considered important for cell proliferation through scrupulous control of solute concentrations. K^+ channels, along with Cl– channels, are known to be important for regulatory volume changes that support cell proliferation (Sanguinetti *et al.*, 1995; Lang *et al.*, 2000; Wondergem *et al.*, 2001). The schematic diagram below (Figure 1.10) highlights the potential role of potassium channels in cellular proliferation outlining the contributing and collaborating factors involved therein.

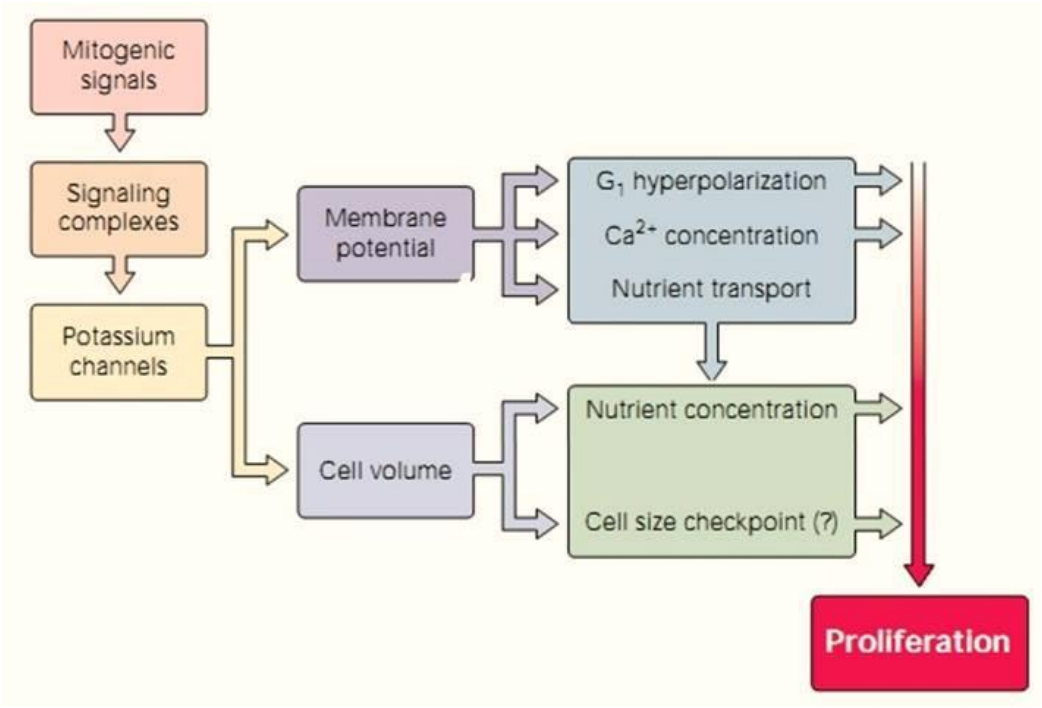

Figure 1.10 Role of K^+ channels in cell proliferation
Cell signals that initiate mitosis through signalling complexes are thought to recruit potassium channels that function as regulators of membrane potential and cell volume. The discrete pathways trigger individual downstream processes (Na^+ & Ca^{2+} fluxes, nutrient management) important in promoting cell proliferation. Recreated and adapted from (Pardo, 2004).

To throw light on the importance of potassium channels in cancer, the expression profile of these channels has been highlighted. Table 1.1 illustrates the extent of expression of one family (KCNK family) of potassium channel expression in 20 human cancers compared to normal tissue (Williams, Bateman and O'Kelly, 2013).

A

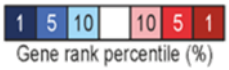

B

Cancer \ Gene / Protein	KCNK1 K_{2P}1.1	KCNK2 K_{2P}2.1	KCNK3 K_{2P}3.1	KCNK4 K_{2P}4.1	KCNK5 K_{2P}5.1	KCNK6 K_{2P}6.1	KCNK7 K_{2P}7.1	KCNK9 K_{2P}9.1	KCNK10 K_{2P}10.1	KCNK12 K_{2P}12.1	KCNK13 K_{2P}13.1	KCNK15 K_{2P}15.1	KCNK16 K_{2P}16.1	KCNK17 K_{2P}17.1	KCNK18 K_{2P}18.1
Bladder															
Brain and CNS															
Breast															
Cervical															
Colorectal															
Esophageal															
Gastrointestinal															
Head and Neck															
Kidney															
Leukemia															
Liver															
Lung															
Lymphoma															
Melanoma															
Myeloma															
Other															
Ovarian															
Pancreatic															
Prostate															
Sarcoma															

Cancer \ Gene / Protein	KCNK1 K_{2P}1.1	KCNK2 K_{2P}2.1	KCNK3 K_{2P}3.1	KCNK4 K_{2P}4.1	KCNK5 K_{2P}5.1	KCNK6 K_{2P}6.1	KCNK7 K_{2P}7.1	KCNK9 K_{2P}9.1	KCNK10 K_{2P}10.1	KCNK12 K_{2P}12.1	KCNK13 K_{2P}13.1	KCNK15 K_{2P}15.1	KCNK16 K_{2P}16.1	KCNK17 K_{2P}17.1	KCNK18 K_{2P}18.1
Bladder															
Brain and CNS															
Breast															
Cervical															
Colorectal															
Esophageal															
Gastrointestinal															
Head and Neck															
Kidney															
Leukemia															
Liver															
Lung															
Lymphoma															
Melanoma															
Myeloma															
Other															
Ovarian															
Pancreatic															
Prostate															
Sarcoma															

Table 1.1: Expression of KCNK genes across different cancers.
Expression of genes coding for K2P channels (*KCNK1–18*) in 20 cancers compared to normal tissue controls. [A] Over-expression of KCNK genes. [B] Underexpression of KCNK genes. Cancer types are organised by their tissue of origin, the degree of colour correlates to the gene rank percentile of the highest ranking analyses. Represented with permission from (Williams, Bateman and O'Kelly, 2013) Appendix 1I.3. 35

1.4.2 Role of K^+ channels in cancer

Voltage-gated potassium (Kv) channels are known to be expressed in different types of cancers and have been shown to be involved in proliferation and cell cycle kinetics (Wonderlin and Strobl, 1996). The translocation of charged molecules across the plasma membrane is considered to be an important mode of action of these channels (Le Gue*n*nec *et al.*, 2007). The Ether-a-go-go (Eag) channel (coded by the Eag gene) (Ganetzky *et al*., 1999) and the Human Eag Related Gene (HERG) are members of the Kv family (Fig 1.18b). They are aberrantly expressed in multiple cancer types and have been associated with oncogenic potential in heterologous systems (Pardo *et al.*, 1999).

Eag channels have been shown to aid cancer cells in their transition through the cell cycle (Camacho, 2006) while HERG channels have been shown to play a primary role in regulation and progression of the cell cycle in different categories of solid tumours (Crociani *et al*., 2003). The non-specific voltage gated K^+ channel blocker 4-aminopyridine (4-AP) arrested ovarian cancer cells in the G1 phase of the cell cycle inhibiting proliferation (Zhanping *et al*., 2007).

Eag and HERG channel blockers significantly inhibit proliferation in the ovarian cancer cell (SK-OV-3), in which there is high expression of these potassium channels (Zhanping *et al*., 2007). Flow cytometry analysis of SK-OV-3 cells treated with HERG blockers has revealed that they are arrested in the S and G2/M phase (Asher *et al.*, 2011).

The HERG gene known to be expressed primarily during the early stages of cell differentiation is also found to be overexpressed in different tumour cell lines (Bianchi *et al*., 1998). In contrast Eag channel blockers like imipramine though have not been found to have any effect on the cell cycle but work from our lab has shown that they trigger early apoptosis in SK-OV-3 cells (Asher *et al.*, 2011). The functional role of voltage gated K^+ channels has thus been attributed to the proliferation of ovarian cancer cells.

1.4.3 Role of pH_e sensitive Ion Channels (K^+ channels) in cancer

Overexpression of K_2P channel subtypes has been observed in a range of cancers including breast, leukaemia and lung while other cancers (brain, colorectal, gastrointestinal, kidney, lung, melanoma, oesophageal) show underexpression of one or more channels (Williams, Bateman and O'Kelly, 2012, 2013). Several of the K_2P channels are pH_e-sensitive. Among these, the TWIK-related acid-sensitive K^+ channels are activated by a wide range of pH_e. The TASK-1 (Duprat *et al.*, 1997; Kim *et al.*, 1998; Leonoudakis *et al.*, 1998) and TASK-3 (Rajan *et al.*, 2000) channels and their heterodimer has been demonstrated to be activated by varying acidic pH_e (Lesage and Barhanin, 2011). The TASK-3 channel alone has a sensitivity that is shifted toward acidic pH_e, only to be inhibited at a pK value of 6.7 (Rajan *et al.*, 2000). Interestingly, although TASK-1 channel (overexpressed in renal clear cell carcinoma, adrenocortical carcinoma, lung squamous cell carcinoma, prostate carcinoma, cholangiocarcinoma) shown by canSAR v 3.0 (Tym *et al.*, 2016), their activity is inhibited by > 90% at pH_e 6.7 (Duprat *et al.*, 1997), the TASK-1-TASK-3 heterodimer is only inhibited at pH_e 7.3 (Czirjak and Enyedi, 2002).

Unlike the TASK1/3 channels, TREK channels are sensitive to variations of the cystosolic pH (pH_i) (Maingret *et al.*, 1999; Honore *et al.*, 2002). TRAAK is stimulated by cytoplasmic alkalinization from pH 7.3. Like TASK channels, TREK-1 and TRAAK are inhibited by external acidification (Cohen *et al.*, 2008; Sandoz *et al.*, 2009). The TREK-2 mechanosensitive channel is overexpressed in colon carcinoma, papillary thyroid carcinoma, metastatic prostate and renal clear cell carcinoma as shown by canSAR v3.0 (Tym *et al.*, 2016) and activated by acidification in the range pK of 7.4 (Sandoz *et al.*, 2009). In contrast TALK-2 potassium channels are inhibited in an acidic tumour microenvironment and hence are activated by increased pH_e (pK**½** for TASK-2 is 8.0) (Lesage and Barhanin, 2011; Sandoval *et al.*, 2011). A significant increase in copy number variation of the *KCNK17* gene coding for TALK-2 channel protein was observed in lung, colon, caecum, large intestine, renal pelvis, bladder, kidney, urinary tract and colorectal carcinoma as shown by canSAR v 3.0 (Tym *et al.*, 2016). With a 3.26 % fold increase in the expression of TALK-2 channel proteins in invasive breast cancer biopsies according to a single study (Williams, Bateman and O'Kelly, 2012) their role is yet to be correlated with increased metastatic potential of breast carcinomas due to an alkaline tumour microenvironment (Khajah *et al.*, 2013). The contrasting activation profile of this potassium channel protein to TASK-3 channels makes it an interesting candidate for comparison when investigating the differential influence of a pH_e on the expression of these proteins in cancer cells.

Among all the K^+ channels TASK-3 is regarded as an oncogenic potassium channel which is expressed in ovarian (Innamaa *et al.*, 2013; Pardo and Stühmer, 2014),

prostate, lung and melanoma cancers (Koztak, 2011). The prognostic significance of TASK-3 in human ovaries has been investigated through evaluation of the effects of its inhibitor on cell proliferation and apoptosis (Innamaa et al., 2013). Overexpression of TASK-3 in the ovarian cancer cell lines SK-OV-3 and OVCAR-3 compared by immunohistochemistry against their expression levels in normal ovarian tissue samples (Innamaa *et al.*, 2013; Pardo and Stühmer, 2014) was confirmed and reflected a significant survival advantage with a median survival of more than 24 months. Inhibitors of TASK-3 channels caused a significant reduction in cell proliferation and an increase in apoptosis in the SK-OV-3 and OVCAR-3, indicating its importance as a possible therapeutic target (Innamaa *et al.*, 2013). Thus, TASK-3 overexpression in epithelial ovarian cancer, conferring a significant survival advantage to patients, can be interpreted as that of a novel tumour marker.

1.4.4 Oncogenic potential of KCNK9 (TASK-3 coding gene) is due to physiological function

One of the key genomic processes that leads to tumour development involves the genomic amplification of important oncogenes. The genetic alteration of *KCNK9* gene is indicative of their direct role of in cancer (Struski, Doco-Fenzy and Cornillet-Lefebvre, 2002; Mu *et al*., 2003). With *KCNK9* in question it has been shown that there is a high incidence of copy number gains that affect the 8q chromosome arm in multiple cancers. In breast carcinomas 8q copy number gains occur in excess of 40% or more when compared to all other solid tumours (Mu *et al.*, 2003).

The oncogenic potential of TASK-3 channel is associated with the possibility of its dysregulated expression as an event subsequent to transformed proliferation. Furthermore, studies also investigated the role of TASK-3 in inducing transformation and preventing tumour cells commitment to apoptosis. The TASK-3 channel is amplified in 10% of breast cancers and is overexpressed at a higher frequency of breast, lung, colon, and metastatic prostate cancers (Mu *et al.*, 2003; Koztak, 2011) normal ovaries and ovarian tumours (Innamaa et al. 2013).

Overexpression of wild type TASK-3 channels help in resisting the TNF-induced apoptosis and thus led to cell proliferation (Pei *et al.*, 2003). TNF-induced apoptosis enabled cancer cells to escape host immune defences. The dominant-negative mutant of TASK-3 can interfere with the activity of TASK1 channels through heterodimerization (Mulkey *et al*., 2007). TASK-3 gene amplification or overexpression was not detected ¡n tumour samples where TASK-3 was amplified (Sauvant *et al*., 2008). The debate about the actual role of TASK-3 channels in relation to tumorigenesis or cancer is unresolved opening more scope for investigation.

Thus, in the present study we investigated how and if an experimental alteration in the component of the microenvironment (pH and oxygen tension) has any influence on the expression and distribution of the pH sensitive potassium channels. The developed culture models would then prove to be useful to evaluate the role of the channels in proliferation and most importantly the functional role of TASK-3 channels in acid homeostasis. As mentioned earlier these investigations

wouild utilise a combination of unique experimental tools, protocols and imaging techniques. The following section describes relevance and properties of the tools required for evaluating cancer cells' potential to regulate pH homeostasis.

1.5 Tools to evaluate pH regulatory potential

Studying the effect of change in either pH_e and/or PO_2 is not without challenges. Coupling these with K^+ fluxes and linking to K^+ channels is not a trivial task but utilising such experimental combinations will help elucidate the potentially altered relationship between K^+, pH and PO_2 in cancer. One of the longer-standing methods to effect and track changes in pH, the ammonium pre-pulse technique, is described below.

1.5.1 Ammonium pre-pulse technique – modifying pH

One of the first pieces of evidence for the theory supporting the active interplay of pH-regulating systems was elucidated in 1981 (Roos and Boron, 1981). This technique, the H^+-suicide technique, was extensively studied for the sodium-hydrogen exchanger-1 [NHE-1] by (Pouysségur *et al.*, 1984). The increased potential of the NHE exchanger in regulating intracellular pH in an acidic environment was demonstrated by the delivery of a loading dose of acid into the cells through a pre-pulse of NH_4Cl (Figure 1.11).

These observations pertaining to the pH_i regulation of NHE exchangers were found to be consistent in tumour cells such as colon carcinoma LS174Tr cells and also in cervical carcinoma HeLa cells (Chiche, Brahimi-Horn and Pouyssegur, 2010). Interestingly in contrast to the above observation, mutant cells devoid of NHE-1 were unable to re-establish pH_i subsequent to an acid overload and succumbed to the deleterious effects of the acidic environment within an hour (Pouysségur *et al.*, 1984; Chiche, Brahimi-Horn and Pouyssegur, 2010). Targeting tumour metabolism

with the ammonium pre-pulse technique is possible in highly glycolytic cell types in response to transformation events exemplified by oncogene activation, suppression of tumour suppressor genes or metabolic changes such as a low oxygen status.

There is unique and substantial evidence that backs the hypothesis that pH_i-regulating systems have a high functional significance in promoting *in vivo* growth (Roos and Boron, 1981; Boyarsky *et al.*, 1988b; Chiche, Brahimi-Horn and Pouyssegur, 2010). These observations indicate the possible existence of multiple pH-regulatory systems that can be understood by challenging cancer cells with an acute acidic exposing their metabolic vulnerability, serving as potential targets for novel and efficacious anti-tumour strategies (Chiche, Brahimi-Horn and Pouyssegur, 2010. In many in vitro experiments targeted at upholding the significance of NHE-1 or CAIX (Swietach *et al.*, 2008, 2009) pH_i regulation was monitored in a bicarbonate as well as a bicarbonate-free extracellular environment, where limiting the bicarbonate concentration in the extracellular milieu is aimed at restricting the involvement of intrinsic anion exchangers.

Thus, the ammonium pre-pulse is a commonly used experimental manoeuvre to challenge cells as it provides a way in which to measure subsequent pH_i modulation by the cells (Figure 1.11) and to estimate the contribution of multiple pH regulators, including bicarbonate-dependent and bicarbonate-independent buffering systems. These processes have previously been studied independently in certain cancer-derived cell lines, non-neoplastic cells and normal cells, primarily

with respect to specific pH regulatory systems and proteins (Roos and Boron, 1981; Boyarsky *et al.*, 1988b; Hulikova, Vaughan-Jones and Swietach, 2011; Hulikova *et al.*, 2013). Hence pharmacological manipulation of specific channel proteins and transporters in tandem with the ammonium pre-pulse manoeuvre can help elicit their involvement in intrinsic pH_i regulation (chapters 5 and 6). Furthermore, the ammonium pre-pulse manoeuvre is thought to contribute in identifying associations between pH_i oscillations with complex cellular processes generating metabolically active areas within the cytosol.

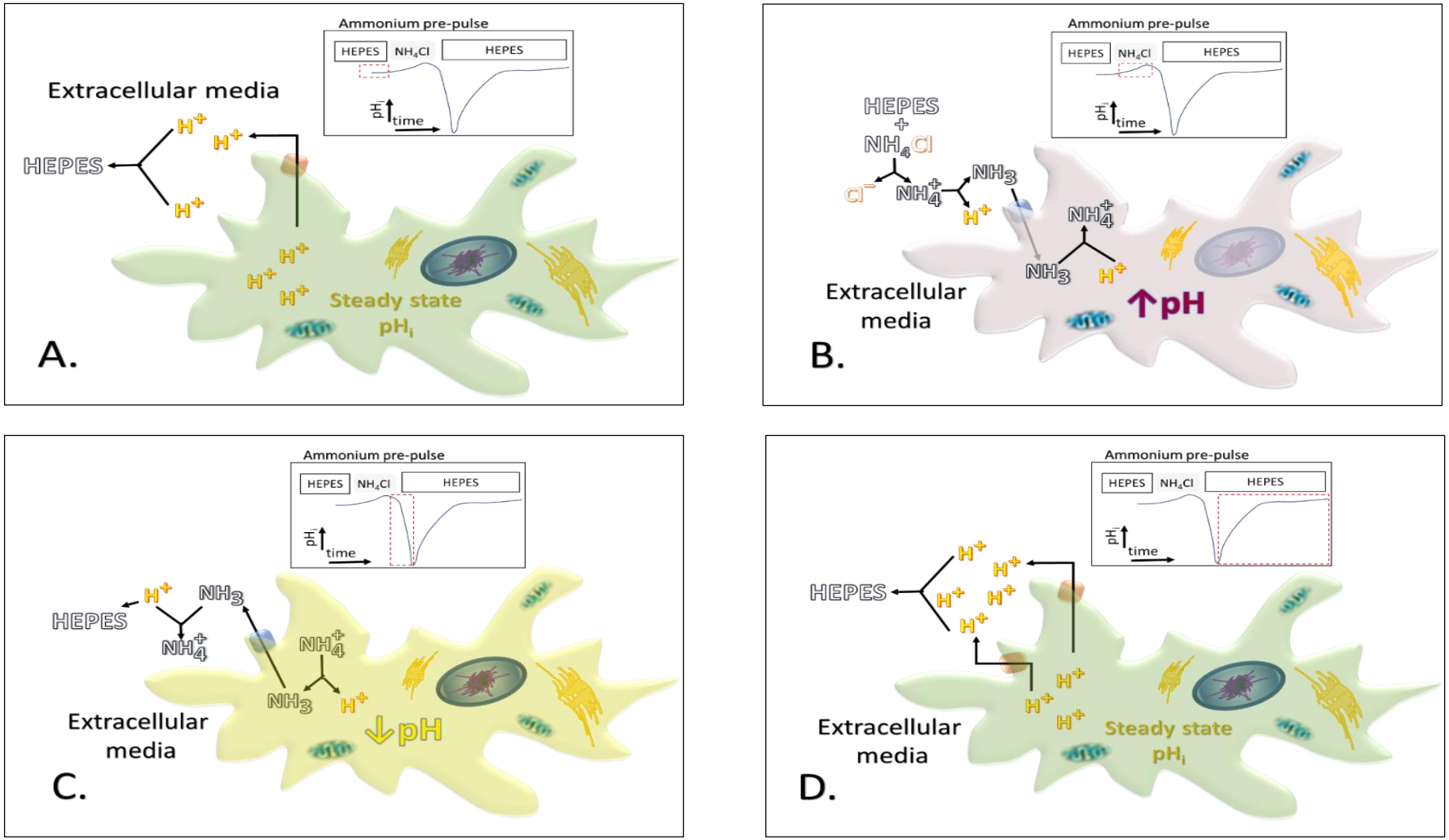

Figure 1.11: Principle of the 'ammonium pre-pulse' technique

Schematically represented human cell subjected to 'ammonium pre-pulse' experiment. Inset represents progress of a conventional time course trace of the experiment highlighted by red dotted box. [A] Stabilisation of steady state pH_i in standard HEPES buffered extracellular media. [B] Intracellular alkalinisation due to NH_4Cl pulse. [C] Intracellular acidification of withdrawal of NH_4Cl. [D] Recovery of steady state pH_i in standard HEPES. (Boyarsky *et al.*, 1988).

1.5.2 Fluorescence and live-cell imaging to evaluate pH of cancer cells

Over the past decades there has been remarkable advancement witnessed in the field of fluorophore technology and development of efficient but synthetic fluorescent proteins (Gaethje, 2007; Suzuki *et al.*, 2007). As the need arises for development of methods to provide critical insight into the fundamental nature of cellular and tissue function demands for live-cell imaging techniques have increased. Consequently, live-cell imaging has become an indispensable means of data acquisition and analysis tool broadly in cell biology research.

Live-cell imaging (Figure 1.12) experiments are considered to be extremely useful to investigate the functional relevance of cellular processes. The strength of the data derived through this technique is well-complemented when combined with data from confocal microscopy (Bischof *et al.*, 1996; Corvini *et al.*, 2000; Ozkan and Mutharasan, 2002; Hulikova *et al.*, 2013).

With access to modern instrumentation the imaging of living specimens can be performed to observe real-time events at high resolution and signal-to-noise ratios, while using extremely low levels of illumination. Hence to analyse dynamics of ion movement and fluxes this technique can be considered to be an efficient tool for the analysis data interpretation from fluorescently labelled cells. Thus several factors like the correct filter sets, lasers and fluorophores and appropriate processing of samples are key to generate data that will enable explanation of cellular and metabolic processes as in cancer research.

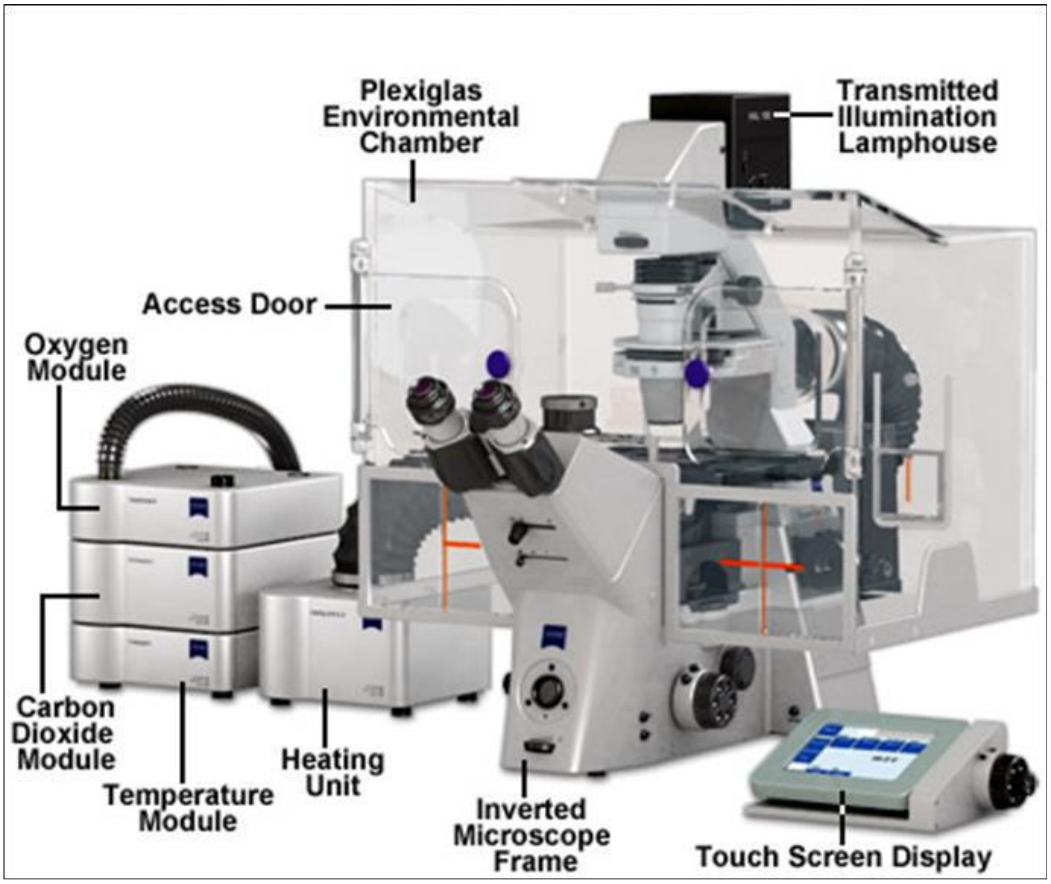

Figure 1.12: Microscope configuration for live cell imaging
The illustrative representation of a microscopy setup with essential components to support living cells whilist a live-cell imaging session.

1.5.3 Selection of pH sensing and pH sensitive dyes/probes as pH indicator

Accurate determination of pH, (through live cell imaging) and particularly its effects on submicron compartments of cells, is of great interest to the scientific community (Roos and Boron, 1981; Wolfbeis, 2002). Advances in optical technology have driven the development of tools small enough to characterise diverse microenvironments (McDonagh, Burke and MacCraith, 2008). Initial efforts were directed towards reducing the dimensions of analyte sensitive optodes (an optical sensor device that optically measures a specific substance). However, it was soon established that the fluorophores at the tip of an optode are all that is required to make measurements

(Clark *et al.*, 1998; Clark, Hoyer, Parus, *et al.*, 1999; Clark, Hoyer, Philbert, *et al.*, 1999).

1.5.3.1 pH dyes

The 2'7'-bis-carboxyethyl-5'-and-6'-carboxyfluorescein (BCECF) and 1,4 (and 5)-benzenedicarboxylic acid, 2-[10-(dimethylamino)-1-fluoro-3-oxo-3H-benzo[c]xanthen-7-yl] (carboxy SNARF-1) are cell impermeant fluorescent dyes that are sensitive to changes in the ambient pH. The high cell permeability of the otherwise inactive acetoxymethyl ester of BCECF (BCECF-AM)/cSNARF-1 makes them befitting candidates to measure only pH_i (Bergman *et al.*, 1991; Lemasters *et al.*, 1999; Tanaka *et al.*, 2003). The acetoxymethylester (AM) when cleaved by intracellular esterases releases the pH sensitive dye serving as a useful experimental parameter. The benefit of AM cleavage is influenced by factors like like cell volume and cell membrane, and can be quantified by calibrating the dye for the different cell types with nigericin - an antibiotic derived from *S. hygroscopicus* that acts as a potassium ionophore promoting K^+/H^+ exchange across cell membranes.

1.5.3.2 Fluorescent pH polymeric nanosensors

This species of pH sensors represents a concept that incorporates the advantages of pulled optical fibres into free fluorophores (Aylott, 2003; Ow *et al.*, 2005; Lee, Smith and Kopelman, 2009). Spherical fluorescence pH probes have a radius of ~500 nm made up of an inert matrix. Polyacrylamide/silicon are considered as suitable matrices inside which are embedded signal transducers. The signal transducers are

usually a combination of fluorescent dyes which can also be covalently bound to the matrices (Clark *et al*., 1998; Sun *et al*., 2006).

The non-reactant matrix provides a physical separation acting as a barrier between the intracellular components reactive salts and enzymes. This benefit provided by the matrix avoids unexpected reactions between the dye and cellular component that might jeopardise cell viability. Unlike free dyes, nanosensor probes have been found to interact with biological components without triggering cellular toxicity, e.g. as a result of photoexcitation. These sensors are also bereft of hindrances from sensing capabilities, due to reduced protein binding (Graber *et al*., 1986).

1.6 Project Rationale and Aims

The contribution of acidic pH_e as an important microenvironmental factor has been realised through its induction of epithelial-mesenchymal transition, also important in some types of cancers (Gos, Miloszewska and Przybyszewska, 2009; Kalluri and Weinberg, 2009; Suzuki *et al.*, 2014). An acidic pH_e is associated with metastatic pain in cancer known to act through certain channels and by sensitization of primary afferent nociceptors (Schmidt *et al.*, 2010). Interestingly membrane receptors for extracellular pH (activated below 6.8 pH_e) have been shown to suppress cell proliferation and migration in prostate and breast cancer cells and enhance cell adhesion of ovarian cancer to the extracellular matrix (Yang *et al.*, 2006; Ren and Zhang, 2011; Li *et al.*, 2013). Ovarian cancer cells in acidic medium (pH 6.6) significantly increase interleukin-8 (IL-8) expression which modulates tumour cell invasion. Alkalinisation (pH 7.7 - 8.3) of the extracellular environment has also been shown to induce morphological changes in some breast cancer cell lines. A change in pH_e has also been attributed to change in migratory and invasive phenotype of breast cancer cells (Khajah *et al.*, 2013).

Together with an acidic extracellular pH_e, hypoxia greatly facilitates cancer cell proliferation and migration. While culturing cancer cells in a hypoxic environment to mimic in vivo conditions, is an accepted methodology, few studies report growing cells in an acidic environment and even less so superimposed with a low O_2 tension (Hulikova, Vaughan-Jones and Swietach, 2011; Hulikova *et al.*, 2013). The reason for this may be due to difficulties in exercising experimental control over pH and the

lack of available commercial culture media. In addition, robust methods for measuring pH in live cancer cells like intracellular, fluorescent non-toxic pH sensor dyes and nanosensor probes demand meticulous calibration in tandem with high resolution microscopy with minimal phototoxicity to the cells during experimentation. In seeking to understand the role of pH in cancer cells, we optimised four culture conditions in order to enable us to address the effects of these conditions on a range of cellular functions, as well as the pH-dependence and intrinsic buffering influences of the cellular pH regulatory mechanism. Following on from previous work in our lab (Asher *et al.*, 2011; Innamaa *et al.*, 2013) this study focusses on investigating the functional importance of K^+, K^+ channel expression not only in cancer cell survival but also in pH regulation in response to a microenvironment with altered pH_e and O_2 tension. The planned study utilised three phenotypically distinct cancer cell lines (ovarian cancer – SK-OV-3; breast cancer - MCF-7; oesophageal cancer - OE-19) to study the role of pH, O_2 tension and K^+ of the tumour microenvironment on cancer cell behaviour.

1.6.1 Working hypothesis

Changes in pH and PO_2 in the tumour microenvironment affect cancer cell behaviour through K^+ transport processes.

1.6.2 Aims of the work

To establish an in vitro culture model designed to test the effects of altered extracellular pH (pH_e 6.3 and 7.4) and oxygen tension (PO_2 of 0.029 atm and 0.21 atm) (Chapter 3) on:

1. Expression and localisation of voltage-gated (Eag, HERG) and pH-sensitive (TASK-3, TALK-2) K^+ channels in the cancer cell lines SK-OV-3, MCF-7, OE-19 (Chapter 3).

2. Cell proliferation of the cancer cell lines SK-OV-3, OE-19 and MCF-7 cells using inhibitors of pH-sensitive channels and migration/invasion of SK-OV-3, MCF-7 (Chapter 4).

3. The intrinsic pH buffering capacity (β_I) and net acid extrusion (NAE) from rate of pH_i recovery of cancer cell lines SK-OV-3 and MCF-7 using the ammonium pre-pulse method (Chapter 5).

4. The role of K^+ and the pH-sensitive TASK-3 channel on pH_i recovery subsequent to acute acid loading in cancer cell lines SKOV-3 and MCF-7 using the ammonium pre-pulse manoeuvre (Chapter 6).

Chapter 2. Materials and methods

The study was primarily conducted at the Clinical Science Laboratory (5101), School of Medicine (Division of Medical Sciences and Graduate Entry Medicine, Derby), University of Nottingham, UK. Some experiments were also conducted at the Advanced Microscopy Unit, School of Medicine, Nottingham, University of Nottingham, UK.

2.1 Cell lines used for the study

The SK-OV-3, an ovarian adenocarcinoma cell line from ascites (metastatic site) was purchased from an authenticated stock provided by the European Collection of Cell Cultures (ECACC). The SK-OV-3 cell vial was labeled as 'Passage +1' for reference. McCoy's 5A medium as supplemented with 2mM glutamine, 15% FBS and 1% penicillin/streptomycin was used as resuscitation medium to revive cryopreserved SK-OV-3 cells from liquid nitrogen (Appendix 2X.1). RPMI-1640 medium was supplemented with 10% FBS and 1% penicillin/streptomycin and was used as maintenance medium for SK-OV-3 cells after quantitative evaluation of doubling time and viability. MCF-7 (breast adenocarcinoma cell line from pleural effusion (metastatic site); Passage +105), OE-19 (male oesophageal cancer cell line; Passage+11) and MCF-10A cell line (non-tumourigenic immortalized breast epithelial cell line; Passage +104) was kindly donated by Dr. Cristina Tufarelli, Division of Surgery; School of Medicine, University of Nottingham, UK. DMEM for MCF-7 and RPMI-1640 for OE-19 cells respectively, supplemented with 10 % FBS and 1% penicillin/streptomycin was used as resuscitation and maintenance medium

(Appendix 2.X.1). The MCF-10A cell line maintained in DMEM/F12 (1:1) was supplemented with 5% charcoal stripped horse serum (CSHS), 0.5mg/ml hydrocortisone (resuspended at 1 mg/ml in 100% ethanol), 1% penicillin/streptomycin, Epidermal growth factor (EGF) final concentration 20ng/ml, insulin 10µg/ml (resuspended at 10 mg/ml in sterile double distilled H_20 (ddH_20) containing 1% glacial acetic acid; shaken well and allowed to reconstitute for 10-15 min) and cholera toxin 100ng/ml (resuspended at 1mg/ml in sterile ddH_20 and allowed to reconstitute for about 10 min). Resuspension media for MCF-10A was prepared with 400ml DMEM/F12, 100ml CSHS (final concentration 20%) and 1% penicillin/streptomycin. Modified MEM (Section 2.4.3) was used for all culture condition specific experiments with cell line specific supplements incorporated for respective cell lines. Only when preparing cells for immunofluorescence, for confocal and wide field microscopy all cell subculture and maintenance were carried out exclusively in phenol red-free media/trypsin/HBSS (Appendix 2X.1).

2.2 Computer software and databases used for the study

The present study relied heavily on the following software and computer programmes. The FIJI 3.0 (ImageJ software) was used for the 'Ratiometric analysis' of fluorescence image signals from pH-sensing dyes (Section 2.7).

Statistical analysis of experimental data was carried out with the use of Prism 6.0 and 7.0 (Graphpad) (Section 2.14). The GeNex 4.0 and 6.0 (MultiD.se) was used for statistical analysis of the 'cycle threshold' values obtained from quantitative RT-PCR experiments to determine relative gene expression (Section 2.13.5)

SoftWorx 3.0 (Applied Precision) was used as a Linux based interface to operate the widefield fluorescence microscope (Section 2.7.5.4).

2.3 Culturing and maintenance of adherent cell lines

2.3.1 Recovery of cells from liquid nitrogen

Cancer cell lines were stored in liquid nitrogen at -180°C. For recovery, the lid of the sterilised vial was loosened in a Class II safety cabinet to release any trapped N_2 gas. The vial lid was then secured back and transferred to a 37°C water bath where it was partially immersed until thawed. The cell suspension was then asceptically transferred using a Pasteur pipette into a T25 tissue culture flask containing pre-warmed medium (approximately 5 ml for a 25 cm^2 flask) (Appendix 2X.2). The flask was capped quickly and viewed under a phase contrast microscope to ensure proper dispersion of the cells within the flask. The flasks with cell suspension in respective complete growth media (CGM) containing 4mM sodium bicarbonate balanced with 10mM HEPES, were placed in a humidified incubator at 37°C in 5% CO_2/95% air (0.21 atm PO_2), intended to attain a pH of 7.4 and maintained until the required degree of cell confluence was achieved. To prevent the exhaustion of medium nutrients from the trauma that the cells underwent on transportation/resuscitation, the spent medium was replaced with fresh medium the following day.

2.3.2 Subculture of adherent cells

At 70-80% confluence, the culture medium was carefully aspirated and the monolayer of cells was washed twice with PBS (Appendix 2X.1). To this, trypsin/EDTA (0.05%) solution was added (1-2 ml for 25cm^2 culture surface area)

(Appendix 2X.1). For SK-OV-3 cells the flask was gently rocked for 30 – 50 seconds at room temperature to ensure detachment. If not detached the flask was again put back into the 37°C incubator for around 5 minutes. For all other cell lines the flasks were directly incubated at 37°C incubator for around 2 -8 minutes (for MCF-10A: 5 – 10 minutes).

At this point the flask could be examined first visually and then under the microscope to confirm the detachment of the cells (except flasks with SK-OV-3 cells, all other flasks needed to be tapped to ensure complete detachment of the cells). Immediately 2ml of fresh FBS pre-warmed to 37°C was added to resuspend the cells in order to quench the deleterious effects of trypsin. The cells were further resuspended in approximately 5ml of pre-warmed fresh HBSS (Ca^{2+}/Mg^{2+}-free without phenol red). The whole suspension was aseptically transferred using Pasteur pipettes (to apply minimum shearing force) into a 15 ml screw-capped Falcon tube. The suspension was centrifuged at 800 rpm for 5 minutes at room temperature (22 – 25 °C) to yield a pellet of healthy cells. The supernatant was carefully aspirated. The cell pellet was again suspended in 10 ml of fresh pre-warmed HBSS and the above procedure was repeated twice to remove any remnant of trypsin/EDTA. The pellet obtained after the final wash was again resuspended in 1ml pre-warmed fresh medium. The viability and count of the resulting cells was determined using the trypan blue cell exclusion assay in a haemocytometer/Neubauer chamber or an automated cell counter (Bio-Rad, Hertfordshire, UK). The cells were then subcultured into fresh T-75 vented flasks

with pre-warmed CGM for respective cell lines. The subculture ratio for SK-OV-3 and MCF-7 cells was 1:3 and for OE-19 and MCF-10A was 1:5 respectively.

	Trypsin 0.5% (1-2 ml/25cm^2 area)		FBS/CSHS (pre-warmed to 37°C)	Repeat twice				Resuspension in CGM	Subculture Ratio
SK-OV-3	30-50 seconds at RT. Refractory cases upto 5 minutes at 37°C	Gentle rocking of flask without agitation (RT)	2 ml for every 1 ml of Trypsin	Aseptically transfer Suspension using Pasteur pipettes to 15 ml Falcon tube	Centrifuge @ 800 RPM for 5 min at RT	Aspirate supernatant gently (strictly avoid suction for SK-OV-3 cells)	Resuspended cell pellet in HBSS	**RPMI-1640**- 2 mM Glutamine 10% FBS and 1% penicillin/streptomycin for maintainence , **McCoy's 5A** – 2 mM Glutamine, 15% FBS and 1% penicillin/streptomycin for resuscitation from cryopreservation	1:3
MCF-7	2-5 minutes at 37°C	Mild physical agitation of flask (RT)	2 ml for every 1 ml of Trypsin					**DMEM** – 2 mM Glutamine 10% FBS and 1% penicillin/streptomycin	1:3
OE-19	2-5 minutes at 37°C	Mild physical agitation of flask (RT)	2 ml for every ml of Trypsin					**RPMI-1640** – 2 mM Glutamine 10% FBS and 1% penicillin/streptomycin	1:5
MCF-10A	5-10 minutes at 37°C	Adequate physical agitation of flask (RT)	2 ml CSHS for every 1 ml of Trypsin					**DMEM/F12 (1:1)**, supplemented with 5% charcoal stripped horse serum, 0.5 mg/ml hydrocortisone, 1% penicillin/streptomycin, Epidermal growth factor final concentration 20ng/ml, insulin 10 µg/ml and cholera toxin 100ng/ml.	1:5

Table 2.1. Cell line subculture profile layout.
Subculture protocol of test cancer derived cell lines and non-neoplastic breast cell line MCF-10A performed to maintain adherent cell cultures. RT = Room Temperature (20-25°C).

2.3.3 Cryopreservation of cells in Liquid nitrogen

In order to store cell lines for long durations, cells were stored in the vapour phase of liquid N_2 by suspending the cell pellet obtained by the subculturing (see Table 2.1) in the following freezing media.

a) Growth media (Section 2.1) + 10% DMSO and 20% CSHS for MCF-10A.

b) Growth media (Section 2.1) + 10% DMSO and 10% FBS for all other cell lines.

An approximate density of 3 x10^6 cells/ml was maintained in cryo-vials. The labelled cryo-vial were kept on ice for 15 minutes and then transferred to a cell freezer over night at -80°C before being stored in vapour phase of liquid N_2. Care was taken to store adequate numbers of cells for future use.

2.4 Establishing a standard cell culture based model to stabilise the pH_e

2.4.1 Methods to determine the buffer concentration to establish specific pH_e model

The focus of the study was to investigate the effect of extracellular pH in regulating cell proliferation and metabolism in cancer. This study required a strategy to improve previously established cell culture models with a steady pH of the culture medium. Sodium bicarbonate and CO_2 were used as a robust buffering system that worked in combination to stabilize pH of the culture medium for long term experiments.

All cell lines during maintenance and after resuscitation were incubated in 5% CO_2/95% air humidified incubator (often referred to as normoxic incubator in this study; MCO-5, Sanyo, Moriguchi, Osaka Prefecture, Japan) at 37°C. The experiments with low oxygen tension were carried out by replacing air with N_2 to achieve 3% O_2

(0.029 atm PO_2), while CO_2 was set at 20% concentration in a multi-gas cell culture humidified incubator at 37°C (MCO-5M, Sanyo, Moriguchi, Osaka Prefecture, Japan). The selection of 3% oxygen as low oxygen was to mimic mild hypoxia conditions that are observed in the tumour microenvironment of solid tumours falling between approximately 0.3% and 4.2% oxygen. The oxygen gradient in tumour microenvironment has been further categorised as that normal levels (6%), mild hypoxia (0.5 to 3%) and anoxia (0%) (Bustin *et al.*, 2009; Paolacci *et al.*, 2009; Chao *et al.*, 2012). Hence, considering the range of hypoxia it was decided to use 3% oxygen as low oxygen conditions.

2.4.2 Preparation of MEM medium without $NaHCO_3$

The sterile powder was added to a volumetric flask and made up by adding 950 ml of distilled water at room temperature (15°C to 30°C) with gentle stirring. When completely dissolved, the pH was adjusted to 4.1 to 4.2 with 1N HCl. The prepared liquid medium after final volume make up and pH monitoring was dispensed into 1000 ml bottles with loosely fitted caps and autoclaved for at least 15 minutes at 121°C on a slow exhaust cycle. The medium was then allowed to cool to room temperature.

2.4.3 Strategies to validate the buffer concentration to establish extracellular pHe model

In this study three basic strategies were adopted to develop novel cell culture models with altered pH_e and PO_2. Firstly, a validation of a cell's response and

viability (tested by trypan blue cell exclusion assay (Section 2.5) in low pH_e and physiological pH_e was examined for all cell lines. The final pH of the respective CGM was adjusted to 6.0-6.3 by slowly adding, with stirring, 1N HCl/1N CH_3COOH and to 7.0-7.5 with 1N NaOH as per the requirement. The principle guiding the experimental design for the above method is represented in Appendix 2I and Appendix 2II respectively.

Secondly, an experimental approach was adopted initially to attain a pHe of 7.42 at low PO_2 with MEM. By adding $NaHCO_3$ (10% concentrated stock prepared in reconstituted MEM) to a final concentration ranging between 25 – 44 mM was balanced with 5 – 10 mM HEPES to reconstituted MEM. Similarly, for low pHe 6.3 at normal PO_2, MEM was reconstituted with less than 4 mM $NaHCO_3$. For media with normal pH_e in normal PO_2 and low pH_e in low PO_2 the reconstituted MEM was balanced with 4 mM $NaHCO_3$. If the concentration of sodium bicarbonate was too high for the CO_2 atmosphere in the incubator, the media became more alkaline (the pH increased). All constituent supplements specific to the cell line used were added to the reconstituted MEM to test the stabilisation of pHe over 48, 72 and 96 hours, with and without cells in culture. In case of subculture, sterile pre-incubated pre-warmed pH adjusted culture media was used to resuspend the subcultured cells. Finally, a theoretical validation and determination of the concentration of the $NaHCO_3$ in the medium must be matched with the concentration of PCO_2 to achieve a desired pH_e. This method was developed to stabilise the pH_e for prolonged culture time points.

The Henderson Hasselbalch's equation was used to determine the concentration of sodium bicarbonate to be matched for the amount of CO_2 atmosphere in the incubator as described in (Section 2.3.2). The use of PCO_2 (available to the cultured cells) and Henry's Law (Henry's constant) helped us to calculate the $NaHCO_3$ to be added in the media (Appendix 2III). The methodology of this derivation is described in Appendix 2IV. The rationale for using $NaHCO_3$ dependent buffering system and calculations to achieve sustained acidic pHe are elaborated in Appendix 2I.

To distinguish between the observed effects from either a change in pH of the medium or due to the availability to oxygen, different pH regulated culture medium were determined. The Henderson Hasselbalch's equation was used to establish four different pH regulated culture medium models:

I. **Low pH_e and PO_2 -** Complete growth medium with pH of 6.3 to 6.58 in 0.029 atm PO_2 (3% O_2) and 20 % CO_2

II. **Normal pH_e and PO_2 -** CGM with pH of 7.42 in 0.21 atm PO_2 (95% air) and 5 % CO_2.

III. **Low pH_e and normal PO_2 -** CGM with pH of 6.3 to 6.58 in 0.029 atm PO_2 (95% air) and 5 % CO_2.

IV. **Normal pH_e and low PO_2 -** CGM with pH of 7.42 in 0.029 atm PO2 (3% O_2) and 20 % CO_2.

2.5 Viability and Proliferation Assays

Cell viability and proliferation were measured as a function of metabolism. Proliferation assays of cancer cell lines were undertaken after culturing them in altered pHe and PO_2, with proliferation assessed by MTS and resazurine assays only. The cell viability was assessed by trypan blue dye cell exclusion assay (qualitative observation) and/or resazurine assay (as a function of metabolic viability) due to its reduction to resofurin by active mitochondrial mechanism of viable cells.

2.5.1 Proliferation assay with MTS and resazurine dyes

The cleavage and conversion of the MTS or resazurine to the insoluble purple formazan or fluorescent resofurin respectively was used for the measurement of cell proliferation. Trypan blue cell exclusion assay was used to assess the viability of the cells.

a) Firstly, for each cell line, cells were counted and seeded in the range $5x10^3$ – $100x10^3$ in triplicates in 96 well plates. The cells were then subjected to serum starvation (incubated for 4 hours in FBS free media) for cell cycle synchronisation and subsequently incubated for 24, 48 and 72 hours under all four culture conditions developed (Section 2.4.3). Now, 20 µl of MTS/10 µl resazurine (to attain 100 µM final concentration) were added to each well in the dark, in parallel replicate plates for MTS and resazurine assays. The plates were then incubated at 37°C for 1-2 hours before measuring absorbance at 490 nm for MTS assays (CellTiter 96 aqueous non-radioactive cell proliferation assay kit (Appendix 2X.3) and fluorescence expressed as Relative Fluorescence Units (RFU at 560 nm, Ex/590 nm, Em) for resazurine assays. The change in OD/RFU values representing the change in the number of

metabolically viable cells was plotted against the increasing seeding density to estimate the most viable seeding density for all cell lines.

Subsequently, serum starved SK-OV-3, OE-19, MCF-7 and MCF-10A cells were seeded onto 96 well plates at optimal seeding density for assessment of proliferation and doubling time in response to altered pH_e/PO_2 (Section 2.4). At consistent time intervals (24, 48 and 72 hours), the effect of the established culture condition (Section 2.4.3) on the proliferation of the test cancer cells SK-OV-3, MCF-7 or OE-19 and MCF-10A (non-neoplastic control), was assessed using CellTiter 96® aqueous cell proliferation assay kit as described above. The relative doubling time for passage numbers 7, 21, 113 and 105 for SK-OV-3, OE-19, MCF-7 and MCF-10A cell lines respectively under altered pH_e and PO_2 was calculated using percent increase in proliferation based on the formula:

$$\text{Doubling Time} = T\ \frac{\ln 2}{\ln(X1/X2)}$$

T is the incubation time in any units. X1 and X2 are the cell number at the beginning and end of the incubation time respectively.

b) Secondly, serum starved cell were again plated at optimal cell density in 96 well plates to assess the long term effect of altered pHe and PO2 with and without pharmacological inhibitors of TASK-3 (methanandamide), HERG (E-4031) and H^+/K^+ATPase (omeprazole) on the proliferation of SK-OV-3, MCF-7 and OE-19 cell lines. The pharmacological reagents for administration to all the above test cells were prepared as described below in 2.5.1.1.

c) All drugs were reconstituted in respective modified medium (Section 2.4.3) as required. The respective media and vehicle control (e.g. < 0.1% Ethanol for methanandamide and DMSO for E-4031) were added to all replicates. The metabolic activity of the cells in altered pH_e and PO_2 for could best tested over long term (more than the doubling time of all the test cancer cells) they were incubated in respective modified culture conditions for 72 hours. At the end of the incubation MTS (Promega 96 Cell Titre) aqueous non-radioactive cell proliferation assay and resazurine sodium salt assays were performed according to the manufacturer's instructions (described above). Optical Density (OD)/absorbance at 490nm for MTS assays and Relative Fluorescence Units (RFU at 560 nm, Ex/590 nm, Em) for resazurine assays were measured for all replicate plates. The change in OD/RFU values representing the change in the number of metabolically viable cells in controls compared with response to different pharmacological agents for specific time points was recorded. All cell proliferation assays were carried out for the cells cultured under the selected four culture conditions and repeated minimum thrice.

d) Finally, the pH_i of the viable SK-OV-3, MCF-7 and OE-19 cells after 72 hour of incubation with the three pharmacological agents in altered pH_e/PO_2 was assessed. At the end of the incubation with the three pharmacological agents the cells adhered to Corning® 96 well clear flat bottom optic plates in monolayer were washed HEPES buffered extracellular solutions (Section 2.11.1). The cells were subsequently loaded (Section 2.7.1 and 2.7.2) with BCECF-AM pH sensing dye (see Section 2.8 for calibration). Fluoroskan Ascent™ Microplate Fluorometer (5210470,

Thermo Scientific, Paisley, UK) was used to obtain fluorescence data from dye loaded cancer cells as described in Section 2.7.4.

2.5.1.1 Preparation of drug solutions

Pre-activation of Omeprazole (H^+/K^+ ATPase Pump inhibitor) was carried out by preparing a 10-fold more concentrated form in 2.5 ml modified DMEM/RPMI. The medium was incubated in 20% CO_2 to yield an acidic solution with pH < 5.2 and incubated for 7-8 hrs. This technique was modified from published literature to accommodate the rate of acidification of the culture medium (Im *et al.*, 1985; Cortes *et al.*, 2009).

After overnight attachment of cells, 10 µl of medium was discarded gently from the surface to prevent accidental removal of cells. Pre-activated omeprazole at a final concentration of 10 µg/ml was added (Luciani *et al.*, 2004; Cortes *et al.*, 2009). E-4031 dihydrochloride (Human Ether ago go Related Gene, HERG channel blocker) and (R)-(+)-Methanandamide, a non-specific K^+ channel inhibitor of the TWIK-like Acid Sensitive K^+, TASK-3 channel (Innamaa *et al.*, 2013) were used at a final concentration of 0.1 µM (Appendix 2X.3). The drugs were prepared initially as stock solutions in respective solvents viz., DMSO/Ethanol (≤ 0.1% at final dilution).

2.6 Assessing the migratory and invasive potential of the tumour cells in altered microenvironment

2.6.1 Scratch wound migration assay

The scratch assay was performed on cancer cells to study the effect of altered culture conditions and pH_e on cell migration:

a) Coating of cell culture dishes: Tissue culture-treated dishes (35 mm diameter, Nunc® dishes) were used (Appendix 2X.2). Some dishes were coated with Poly-L-lysine as control. The tissue culture-treated dishes and Poly-L-lysine coated dishes were rinsed once with PBS and refilled with 3–5 ml of medium before seeding the cells. The appropriate amount of serum for the particular cell type used, in the medium during the in vitro scratch assay was required to be determined. A lower percentage of serum was used than that required for the growth medium (pH_e/PO_2 specific culture conditions; Section 2.4.3) to minimize cell proliferation, but sufficient to prevent apoptosis and/or cell detachment. This comprised of scratch wound assay-specific media while still maintaining the modifications required to yield culture conditions for all cell lines in with their specific supplements (Section 2.4.3).

b) Passaging the cells in culture: Sub-confluent growing cells in tissue culture flasks were passaged (Section 2.3). Cells obtained were plated onto the 35 mm dish to create a confluent monolayer. The dishes were incubated as per the requirements for specific culture conditions (Section 2.4.3) for approximately 6 h at 37°C, allowing cells to adhere and spread on the surface completely. The required number of cells for a confluent monolayer was adjusted appropriately by considering the particular

cell type and the working surface area of dishes (~ 1.2 X 10^6 cells/dish for all cell lines).

The cell monolayer was scraped in a straight line with a p200 pipette tip to create a ‘‘scratch’’. The debris was removed and the edge of the scratch was smoothened by washing the cells once with 1 ml of the growth medium and then replaced with 5 ml of medium specific for the in vitro scratch assay. Scratches of approximately similar size were created in the target cells and control cells to minimize any possible variation caused by the difference in the width of the scratches. To obtain the same field during the image acquisition, markings were created as reference points close to the scratch wound. The reference points were made by etching the dish lightly with a razor blade on the outer bottom of the dish. After the reference points were made, the dish was placed under a phase-contrast microscope. Care was taken to keep the reference mark outside the capture image field but within the eye-piece field. The image of the scratch was saved at specified intervals and the time was noted. The dishes were placed in a tissue culture incubator at 37 ◦C under defined culture conditions for a minimum of 8–10 h. The time lag for incubation in all the culture conditions was determined empirically for respective cell types. The dishes were removed carefully out of the incubator to be examined at regular intervals and then returned to resume incubation. A time frame of incubation was selected i.e. 12, 24 and 48 hours. The time points were chosen such that serum synchronisation and image acquisition were accommodated and also allowed us to work with cells under the fastest migrating condition to just achieve the complete closure of the scratch. After the incubation in specific culture condition, the dishes were imaged

by matching the reference point. By aligning the photographed region previously acquired the subsequent images were acquired. The distances between one margin of the scratch and the other were measured at certain intervals using ImageJ. The scaled images were compared from hour 0 to the last time point obtained. The distance between the two boundaries of cells on either side of the scratch was measured. The reduction in the distance at these two time points was taken as the time for closure of the scratch. The 30 readings of distances were measured in triplicate for each cell type and culture condition.

By comparing the images from time 0 to the last time point, scratch closure was assessed on the basis of the cell free space existing between the opposite scratched margins. This assay was performed primarily to assess the scratch closure phenomenon when the time duration for the 'scratch closure' was primarily recorded (quantitative assessment). The change in the time required for different cells cultured under altered microenvironmental conditions was recorded to assess the rate of migration.

2.6.2 PCF membrane assay

Millicell®- PCF (12 µm pore size) cell culture plate inserts were placed in a multiwell cell culture plate (Appendix 2X.2), thereby forming two compartments: the upper compartment of the insert and the lower compartment of the plate well. Both compartments form the migration chamber, separated by the porous polycarbonate (PCF) membrane. Cells seeded on the PCF membrane in serum-free medium may be induced to actively migrate through the PCF membrane into the lower compartment with medium containing serum or another chemoattractant.

Adherent cells remain attached to the under-side of the PCF membrane. This is followed by fluorescently labelling all cells with a pH-nanosensor. Subsequently the migratory cells detached from the underside of the PCF membrane. Finally, the migratory cells were quantified in a fluorescence microplate reader (Figure 2.1).

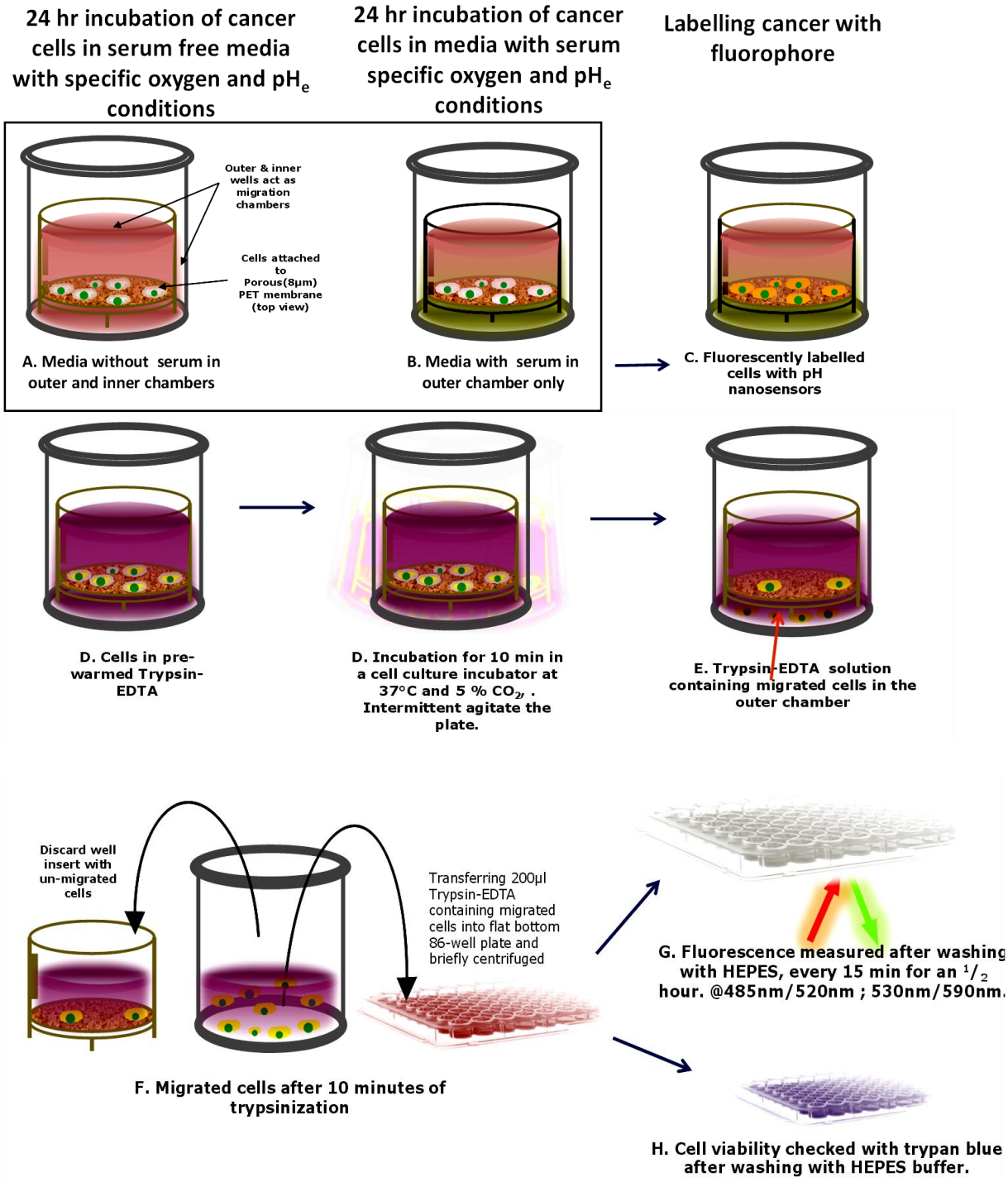

Figure2.1: Scheme of PCF membrane migration assay.
Diagrammatic illustration describing quantitative migration assay with adherent cells. The individual steps are schematically illustrated.

Cell cultures were prepared according to standard cell culture procedures (Section 2.3). They were starved overnight in serum-free medium with 0.2 % BSA before harvesting and then washing twice with PBS. Cells were resuspend in serum free culture medium with 0.2 % BSA and different concentrations of $NaHCO_3$ (to achieve desired pH relative to the PO_2/PCO_2) (Section 2.4) to an appropriate final cell concentration (e.g. $1X10^6$ cells/ml; MCF-7). The 24 well cell culture inserts were placed in the wells of a 24 well cell culture plate. The inserts with PCF membrane of 12 µm pore size were used to assess the migratory and invasive potential of the tumour cells. With the appropriate use of these microporous inserts, tumour cells were provided a three dimensional environment in which a degree of freedom would enable them to access medium from both the apical and basolateral sides.

Culture medium (600 µl) with different concentrations of $NaHCO_3$ (with or without FBS as a chemoattractant) was added to each well of the cell culture plate. Cell suspension (200 µl) was added to each cell culture insert. The cell culture plates were incubated for 24 hours in a cell culture incubator at 37°C and 5% CO_2. The cell culture medium from each well of the cell culture plate was removed and replaced with 450 µl serum-free culture medium with 100 µg/ml Nanosensor (pH Nanosensor Polyacrylamide Stock: 2 mg/ml) containing FITC and Oregon green in 1:1 ratio. In parallel wells were prepared for calibration of pH nanosensors as described in Section 2.8. This was followed by incubation for 45 min in a cell culture incubator at 37°C and 5% CO_2. The culture media from the tissue culture plate well inserts were removed. The cell culture inserts were carefully transferred into freshly prepared 24 well cell culture plate containing 500 µl pre-warmed trypsin-EDTA. Incubation for

10 min in a cell culture incubator was then performed as before, followed by agitating the plate from time to time. The cell culture inserts were then discarded and 200 µl of the trypsin/EDTA (0.05%) solution (now containing the migratory cells) was transferred from each well into a flat bottom black 96 well plate and briefly centrifuged. Cell viability was assessed with trypan blue after washing with HEPES buffer. The assay was concluded by reading fluorescence in a Fluroskan microplate reader every 15 min for an 1/2 hour at Excitation/emission wavelengths of 485 nm/520 nm; 530 nm/590 nm (Section 2.7.3). The pH_i of viable cells (verified by trypan blue assay (Section 2.5) was determined ratiometrically (Section 2.7.5).

2.7 Determination of pH_i in cells

Determination in intracellular pH (pH_i) was carried out with the use of cell permeable and intracellularly-activated pH-sensing dyes (Busa and Nuccitelli, 1984). These include 2',7'-Bis-(2-Carboxyethyl)-5-(and-6)-Carboxyfluorescein, Acetoxymethyl Ester (Bergman *et al.*, 1991; Ozkan and Mutharasan, 2002) and Carboxy seminaphthorhodafluor-1-acetoxymethyl ester (Appendix 2X.4), a long-wavelength fluorescent pH indicator from Molecular Probes (Busa and Nuccitelli, 1984). The pH-nanosensors (Appendix 2X.4) are another set of pH sensing ratiometric probes prepared by entrapping combinations of two pH-sensitive fluorophores (A. S. Des*ai et al*., 2013).

2.7.1 Experimental design and plans for live-cell observations over long-term sessions

To enable consistent results from such experiments, a handful of important aspects of imaging demand adequate validation of quality and precision. (Note: The

following salient points are also applicable when acquiring live cell imaging with fluorescent proteins (MitoTraker))

I. The cultured cells were labelled with precise concentrations of the synthetic fluorophore (cSNARF-AM/BCECF-AM/pH-nanosensors).

II. It was ensured that these values complied with the concentrations used during calibration (Section 2.8 and 2.10) in order to clearly visualize the target biological/biochemical components.

III. The cells were maintained in a condition that simulates experimental requirements while sustaining normal function. This enables avoiding potential risk of collecting false positive signals from debris that can interfere with interpretation of experimental results.

IV. Selection of the right objective (60X/40X, oil immersion), exposure and intensity setting and entering the right value in the software was integral in achieving accurate results as the machine doesn't transfer this information to the software. This ensured that the cells would be imaged with sufficient spatial and temporal resolution such that phototoxicity is not induced or uptake and visualization of the fluorescent probes is affected as described by (Frigault *et al.*, 2009).

Images obtained were loaded onto ImageJ (FIJI) interface for conversion of fluorescence signal intensities into quantitative ratios for relative fluorescence unit values (Section 2.7.5). The data was then analysed for ratiometric estimation of pH_i as described in Section 2.11.

2.7.2 The use of pH-sensing fluorescent dyes/probes with monolayer cells: Delivery of fluorescent dyes/probes within the cells

The, BCECF-AM, cSNARF-1 and polyacrylamide nanoparticles were assessed for adequate cellular uptake. The uptake assays of the positively charged nanosensors was most crucial but was tested for all dyes used for pH_i estimation.

Selection of cell seeding surfaces: The cells should be seeded onto specific surfaces (with precise thickness, flatness and clarity) that would render anchorage without refracting or distorting fluorescent light signals. The best images were obtained by using #1.5 glass bottomed dishes or #1.5 thickness round cover glass. Corning® 96/24 well clear flat bottom optics plates compatible with Fluoroskan Ascent™ Microplate Fluorometer (5210470, Thermo Scientific, Paisley, UK). Poly-D-lysine hydrobromide (Sigma-Aldrich, Dorset, UK) were used to adhere cells cultured under specific culture condition (Section 2.4.3) to attain 50–60 % confluence.

1. Uptake of fluorescent dyes/probes: Fluorescent dyes/probes were dissolved in DMSO (cSNARF-1 and BCECF-AM – 10 mM stock) or in PBS (pH-nanosensor – 2 mg/ml stock) at pH 7.4. The pH-nanosensors were sonicated for 10–20 minutes until a clear solution is obtained. The cells were rinsed twice with FBS-free media. Vehicle control with DMSO-buffer only assays were performed in parallel. A working stock of each fluorescent dyes/probes (10µM for BCECF-AM and cSNARF-1 and 100 µg/ml for pH-nanosensors) was prepared in physiological media solution buffered with HEPES. This solution of the dyes was used to replace the complete growth media. The cells are then incubated with the fluorescent dyes/probes at 37°C,

predetermined concentration of CO_2 (in different culture condition; (Section 2.4.3) (A. S. Des*ai et al*., 2013).

2. Reducing background signals: The background signals from the nanosensors outside the cells can be removed by replacing the nanosensor containing growth media and rinsing the cells by adding fresh phenol red free HEPES buffered growth media 3 times. Although, BCECF-AM and cSNARF-1, activated by intracellular esterases produce minimal background signals, unused dye from the media was removed by washing the cells with HEPES buffered media.

2.7.3 Image acquisition with Wide-Field microscopy

Cells imaged by wide-field microscope (Deltavision Olympus Inverted microscope). Special precaution should be taken to make sure that the instrument settings filter sets (ex/em details see Section 2.7), exposure and intensity ratios are consistent throughout the imaging processes including uptake and calibration to prevent saturation of signals.

According to specifications from the manufacturing group a single point was imaged repeatedly for 1.2 hours to rule out any issues related to fluctuations with the light source. To ensure the excitation source is responding as per specification the nanosensor particles should be recalibrated in case of recorded fluctuations.

To reduce phototoxicity of the live cells the intensity and exposure settings of the light source should be carefully selected. This can involve measuring the brightest spot of a set of images to detect any saturation of signals. This will help determining appropriate exposure time and intensity of excitation that would minimize signal to noise ratio (1:5) without saturating the image. This is to minimize photobleaching

from extended exposure to fluorescent light. In terms of using an adherent like poly-d-lysine (0.1 mg/ml for coating glass coverslips) it is important to ensure that the intensity of the background signals be minimized as much as possible by:

a: Ensuring uniform coating of the glass surface with poly-d-lysine to prevent trapping of nanosensor particles that resist their removal even on repeated washes.

b: Focussing the cells on a plane along the z-axis far above the plane of the poly-d-lysine coating. Nanosensors containing a combination of FITC-D and OG-D fluorophores internalised in polyacrylamide nanoparticles and preserved in a 1:1 ratio. This has been optimised to ensure that the effective dynamic range is maximised, to 2.01 pH units (A. S. Des*ai et al.*, 2013).

The instrument settings of the wide-field microscope or multiwell fluorometer was maintained throughout the readings taken with the 96 well plate. The filter sets were chosen in accordance with the specifications of the excitation and emission wavelengths. The background signals should be recorded to be deducted from the signals acquired from the images. The use of a plate reader enables simultaneous recording of multiple experiments although reduces quality of the signals acquired.

2.7.4 Data collection from Fluroskan microplate reader

In parallell, for similar experiments, cells for investigation were cultured in Corning® 96 well clear flat bottom optic plates in monolayer were maintained either in HEPES or $NaHCO_3$ buffered solutions. The solutions' pH was adjusted to normal or low and maintained at nornal or low atm PO_2 (Section 2.4). Fluoroskan Ascent™ Microplate Fluorometer (5210470, Thermo Scientific, Paisley, UK) was used to obtain fluorescence data from BCECF-AM or pH nanosensor dye loaded test cells. For

validation of methods, the dye calibration experiments in normal pH_e & PO_2 (Section 2.8) were simultaneously carried out with live cell imaging technique (Section 2.7) with all test cells.

To measure pH_i, the pH-nanosensors were used by exciting the entrapped dye combinations at a wavelength, ranging between 488 nm and 530 nm, while collecting the emitted fluorescence signals at two unique wave lengths, typically spanning between about 580 nm and 640 nm. BCECF-AM dye was excited at 490 and 440 nm and emission collected at 535 nm wavelengths. The background RFU values was deducted from those derived from wells containing the cells. The signals were analysed ratiometrically to determine the pH_i of the cells as described below (Section 2.7.5).

2.7.5 Ratiometric analysis of RFU signals from pH sensing dyes

2.7.5.1 Ratiometric analysis of images using wide field microscopy in live cell setup

Images acquired were loaded onto ImageJ (version 1.0, FIJI image processing package) interface. Once the images (in TIF format) were opened and split into two channels Image>Stack>Stack to images, a false colour was rendered to these images (eg. Image>Lookup Tables>Yellow). Also the contrast was adjusted uniformly if needed (e.g. Image>Adjust>Brightness/Contrast then 'Auto'-Run).

2.7.5.2 Deducting background from images

Depending on the image analysis software, the appropriate area of the image can be selected with a Region of Interest (ROI). As described this region should produce

minimum or no signals and outside a cell. The mean intensity of the area can be deducted from the total intensity signal of the image. As might be evident in the case of a microplate reader, the background value can be obtained from imaging cells not loaded with sensors.

2.7.2.3 Generating ratio image

The 'Ratio Plus' plugin >Ratio Plus is used to generate ratio images. The plugin determines the ratio of the signals from Image1 (protonated)/Image2 (unprotonated) form of dye. The image addresses were swapped over and background values were added. The new created image, looked rather flat. The contrast on this image was adjusted. Once the ratio image is generated the ROI around the masked region will produce mean intensity of the ratio image. Thus by supplementing the background data from the generated ratio image and analysing the unique images from both indicator channels, the mean intensity value was recorded.

2.7.5.4 Weighted measurements for pH-nanosensor only

Based on the concentration of pH-nanosensor in each pixel, a weighted value was assigned. Such a weight associated with a discreet measurement registered in each pixel indicates the intensity in the reference channel of the pH-nanosensors.

Note: The mean intensity of the ratio images from Wide-field 'Live cell' imaging setup and the background corrected RFU values obtained from experiments conducted using the **Fluoroskan microplate reader** (Section 2.7.4) was used to determine the pH_i of the cell using the equation:

$$Y = pK_a + \frac{\text{Top-Bottom}}{1+10^{(pK_a - \chi) \times \text{Hillslope}}}$$

Where:

Y = indicator to reference ratio.
χ = pH_i of the cell.
Bottom = Minimum detectable response of pH sensing dye/probe from calibration experiments (lower asymptote)
Top = Maximum detectable response of pH sensing dye/probe from calibration experiments (upper asymptote)
pK_a = Point at half maximum response
Hillslope = Steepness of the curve

The equation used to generate the calibration curve can be rearranged to represent pH_i as a function of intensity.

$$pH_i = pK_a - \log_{10} \frac{\text{Top-Bottom} / \text{Y-Bottom}}{\text{Hillslope}}$$

This equation is used to estimate the pH_i from the images from nanosensor uptake experiments.

2.8. *In vitro* calibration and optimisation of fluorescent dyes/probe

2.8.1 *In situ* calibration of pH nanosensors, BCECF-AM and cSNARF-1-AM

The efficiency of these pH sensing dyes/probe being subjective to parameters like cell volume, cell membrane was determined by calibrating the dye for the different cell types with the help of nigericin an antibiotic derived from *S. hygroscopicus* that acts as a K^+ ionophore promoting K^+/H^+ exchange across cell membranes (see Appendix 4I and 4II). Nigericin was solubilised as a 10mM stock solution in ethanol. In situ calibration was carried out on BCECF-AM and cSNARF-AM and pH-nanosensor loaded cells administered at 10 µM, 10 µM and 100 µg/ml respectively

in serum free phenol red free medium. The dye loaded cells were washed briefly with high K^+ media/buffer (145 mM KCl, 5 mM NaCl, 1 mM $MgCl_2$, 1 mM $CaCl_2$, 5.5 mM D-glucose, 7 mM HEPES (± 25 mM $NaHCO_3$), 0.1 mM KH_2PO_4, 0.4 mM $KHPO_4$) adjusted to pH 7.4. The stock of high K^+ buffer was split into 12 aliquots of equal volumes adjusted to 12 pH points over the range 4.5 to 8.5.

For each of the 12 aliquots, the pH was adjusted by adding 0.1 M HCl and/or 0.1 M KOH as necessary. The shift in pH was in the range of 0.25 to 0.40 within three days owing to the complexity of the constituents. This was unacceptable when the target resolution window was very narrow. This issue was addressed through a multipronged approach. First, the pH of the aliquots was only adjusted at 37°C as this stabilised the pH over the duration of the experiments.

For the experiments with long time points, pH stability was ensured by controlling the environment of the solution. The buffer HEPES, which is capable of buffering in the pH range 6.8 – 8.2, would ideally maintain the pH_e within the range largely covered by pH sensing dyes/probe. Second, intermittent measurement of pH of the dispensed and aspirated solutions throughout the optical measurement would help monitor a drift in the pH reading. Furthermore, the experiments were performed in a temperature and gas controlled enclosed environment that was pre-set to mimic physiological conditions. The solutions were pre-warmed and delivered in gas impermeable tubes to prevent any shift in composition and pH during administration. A reasonably large volume of each aliquot enabled greater pH stability.

The cells were then imaged during equilibration in the high K^+ buffer of a specific pH for 5-10 min before replacing it with the buffer of a different pH until all 12 pH points are covered. The RFU ratios of the fluorescence signals from the acquired images was plotted against corresponding known pH_e of the high K^+ buffers. This correlation represents the change in the protonated/unprotonated fraction of the corresponding pH-sensing dye/probe relative to the pH_i equilibration with the buffer pHe. Using a sigmoid curve fitting function (Graphpad PRISM, ver. 6.0) the calibration curve was generated for pH sensing fluorescent dye/probes. Calibration of the pH-nanosensor probe used for evaluation of pH_i, was performed before each experiment on all the cancer cells.

2.9. Construction of calibration curve

This involves using a high K^+ HEPES buffered solution with pre-adjusted pH over a range of 4.5 to 8 to acquire the relative change in the pH_i of the cell. The above steps can be used to measure signal intensities pertaining to these pH_e points. The mean ratios can be used to construct a calibration curve by fitting a sigmoidal curve to the calibration points. In order to cross validate the pHi determination data from 'Live-cell microscopy as well as in 'Fluoroskan microplate-reader format, the in-situ calibration of all three pH-sensing dye was carried out in both experimental setups. Moreover, in-situ calibration of each pH sensing dye was performed before every experiment whether in 'Live-cell microscopy' or 'Fluoroskan microplate-reader format.

Thus the calibration of the pH-nanosensors probe and dyes was performed before each experiment on SK-OV-3 cells MCF-7 and MCF-10A cells. The mean pK_a values

were 5.5 - 5.7 for pH-nanosensor probe (n = 12), 7 - 7.2 (n = 8) for cSNARF-AM dyes (n = 15) and 6.5 – 6.8 BCECF-AM derived from the curve fit to non-linear regression for each pH sensing probe/dye (Figure 2.2 A, B & C) and are consistent with published data.

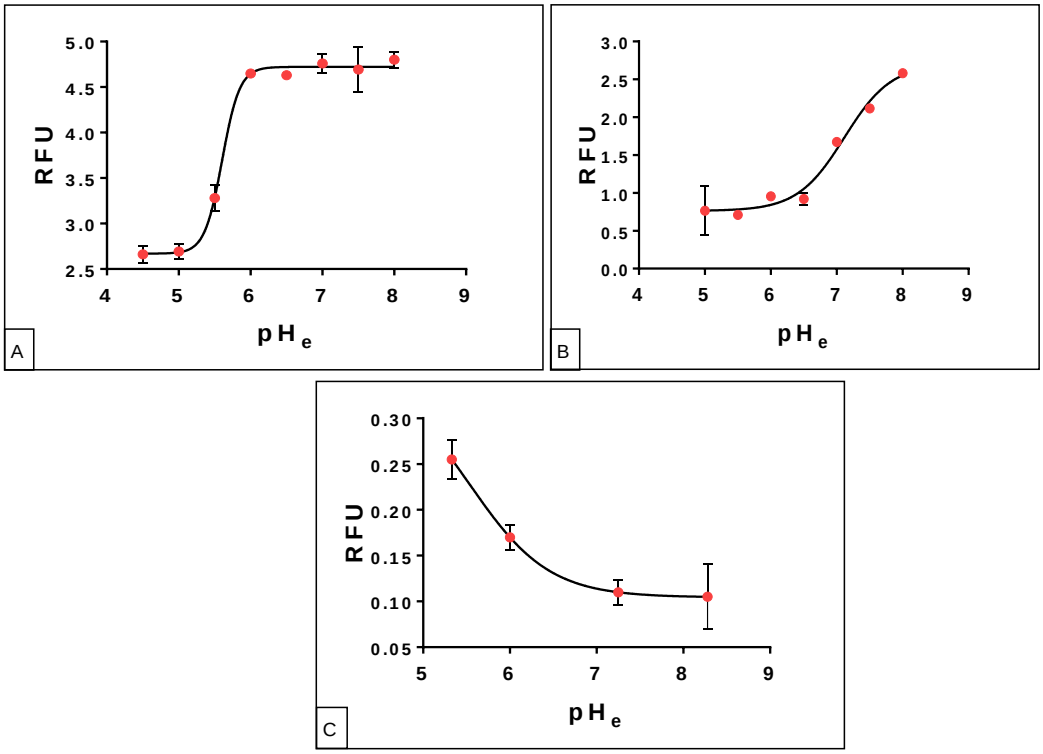

Figure 2.2: Calibration of pH sensor dyes/probes
Calibration curve for pH sensors loaded in SK-OV-3 cells. [A] pH-nanosensor (pKa = 5.5-5.7); n = 12 [B] cSNARF-AM (pKa = 7-7.20); n = 15, and [C] BCECF-AM (pKa = 6.5 – 6.8); The pH-nanosensor curve is steeper in the exponential phase compared with shallower curves for cSNARF and BCECF-AM. n = 8.

2.10. Optimisation of Mito Tracker dye

Optimisation of mitochondrial membrane potential sensitive fluorescence dye: The optimisation of MitoTracker dye (Appendix 2X.4) was performed on SK-OV-3 cells. SK-OV-3 cells were mintained in normal pH_e and PO_2 at 37°C. Following etoposide administration, intrinsic apoptosis pathway was initiated in SK-OV-3 cells indicated by the loss of signals from Mitotracker dye due to drop in mitochondrial membrane

potential within 20 minutes (Figure 2.3). Completion of apoptosis was identified through the activation of caspase 3 (Porter and Janicke, 1999) in SK-OV-3 cells.

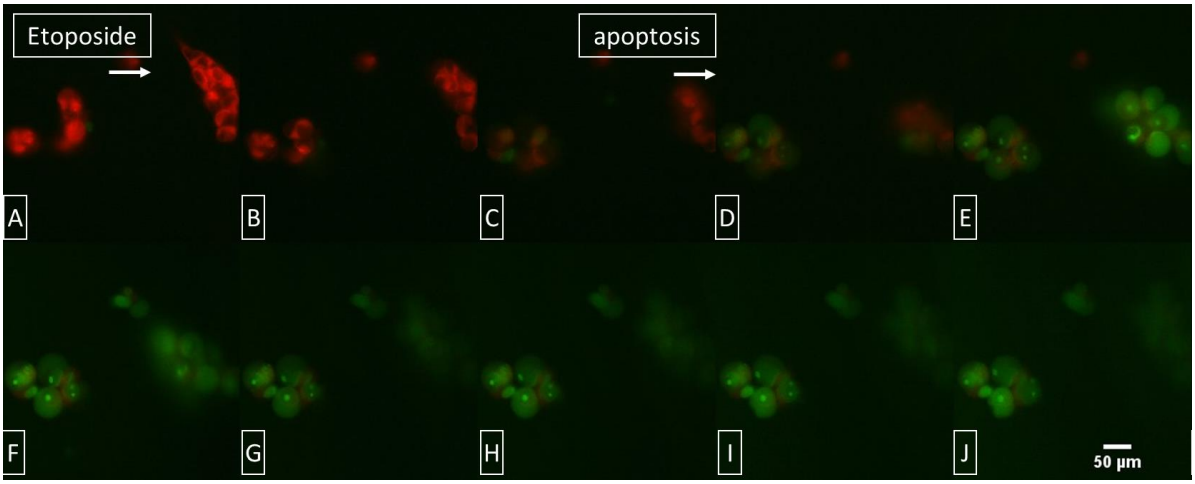

Figure 2.3. Etoposide induced apoptosis of cancer cells: Etoposide loaded cells undergo apoptitic changes in SK-OV-3 resulting in loss of mitochondrial membrane potential signals (Mitotracker Deep Red). Increase in Caspase 3 signals indicate completion of apoptosis.

The change in MitoTracker dye signals representing the fall in mitochondrial membrane potential following etoposide induced apoptosis (Ly, Grubb and Lawen, 2003) was plotted against time (Figure 2.4).

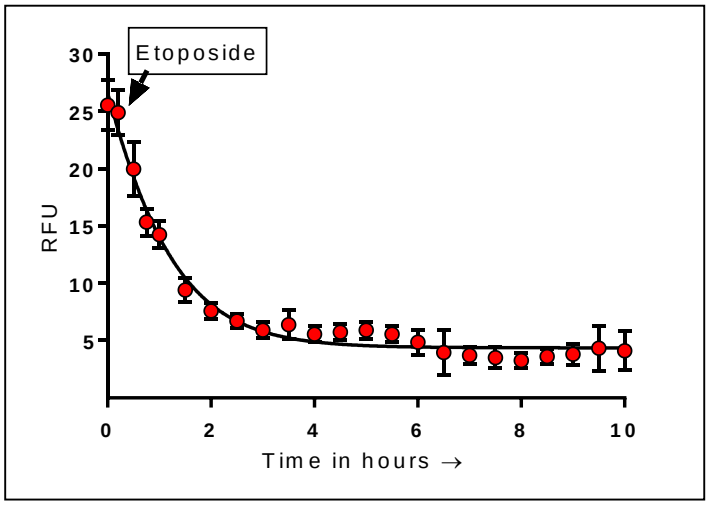

Figure 2.4. Depletion in Mito Tracker Deep Red dye signal intensity following apoptosis of cancer cells.
The signal intensity (rpresented as Reative Fluorescence Unit (RFU)/ time) of Mitotracker Deep-Red dye is shown to decrese in apoptotic SK-OV-3 cells following the administration of 50 µM etoposide.

2.11 Data Analysis

2.11.1 Intracellular acidification by 'Ammonium Pre-pulse manoeuvre'

Cells in monolayer were superfused with solutions buffered by $NaHCO_3$ or HEPES. The extracellular solutions contained *5 mM KCl, 135 mM NaCl, 5.5 mM glucose, 0.1mM NaH_2PO_4, 0.4mM $NaHPO_4$, 1 mM $CaCl_2$, 1 mM $MgCl_2$*. HEPES-buffered solutions contained 1–20 mM HEPES, and the pH of the solutions was adjusted with 5M NaOH. The $NaHCO_3$ buffered solutions were maintained in an atmosphere of 5% CO_2/air or 20% CO_2/3% O_2 and contained a concentration of $NaHCO_3$ that yielded the desired pH, in accordance with the Henderson-Hasselbalch equation. For all solutions, NaCl was added to produce a total osmolarity of 250–300 mosM/L.

Cytoplasmic acidification: The design of this assay was meant to elicit the cellular response from:

i. cSNARF pH sensing dye under normal PO_2 and when in normal and low pH_e (SK-OV-3 and MCF-10A cells) in live cell setup.
ii. pH-nanosensors when normal and low PO_2 (microplate fluorometer) and normal and low pH_e (measured in microplate fluorometer) was applied (for MCF-7).

The intracellular acidification was established using a prepulse of NH_4Cl in either HEPES-buffered or $NaHCO_3$-buffered solutions. The pH-sensing dye/probe loaded cells were first stabilised in $NaHCO_3$-buffered or HEPES-buffered solution in normal/low pH_e & normal/ low PO_2 for a minimum of 5 minutes. Next the buffered solutions were replaced with that containing 20 mM NH_4Cl (by equimolar replacement of NaCl) for 3 minutes. This ammonium pulse would force the cells to

initially undergo a slow alkalinisation followed by a gradual acidification. The washout of the extracellular ammonium (replaced by fresh HEPES/$NaHCO_3$ buffered medium (referred here as the pH_i recovery solution)), was performed to further challenge the cells' pH buffering potential to dump the intracellularly accumulated NH_4^+, forcing rapid acidification. The NH_4Cl was washed out with either HEPES/$NaHCO_3$ buffered extracellular solution under desired pH_e/PO_2 to aid in acid dumping and recovery of pHi to steady state levels.

2.11.1.1 Intrinsic buffering capacity (β_I) of test cells:

Assessing pH_i at the steady state of pH equilibration before the ammonium pre-pulse manoeuvre in HEPES buffered extracellular solution was a perquisite to calculate the β_I in SK-OV-3, MCF-7 and MCF-10A (normal control). The mean, intensity of the pH sensing dye was recorded along with relevant metadata that will be used to estimate the mean steady-state pH_i of test cells cells.

Thus, β_I, is the buffering power of all buffers other than those dependent on $NaHCO_3$. β_I is represented as:

$$\beta_I = \Delta B / \Delta pH = -\Delta A / \Delta pH$$

Where ΔB is the amount (in mM) of strong base added to the solution, ΔA is the amount of strong acid, and ΔpH is the resultant change in pH.

These values were used to calculate the concentration of NH_4^+ at a point when the cell has loaded itself with excessive protons before recovery of pH_i commences on The approach of studying acid-extruding mechanisms is to acutely load the cell with acid. These values denote the change in acid flux over a change in

external pH change. Hence intrinsic buffering capacity of the cell in altered pH_e/PO_2 was calculated.

2.11.1.2 Rate of pH_i recovery

The NH_4Cl washout with HEPES/$NaHCO_3$-bufffered solution at the end of the ammonium pre-pulse monoevure was used to asses the steady state pH_i and recovery of pH_i following acute acid loading (Section 2.11.1). This approach was used in studying the recovery of pH_i toward its initial level. It is this pH_i recovery (i.e., alkalinisation) that is produced by one or more acid-extruding mechanisms. This is determined as the slope of the change in pH_i following washout of NH_4Cl in an ammonium prepulse experiment (Roos and Boron, 1981; Boyarsky *et al.*, 1988b). The pH_i recovery rate in altered pH_e/PO_2 (secion 2.04a) was calculated for individual experiments

2.11.1.3 Net acid extrusion (NAE)

The Net efflux of acid (i.e., acid-extrusion rate) is the product of the total intracellular buffering power (β) and the rate of pH_i recovery (dpH_i/dt), denoted by the slope of the pH recovery (under any given set of condition; Section 2.4.3). Rate of recovery is measured as a function of the change in the pH_i of a cell to attain a steady state pH_i. The NAE can be calculated to evaluate the contribution of a growth influencing factor or its interaction with one or a set of pH regulating mechanism in cancer cells.

The component of the net acid extrusion can be evaluated by taking into consideration the role of sodium bicarbonate mediated buffering. This method was

adopted to sequentially reveal the dependence of the cancer cell survival on a change in pH_e subsequent to change in oxygen availability.

The product of total buffering capacity (β = intrinsic buffering capacity (β_I) + extrinsic buffering capacity (β_{HCO_3})) and the slope of pH_i recovery (dpH/dt) measured separately by gradual ammonium removal in the presence and absence of potassium in HEPES buffered extracellular media in altered pH_e/PO_2 (Section 2.4.3).

2.11.1.4 Mapping the distribution of pH_i of cancer cells

In order to match the distribution of hydrogen ions within intracellular regions FIJI's image processing package was used. Once the cells have been imaged using the Widefield DV microscope the images are opened as a composite stack image. The composite colour mode and auto-scaling were selected. At this point splitting the individual channels was avoided.

To convert the opened image to RGB format the 'Stack to RGB' option was selected from the 'Image' tab on the FIJI main window. Once the composite image is converted into a RGB image the 'Threshold Color' window was opened through the 'Adjust' drop-down menu from the 'Image ' tab.

The 'Threshold Colour' window depicts the existing status of the image hue, saturation of signals and the level of brightness. At this point the dark background option was selected to ensure that the background of the image does not interfere with the measurements.

The image brightness was adjusted to select the total region of interest. This converted the selected area into a brick red colour concealing the underlying

details. The selected region was demarcated by the 'Select' button on the 'Threshold Color' window.

This generated a ROI around the selected cells. The saturation and hue levels were sequentially adjusted to specify the ROI to determine the pH_i (Section 2.7.5). The ratio image obtained was overlaid with the ROI created on the RGB image. This helps separate the original RGB image from the overlying ROI into two different slices within one frame. The mean intensity value from within the region of the cells is recorded and converted into pH_i.

To restore the ROI only a slice was added to the RGB image. In order to obtain ROIs that should denote specific/localised pH_i, variable areas of the saturation and hue was manipulated. The RGB image was removed through the 'Stack' option to restore only the ROI overlay with a black background.

Once the ROIs are separated from the parent RGB image they were saved as Tiff files with a specific colour weighted to the corresponding pH_i value derived through ratiometric measurements. These colour labels were used as reference points to denote the distribution of pH intracellularly within a cancer cell. The individual ROI slices were superimposed (dark background removed) to reconstruct the image denoting the different pH_i zones associated with the treatment and culture condition (as described in Section 2.4.3) of the cancer cells.

2.11.2 Visualizing mitochondrial distribution in cancer cells cultured in altered pH_e

To identify regions within the cell that showed interesting distribution of protons defining pH changes, organelle tracking was sought necessary. Mitochondria

labelling was considered as they represent the metabolic activity of the viable cell following optimisation in SK-OV-3 cells (Section 2.10). The effort was to visualise the mitochondria in a cell that underwent active pH_i changes influenced by the altered microenvironment.

The MitoTracker® Deep Red, JC10 and MitoTracker® Red CMXRos (Appendix 2X.4) were screened for use in cells preloaded with cSNARF-AM dye or pH-nanosensor probes. Owing to the wide fluorescence image acquisition wavelength the MitoTracker® Deep Red excitation and was selected to be used with cSNARF and pH-nanosensor loaded cells. The cells loaded with this dye.

Preparing Stock Solutions: Thawed (at RT) lyophilized MitoTracker® product was dissolved in high-quality, anhydrous dimethylsulfoxide (DMSO) to a final concentration of 1 mM. The solution aliquots of the MitoTracker® Deep Red was frozen at ≤ –20°C and protected from light.

Preparing staining solutions: 1 mM MitoTracker® stock solution was diluted to the final working concentration in normal HEPES buffered solution (Section 2.11.1). As working solution final concentrations of 25–500 nM was used

Staining adherent cells. Test cells on 35mm glass bottom petri dishes were filled with serum free modified culture medium in altered pH_e/PO_2. The cancer cell or non-neoplastic cells were loaded with the respective pH sensing probes as described in Section 2.7. The media was then replaced with pre-warmed (37°C) staining solution containing MitoTracker® Deep Red. Incubation time of 15–45 minutes under growth conditions was optimized. Passive diffusion of the MitoTraker® Deep Red was achieved following a standard incubation of the cells

loaded with respective pH-sensor probe/dye maintained in altered pH_e. This provided enough equilibration time for the MitoTracker dye to accumulate in active mitochondria. After staining is complete the staining solution was replaced with fresh pre-warmed HEPES buffer (Section 2.11.1).

The dye loaded cells were imaged with an exposure time of 0.100000 secs with CY-5 (covering the excitation and emission profile of 644/665 nm) as both excitation and emission filters redirected through Quad polychroic mirrors. The images were processed using FIJI software.

2.11.3 Functional association between potassium and pH_i regulation in cancer cells

2.11.3.1 Estimation of intracellular K^+ $[K^+]_i$ in test cell lines

Inter-relationship between pH_i and $[K^+]_i$ in nigericin-treated SK-OV-3 and MCF-7 cells:

The cells were washed in modified HEPES buffered solutions with varying K^+ concentrations. Test cells after being loaded with cSNARF-AM (Section 2.7.2) were washed with normal HEPES buffered extracellular solution (Section 2.11.1) followed by suspension in high K^+ buffers. These solutions were maintained at 37°C. Two stock solutions containing 120 mM KCl and 30 mM KCL respectively were prepared. 120 mM KCL containing solution comprised *120 mM KCl, 15 mM NaCl, 10 mM NMDG, 5.5 mM glucose, 0.1mM NaH_2PO_4, 0.4mM $NaHPO_4$, 1 mM $CaCl_2$, 1 mM $MgCl_2$ and 10 mM HEPES.* In 30 mM KCL containing solution 90mM NMDG was introduced to the above solution for maintaining osmolarity. Each of the

aforementioned two solutions were split into 8 - 12 aliquots of equal volumes adjusted to 8 pH points ranging from 6 to 8.

The SK-OV-3 and MCF-7 cells maintained in normal pH_e/PO_2 were loaded with cSNARF-AM pH_i sensing dye (Section 2.7.2). The dye was calibrated before each experiment using nigericin (Section 2.8). The monolayer of cells was washed with HEPES buffered normal extracellular solution (Section 2.11.1) and then loaded with 3 µM nigericin. The cells were again rinsed with normal extracellular solution and then perfused with 8 - 12 different pH adjusted aliquots of pre-warmed high K^+ buffer solution and fluroscence intensities of cSNARF-AM dye was recorded (Section 2.7.2) for each pH_e using Wide-field fluorescence microscopy with the live cell setup. At the end of the experiment the process was repeated with the all the pH adjusted aliquots of 30mM K^+ solution.

The ionophore sets were $[H^+]_i/[H^+]_e = [K^+]_i/[K^+]_e$ (see derivation in Appendix 2IX); thus, in the case of $[K^+]_i = [K^+]_e$, the intracellular H^+ concentration is clamped to that of the buffer. A shift in the curve plotting pH_i vs pH_e from ratiometric measurements of fluorescence intensities was used to validate the interrelationship between pH_i and extracellular pH_e and $[K^+]_i$ (Chakrabarti, Ekuta and Onaivi, 1998; Chaperon and Thiébot, 1999). The evaluation of the pH_i values from ratio (Section 2.7.5) data facilitate to rescale the ordinate according to pH_i. Hence the calibration curve (Section 2.8) was used to determine the pH_i (Section 2.7.5) (Chakrabarti, Ekuta and Onaivi, 1998; Chaperon and Thiébot, 1999).

2.11.1.2 Potassium dependence on steady state pH_i of cancer cells

The time course of change in pH_i of SK-OV-3, MCF-10-A and MCF-7 cells (to achieve steady state pH_i recovery) in increasing $[K^+]_e$, following acute acid loading from a pulse of 20mM NH_4Cl (by equimolar substitution of extracellular NaCl) (Section 2.11.1) was recorded. HEPES buffered solution (Section 2.11.1) was modified to contain variable $[K^+]_e$ (0, 1, 2, 3, 4 and 5 Mm $[K^+]_e$) and used for pH_i recovery. Caesium was used to substitute $[K^+]_e$ deficit, to preserve the molarity of these solutions. All experimental solutions were maintained at normal PO_2 and adjusted either to normal pH_e or low pH_e. In each individual experiment, following acute acid loading, the time course and mean pH_i recovery (from the intracellular acidification produced by NH_4^+ washout), in different $[K^+]_e$ (0 - 5 mM) was recorded.

pH_i recovery from ammonium pre-pulse was ploted in nonlinear least-squares curve fit to a form of Michaelis-Menten equation. Michaelis-Menten constant K_m (mM), predicts the $[K^+]_e$ needed to achieve a half-maximum pH_i recovery (from intracellular acidification after ammonium prepulse). The data was generated as a response of test cells to normal/low pH_e and normal PO_2 (Section 2.4.3).

2.11.3.3 Pharmacological modulation of acid extrusion:

Intracellular acidification of test cells was established in HEPES-buffered extracellular solutions using the ammonium manoeuvre as described in Section 2.11.1. To evaluate the role of the acid sensitive K^+ channel (TASK-3) in pH_i regulation, the SK-OV-3 (using Wide-field microscopy with live cell setup) and MCF-7 (using Fluoroskan microplate format) cells were recovered from ammonium pre-pulse in HEPES-buffered extracellular solution loaded with methanandamide (3

μM). The resulting intracellular alkalinisation was measured. The data obtained from ammonium prepulse experiments on test cells in standard HEPES-buffered solution in altered pH_e/ PO_2 Section 2.4.3) were taken as no-drug controls. Similar experiments were conducted on MCF-10A cells in normal pHe & PO2 and were considered as non-neoplastic control cells. The results of experiments were used to calculate the NAE (Section 2.11.1.3) after TASK-3 inhibition by multiplying the the total buffering capacity (β) (Section 2.11.1.1) by rate of pH_i recovery (Section 2.11.1.2) from ammonium pre-pulse observed in the presence of methanandamide.

2.12 Identification of channels protein expression

2.12.1 Immunofluorescence experiments

Immunofluorescence was performed to assess the cellular location of TASK-3 and TALK-2 K^+ channels in SK-OV-3 and MCF-7 cells. After culturing the cells for 72 hours in altered pH_e and PO_2 conditions Section 2.4.3) they were seeded on sterile glass cover slips (13 mm) placed in 24 well tissue culture plates. The cell seeding density was maintained at approximately 50 x 10^3 cells in each well for both cell lines. The cells were allowed to grow to 60-80% confluence before fixing them with Paraformaldehyde (PFA) (Appendix 2X.5).

Cell fixation: Following aspiration of media from wells and washing twice with 1 ml of PBS, cells (at 60-80% confluence) were fixed at room temperature with 2-4% PFA for 5 min with gentle shaking. The fixed cells were then incubated with Igepal (0.5% in PBS; 5 minutes: room temperature) with shaking and then with BSA/Glycine (3%/1%in PBS; 15 minutes; room temperature) before blocking with goat serum (20% in PBS; 30minutes: room temperature) in preparation for immunostaining

(Appendix 2X.5). Solutions were aspirated, and cells were washed three times with PBS between all these steps.

Immunostaining:

Next the primary antibody (Section 2.12) at predetermined concentrations TASK-3 (1:50) and TALK-2 (1:500) and Cytokeratin (positive control 1:250) in blocking solution (20% goat serum in PBS) was added according to the experimental plan which also included negative controls to which blocking solution alone was added. All were incubated with shaking (18 hours; 4°C) (Appendix 2X.5). Subsequently the primary antibody was removed by aspiration and washed thoroughly three times with PBS and shaking (5 minutes; room temperature) after which appropriate dilutions of FITC-conjugated secondary antibody (anti-mouse-FITC and anti-rabbit_FITC in 1:500 concentrations respectively) were applied to all wells and incubated in the dark (30minutes; at RT).

From this point onwards the plate was wrapped in foil to protect from light. After the incubation the secondary antibody was aspirated and the wells were again washed with 1ml PBL for 5 minutes with shaking in foil. Finally, PBS (1ml) was added to visualize under microscope. To enable accurate localisation of these proteins nuclei were often counter stained with (4',6-diamidino-2-phenylindole) DAPI stain (Appendix 2X.5).

2.12.2 Confocal imaging of pH sensitive TASK-3 and TALK-2 protein in cancer cells

To understand the cellular localisation and trafficking of extracellular acid sensitive potassium channels (TASK-3 and TALK-2), SK-OV-3 and MCF-7 cell images were

captured with confocal microscopy. This technique involved imaging cells with fluorescently labelled membrane bound or cytosolic proteins when scanned along the Z-axis of the imaging acquisition plane. The two cell lines were initially cultured in pH regulated culture models where PO_2 and pH_e was altered. The cells were fixed with 2% Paraformaldehyde (PFA) following cell fixation protocol (Section 2.12.1).

The fixed cells were incubated with TASK-3, TALK-2 antibodies with (Fluorescein isothiocyanate) FITC stain. Thes nuclei were counter stained with (4',6-diamidino-2-phenylindole) DAPI stain. ProLong® anti-fade mountants was used with the pre-stained cells to suppress photobleaching and preserve the signals of fluorescently labelled target molecules for long-term storage and analysis. The coverslips were placed upside down on glass slides and edges sealed with nail varnish to preserve moisture and distance between the coverslip and the slide surface.

The images were acquired with the Leica TCS SP2 confocal laser aided microscope at the Advanced Microscopy Unit in Queens Medical Centre, University of Nottingham. Special care was taken to acquire the clear images by adjusting the optimum number of imaging sections and averaging between sections for each cell type. Pinhole aperture was kept at 1.0 to prevent the capture of scattered light.

The prepared slides were placed inverted on the microscope stage. For oil/multi-immersion (IMM) objectives only a single drop of the oil or the IMM was applied on the objectives. The laser channels were selected from the range of channels available depending on the fluorophore used in the sample. The respective signal was selected as spectral graph display. The intensity of the laser for FITC is selected

at 25% to prevent quenching of the signals from the sample when imaging is under progress.

2.12.3 Signal collection: Z POSITIONING and continuous image acquisition

2.12.3.1 Z positioning and image acquisition in stacks

To acquire images along the Z axis the software provides a point of reference as a three dimensional a box representing the object to being imaged. The series button on the acquire window was brought up a three-dimensional box with a yellow line along the equator of the box. This yellow line represented current plane of focus. Now, with the Z-POS knob on the manual interface the top or the bottom of the image is reached. At these points the intensity of the image was adjusted. These settings are saved. The number of sections to be acquired was simultaneously selected. Depending on the excitation and emission wavelength the software selects the number of sections to be taken for each of the channels. Averaging of the background noise was then set (ie 1 for clear and bright images and 3 for low intensity images).

Once the z stacks details were set, the samples were ready to be imaged by selecting 'CONTINUOUS' in the AQUIRE panel. If the image was too bright QLUT was selected. The image becomes filled with green pixels with blue patches showing areas of high brightness. This was adjusted by selecting the image and rotating the photo multiplier tube (PMT1) knob to reduce the 'GAIN' or the intensity till the blue regions were removed and often replaced by bronze coloured patches. The green pixels can be also adjusted by rotating the PMT2 knob which controls the contrast of the image.

Once these details were fed to the software the AQUIRE button was selected to start acquisition. The image slices were digitally aligned and processed with imageJ software to reconstruct the 3d image of the cell with fluorescently labelled target proteins.

2.13 Expression of genes coding for pH sensitive K^+ channels in cancer

2.13.1 Extraction and quantification of total RNA

RNA extraction from monolayer: Monolayer of cells cultured in specific culture models (Section 2.4.3) was washed with HBSS (5ml) and scraped into 950 µl Tri® reagent per 10 cm^2 of wells of 6 well plates. The cell-Tri® reagent mixture was stored at 80˚C for long-term usage or until required for RNA extraction (Appendix 2X.6). On retrieval from the freezer the mixture was incubated for 5 minutes at room temperature and 0.2ml of Chloroform was added per 1ml of cell-Tri® reagent mixture.

The mixture was shaken for 15s and again incubated at room temp for 3 minutes before spinning at 12,000 g for 15 minutes at 4°C. The aqueous phase was carefully removed and then transferred into a fresh tube before adding 100µl of isopropanol (Appendix 2X.6). The mixture was incubated at room temp for 10 minutes and spun at 12,000 g for 10 minutes at 4°C.

The supernatant was carefully removed and 100 µl 75% Ethyl alcohol was added and spun at 7,500 g for 5 minutes at 4°C. Once again carefully the supernatant was removed and the pellet was air dried for 5 minutes. This was re-suspended in 100µl of RNAse free water and the concentration and purity (260/280) was measured on the NANODROP equipment to check the quality before storing at -80°C.

2.13.2 Assessing the integrity of the extracted RNA

Preparation of the Agarose gel: Agarose (1g) was dissolved in 100ml of Tris/Borate EDTA buffer and placed in a microwave for 2 minutes on high power. The flask was removed from the microwave and contents were mixed thoroughly by swirling. 10mM ethidium bromide (1 µl) was added to the cooled 1% agarose solution and swirled to mix. A 10-well comb (1.5 mm) was placed into the gel casting tray of the horizontal electrophoresis system. About 80 ml of the agarose solution was poured into the tray cover the top of the wells, which was left to set at room temperature. The tray with the gel was placed into an electrophoresis tank until ready for use.

2.13.3 Sample preparation

Preparation of RNA samples was done by mixing 1µl of total RNA (diluted 10 1/5th concentration) with 2 µl of staining dye and 9 µl of nuclease-free water to attain a total volume of 12 µl. After removing the comb from the solidified gel, 12 µl of the 1kb plus DNA ladder (1kb ladder) was loaded on to the first well by submerging the tip of the pipette into the top of the well and slowly dispensing content. Application of other samples into the subsequent wells was done by the same way as above. The electrophoresis tank electrodes were engaged and the gels were run at 100V for 1.5 hour which helped the samples migrate towards the positive electrode.

On completion the RNA was visualised and checked for integrity under the UV light. This can be appreciated by visualising two intact bands and the ratio of 2:1 representing the mammalian 28S/18S ribosomal RNA.

2.13.4 Synthesis of cDNA by Reverse Transcription PCR

Reverse Transcription PCR: The RT PCR reaction was carried out in 20 µl final volume. This contained 10 µl of RNA at 120 ng/µl concentration i.e each RT was done using 1200 ng total RNA (total RNA). RNA was denaturation (at 70°C for 10 minutes with the random primers) to resolve any secondary structure that the RNA might have in solution. The denatured RNA was added to each +RT and -RT well/tube. The cDNA obtained was used for real time PCR. In each tube for each sample 10XRT Buffer 2.0 µl, dNTP mix 0.8 µl, Random Primers 2.0 µl, RNAse inhibitor 1.0 µl, Nuclease free water 3.2 µl, Reverse Transcriptase 1.0 µl and denatured RNA-random primer mix (15.2 µl) were added for the reverse transcription reaction (Appendix 2X.6). Each RT reaction was done in duplicate, one containing the RT enzyme (+RT) and one where reverse transcriptase enzyme was substituted with water (-RT). This was to control for any genomic contamination in RNA samples as well as other reaction components. The reaction temperature conditions on PCR machine were as follows: Initially 10 minutes at 25°C followed by 37°C for the next two hours. Finally, the temperature was set to 85°C for the last 5 min followed by incubation at 4°C. The cDNA was used for quantitative PCR and relative gene expression of genes coding for pH regulators in cancer.

2.13.5 Quantitative (real-time) Polymerase Chain Reaction

To evaluate the gene expression of *KCNK9*, *KCNK17*, *KCNH1* and *KCNH2* pH regulatory proteins in the SK-OV-3, MCF-7, OE-19 cells cultured in altered pH_e/PO_2 (Section 2.4.3), qPCR technique was recruited (Appendix 2X.6). The technique

involves the identification of three most stably expressed reference genes. Subsequently the level of expression of the gene of interest could be evaluated by measuring against the expression levels of the reference genes.

Determination of reference genes: Quantitative PCR assay was employed to assess the stability of *GAPDH*, *HPRT*, *ACTB*, *B2M* and *YWHAZ* genes (Appendix 2X.6) in all cell lines cultured in media with altered pH_e and PO_2 conditions as described in Section 2.4.3.

Each q PCR reaction is carried out in 20 µl final volume. All reactions were done in triplicates. PCR was done on both +RT and -RT cDNA samples plus a no template control (NTC) in which template (cDNA) was replaced with distilled water. To each wells/tubes 18 µl of master mix and 2 µl of template containing the TaqMan® assay 20X (Appendix 2X.6), for all the genes of interest were added. The plates were covered with optically clear covering slips/lids and briefly centrifuged. The PCR plate/tubes containing the samples were loaded onto the PCR machine and set on the right protocol. The plate layout was used to indicate the location of the samples and NTC and other labels for the plates. The reaction conditions used were optimised for 20µl of the reaction volume.

Step1: Hold at 95°C for 10 minutes.

Step 2: {95◦C for 15 seconds, 60◦C or 1minute} X 40.

Step 2: Hold at 4°C.

On completion the plates were stored at -20°C and the mean cycle threshold (CT) values were recorded.

The efficiency of the 20X Taqman gene assays mixes were evaluated by standard curve method. The cDNA (synthesised from 120 ng/µl total RNA) from a positive control cell line (expressing the respective gene of interest) was serially diluted into 5 tubes (1:10 dilution gradient). Each of the diluted cDNA was used as template and respective real time PCR reaction was run in triplicate with Taqman assay of interest. The CT values from triplicate reactions for each diluted template was recorded. A standard plot was created by plotting the mean CT values against respective dilution. The slope and equation of the standard curve was used to derive the efficiency (using Effeciency (%) = $[10^{(-1/slope)} - 1]X100$) of the Taqman assay mix. The efficiency percent within 85% to 105% was considered for this study.

2.14 Statistical analysis

The data from the proliferation and scratch wound-migration and PCF membrane migration assay were analysed by two-way ANOVA to determine the significance of difference in the observed changes. The data from β_I, 'Rate of pH_i recovery' NAE and gene expression assays (obtainted from the ammonium prepulse time course experiments on the test cells) were analysed by two tailed unpaired t-test and oneway ANOVA respectively to evaluate significance of statistical difference from control. The pH_i recovery from acute acid loading, sequential potassium removal and TASK-3 inhibition by methanandamide were evaluated by comparing the significance of difference in the NAE (obtainted from the ammonium prepulse time course experiments in the respective solutions on the test cells). The most stable reference gene selection was assessed using GNorm and Normfinder algorithms of GeneX® software. The relative gene expression of target genes normalised against stable reference genes was calculated using pre-processing feature of Genex®. The data was finally analysed to evaluate statistical variance using comparative analyses with one-way ANOVA test with post-hoc analysis using the Tukey's or Dunnett's multiple comparisons tests.

Chapter 3. Expression of pH sensitive K^+ channels in cancer cells cultured in altered microenvironments

3.1 Introduction

As described in the main introduction, regulation of pH homeostasis is critical for maintenance and alterations of metabolic patterns that play key roles in tumour development and progression. pH-sensitive ion exchange proteins and channels are pivotal in either modifying or adapting cellular responses to the alterations in pH_e and oxygen tension in the microenvironment (Sennoune, Luo and Martínez-Zaguilán, 2004; Krahling *et al.*, 2009; Chiche, Brahimi-Horn and Pouyssegur, 2010; Lucien *et al.*, 2011). To fully understand their functional association with pH homeostasis and regulation, it is important to determine the expression profiles of these proteins in cancer cells and whether they are altered by changes in pH.

In this chapter, I have focused on investigating the expression of pH-sensitive potassium (K^+) channels in established cell lines from different cancer types (SK-OV-3 from ovarian cancer; MCF-7 from breast cancer; and OE-19 from oesophageal cancer) and developed a culture system that allowed me to determine their expression patterns in altered pH and PO_2 of the microenvironment. This was achieved using organic buffers at optimised concentrations, to culture cells at high or low extracellular pH (pH_e) in 0.04 atm PCO_2 (5% CO_2) and 0.21atm PO_2 (95% air) at 37°C (Section 2.4.3). This approach has been shown to be physiologically comparable across the pH_e range in terms of in vivo carbon dioxide/ oxygen tension (Gullino, Clark and Grantham, 1964; Gullino *et al.*, 1965; Gullino, 1966; Hulikova, Vaughan-Jones and Swietach, 2011; Baronzio *et al.*, 2014).

The extrusion of other organic acids and the lactate dehydrogenase activity of rapidly proliferating cancer cells can destabilise pH_e buffering ability over long periods of incubation (Fischer *et al.*, 2007; Sauvant *et al.*, 2008). Therefore, in this thesis, it was necessary to develop a culture system in which long term experiments could be carried out with minimal shift in pH_e. This system was used to mimic the acidification of the environment cancer cells are exposed to within tumours and enabled the investigation of its effects in altered oxygen tension on the expression of potassium channels. Hence, this approach permited us to study the long term oncogenic reprogramming resulting in altered potassium channel trafficking in cancer cells due to persistent exposure to tumour specific microenvironment.

3.1.1 Aims

The overarching scope of this chapter was to determine whether there is a relationship between changes in pH_e and PO_2 and altered expression of potassium channel proteins in cancer cells. Thus the aims were to:

a) Develop a cell culture system to study established cancer cell lines (SK-OV-3, MCF-7, OE-19 cells) cultured under 4 different pH_e and PO_2 conditions;
b) Investigate expression of selected potassium channels genes (*KCNK9, KCNK17, KCNH1* and *KCNH2*) at the mRNA level by quantitative RT-PCR in cell lines under different culture conditions.
c) Study protein expression and localisation of TASK-3 and TALK-2 by immunofluorescence in cell lines under different culture conditions.

3.2 Results

3.2.1 Development of a cell culture system to study established cancer cell lines under 4 different pH_e and PO_2 conditions

Previous reports have shown that the metabolic activity of cancer cells with enhanced proliferation can rapidly destabilise the pH_e of the culture media (Fischer *et al.*, 2007; Sauvant *et al.*, 2008). To overcome this, it was important to develop a system that allowed me to mimic the conditions found in physiological as well as tumour microenvironments. As described in Section 2.4.3 and Appendix 2I, I used the Henderson Hasselbalch equation to calculate the different concentrations of $NaHCO_3$ necessary to maintain over a longer duration, the pH of the growth medium at 7.4 (normal pH_e) or 6.3 (low pH_e) when cells were incubated at 37°C in an atmosphere of normal PO_2 (0.21atm (in air) with 0.04 atm PCO_2 (5% CO_2) or low PO_2 (0.029 atm (3% O_2)) with 0.18 atm PCO_2 (20% CO_2). In this way, four culture conditions were established to study different combinations of pH_e and PO_2:

I. **Normal pH_e & PO_2** – [$NaHCO_3$] = 23.817mM
II. **Low pH_e & PO_2** – [$NaHCO_3$] = 7.22mM
III. **Low pH_e & normal PO_2** – [$NaHCO_3$] = 1.805mM
IV. **Normal pH_e & low PO_2** – [$NaHCO_3$] = 95.271mM

Cancer cells (viz., SK-OV-3) with high seeding density cultured under these conditions were able to maintain their pH_e for 48 hours of culture until 80%

confluence. Cells at confluence offset the pH buffering of the media (Figure 3.1). On achieving confluence, cells were subcultured to the optimum subculture ratio (Section 2.3.2) using the modified media to continue incubation in respective culture conditions. The 'Y' intercept of the slope for the linear regression of recorded pH_e, ranged between 7.383 to 7.486 for normal pH_e and PO_2, 7.316 to 7.389 for normal pH_e with low PO_2, 6.294 to 6.366 for low pH_e and PO_2 and 6.28 to 6.356 for low pH_e with normal PO_2.

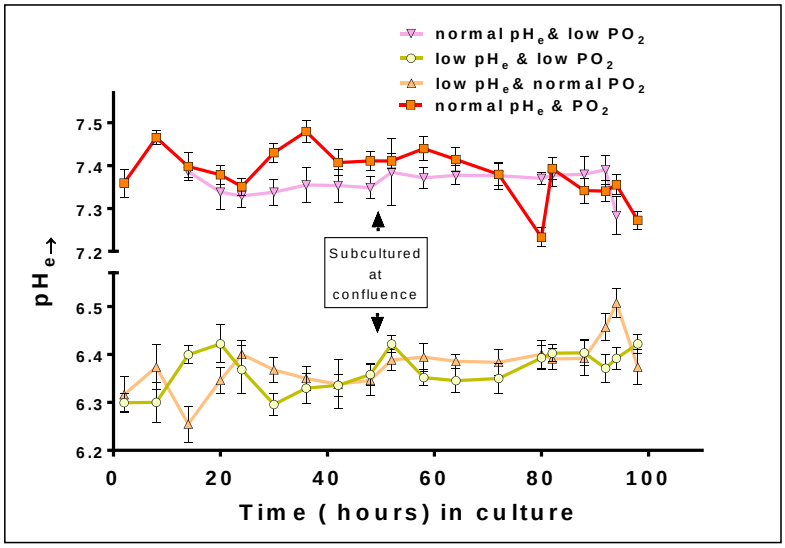

Figure 3.1: The different culture conditions in MEM, maintain the pH_e over long period with SK-OV-3 cells in culture

The pH of the culture media was regulated by dissolved CO_2 availability (as described in the text) and also assisted by cellular metabolism. n = 5

3.2.2 Expression of potassium channel genes *KCNK9, KCNK17, KCNH1* and *KCNH2* at the mRNA level by quantitative RT-PCR in cell lines under different culture conditions

3.2.2.1 Selection of reference gene suitable for quantification in cancer cell lines under different culture conditions

To determine if it was possible to identify reference genes that could be used across the different cell lines and conditions for quantification purposes, I used the methodology described in Section 2.13, to test the expression of five commonly used reference genes for which we had readily available assays (*GAPDH*, *HPRT1, B2M, ACTB* and *YWHAZ*), by quantitative RT-PCR in SK-OV-3, MCF-7 and OE-19 cells cultured under altered pH_e and PO_2 conditions. The normalisation for the selection of reference gene was carried out using the GenEx software that exploits the GeNorm and Normfinder algorithms (Bustin *et al.*, 2009). The most stable reference gene for MCF-7 cells across all the different culture conditions was *YWHAZ* with *ACTB* identified by GeNorm as a potential additional reference gene (Figure 3.2A - C).

A

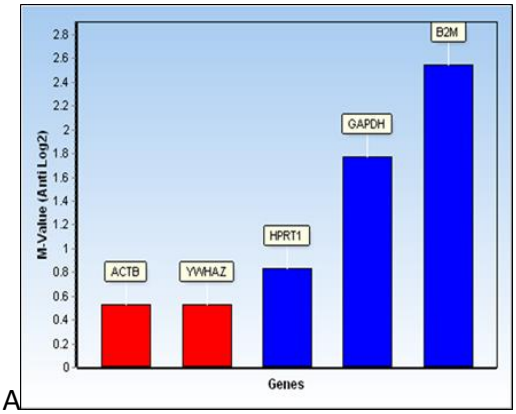

B

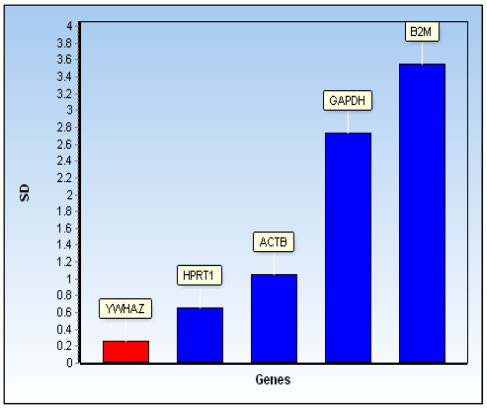

C

NormFinder (Variability)

Gene Name	SD	Acc. SD	SD	0.2555
YWHAZ	0.2555	0.2555		
HPRT1	0.6523	0.3503	Best Gene	YWHAZ
ACTB	1.0514	0.4211		
GAPDH	2.7252	0.751		
B2M	3.5507	0.9302		

Figure 3.2: Expression of five reference genes was tested in the MCF-7 cell lines under the different culture conditions to select the most appropriate for quantitative analysis. [A] GeNorm software output showing that *ACTB* and *YWHAZ* have the most stable expression within the test cancer cells closely followed by *HPRT1*. [B], [C] NormFinder software plot & table demonstrating *YWHAZ* as the most stably expressed gene within test cell lines across all the culture conditions closely followed by *HPRT1*. GenEx 5.0 uses 'Red bars' to denote most stably expressed genes.

For OE-19 cells, *B2M* and *YWHAZ* seem to be most stable across all the culture conditions (Figure 3.3 A – C).

A

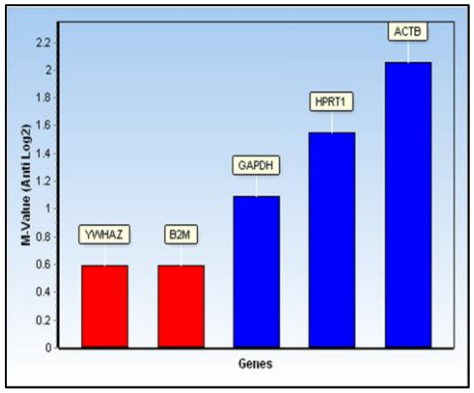

B

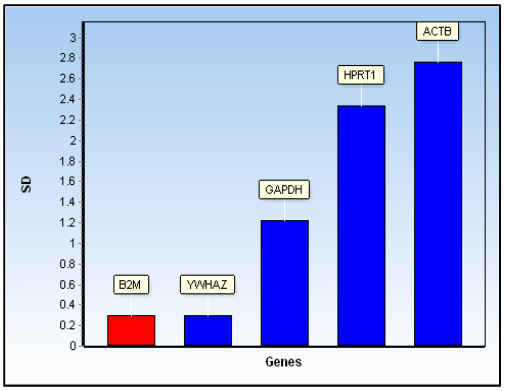

C

NormFinder (Variability)

Gene Name	SD	Acc. SD	SD	0.2946
B2M	0.2946	0.2946		
YWHAZ	0.2946	0.2083	Best Gene	B2M
GAPDH	1.2193	0.4295		
HPRT1	2.3319	0.6661		
ACTB	2.7615	0.7674		

Figure 3.3: Expression of five reference genes was tested in the OE-19 cell lines under the different culture conditions to select the most appropriate for quantitative analysis. [A] GeNorm software output showing that *YWHAZ* and *B2M* have the most stable expression within the test cancer cells. [B], [C] NormFinder software plot & table demonstrating *B2M* as the most stably expressed gene across all the culture conditions closely followed by *YWHAZ*.

By contrast, *HPRT1* and *GAPDH* emerged as the most stably expressed reference genes in SK-OV-3 cells across all the culture conditions (Figure 3.4 A - C), a finding consistent with our previously published data on primary ovarian tumours (Ofinran et al., 2016)

A

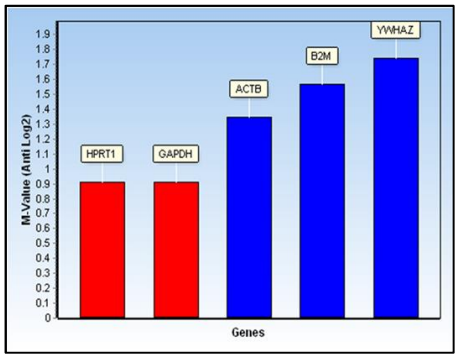

B

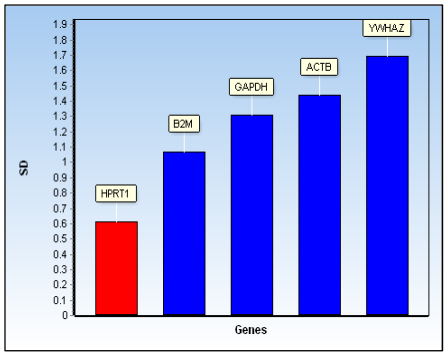

C

NormFinder (Variability)

Gene Name	SD	Acc. SD	SD	0.6105
HPRT1	0.6105	0.6105		
B2M	1.0681	0.6151	Best Gene	HPRT1
GAPDH	1.3094	0.5989		
ACTB	1.4364	0.5751		
YWHAZ	1.6934	0.5713		

Figure 3.4: Expression of five reference genes was tested in the SK-OV-3 cell lines under the different culture conditions to select the most appropriate for quantitative analysis.
[A] GeNorm software output showing that *HPRT1* and *GAPDH* have the most stable expression within the test cancer cells closely followed by *ACTB*. [B], [C] NormFinder software plot & table demonstrating *HPRT1* as the most stably expressed gene within test cell lines across all the culture conditions followed by *B2M* and *GAPDH*.

These data indicate that it will be necessary to test additional reference genes to identify a set of three reference genes that can be used for each cell lines and determine if there is a combination that can be used across all cell lines and conditions tested and thus adhere to MIQE guidelines (Bustin *et al.*, 2009). Due to time constraints, two reference genes were used for each cell line according to the data reported above: *ACTB* and *YWHAZ* for MCF-7; *B2M* and *YWHAZ* for OE-19; and *HPRT* and *GAPDH* for SK-OV-3.

3.2.2.2 Quantification of potassium channels mRNAs in cancer cells under different culture conditions

KCNK9 and *KCNK17* are genes encoding for the potassium channels TASK-3 and TALK-2 respectively, whose expression is known to be affected by pH changes (Lesage and Barhanin, 2011). *KCNK9* and *KCNK17* mRNA expression was measured in SK-OV-3, MCF-7 and OE-19 cells cultured under normal or low pH_e & PO_2 conditions. A significant ($P < 0.001$) decrease in *KCNK9* mRNA expression was observed in normal compared to low pH_e & PO_2 for SK-OV-3 whilst the difference was not statistically significant ($P > 0.05$) in MCF-7 cells (Figure 3.5A). In OE-19 cells, the relative expression of *KCNK9* mRNA was significantly ($P < 0.001$) higher in normal than in low pH_e & PO_2 culture conditions (Figure 3.5A). *KCNK17* levels were significantly ($P < 0.0001$) lower in SK-OV-3 cells cultured in low pH_e & PO_2 compared to normal pH_e & PO_2, while its levels were negligible in MCF-7 and OE-19 (Figure 3.5B).

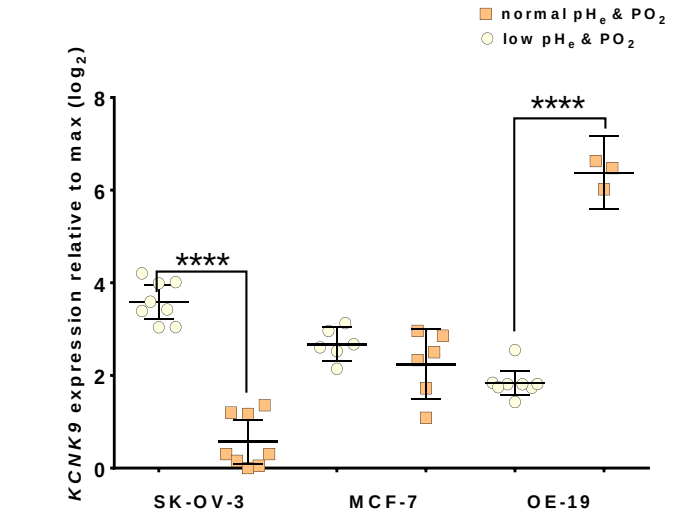

A

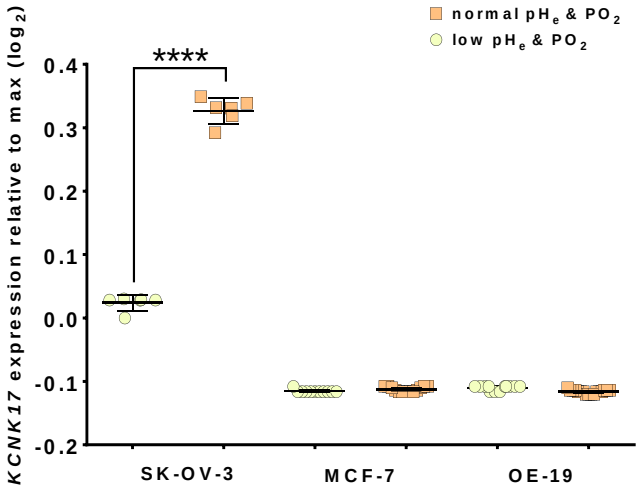

B

Figure 3.5: Relative expression of *KCNK9* and *KCNK17* in cancer cells in altered pH$_e$ & PO$_2$.
Log$_2$ of the expression relative to max of [A] *KCNK9* and [B] *KCNK17*. Statistical analysis was performed with One-way ANOVA using Tukey's multiple comparisons test; **** P < 0.0001.

It is not known whether expression of the HERG and Eag potassium channels is affected by pH changes. Eag and HERG potassium channels are encoded by the genes *KCNH1* and *KCNH2* respectively. Significant increases in *KCNH1* expression in normal compared to low pH$_e$ & PO$_2$ culture conditions were seen in SK-OV-3 (P < 0.0001), MCF-7 (P < 0.001) and OE-19 cells (P< 0.01) (Figure 3.6A). *KCNH2* mRNA levels were also significantly (P < 0.0001) increased in SK-OV-3 cells in normal pH$_e$ &

PO_2 compared to low pH_e & PO_2 culture conditions, but less significant ($P < 0.01$) increase was observed for MCF-7 and OE-19 cells in normal pH_e & PO_2 compared to low pH_e & PO_2 (Figure 3.6B).

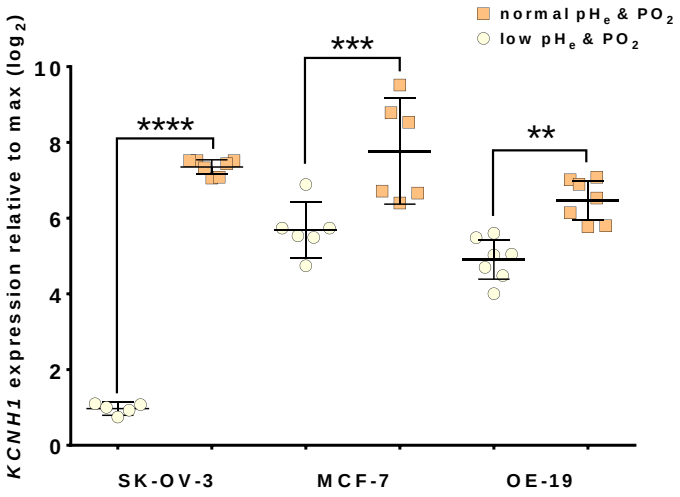

A

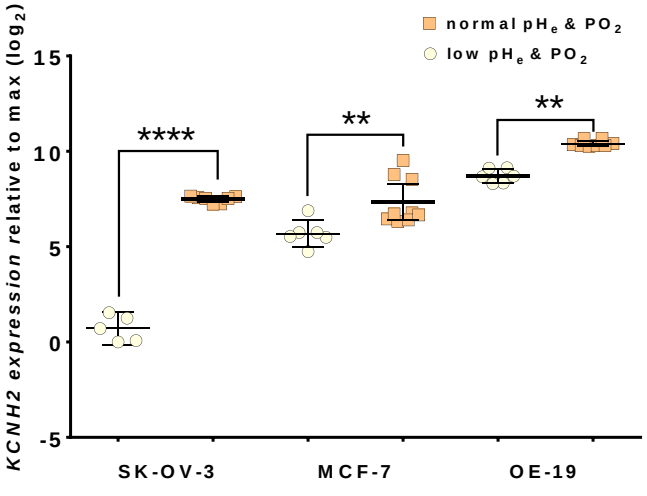

B

Figure 3.6: Relative expression of *KCNH1 and KCNH2* genes in cancer cells in altered pH_e and PO_2. Differential expression of [A] *KCNH1* and [B] *KCNH2* genes in cancer cells in response to a change in pH_e and PO_2. Statistical analysis was performed with One-way ANOVA using Tukey's multiple comparisons test; ** $P < 0.01$; **** $P < 0.0001$.

3.2.3 Expression and localisaton of TASK-3 and TALK-2 potassium channel proteins by immunofluorescence in cell lines under different culture conditions

Having established the RNA expression profiles, I wanted to determine whether these corresponded to the presence of the channels at the protein level. For these studies, I focused on the known pH-sensitive channels TASK-3 and TALK-2 in SK-OV-3 and MCF-7 cells because at the RNA level they show opposite behaviour in SK-OV-3 cells under different culture conditions and no change in MCF-7 cells (Figure 3.5).

3.2.3.1 TASK-3 expression and localisation

Using immunofluorescence, TASK-3 expression in SK-OV-3 cells exhibited a punctate distribution in low pH_e and PO_2 (Figure 3.7A), in comparison to the smooth distribution observed when cultured in normal pH_e & PO_2 (Figure 3.7B). Confocal imaging of SK-OV-3 cells in low pH_e & PO_2 (Figure 3.7C), further confirms the punctate nature of the TASK-3 channel. By contrast, MCF-7 cells maintained in low pH_e & PO_2 exhibit a uniform distribution of TASK-3 (Figure 3.7D).

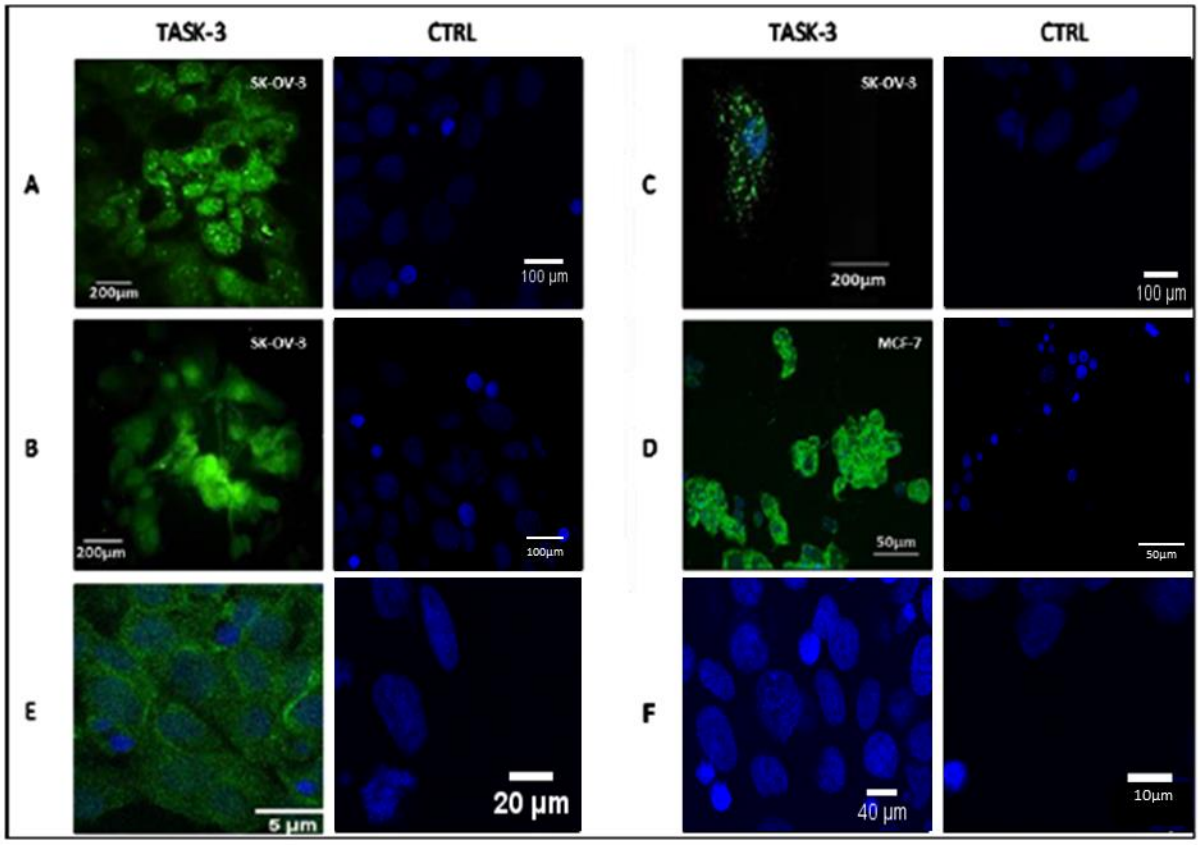

Figure 3.7: Expression of TASK-3 proteins in SK-OV-3 and MCF-7 cells in altered pH_e/PO_2
Localisation of TASK-3 in SK-OV-3 cells in low (A) and in normal (B) pH_e & PO_2. Confocal composite image of TASK-3 protein expression in low pH_e & PO_2 in SK-OV-3 (C) and MCF-7 (D) cells. Green: FITC labelled TASK3 antibodies; Blue: DAPI; Ctrl panels are the secondary antibodies only negative controls. Human placental tissue is used as a positive control for TASK-3 (E). Peripheral leucocytes without TASK-3 expression are used as a negative control (F). A representative image from each condition is shown. All experiments were performed in triplicate on different occasions (n=3).

To determine whether pH_e or PO_2 was the main variable to cause the change in TASK-3 distribution between the two conditions, I studied the staining of TASK-3 in test cells. Interestingly, in low pH_e and normal PO_2 TASK-3 protein localised in close proximity to the nucleus both in MCF-7 and SK-OV-3 cells (Figure 3.8A and B, respectively). The poor resolution of the image is likely due to low cell number and composite nature of the image (compressing Z-stack into 2D image). The observation was confirmed by repeating all imaging four times.

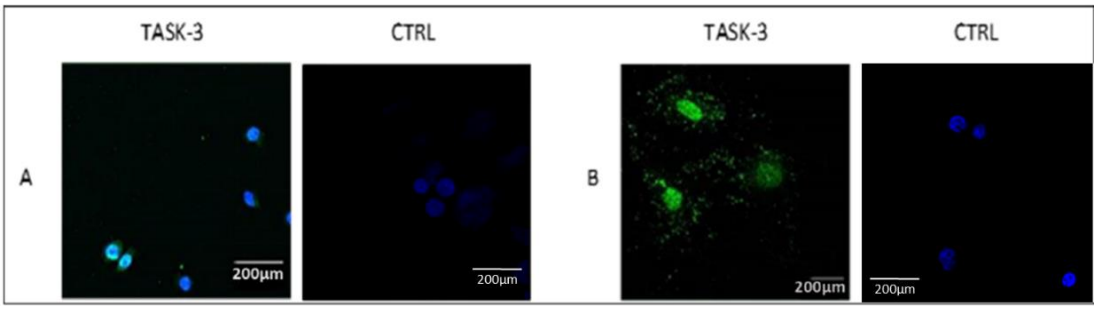

Figure 3.8: Expression of TASK-3 proteins in SK-OV-3 in low pH_e & normal PO_2. Confocal composite image of TASK-3 immunofluorescence in MCF-7 (A) and SKOV-3 (B) cells cultured in low pH_e & normal PO_2 with FITC labelled TASK-3 protein (TASK-3). CTRL panels are the secondary antibodies only negative controls. An example of positive control human placental tissue is shown in Figure 3.3E. A representative image from each cell line is shown. All experiments were performed at least in duplicate (n=2). Blue: nucleus stained with DAPI

3.2.3.2 TALK-2 expression

TALK-2 expression was analysed in SK-OV-3 cells cultured in normal pH_e & PO_2 using the same approaches described for TASK-3. Under these culture conditions, TALK-2 signals seem to localise at the cell membrane and near the nucleus in these cells (Figure 3.9).

These extracellular alkali sensitive potassium channels were not reasonably expressed in MCF-7 cells in normal pH_e & PO_2. No prominent expression of TALK-2 protein was observed in SK-OV-3 and MCF-7 cells in other culture conditions.

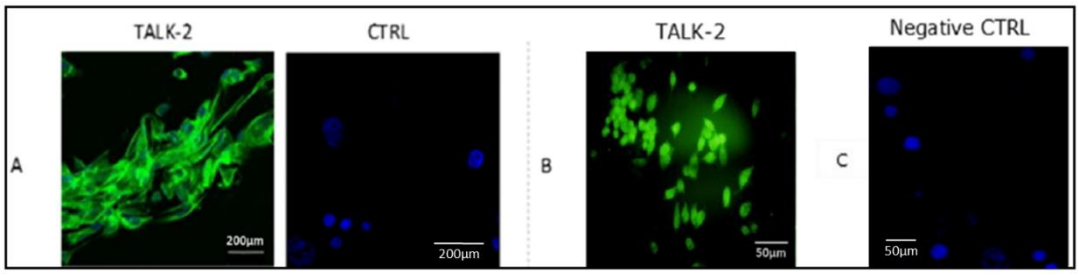

Figure 3.9: Expression of TALK-2 proteins in SK-OV-3 cells under normal pH_e & PO_2.
[A] Confocal images of SK-OV-3 cells with FITC labelled TALK-2 antibodies. CTRL panel is the secondary antibodies only negative control. [B] MiaPaca (pancreatic carcinoma) cells as positive control. [C] Osteosarcoma cells without TALK-2 expression shown as negative control. Blue: nucleus stained with DAPI.

3.3 Discussion

Tumour cells are uniquely associated with abnormal and uncharacteristic expression of several ion channels often identified as hallmarks of tumour progression (Schwab *et al.*, 2012; Huber, 2013). Recent investigations suggest alterations in the "channelome" can contribute to disease progression and pathogenesis (Huber, 2013). Experimental interventions targeting ion channels often impede survival, proliferation, malignant behaviour and invasive properties that can ultimately contribute to resistance to cancer therapy (Lobikin *et al.*, 2012). Potassium channels influence cellular membrane potential through ion fluxes thus altering the electrical activity and behaviour of the cells in which they are expressed (Williams, Bateman and O'Kelly, 2013). There is evidence that in cancer these channels are involved in regulating functions such as proliferation, angiogenesis, invasion, migration and apoptosis (Pardo and Stühmer, 2014). Given the great potential of these proteins as therapeutic targets due to their membrane location and their well characterized pharmacology, there is immense potential in further investigating the expression of these channels in cancer cells under culture conditions that mimic those occurring *in vivo*.

In this chapter, I have described the development of a self-sustaining, metabolically conducive buffering system. This system enabled me to carry out experiments over extended periods (98 hours) with minimal shift in pH_e in culture, designed to mimic physiological conditions (normal pH_e & PO_2) or the tumour microenvironment (low pH_e & PO_2) as well as possible intermediate states (low pH_e/normal PO_2 or normal pH_e/low PO_2). Using this system, I determined the RNA expression profile of the

genes coding for the potassium channels TASK-3 (*KCNK9*), TALK-2 (*KCNK17*), Eag (*KCNH1*) and HERG (*KCNH2*) in the different culture conditions (Figures 3.3. and 3.4). In normal pH_e & PO_2, SK-OV-3 cells express all four channel genes, with *KCNK9* being the lowest, followed by *KCNK17* and finally, at comparable levels, *KCNH1 and KCNH2* with the highest values. When SK-OV-3 cells are cultured in low pH_e & PO_2, dramatic and highly significant increases in *KCNK9* and decreases in *KCNK17*, *KCNH1* and *KCNH2* are observed. In MCF-7 cells, no changes in the levels of *KCNK9* and *KCNK17* mRNA are seen and these are very low or barely detectable in both conditions; by contrast, *KCNH1* and *KCNH2* are expressed at high levels in these cells at normal pH_e & PO_2, and whilst *KCNH1* levels show a significant decrease in low pH_e/PO_2, those of *KCNH2* are unaffected. Expression of *KCNK9* is high in OE-19 cells in normal pH_e & PO_2, and remained so relatively to other cell lines despite a significant downregulation in low pH_e & PO_2; *KCNK17* is barely detectable in both conditions in these cells, whilst *KCNH1* and *KCNH2* are both expressed at high levels in normal pH_e & PO_2 and are decreased or unchanged levels respectively when OE-19 cells are cultured in low pH_e & PO_2.

Given that the different cell lines are representatives of individual tumours from different tissue types (ovaries, breast, bone and oesophagus), these findings may indicate that the tissue of origin may be important in determining whether or not a change in the environment will cause changes in expression of these channels. Consistent with this, work previously published by our group has shown that TASK-3 is overexpressed in ovarian cancer where it renders a survival advantage and has

prognostic significance (Innamaa *et al.*, 2013), whilst a comparative meta-analysis including 12 invasive breast carcinoma tissues suggested no increase in *KCNK17* gene expression in these tumours (Williams, Bateman and O'Kelly, 2012).

Visualisation of the TASK-3 protein by immunofluorescence technique confirmed expression of TASK-3 in ovarian and breast cancer cells and in our culture system we could show a change in the cellular distribution of TASK-3 between cells cultured in normal compared to low pH_e & PO_2 (Figure 3.7). It is known that the predominantly cell-surface distribution of TASK family members observed in non-malignant cells is replaced by high internal labelling; the high intracellular accumulation and low TASK-3 membrane expression in many cancers has been attributed with a potential problem with membrane trafficking of TASK-3 channels (Zuzarte et al., 2009; Mathie et al., 2010). Taken together with the proposed correlation between pH_e and expression of TASK-3 channels (Duprat et al., 1997), the observation of TASK-3 change of localisation in our culture system indicates that pH could be directly involved in distribution and localisation of this protein. DAPI counterstain channel often had to be removed as they interfered with FITC signals used with secondary antibody to stain potassium channels expressed on nuclear membrane.

Similar to what was observed at the RNA level, I could detect TALK-2 expression only in SK-OV-3 cells maintained under normal pH_e and PO_2 conditions, with no expression detected in low pH_e & PO_2, or under either conditions in the other cell lines (Figure 3.9). Our analysis of TALK-2 is too limited and further experiments are needed to draw any specific conclusions. Interestingly, TALK-2 has been found to be

overexpressed in breast cancers of invasive subtypes (Schwab *et al.*, 2012; Williams, Bateman and O'Kelly, 2013); therefore, it can be speculated that expression of TALK-2 channel protein in normal pH_e & PO_2 in SK-OV-3 cells denotes the selective effects of physiological pH_e towards the expression of this alkali activated potassium channel.

In summary, in this chapter I aimed to investigate the role of a changing or dynamic microenvironment on expression of potassium channel proteins to investigate their potential involvement in regulating the pH homeostasis that contributes to cancer metabolism. The role of altered culture conditions was aimed at mimicking a tumour environment to elicit reliable response on multiple aspects of pH regulation in cancer cells. Limitations of this work include the use of established cancer cell lines and the absence of strict control of PO_2 and PCO_2 levels. It will be important to validate these findings in future studies using primary tissue biopsies and anaerobic/hypoxic chambers to appropriately mimic the severe hypoxic conditions of the tumour microenvironment and reveal more information regarding pH regulation and pH homeostasis pertaining to cellular metabolism in cancer.

Given the observed links between pH_e and expression of channel proteins and between pH_e and cell proliferation, in the next chapter I will study the relatively long term effects on cell proliferation and migration and pH_I in response to different culture conditions and investigate whether treating cells with antagonist of potassium channels alters this phenotypic readout.

Chapter 4. Role of pH_e/PO_2 and pH regulation in cancer cell progression

4.1 Introduction

Determining the expression profiles of these proteins in cancer cells and whether they are altered by changes in pH led us to an open question on the association between cancer hallmarks and pH homeostasis and regulation. The relevance of intracellular pH homeostasis as a key player in regulating cancer cell proliferation through alteration in metabolic patterns has been emphasised in various studies (Tannock and Rotin, 1989; Vander Heiden, Cantley and Thompson, 2009) (Chapter 1). Effects of pH_e and PO_2 on cancer cells has been studied independently (Damaghi, Wojtkowiak and Gillies, 2013; Masson and Ratcliffe, 2014) to understand their role as hallmarks of cancer. While some studies focussed on plasma or cellular pH regulatory/buffer systems in reduced pH_e (by increased PCO_2 or use of bicarbonate/ HEPES buffer) (Lauritzen *et al.*, 2010; Swietach *et al.*, 2010), others investigated the influence of low oxygen tension on these cancer cells (Ruan, Song and Ouyang, 2009; Lucien *et al.*, 2011).

It is necessary to use culture conditions that mimic tumour microenvironment (low pH_e and low PO_2) to investigate their collective contribution in pH homeostasis and cancer metabolism. In this chapter the effects of pH_e and PO_2 on some cancer hallmarks that include cell viability, proliferation, migratory potential in breast, ovarian and oesophageal cancer cells are described. To achieve this, organic acids were used to establish culture conditions with decreased extracellular pH (pH_e) of the medium in optimised concentration augmented with appropriate gas mixtures

(Section 2.4.3; Section 3.2.1). Finally, given that a relatively low pH_e promotes aggressive development of tumours by inducing migration and invasion (Hanahan and Weinberg, 2000), experiments were also performed to address the role of changes in pH_e and PO_2 on progression of cancer.

4.1.1 Aims

The overarching aim of the study was at evaluate the effect of altered pH_e and PO_2 on:

a) The proliferation and doubling time of SK-OV-3, MCF-7, and OE-19 cells.
b) The proliferation of SK-OV-3, MCF-7 and OE-19 cells with and without pharmacological manipulations of TASK-3, HERG and H^+/K^+/ATPase.
c) The long term pH_i stabilisation during proliferation of SK-OV-3, MCF-7 and OE-19 cells with pharmacological inhibitors of TASK-3, HERG and H^+K^+ATPase.
d) The migratory and invasive potential of viable SK-OV-3 and MCF-7 cells and record their pH_I post migration.

4.2 Results

4.2.1 Evaluate the viability and proliferation of cancer cells in altered pH_e and PO_2

The current section illustrates the experimental observations demonstrating the effect of altered pH_e/PO_2 on the viability, proliferation and migration potential of cancer cells. A change in pH of the culture medium was found to influence cancer cell proliferation depending on the given population. Oneway ANOVA showed that the test cancer cell lines had a significantly ($P < 0.001$) lower rate of proliferation at all three time points in normal and low pH_e & PO_2, compared to MCF-10-A (normal control, Figure 4.1). On comparing percent change in cell growth from the start of the experiment, by oneway ANOVA, it was observed that percent change in cell growth from the start of the experiment, by oneway ANOVA, it was observed that the SK-OV-3 cells significantly ($P < 0.001$) proliferated after long-term incubation in low pH_e and PO_2 (Figure 4.1) compared to those in normal pH_e & PO_2.

This effect on cell growth was relatively stable after 48 hours but again significantly ($P < 0.001$) increased with a continued incubation (72 hours) under low pH_e & PO_2 compared to normal pH_e & PO_2. There was a significant ($P < 0.001$) drop in the overall metabolic activity of the cultured OE-19 cells, which potentially indicates their diminished cell growth for 24 and 48 hours in low pH_e and PO_2 compared to that in normal pH_e and PO_2 (Figure 4.1).

Unlike SK-OV-3 and OE-19 cells (Figure 4.1), the MCF-7 cells showed no significant decrease in cell growth within 24 hours at low pH_e & PO_2. Significant decrease in MCF-7 cell growth was observed from 24 to 72 hours in low pH_e & PO_2 ($P < 0.0001$) and normal pH_e & PO_2 ($P < 0.0001$) respectively (Figure 4.1).

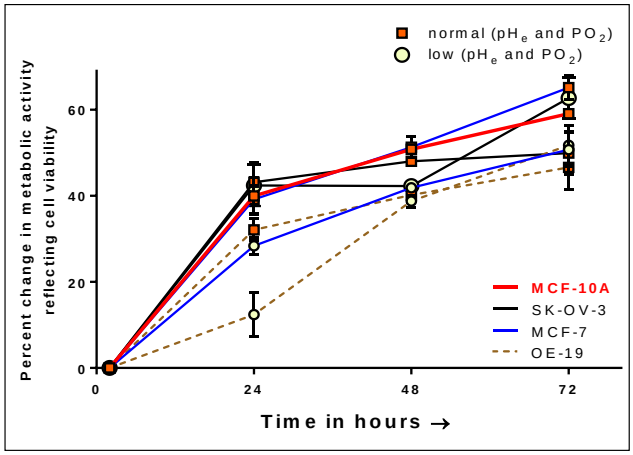

Figure 4.1: Percent change in metabolic activity and viability of cancer cells in altered pH_e/PO_2. Percent change in overall metabolic activity of indicating cell growth from initial seeding time of SK-OV-3, MCF-7 and OE-19 cells (5000 cells seeding density) measured as a function of cellular metabolism dictates the role of normal pH_e and PO_2 as well as low pH_e and PO_2. Percent change in proliferation of MCF-10A cells in normal pH_e and PO_2 was considered as control. n = 3

The test cancer cell lines had a significantly ($P < 0.001$) lower rate of proliferation at all three time points in normal pHe and low PO_2 as well as in low pH_e and normal PO_2, compared to normal control (Figure 4.2). Although these conditions, where either pH_e or PO_2 were low, served as good experimental reference conditions they neither simulated true tumour specific conditions nor mimicked ideal physiological microenvironments.

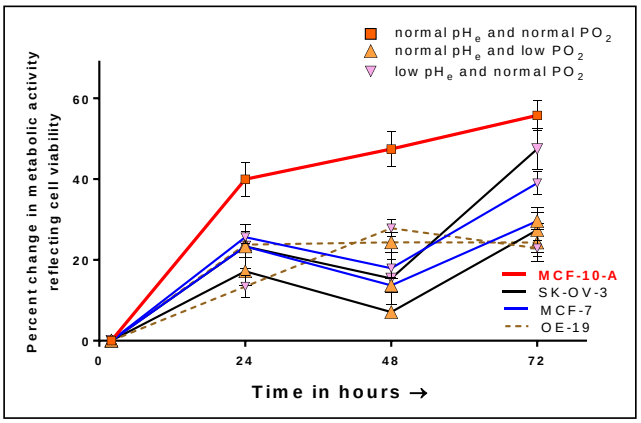

Figure 4.2: Percent change in metabolic activity and viability of cancer cells in altered pH_e/PO_2. Percent change in overall metabolic activity of indicating cell growth from initial seeding time of SK-OV-3, MCF-7 and OE-19 cells (5000 cells seeding density) measured as a function of cellular metabolism dictates the role of normal pH_e and low PO_2 as well as low pH_e and normal PO_2. Percent change in proliferation of MCF-10A cells in normal pH_e and PO_2 was considered as control. n = 3.

At this point it was important to evaluate the effect that a low pH_e & PO_2 condition (more closely simulating tumour specific microenvironment) would produce on the proliferation of the test cell lines in comparison to normal pH_e & PO_2 condition (simulating physiological microenvironment). As a result, it was important that further analysis was primarily focussed on these two culture conditions. Relative doubling time (Section 2.5) was calculated for passage nos. 7, 21, 113 and 107 for SK-OV-3, OE-19, MCF-7 and MCF-10A cell lines respectively, in normal pH_e and PO_2 as wel as in low pH_e and PO_2.

The relative doubling time of SK-OV-3, MCF-7 and OE-19 cells at normal pH_e & PO_2 was observed to be approximately 35 hours, 16 hours and 42 hours respectively (Table 4.1). The change in relative doubling time was critical in SK-OV-3 cells, where low pH_e & PO_2 decreased the relative doubling time to less than half (comparable to MCF-10-A normal control as in table 4.1 and (ATCC®, 2017). In MCF-7 cells, no significant difference was observed in the relative population doubling times between cells cultured in low pH_e & PO_2 and those in normal pH_e & PO_2. However, in OE-19 cells low pH_e & PO_2 significantly ($P < 0.01$) increased the relative doubling time (Table 4.1).

	Normal pH_e/PO_2	Low pH_e/PO_2	Passage number
SK-OV-3	34.7 ± 0.8	14.4 ± 0.3	7
MCF-7	15.5 ± 0.32	14.5 ± 0.3	113
OE-19	41.7 ± 0.51	60.7 ± 0.14	21
MCF-10A	18 ± 0.02	NA	107

Table 4.1: Effect of pH_e and PO_2 on relative doubling time of proliferating cancer cells. The table describes the proliferation of test cancer cell lines in response to altered culture conditions viz., normal pH_e and normal PO_2; low pH_e and low PO_2. An increase in proliferation from initial cell seeding density was monitered. Doubling time was calculated for passage nos. 7, 21, 113 and 107 for SK-OV-3, OE-19, MCF-7 and MCF-10A cell lines which differed in respective culture conditions.

4.2.2 Determine the proliferation of SK-OV-3 cells in the presence and absence of the inhibitors of TASK-3 and HERG potassium channels

The effect of methanandamide and E-4031 on their respective receptors depends on the relative specificity to their target receptors. I used these pharmacological agents to initially observe variable effect of all four modified culture conditions on the proliferation of viable SK-OV-3 cells. The viability was assessed using Cell titre 96 well MTS protocol (Section 2.5).

The highest proliferation observed in drug free culture medium for the respective cell line under low pH_e and low PO_2 was considered as no-drug control.

4.2.2.1 Effect of TASK-3 blocker, methanandamide on SK-OV-3

I observed a significant ($P < 0.001$) inhibition in proliferation of SK-OV-3 cells under all four culture conditions in presence of methanandamide compared to no-drug control (Figure 4.3A). No significant difference in the percent inhibition of proliferation was observed among normal pH_e & PO_2, normal pH_e/low PO_2 and low pH_e/normal PO_2 conditions with methanandamide. However, a significant ($P < 0.05$) inhibition in cell proliferation by methanandamide was observed in SK-OV-3 cells after 72 hours in low pH_e and low PO_2 in comparison to normal pH_e and normal PO_2. The assays were performed in both low and normal pH_e, by maintaining the gas supply constant for each pair of experiments (Section 2.4.3).

4.2.2.2 Effect of E-4031 inhibitor on SK-OV-3 proliferation

The long term inhibition (72 hours' incubation) of HERG potassium channel in SK-OV-3 cells (by E-4031, 0.1 µM) showed significant ($P < 0.001$) reduction in

proliferation when compared to no drug control. However, low pH_e & PO_2 produced significantly ($P < 0.0001$) greater inhibition in proliferation not only in comparison to control and after HERG inhibition in normal pH_e & PO_2 but also under normal pH_e/low PO_2. Similarly, normal pH_e/low PO_2 produced significantly ($P < 0.0001$) greater inhibition in proliferation not only in comparison to control and after E-4031 mediated HERG inhibition in normal pH_e & PO_2 but also under normal pH_e/low PO_2 (Figure 4.3 B).

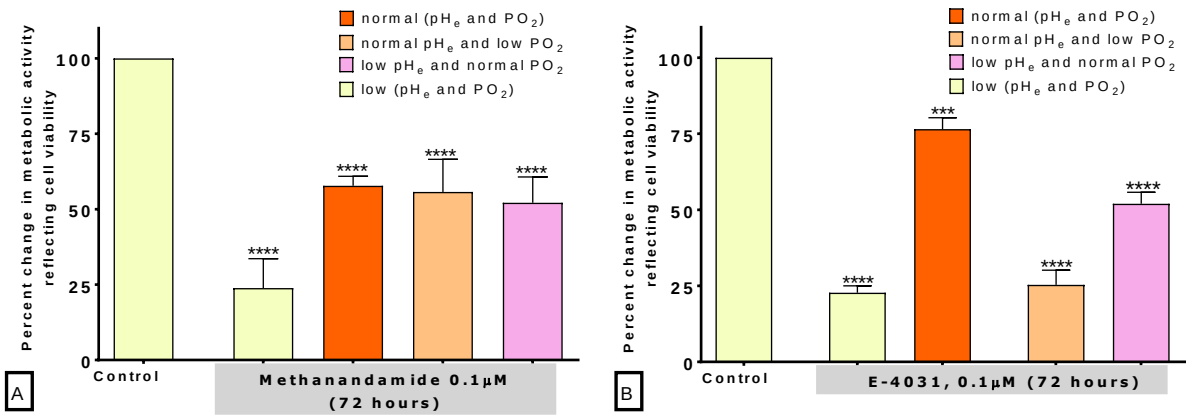

Figure 4.3: Effect of K^+ channel inhibitors on cancer cell proliferation. The effect of [A] methanandamide and [B] E-4031 on SK-OV-3 cell viability after 72 hours incubation in altered pH_e/ PO_2 is shown. The experiments were performed in normal and low pH_e under normal PO_2 as well as normal and low pH_e under low PO_2 (*** = P<0.001; **** = P<0.0001). n = 3

Further on, the long term effect of these pharmacological agents on proliferation and pH_i of SK-OV-3, MCF-7 and OE-19 cells in low pH_e/PO_2 (closely simulating tumour specific culture condition) compared to normal pH_e/PO_2 (closely simulating physiological culture condition), is reported in the following section.

4.2.3 Determine the pH_i during proliferation in the presence and absence of the inhibitors of TASK-3, HERG and H^+/K^+ATPase

The overarching aim was to assess the pH_i recovery status of the test cancer cells after long term incubation (more than the highest recorded relative doubling time;

72 hours) with pharmacological inhibitors of potential pH associated membrane proteins (methanandamide (M), E-4031 (E) and omeprazole (O)) (Figure 4.4). The viability of test cancer cells was assessed using Cell titre 96 well MTS protocol (Section 2.5). The pH_i of the cells that survived the proliferation assay in the presence and absence of the three pharmacological agents (Section 2.5.1.1) was determined using BCECF-AM as described in Section 2.7.4, 2.7.5. Calibration of the pH-sensing dye was performed before each experiment on the test cells as described in Section 2.8. Increased cell death was observed in low pH_e/normal PO_2 as well as in normal pH_e/low PO_2 for MCF-7 and OE-19 cells over 72 hours. Hence, no data was available for proliferation assays under these two conditions.

The proliferation of SK-OV-3 cells was significantly reduced in low pH_e & PO_2 compared to normal pH_e & PO_2 in the presence of omeprazole (Figure 4.4 D). However, this decrease was not significantly different from that observed with methanandamide or E-4031 in the same culture conditions. A significant ($P < 0.0001$, $P < 0.001$, $P < 0.0001$) fall in pH_i was observed in SK-OV-3 cells (in normal pH_e & PO_2) associated with a significant ($P < 0.0001$, $P < 0.0001$, $P < 0.01$) decrease in proliferation when exposed to inhibitors of H^+/K^+ATPase, TASK-3 and HERG channels respectively (Figure 4.4A, D).

In contrast, MCF-7 cells had a decrease ($P < 0.0001$ after inhibition of H^+/K^+ATPase, TASK-3 and HERG) in pH_i in low pH_e & PO_2 compared to that in normal pH_e & PO_2 even though a significant decrease in cell proliferation was not observed after exposure to the drugs in either conditions (Figure 4.4B, E).

However, viable OE-19 cells showed a highly alkaline pH_i ($P < 0.001$, $P < 0.01$, $P < 0.001$ after inhibition of H^+/K^+ATPase, TASK-3 and HERG respectively) after exposure to the drugs under low pH_e & PO_2 (Figure 4.4C). Although an increased cell death was observed in OE-19 cells in comparison to SK-OV-3 cells after exposure to drugs under normal pH_e & PO_2, the viable cells of both cell lines demonstrated a normal pH_i profile (Figure 4.4A, D, C and F). After exposure to the drugs under low pH_e & PO_2, a sharp rise in pH_i was observed although a significant ($P < 0.0001$) decrease in OE-19 cell proliferation was recorded (Figure 4.4F).

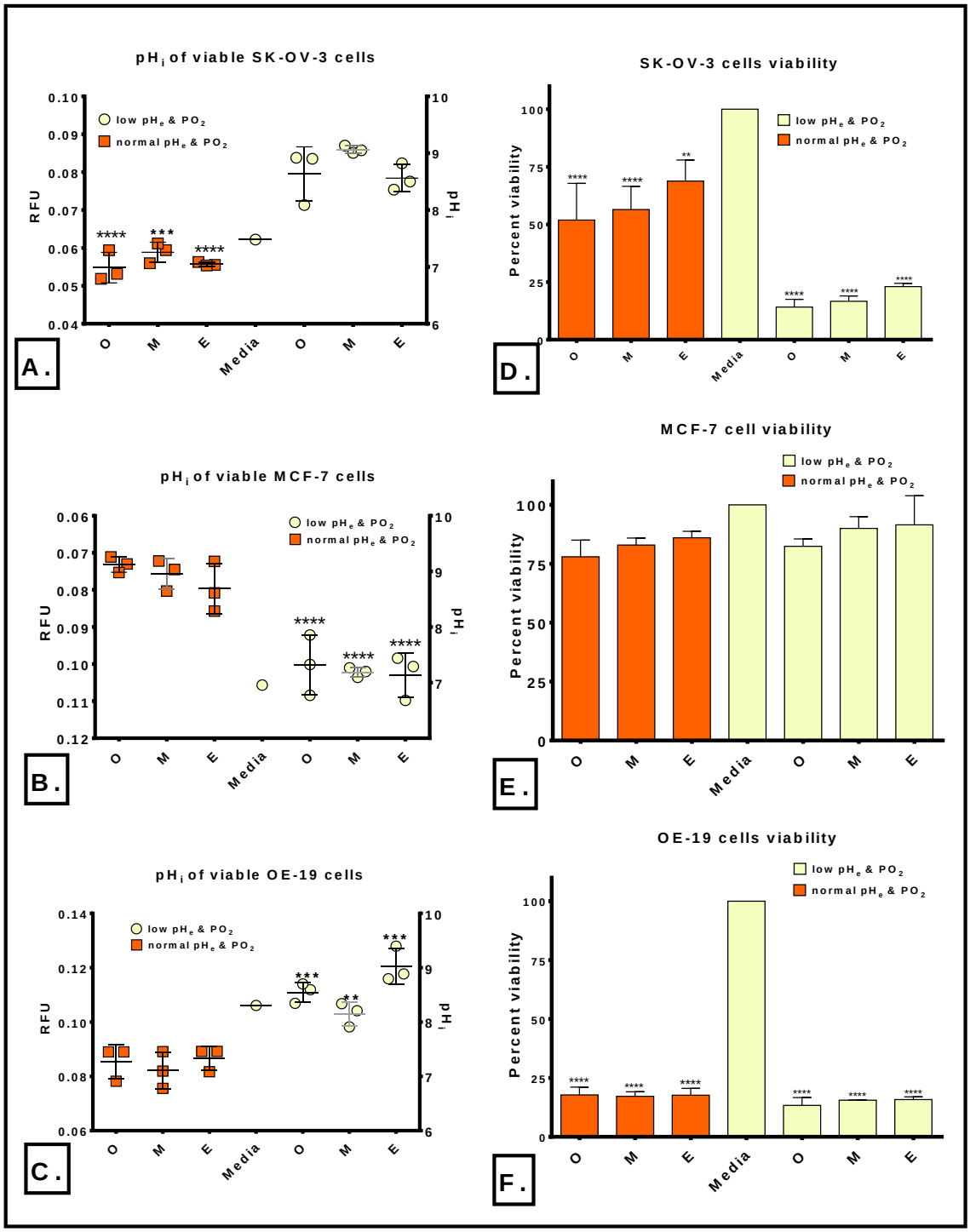

Figure 4.4: Correlation between proliferation and pH_i of cancer cells.
Relation between proliferation and pH_i of cancer cells treated with omeprazole (O), methanandamide (M) and E-4031 (E) is shown. The data was collected after 72 hours reflecting the influence on the pH_i of survived (A) SK-OV-3, (B) MCF-7 and (C) OE-19 cells. Effect of the drugs over 72 hours on viability of (D) SK-OV-3, (E) MCF-7 and (F) OE-19 cells, which survived drug treatment is shown. (**= P <0.01; ***= P <0.001; ****= P <0.0001). n = 4

4.2.4 Determination of the migratory and invasive potential of cancer cells and their pH_i post migration in altered pH_e/PO_2

4.2.4.1 Determination of the migratory and invasive potential of cancer cells by scratch wound assay

The migration of SK-OV-3 and MCF-7 cells across a scratch wound, in altered microenvironments at different time points are shown in Figure 4.5 and 4.6 respectively. The representative images A and D (12 hours of incubation), B and E (24 hours of incubation) and C and F (48 hours of incubation) represent the migration of SK-OV-3 cells. The representative images G and J (12 hours of incubation), H and K (24 hours of incubation) and I and L (48 hours of incubation) represent the migration of MCF-7 cells.

The migration of SK-OV-3 cells on the boundary of the 130 µm scratch wound was initiated towards the center of the scratch by 30 hours in normal pH_e and normal PO_2 and by 18 hours for those maintained in low pH_e & low PO_2. The SK-OV-3 cells were found to align along the wound margin leading to the formation of a solid wound margin protruding into and compromising 10% of the mean wound space. In contrast to the SK-OV-3 cells maintained in low pH_e & PO_2, the cells maintained under normal pH_e & PO_2, along the wound margin traversed ≥ 60% mean wound space. The results from 48 hours of incubation show complete wound closure in sub-optimal serum levels (< 5% FBS in media used to prevent any proliferation (Cory, 2011)) only in low pH_e and low PO_2 but wound closure is compromised in normal pH_e and normal PO_2. The MCF-7 cells in normal pH_e & PO_2 demonstrated a slower

rate of migration in comparison to SK-OV-3 cells (Figure 4.8). A drop in both pHe and PO_2 below normal levels could only marginally increase scratch wound gap closure by 30%. In culture conditions where either pH_e or PO_2 were individually lowered from their normal values, minimum plate adherence and viability in optimum serum medium for both the cell lines was observed.

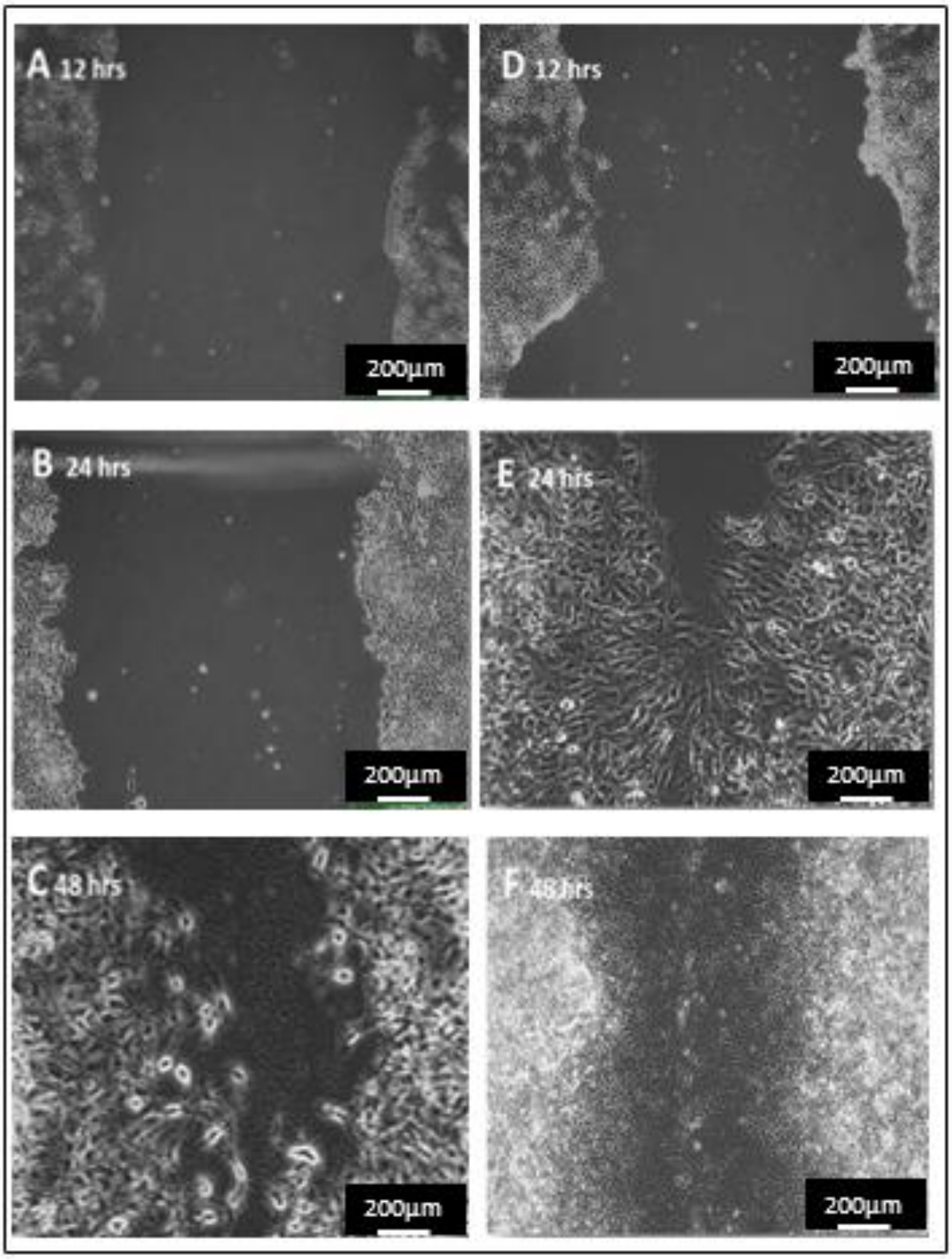

Figure 4.5: Scratch wound migration assay of SK-OV-3 cells. The figure depicts the migration of SK-OV-3 cells influenced by [A-C] normal pH_e/PO_2 and [D-F] low pH_e/PO_2. Representative images of scratch wound healing by migrating SK-OV-3 cells is shown under the influence of altered microenvironment. n = 5

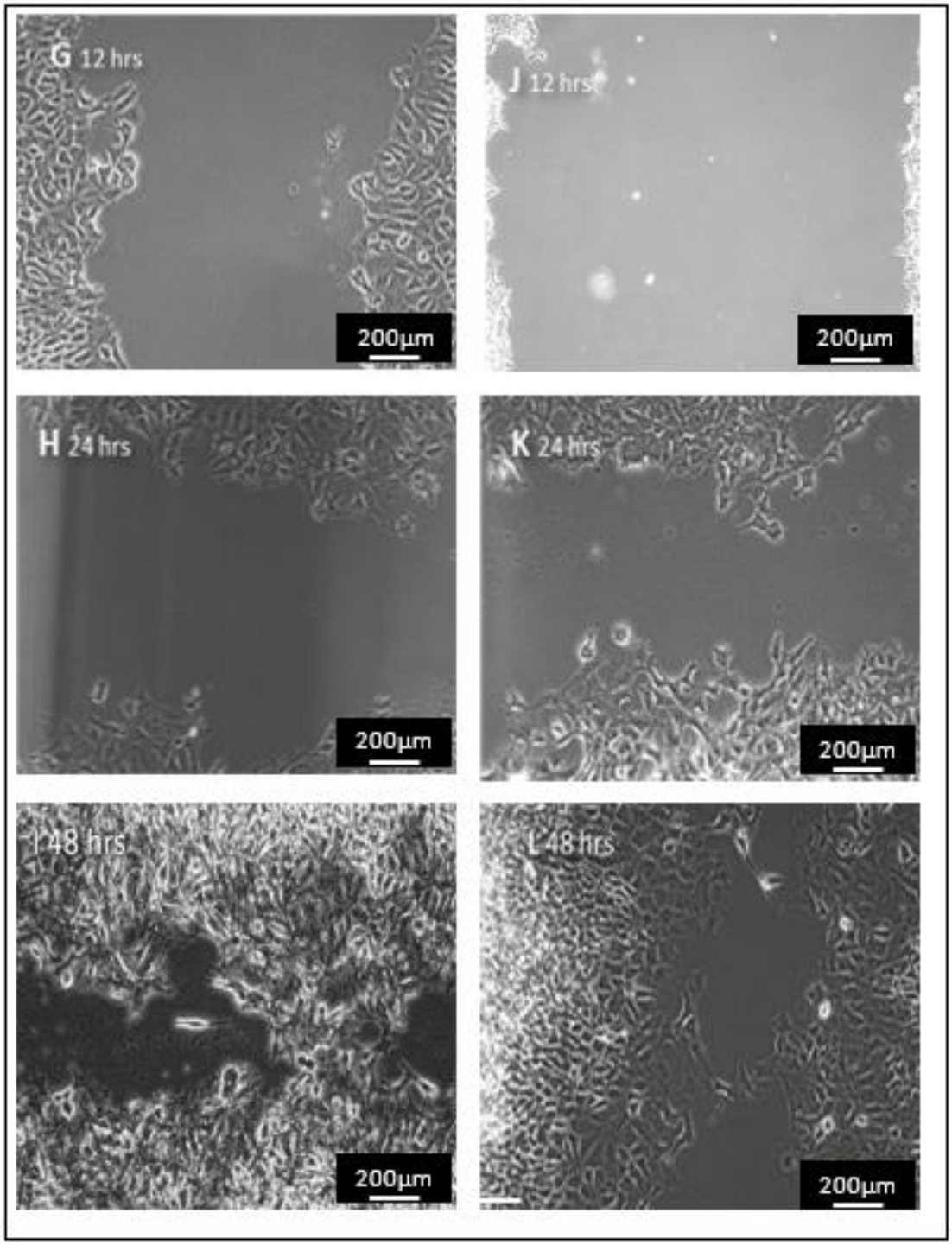

Figure 4.6: Scratch wound migration assay of MCF-7 cells. The figure depicts the migration of MCF-7 cells influenced by [G-I] normal pH_e & normal PO_2 and [J-L] low pH_e & PO_2. Representative images depicting scratch wound healing by migrating MCF-7 cells is shown under the influence of altered microenvironment. n = 5

Migratory potential of cancer cells under altered pH_e/PO_2 was assessed as a function of scratch wound healing (Section 2.6.1), observed over incubation time points (Figure 4.7). Significant ($P < 0.0001$) increase in migration was observed in both cell lines under altered pH_e/PO_2. SK-OV-3 cells showed significant ($P < 0.0001$) reduction in wound area after 24 and 48 hours of incubation in low pH_e & PO_2 compared to that in normal pH_e & PO_2. MCF-7 cells showed significant ($P < 0.0001$) reduction in wound area only after 48 hours of incubation in low pH_e & PO_2 compared to that in normal pH_e & PO_2 respectively.

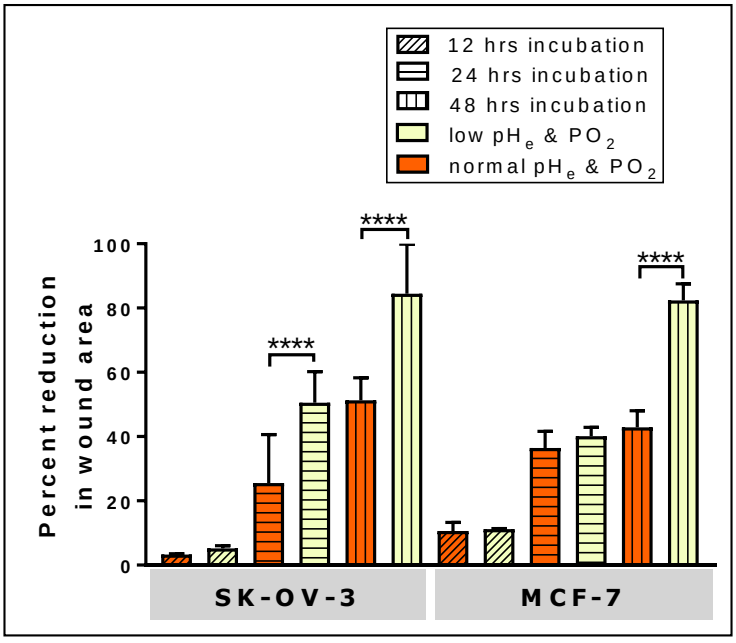

Figure 4.7: Effect of altered pH_e/PO_2 on migration (scratch wound assay) in cancer cells. Migratory potential of SK-OV-3 and MCF-7 cells after 12, 24 and 48 hours of incubation is represented. The migration of both cell lines in order to heal scratch wound was recorded under normal pH_e & PO_2 as well as low pH_e & PO_2. n = 5. (****= $P < 0.0001$)

4.2.4.2 Determination of the invasive and migratory potential of the test cancer cells across PCF membrane

The invasive and migratory potential of the MCF-7 and SK-OV-3 cells in altered pH_e and PO_2 was further tested using PCF membrane culture plate inserts (Section 2.6.2). The migration of MCF-7 cells maintained in low pH_e/PO_2 was significantly ($P < 0.0001$) greater than those maintained in normal pH_e & low PO_2 (Figure 4.8 A). Significant ($P < 0.01$) increase in migration was observed between cells maintained in low pH_e & PO_2 and low pH_e/normal PO_2.

Similarly, cells maintained in low pH_e & PO_2 migrated in significantly ($P < 0.001$) large numbers compared to those maintained in normal pH_e and low PO_2. Oneway ANOVA also showed that the pH_i of cells that migrated in low pH_e & PO_2 were significantly ($P < 0.01$ and $P < 0.0001$) greater than those maintained either in normal pH_e & PO_2 and low pH_e/normal PO_2. Similarly, the pH_i of cells that migrated in normal pH_e/low PO_2 were significantly ($P < 0.0001$) greater than those maintained either in normal pH_e & PO_2 and low pH_e/normal PO_2. A high pH_i ranging between 7.2 and 7.45 was observed only in the migrated MCF-7 cells that were maintained in normal pH_e with low PO_2 (Figure 4.8B).

Interestingly, for SK-OV-3 cells, although no significant difference was observed in the percent change in migration among different culture conditions (Figure 4.8A), their pH_i varied remarkably. Only SK-OV-3 cells maintained in normal pH_e & PO_2 showed significantly ($P < 0.0001$, $P < 0.001$ and $P < 0.01$ respectively) lower pH_i compared to those in low pH_e & PO_2, low pH_e/normal PO_2 and normal pH_e/low PO_2, respectively Figure 4.8B).

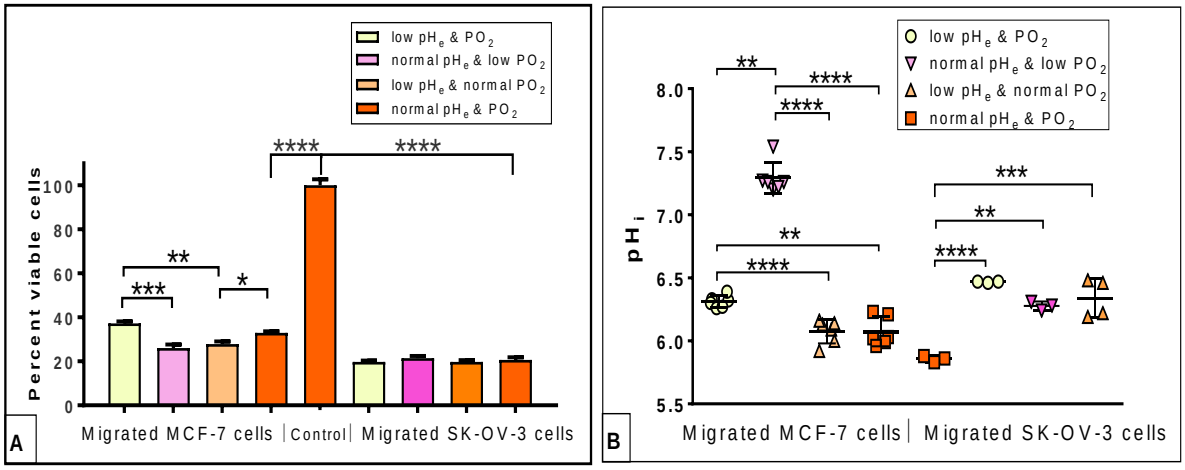

Figure 4.8: PCF membrane migration assay in cancer cell lines [A] Migration of MCF-7 and SK-OV-3 cells across PCF membrane towards FBS supplemented (Section 2.6.2) complete growth medium under alterd pH_e/PO_2. Initial seeding density of 1000 cells is taken as control. [B] Change in pH_i of migrated MCF-7 and SK-OV-3 cells in altered pH_e/PO_2 as mentioned in the main text. (* = P < 0.05; ** = P < 0.01; *** = P < 0.001; ****= P < 0.0001). n = 4

4.3 Discussion

In this chapter we aimed to describe the effect of altered pH_e/PO_2 on two hallmarks of tumour progression in relation to proliferation and migration, by testing the theory with altered microenviroment conditions developed through this study, on different cancer cell lines. Studies show that experimentally culture medium can be buffered with (1–40 mM) HEPES or bicarbonate/CO_2 system and the pH_e adjusted with 4M NaOH without introducing substantial changes in cellular metabolism (Hulikova, Vaughan-Jones and Swietach, 2011). As described in Chapter 3, the standardised concentration of $NaHCO_3$ helped yield and stabilise the intended pH_e according to the Henderson-Hasselbalch equation over 24-72 hours incubation periods to accommodate cell based assays (Hulikova, Vaughan-Jones and Swietach, 2011). Conventionally the concentration of $NaHCO_3$ for optimum stabilization of pH_e in a 5% CO_2 atmosphere was determined to be 1.5 g/L, started first in the early 1960's by American Type Culture Collection (ATCC). This helps to stabilise the pH of culture media within physiological range (7.2 -7.4) which is ideal for experiments that involve normal cell culture conditions that require physiological pH_e and atmospheric PO_2 (different from tumour microenvironment i.e. low pH_e & PO_2).

4.3.1 Implications of using culture conditions with altered pH_e and PO_2 to target cell proliferation

The uniqueness of this study lies in the transition from using normal pH_e & PO_2 only to harness the potentials of established culture conditions with low pH_e & PO_2, low pH_e/normal PO_2 and normal pH_e/low PO_2 (Chapter 3) to culture cancer cell lines for experimental assessment. In comparison to conventional protocols that are

commonly used to study both normal cells and cancer progression and metabolism alike, this approach is deemed useful in testing the assays specific to cancer viability, proliferation and migration in altered pH_e and PO_2. Thus, the developed cultured conditions were designed to provide a combination of the culture conditions (in accordance to Section 2.4.3) to evaluate the response of cancer cells cultured in environments simulating to *in vivo* tumour microenvironment.

We demonstrated for the first time how experiments conducted in four discrete culture conditions can help sequentially evaluate the requirement of altered individual components of the tumour microenvironment. Thus, we were able to distinguish if altered pH_e or oxygen tension alone and/or in combination influence cancer progression. Hence the culture conditions developed could help validate the use of different concentrations of $NaHCO_3$ as media buffer. The information presented can be used to develop and assess cancer models not only in low PO_2 (5% CO_2) but also allow us to test more realistic tumour microenvironment mimicking experimental models with increased PCO_2 (ATCC ®, 2011).

The rationale behind using PCO_2 more than 0.04 atm (35mm Hg) stems from the fact that interstitial fluid is known to maintain high PCO_2 values ranging between 59–84 mm Hg within various solid tumours (Gullino *et al.*, 1965; Martinez-Zaguilan *et al.*, 1996). In some studies involving 'Tissue Interstitial Fluid technique in murine tumour models, the PCO_2 value of 200 mm Hg was reached in the interstitial fluid of the tumour (Gullino, Clark and Grantham, 1964; Gullino *et al.*, 1965; Gullino, 1966; Hulikova, Vaughan-Jones and Swietach, 2011; Baronzio *et al.*, 2014). These

values are significantly high and correlate to approximately more than double the values in normal tissue (35-49 mm Hg); (Aller *et al.*, 2005).

The observations of this study demonstrated a substantial increase in oesophageal cancer cell viability during short term exposure to normal pH_e and PO_2 in comparison to low pH_e and PO_2 conditions. As observed in our study, it adds greater credence to an association between increased occurrence of oesophageal adenocarcinoma with prolonged acid suppression therapy in the treatment for acid reflux disease (McColl, 2006). The susceptibility of OE-19 cells to acidic pH_e and low PO_2 expose their vulnerability and probable lack or delay in recruitment of robust pH buffering mechanisms. We suggest that normal pH_e and PO_2 together provide a multifactorial yet beneficial role in the viability and development of oesophageal cancer. This finding contributes to the involvement of hypoxia as an additive factor to acidic pH_e contributing to oesophageal cancer senescence; a factor that conversely is not observed under the normal proliferative environment of oesophageal cancer cells. Hypoxia can be indirectly related to prevention of geroconversion (cell arrest to senescence) in cancer cells (Leontieva, Demidenko and Blagosklonny, 2014). The additional facilitation of low oxygen tension to promote cell viability and proliferation has been shown through inhibition of mTOR to suppress p21-induced senescence (Leontieva, Demidenko and Blagosklonny, 2014).

In contrast, a quick adaptive/compensatory response (within 24 hours) from ovarian and breast cancer cells to low pH_e and PO_2 was manifested as lack of significant change in their viability from that observed under normal pH_e and PO_2. This can be

explained by the hypoxia resistant characteristics of SK-OV-3 cells and the short population doubling time of MCF-7 cells observed at a low seeding density in their exponential growth phase (Sutherland, Hall and Taylor, 1983). The data from the 72 hours' exposure assay revealed that the long term growth advantage to cancer cells from acute drop in pH_e is potentiated with assistance from subsequent low PO_2, closely mimicking tumour microenvironment. The differential role of acidic pH_e on the array of cancer cells, demonstrated its time dependant influence that takes into account physiological factors including pH_i buffering capacity, acid extrusion potential and ability of the cancer cell to re-establish steady state pH_i (Swietach *et al.*, 2014).

Acute exposure to atmospheric PO_2 and pre-adjusted acidic pH_e has been shown to elevate expression of GRP78, CHOP, phospho-eIF2α, IRE-1α, spliced XBP-1, and phospho-JNK inducing ER stress on ER contributing towards a cumulative pro-apoptotic potential on MG-63 cells (Lee *et al.*, 2011). The study by (Lee *et al.*, 2011) used a culture condition similar to low pH_e & PO_2 modification of the culture condition developed in our study and thus the contribution of low oxygen tension was not investigated. However, unlike in our study design, (Lee *et al.*, 2011) demonstrated a reduction in the pH_e at the expense of nigericin induced proton extrusion. We suggest that irrespective of the method recruited to lower the pH_e, a reduction in cell viability of cancer cells in low pH_e alone can only reveal their growth potential in conditions that partially simulates tumour microenvironment. Hence our study contributed to fill this gap by further investigating the contribution of decreased oxygen tension in combination with low pH_e (closely mimics the cancer

microenvironment) on cancer cell viability. Thus results from our experiments demonstrated that the tumour microenvironment-simulating conditions have positive influence on the viability of breast adenocarcinoma and ovarian adenocarcinoma cells.

4.3.2 Influence of pH_i regulation in cancer cell proliferation

Through our observations, we demonstrated that the proliferation of cancer cells vary differentially as a function of altered cellular metabolism when exposed to a change in pH_e and PO_2. On short exposure to acidic pH_e, the increased proliferation of oesophageal cancer cells cultured in a normal PO_2 environment is a classic example of this phenomena. We infer that although acute exposure to low PO_2 alone promotes an initial steep growth spurt, long term maintenance in low PO_2 contributes towards the plateauing of the logarithmic growth phase. These observations also highlight the fact that cell seeding density is associated with the initial increase in logarithmic growth. It can be argued wthin reason that as the cell density increases, the growth impetus provided initially by the hypoxia in low pH_e decreases gradually as the competition for resource acquisition among viable cells increase.

The maintenance of cells in their exponential growth phase, post cell cycle synchronisation, contributed towards the short mean doubling time of homogenous population of MCF-7 cells when cultured in normal pH_e and PO_2 (Sutherland, Hall and Taylor, 1983). A short doubling time has been attributed to low seeding density and also when uninterrupted growth was allowed for up to a week in appropriate culture conditions (Lacroix and Lippman, 1980).

We conclude that acidification of the medium, assisted by the cellular metabolism and bicarbonate buffering system in high PCO_2, potentiates proliferation in cancer cells resistant to hypoxia. Thus at low cell densities during early phases of tumourigenesis, a drop in pH_e and oxygen tension due to poor perfusion, can potentiate pH_i regulation to influence cellular metabolism promoting rapid proliferation. Our data demonstrates that this phenomena can be attributed to hypoxia resistant ovarian cancer cells primarily at low densities. The proliferation rate constant and non-linear proliferation curve are important indicators that demonstrate how low pH_e and PO_2 favours proliferation in some cancer cells when they achieve a critical population density. Thus conventionally used normal pH_e and PO_2 condition to assess cancer proliferation can be inefficient to provide reliable proliferation data as they lack such growth promoting potential. Our data reiterates that even in the absence of adequate perfusion, an acidic pH_e in combination with low oxygen tension has minimal growth prohibiting influence at optimal cell density (equivalent critical mass of a tumour *in vivo*). However, we infer that at very low cell density, acidic pH_e and low PO_2 would not provide any advantage to cancer cell proliferation over normal interstitial microenvironment associated with the increased metabolism. Although low pH_e and PO_2 closely mimic tumour microenvironment, we demonstrated that cancers from different tissue origins have variable levels of susceptibility towards these altered conditions. In contrast, high susceptibility of oesophageal cancer cells to low PO_2 and acidic pH_e can be attributed to their embryological origin as they predominantly survive in atmospheric PO_2 and physiological pH_e. It can be inferred that tumour

microenvironment mimicking culture condition is equally efficient in promoting proliferation of viable breast cancer cells as normal pH_e and PO_2. Thus unlike normal cells breast cancer cells are resistant to the deleterious effects of low PO_2 and pH_e (although significantly less compared to ovarian cancer cells) and thereby retain proliferative potential.

4.3.3 Further implication of altered microenvironment on cell proliferation

Tumour cells are known to prevent cytosolic acidification (Gillies *et al.*, 1990) by activating different transporters, ion channels and proton pumps that extrude the protons produced during metabolism (Pei *et al.*, 2003; Asher *et al.*, 2011; Innamaa *et al.*, 2013). The proliferation of SK-OV-3 cells was increased in a low pH_e. Inhibitors of ion channels and proton pumps elicited a variant response from proliferation experiments with breast, oesophageal and ovarian cancer cells.

4.3.3.1 Role of acid sensitive K^+ channel inhibition

We demonstrated the increased anti-proliferative effect of methanandamide in cancer cells by inhibition of TASK-3 in the low pH_e with/without associated low PO_2 compared to physiological pH_e and PO_2 (Innamaa *et al.*, 2013). We suggest that this stems from the possible loss of TASK-3 mediated protection from cellular stress (Liu *et al.*, 2005) including low pH_e and low oxygen tension. It can be inferred that support provided by TASK-3 receptors to the cancer cell proliferation is attenuated with its pharmacological inhibition. The inhibitory curve of TASK-3 is known to be shifted by acidic values of 0.8 pH units more than other K_2P channels which lies in the 6.5 to 7.5 pH_e range (Pei *et al.*, 2003). TASK-3-blockade inhibited proliferation and appears to prevent the indirect interaction of these membrane proteins with

specific cellular mechanisms that modulate proliferation as shown by (Pardo and Stühmer, 2014). These include influencing the intracellular Ca^{2+} concentration or by regulating cell volume (Pardo and Stühmer, 2014). In our study, although the interaction between oxygen tension and pH_e is shown to promote cancer cell proliferation, their contribution is understood to be largely through modulation of pH sensitive membrane proteins. The growth promoting thrust provided by low oxygen tension (through oncogene activation and inhibition of tumour suppressors (Kunz and Ibrahim, 2003) is essential in the presence of low pH_e for disease progression. Our data reveals that the cells expressing acid-sensitive K_2P channel already affected by low pH_e and PO_2, exhibit increased vulnerability towards the respective channel inhibitors compared to those cultured in normal pH_e. To understand the contribution of methanandamide's CB1 receptor agonism in our results, experiments were carried out to validate the TASK-3 inhibitory response from methanandamide (using AM-251 (100nM, antagonist of CB1)). Although controversially this phenomena has been shown to be pro-proliferative (Hart, Fischer and Ullrich, 2004) and anti-proliferative (Olea-Herrero *et al.*, 2009) in cancer cells, our preliminary data implicates methanandamide at 0.1 µM (dose used in our study) produces a larger antiproliferative effect in SK-OV-3 cells when acting only through TASK-3 inhibition (Appendix 2VI). The dampening of the TASK-3 inhibitory effect of methanandamide from its unmasked CB1 receptor agonism was taken into consideration in this study.

4.3.3.2 Role of H^+/K^+ ATPase inhibition

The anti-proliferative effects of omeprazole on the end stage acidification in cancer cells has been widely investigated (Luciani *et al.*, 2004; De Milito *et al.*, 2010; Patlolla *et al.*, 2012; Ferrari *et al.*, 2013). In our study, the anti-proliferative effect being prominently observed after its long term exposure in acidic medium raises many questions. Firstly, the dose at which this effect was observed was chosen much lower than the conventionally administered inhibitory concentration for 50 percent cells (Luciani *et al.*, 2004). The delay in the action of activated omeprazole inhibits the acid release due to H^+/K^+ ATPase activity without neutralising already secreted acid (Im *et al*., 1985; Besancon *et al*., 1997). Hence the inhibition appears to be time dependant (long-term exposure) due to occupancy of the target site followed by buffering of the existing acid pool and then through inhibition of proliferation of the cancer cells. Although omeprazole is activated in acidic pH_e, we demonstrated that breast cancer cells evade the antiproliferative effects of omeprazole (at the standard dose used across all cell lines) after long term exposure to both normal interstitium and tumour microenvironment mimicking conditions. Interestingly, the pH_i profile of the viable breast cancer cells demonstrated that healthy physiological levels was maintained only under the influence of low oxygen tension and low pH_e. We suggest that during long term inhibition of H^+/K^+ATPase by omeprazole, the tumour microenvironment mimicking condition possibly contributes towards steady state pH_i recovery in breast cancer cells compared to an over compensation of pH_i regulation by normal pH_e and normal PO_2.

4.3.3.3. Role of HERG potassium channel inhibitor

Pharmacological inhibition of HERG channels demonstrated a significant inhibitory effect on ovarian and oesophageal cell proliferation at low pH_e irrespective of the PO_2. However, we demonstrated that both these growth conditions are effective in developing alarming resistance, specifically to breast cancer cells towards this pharmacological inhibitor. The altered microenvironment also has a differential influence on the antiproliferative effects of the inhibitor of HERG channels. A precisely pre-adjusted dose in low pH_e & PO_2 conditions appears to potentiate the inhibition of HERG channels in ovarian and in oesophageal cancer cells. However, under normal pH_e & PO_2 significantly ($P < 0.0001$) less effect of the inhibitor of HERG channels is observed in SK-OV-3 cells compared to oesophageal cells (figure 4.4D and F).

4.3.3.4 Role of proliferation on pH_i regulation

The effect of the methanandamide on the pH_i modulation of different cell types demonstrated the difference in metabolic capabilities of the cells in terms of pH regulation (Figure 4.4D, E and F). In our study the pharmacological inhibitors of HERG and TASK-3 channels had significant inhibitory effects on most cell lines at low pH_e and PO_2 over physiological conditions (Figure 4.4D, E and F). However, we demonstrated that both these growth conditions are effective in developing resistance, specifically to breast cancer cells towards these pharmacological inhibitors. The high pH_i of the surviving cells after drug exposure demonstrated their resistance to a fall in pH_e (Figure 4.4E).

We also demonstrated that the pharmacological inhibition of HERG and TASK-3 channels in hypoxia resistant ovarian cancer cells (SK-OV-3) have differential effects

on the pH regulation in response to an altered microenvironment (Figure 4.4D). In contrast to oesophageal cancer cells, ovarian cancer cells acquire a benefit from physiological pH_e and PO_2, to maintain steady state pH_i, even at the expense of a long-term exposure to these pharmacological agents (Figure 4.4C and F). We demonstrated through these studies that the hypoxia resistant ovarian cancer cells are inefficient in compensating for the pharmacologically induced loss of pH_i regulation.

The pH_i of the surviving ovarian cancer cells demonstrated their relatively impaired pH_i regulatory systems either in normal pH_e & PO_2 or in low pH_e & PO_2 respectively. This observation was analogous to that observed in oesophageal cancer cells in both microenvironmental modifications (Figure 4.4A, F, D and F). However, it can be argued that the near normal pH_i regulation in surviving breast cancer cells only, in the different alterations in the culture conditions may indicate the differential response of cancer cells of different tissue origin towards pharmacological inhibition of pH regulatory proteins. In summary, we conclude that an altered microenvironment has a differential influence on the antiproliferative effects of the inhibitors of pH regulators where a pre-adjusted dose in one condition can prove to be inefficacious in an altered condition. Further research can help in developing strategies to synchronise drug dosage or drug administration interval time, in combination with other inhibitors of pH regulatory systems by identifying multiple targets of cancer metabolism and pH modulation.

4.3.4 Migration and Invasion potential of cancer are influenced by pH_e

In this study we demonstrated how a change in pH_e assisted by a controlled oxygen tension and balanced bicarbonate-mediated buffering system can influence aggressive phenotypical development in cancer cells. We infer that ovarian cancer cells appeared to positively utilise a low oxygen tension coupled acidic pH_e that resulted in an increase in their migratory potential defined by the rate of 'scratch' or wound closure. The minimal permissible concentration of FBS was optimised to sustain viable cells and surface adherence but not adequate to promote proliferation (Cory, 2011).

Progression of cancer has been attributed to establishment of a low pH microenvironment which is a reversed pH gradient compared to non-malignant cells. It has been shown that a relatively low pH_e promotes aggressive development of tumours by inducing migration and invasion (Hanahan and Weinberg, 2000). Interestingly cancer cell processes including vesicle trafficking, contraction, migration, invasion and metastasis are hugely dependant on tight regulation of pH_i in response to pH_e. A diversion of pH_i on either end can impose deleterious impact on the movement of cancer cells and in turn influence metastatic potential of cancer cells (Hansen *et al.*, 2013).

In our study, the use of minimal FBS as a chemoattractant helped reduced selection bias for migratory potential of cells over their capacity to proliferate. The migratory potential of the test cells were further assessed subject to the influence of the dynamic and altered microenvironment. The observed phenomena that neither normal pH_e (at low PO_2) nor low pH_e (at normal PO_2) could not sustain cell adherence

in optimal FBS ruled out these culture conditions from being included in the assay. This observation addresses the fact that any change in migration of viable ovarian cancer cells requires the intervention of both pH_i regulation and optimum PO_2 control of the microenvironment.

The 130mm 'scratch'(250pixels = 66145 µm) created was reasonably traversed by more than ~50% of the ovarian cancer cells located near the wound boundary in normal pH_e only after adequate incubation time that exceeded their population doubling time (35 hours (SOP:SK-OV-3)). This observation could probably be attributed to reduced levels of nutrients, hormones, amino acids, sugars, and growth factors in the medium coupled with lack of dynamic remodelling of actin filaments at focal adhesion sites. These sites are known to be associated with high pH_i sensitive regulation which is critical at the leading edge of migrating cells (Stock and Schwab, 2009).

Furthermore, a higher pH_e would promote dynamic HCO_3^--dependent buffering, preventing extracellular matrix (ECM) remodelling and inhibiting acid-activated proteases to hinder tumour cell invasion and dissemination (Schonichen *et al.*, 2013). In contrast in low pH_e and low PO_2 the cells traversed midway between the 'scratch' wound within 24 hours to cover approximately 60µm from the wound boundaries. The low pH_e and the associated high PCO_2, (0.192 atm) exhausts the bicarbonate buffering system exercising its influence on regulation of the dynamics of integrin-ECM attachments as observed in fast migrating melanoma cells (Stock and Schwab, 2009).

The rate and extent of migration across PCF membrane was assessed in all culture conditions in test cells. From our data an inference can be drawn that that low pH_e and low PO_2 promotes maximum migration of MCF-7 cells (across the PCF membrane) significantly more than those maintained under normal pH_e and normal PO_2. We observed that substantial acidification of the media alone cannot promote the migratory potential in oestrogen receptor positive cell lines. The acidic pH_e of the tumour microenvironment represents a "niche engineering" (Estrella *et al.*, 2013) strategy to facilitate migration which is potentiated by hypoxia mediated induction of metastatic potential.

These mechanisms include HIF-dependent upregulation of transcription repressors of E-cadherin (Lu *et al.*, 2010), PERK/ATF4/LAMP3-arm of the unfolded protein response (Nagelkerke *et al.*, 2013), activation of LOX, MET and VEGFA (also induced by acidic pH_e (Fukumura *et al.*, 2001; Lardner, 2001; Xu, Fukumura and Jain, 2002) that promotes local invasion and subsequent *in vivo* growth of malignant tumours. Our data also provides a basic understanding that a drop in the pH_e alone might not provide a selection benefit for the migratory together with invasive potential. Apparently low PO_2 did not provide a further benefit to the migration of breast cancer cells (although originally obtained from metastatic site) that were maintained in physiological pH_e.

4.3.5 Influence of pH_e on migratory potential of cancer cells

The results in this chapter describe the alteration of pH_i of migrated cancer cells loaded with pH sensitive nanosensors. The lowest recorded pH_i was observed in the normal PO_2 and normal pH_e condition implying the amount of proton accumulation

in these cells upon migration across the PCF membrane. Normal pH_e in a low PO_2 environment, facilitates significantly less migration in breast cancer cells. However only under low PO_2 does normal pH_e enable the cells to regain physiological pH_i after migration. When compared to normal pH_e and PO_2, a substantial drop only in the ambient PO_2 induces a rise in pH_i of migrated target cells. This highlights the interaction of PO_2 in pH_i homeostasis of migrated cells to maintain steady state pH_i facilitating cellular functions. Marginal increase in the pH_i was observed in the breast cancer cells that demonstrated maximum migration.

Although the pH_i recorded with cells from low pH_e and low PO_2 was also acidic, and was significantly higher than the pH_i of cells maintained in physiological PO_2 and pH_e. Previous studies have demonstrated how an internal proton gradient is maintained by cancer cells to establish the direction of movement during migration (Figure 1.6 in the thesis) (Koltai, 2016). Furthermore, the micromanagement of the local pH gradient across the cell surface of the plasma membrane has been shown to be dependent on proton exchange under constant pH_e (Stock et al., 2005; Stüwe et al., 2007). In addition our data demonstrate that altered pH_e affected migration of cancer cells which resulted in differential pH_i. Thus the present data indicates that the acidic intracellular milieu could be a consequence of modulation of cellular processes throughout the process of migration. We propose that this accumulated acid may be dumped by the cells upon migration into newly migrated location with physiological pH_e, subsequently inducing niche engineering. Interestingly, the only survival advantage in terms of steady state pH_i regulation was provided from physiological pH_e when the oxygen tension of the microenvironment is reduced.

Our data suggests that although the individual culture conditions introduced different dynamics of pH_i equilibration, they maintain 80 - 90% viability of the migrated target cells.

The limitations of this study is inadequate use of proliferation and viability markers that could be more informative on the effect of the dynamic microenvironment on the cancer hallmarks. Further analysis of population data on cell cycle analysis could be of much use in assessing the role of microenvironment on cancer cell metabolism.

In summary our observations indicate that viability of the cancer cells is increased by substantial drop in the pH_e and oxygen tension that closely mimic the *in vivo* conditions existing in most solid tumours. While proliferation of viable cancer cells is also largely positively influenced by this condition, optimum cell density and confluence plays a major role in modifying this response in their favour.

Moreover, proliferation rate differs among different cancer cells in response to altered microenvironment. This study elucidated how cancer cell's response to inhibition of pH sensitive and regulatory proteins is altered drastically under altered pH_e and PO_2. This cautions the controlled use of conventional cell culture conditions over strategies tailored to cancer microenvironment for relevant outcome in cancer research.

The migration studies revealed how the contribution of low oxygen tension potentiates the pH_e induced migratory potential in cancers. We demonstrated that maintenance of steady state pH_i in viably cancers depends heavily on the environment and is affected by cancer proliferation and migration. In accordance to

this it is important to investigate the indicators of pH regulation in cancer and how they differ in altered pH_e and oxygen tension as is explained in the following chapter.

Chapter 5. The effect of pH on acid buffering and extrusion.

5.1 Introduction

Enhanced rates of proliferation, migration and invasion are metabolically exhaustive processes that demand strict control of pH buffering in cancer cells (described in Chapter 4). The extrinsic ($NaHCO_3$-dependent) and intrinsic ($NaHCO_3$-independent) buffering potentials (Section 2.11.1) have been independently studied to evaluate their functional role in pH regulation of normal tissues and cancer cells mostly under physiological conditions (Amos and Richards, 1996). However, there are limited studies on the interaction of such pH-buffering mechanisms with (a) overall acid extrusion and (b) steady-state pH_i restoration in a modified tumour microenvironment involving simultaneous alterations in pH_e as well as oxygen availability (Hulikova, Vaughan-Jones and Swietach, 2011; Swietach *et al.*, 2014).

A commonly used technique to test the pH regulatory potential is to challenge cells with an ammonium pre-pulse (APP) manoeuvre (Section 1.81, Section 2.11.1). This provides a way in which to measure subsequent acid extrusion and pH_i adjustment by cells in order to identify differences in pH buffering potentials between normal and cancer cells (Roos and Boron, 1981; Boyarsky *et al.*, 1988a; Amos and Richards, 1996). Thus, by experimentally challenging the pH regulating system using weak acids in a $NaHCO_3$ free environment (by replacing $NaHCO_3$ with HEPES buffer to block the extrinsic buffering mechanism of cells), one can evaluate the intrinsically active buffering capacity (β_i; Section 2.11.1.1) of cancer cells in comparison to their normal counterparts. The role of extrinsic buffering mechanism in pH regulation has

been studied previously by performing APP in cells maintained in $NaHCO_3$ containing medium (Roos and Boron, 1981; Boyarsky *et al.*, 1988a; Hulikova, Vaughan-Jones and Swietach, 2011; Swietach *et al.*, 2014). Although these studies revealed the role of the extrinsic buffering mechanism in normal as well as colorectal, breast and pancreatic cancer derived cells, primarily with respect to specific pH regulatory systems and proteins, the role of the intrinsic buffering mechanism in pH regulation and its interaction with alterations in pH_e and PO_2 is poorly understood. Moreover, the sites of pH_i oscillations within the cytosol due to an altered microenvironment may shed light on pH regulation in cancer cells.

Additionally, the rate of pH_i recovery (measured as change of pH over time, i.e. $\Delta pH/\Delta time$, Section 2.11.1.2) after APP may be estimated in the presence or absence of $NaHCO_3$ in an environment of altered pH_e and oxygen tension. This will help in evaluating the collective contribution of all pH regulators in the net acid extrusion potential (Section 2.11.1.3) of the test cells.

Interestingly, complex cellular metabolic processes have been shown to regulate the distribution of metabolically active organelles like mitochondria (Corrado, Scorrano and Campello, 2012). However, the potential role of pH_i oscillations in the dynamics and spatial distribution of this metabolically active organelle in response to altered tumour microenvironment needs elucidation.

5.1.1. Aims

The aims of this chapter were to use the 'Ammonium pre-pulse' manouvre in ovarian (SK-OV-3), breast cancer cells (MCF-7) and the non-tumourigenic breast cell line (MCF-10A, control) in altered pH_e/PO_2 to:

a) Determine the time course of pH_i maintenance and pH_i regulation in HEPES versus $NaHCO_3$ buffered extracellular solutions.

b) Determine and compare β_I in HEPES buffered extracellular solution.

c) Estimate pH_i recovery rates in HEPES compared to $NaHCO_3$ buffered extracellular solution.

d) Derive the net acid extrusion (NAE) in HEPES and $NaHCO_3$ buffered extracellular solution.

e) Map the distribution of pH_i in the cell lines using widefield fluorescence microscopy in a live cell imaging setup and determine associations between intracellular zones of pH_i oscillations with the spatial distribution of mitochondria in test cancer cell lines under altered pH_e/ PO_2.

5.2 Results:

In order to study how the established cancer cell lines SK-OV-3 and MCF-7 regulate their pH_i in response to altered pH_e/PO_2, the ammonium pre-pulse technique combined with live-cell imaging and fluorometric measurement respectively was used.

Calibration of the pH-sensing fluorescence dyes: As for all experiments assessing pH effects, described in this thesis, calibration of the pH-nanosensor probe and pH-sensing dyes used for evaluation of pH_i, was performed before each experiment on SK-OV-3 cells, MCF-7 and MCF-10A cells (Section 2.8). The mean pK_a values were 5.5 - 5.7 (n = 12) for the pH-nanosensor probe and 7.0 - 7.2 (n = 8) for cSNARF-AM dyes. These values are derived from the curve fit to non-linear regression for each pH sensing probe/dye and are consistent with published data (Graber *et al*., 1986; Ozkan and Mutharasan, 2002; Desai *et al*., 2013). Moreover, as part of validation, the test pH_i values of the three cell lines were also ratiometrically measured using BCECF-AM pH sensing dye to detect the efficiency of cSNARF-AM dye and pH-nanosensor probe.

5.2.1 Time course of pH_i regulation from acute acid overload under altered pH_e/PO_2

5.2.1.1 pH_i regulation of cancer cells in HEPES ($NaHCO_3$-independent) buffered media

To study the intrinsic pH buffering potential (β_i) and transmembrane extrusion of acid in SK-OV-3 and MCF-7 cells, pH_i recovery from an intracellular acid load was characterised in cells maintained in $NaHCO_3$-free (HEPES buffered) media with

normal and low pH_e & PO_2. The response of MCF-10A cells to an ammonium pre-pulse (Section 2.11.1) in normal pH_e and normal PO_2 was taken as normal control. Low pH_i was attained using the ammonium pre-pulse technique in all cells. The response to acid loading following an ammonium pre-pulse was characterised by a sharp decrease in pH_i which returned to normal pH_i on washing with HEPES buffer (Figure 5.1 A-D). Figure 5.1A illustrates the time course of response to APP in SK-OV-3 and MCF-7 cells in normal pH_e and normal PO_2. On comparing the change in pH_i due to acidification, both cell lines demonstrated a significantly ($P < 0.01$ for SK-OV-3 and $P < 0.05$ for MCF-7) greater acidification than MCF-10A control (Figure 5.1 A, B). Interestingly, SK-OV-3 cells also underwent a significantly ($P< 0.001$) larger acidification compared to MCF-7 cells (Figure 5.1 A).

In the case of SK-OV-3, the recovery to steady state pH_i is characterized by an alkalinisation within 10 minutes' post washout which is faster than that observed in MCF-7 and MCF-10A cells. Compared with SK-OV-3 cells, the acidification response of MCF-7 cells to the ammonium pre-pulse was much shallower, indicating a faster buffering mechanism compared to SK-OV-3 cells (Figure 5.1A).

Figure 5.1B indicates that in low pH_e/normal PO_2 conditions, SK-OV-3 cells still recorded an increased rate of acidification compared to MCF-7 cells, after NH_4Cl washout. Under these conditions SK-OV-3 cells had the fastest pH_i recovery rate (0.115 mM/min) > MCF-7 (0.059 mM/min) > MCF-10A control (0.127 mM/min). In contrast, low pH_e appeared to delay the complete pH_i recovery in MCF-7 cells under normal PO_2 (Figure 5.1B).

Furthermore, MCF-7 cells persistently maintained a low baseline steady state pH_i when PO_2 was lowered from normal values to 0.029 atm (i.e. low PO_2) irrespective of the pH_e (Figure 5.1 C, D). Interestingly, under low PO_2, the acidification of MCF-7 cells post NH_4Cl washout was larger than MCF-10A control only upon lowering the pH_e from normal to 6.3 (low pH_e). Low pH_e and low PO_2 also promoted the pH_i recovery rate in MCF-7 cells (0.018 mM/min) which was similar to MCF-10A control (Figure 5.1D).

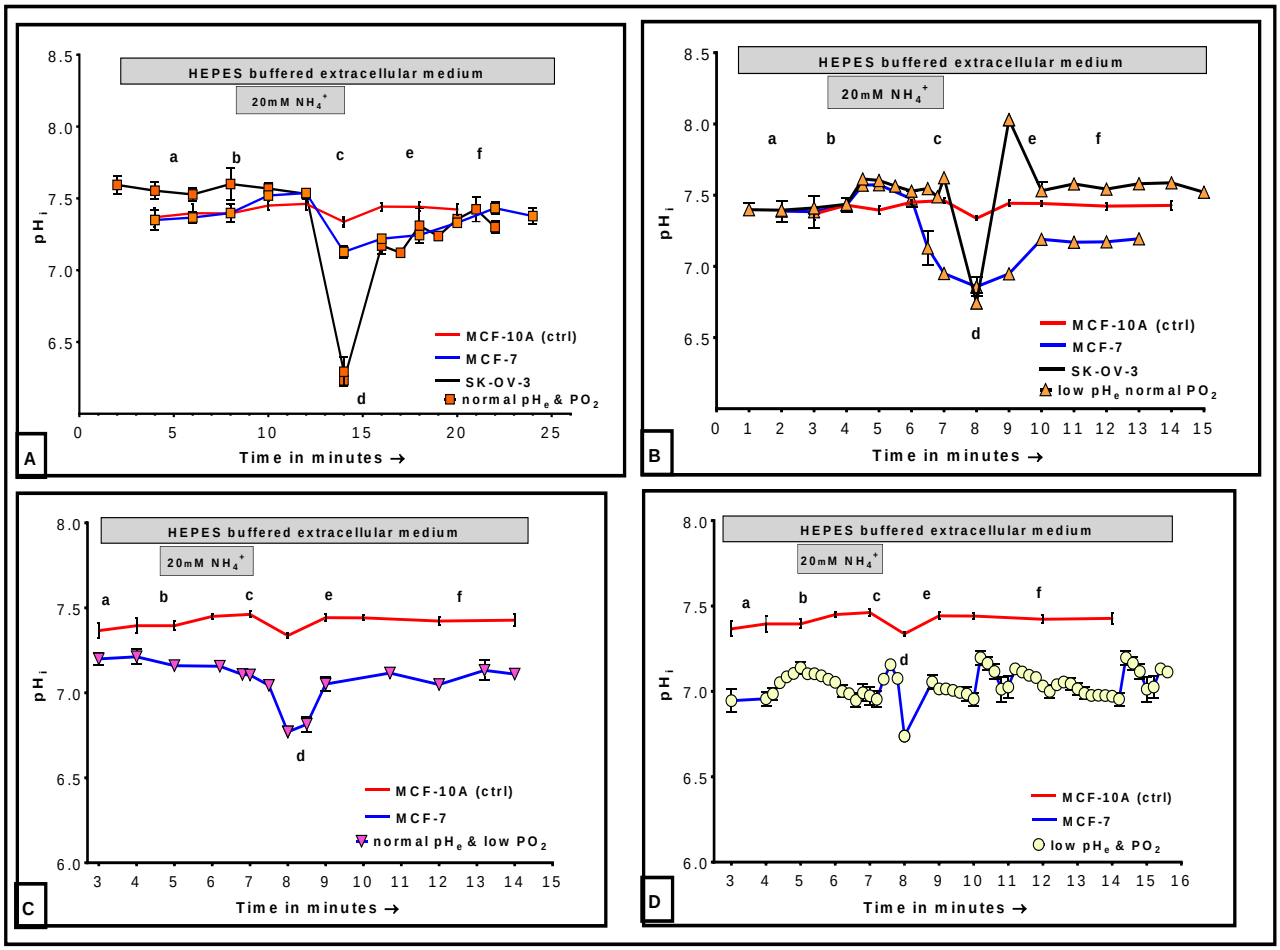

Figure 5.1: pH_i regulation by the $NaHCO_3$-independent component of cancer cells in altered pH_e and PO_2.

Time course of pH_i recovery in HEPES buffer- of SK-OV-3, MCF-7 cells in [A] normal pH_e& PO_2 [B] low pH_e/normal PO_2;- of MCF-7 cells only in [C] normal pH_e/low PO_2 [D] low pH_e & PO_2; -of MCF-10A (control) in [A] – [D] normal pH_e &.PO_2 .Letters '*a, b, c, d, e and f*' indicate the timepoints at which data were compared. n = 8.

5.2.1.2 The pH_i regulation of cancer cells in $NaHCO_3$ buffered medium ($NaHCO_3$ dependent component)

The time course of pH_i regulation in $NaHCO_3$ buffered medium was only aimed at deriving the extrinsic buffering capacities (β_{HCO_3}) of the cancer cell lines. The derivation of the NAE (Section 5.2.4) takes into account the β_{HCO_3} and β_I. The pH_i recovery from an ammonium pre-pulse in $NaHCO_3$ buffered media differed between SK-OV-3 and MCF-7 cells. Specifically, after NH_4Cl washout, a large drop in pH_i was observed in MCF-7 cells compared to SK-OV-3 and MCF-10A cells, under normal pH_e & PO_2 (Figure 5.2A). This manoeuvre was aimed to elucidate the response of the test cells, involving $NaHCO_3$-dependent flux of ion species that largely function extrinsically. The pH_i recovery was also delayed in the order MCF-7 > SK-OV-3. For SK-OV-3 cells, normal PO_2/low pH_e promoted increased acidification from the ammonium pre-pulse (Figure 5.2B). However, compared to MCF-10A control cells (Figure 5.1), pH_i recovery in SK-OV-3 and MCF-7 cells was incomplete under normal PO_2 conditions, irrespective of the pH_e. Low PO_2 consistently accelerated acidification and pH_i recovery from an ammonium pre-pulse in MCF-7 cells (Figure 5.2C, D).

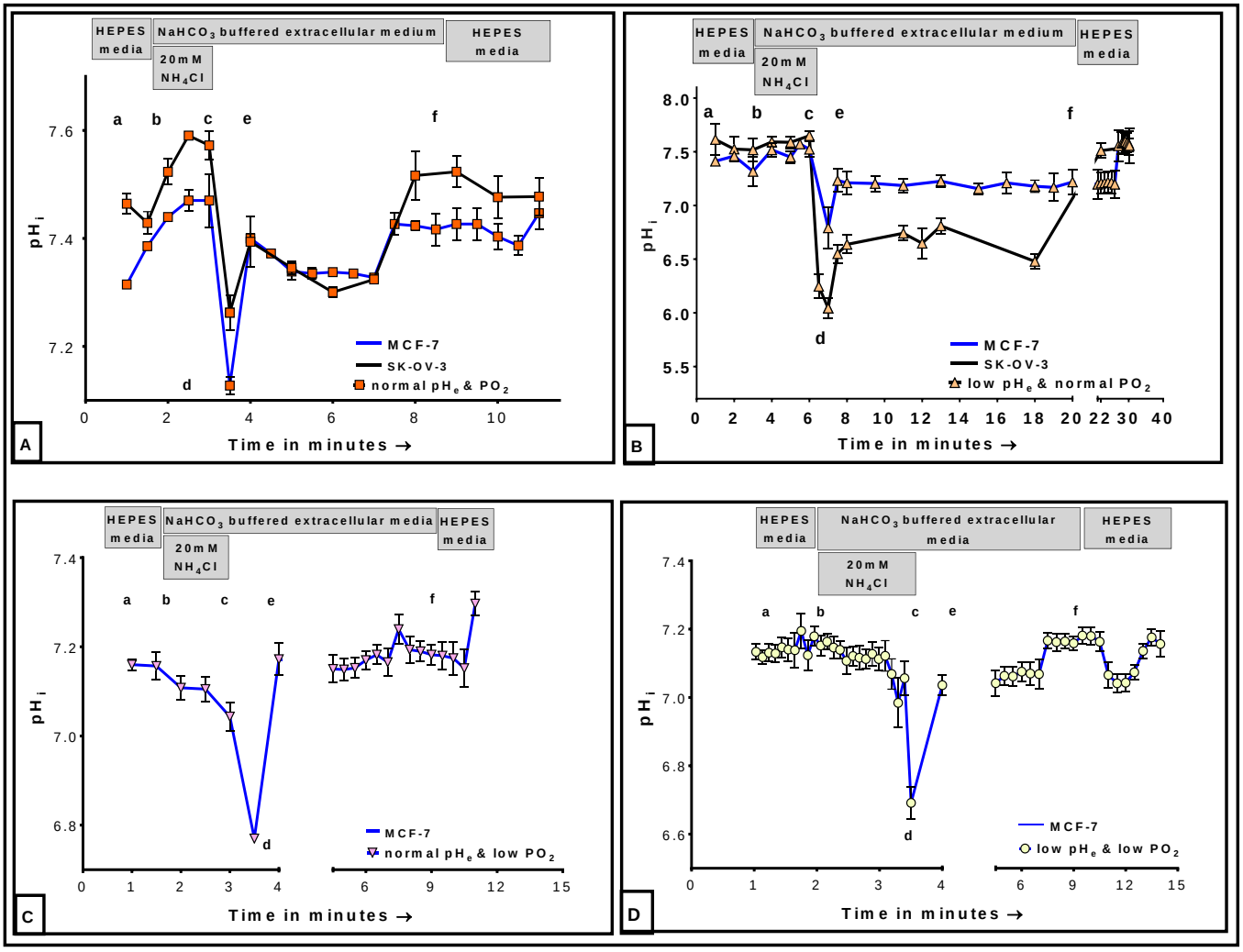

Figure 5.2: pH_i regulation by the $NaHCO_3$-dependent component of cancer cells in altered pH_e and PO_2.

Time course of pH_i recovery (to achieve steady state pH_i) of SK-OV-3 and MCF-7 cells in 22mM $NaHCO_3$ buffered medium at [**A**] normal PO_2 & pH_e; [B] low pH_e/normal PO_2; [**C**] normal pH_e/low PO_2 and [**D**] low pH_e/PO_2. Indicated with '***a, b, c, d, e and f***' are the points compared between conditions and cell lines as described in the main text. n = 10

5.2.2 Determination of β_I of cancer cell lines in HEPES buffered media under altered pH_e/PO_2

The β_I was computed (Section 2.11.1.1) from the pH_i values obtained for SK-OV-3, MCF-7 and MCF-10A cells in response to the ammonium pre-pulse (Figure 5.1 A-D). The β_I values shown in Figure 5.3A illustrates the β_I (0.24 ± 0.12 mM/pH) observed in SK-OV-3 cells, maintained in normal pH_e and normal PO_2. This indicates that the

cells are mobilising 0.2 to 0.4 mM of pH equivalents for every pH point shift. Furthermore, this dependence increases (β_I = 0.73 ± 0.20 mM/pH) in normal PO_2 only with a simultaneous decrease in the pH_e to 6.3.

In contrast to MCF-7 cells, the β_I of SK-OV-3 cells showed a significant increase ($P < 0.0001$) with a decrease in the pH_e under atmospheric PO_2 (Figure 5.3 A, B). Interestingly, significantly higher values for β_I (91.3 ± 4.24 mM/pH) in MCF-10A cells (in normal pH_e/PO_2) and β_I (83.2 ± 4.16 mM/pH) in MCF-7 cells (in normal pH_e/low PO_2; Figure 5.3C) were observed when compared to SK-OV-3 or MCF-7 cells maintained in all other conditions.

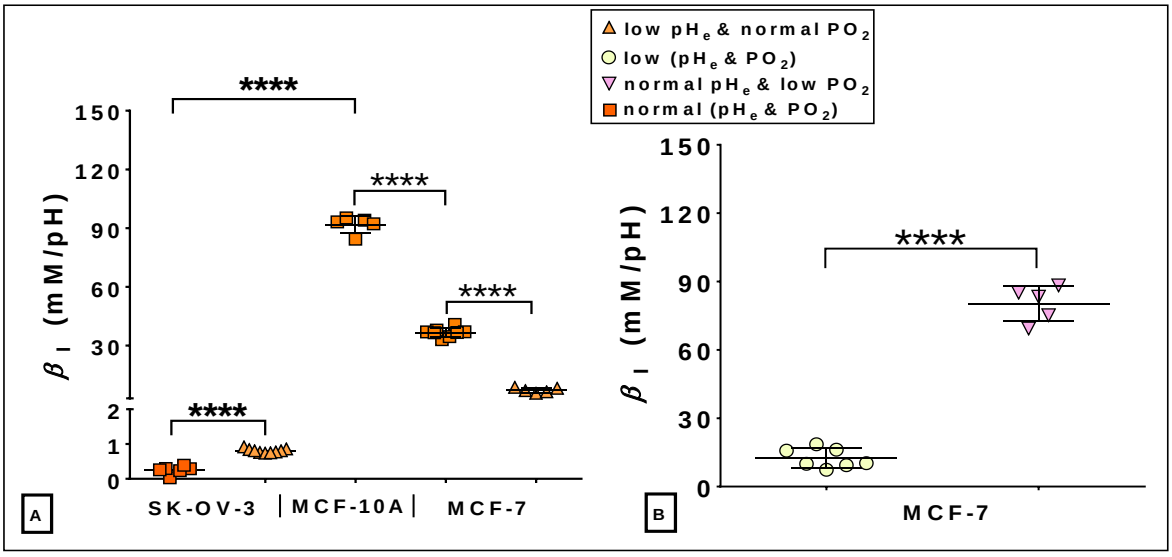

Figure 5.3: β_I of SK-OV-3, MCF-7 and MCF-10A cells in altered pH_e/PO_2 in HEPES buffered medium. β_I was measured for SK-OV-3 and MCF-7 cells [**A**] at either normal pH_e/PO_2 (orange squares) or low pH_e normal PO_2 (orange triangles) and [B] for MCF-7 cells in low pH_e/PO_2 (yellow circles) or normal pH_e/low PO_2 (inverted purple triangles). The β_I of MCF-10A cells measured in normal pH_e/PO_2 was taken as control. * = $P < 0.05$; **** = $P < 0.0001$. n = 6

5.2.3 Estimation of the 'Rate of recovery' of cancer cells from acute acid loading in HEPES buffered medium under altered pH_e/PO_2

The rate of pH_i recovery from acute acid loading in MCF-7 and SK-OV-3 cancer cells in HEPES buffer (i.e. $NaHCO_3$-independent buffering) was not significantly different ($P > 0.05$) from MCF-10A control (summarised in Table 5.1).

SK-OV-3		MCF-7				MCF-10A ctrl
HEPES buffered media						
normal pH_e normal PO_2	low pH_e normal PO_2	normal pH_e normal PO_2	low pH_e normal PO_2	normal pH_e low PO_2	low pH_e low PO_2	normal pH_e normal PO_2
0.09 ± 0.001	0.115 ± 0.001	0.06 ± 0.011	0.06 ± 0.01	0.05 ± 0.01	0.02 ± 0.001	0.13 ± 0.001
$NaHCO_3$ buffered media						
0.12 ± 0.003	0.39 ± 0.001	0.07 ± 0.001	0.34 ± 0.001	0.53 ± 0.08	0.15 ± 0.001	

Table 5.1: pH_i recovery rate (pH/min) of cancer cells maintained in altered pH_e and PO_2.
The pH_i recovery rate of SK-OV-3, MCF-7 and MCF-10A cells in altered pH_e/PO_2 is represented. The data was obtained from ammonium pre-pulse experiments performed independently in HEPES or $NaHCO_3$ buffered media. n = 6

This observation was consistent in HEPES buffered media only (Figure 5.4). However, we noted that in the presence of $NaHCO_3$ dependent pH buffering, normal pH_e and normal PO_2 failed to provide any additional benefit to modify their pH_i recovery. In contrast, significantly ($P< 0.0001$) increased rates of pH_i recovery in SK-OV-3 (normal PO_2/low pH_e only) and MCF-7 cells (normal PO_2/low pH_e and low PO_2/normal pH_e) were observed when $NaHCO_3$-dependent pH buffering was provided to recover pH_i from acute acid loading (Figure 5.4).

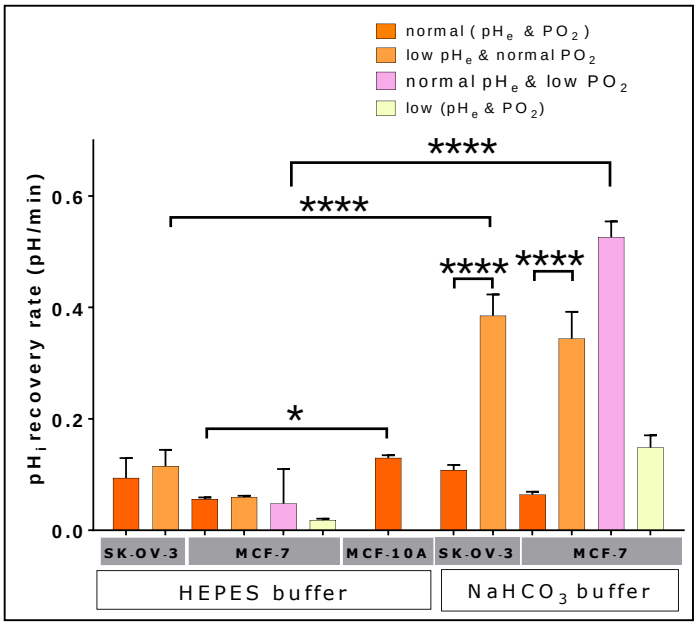

Figure 5.4: pH_i recovery rates of SK-OV-3, MCF-7 and MCF-10A cells in altered pH_e/PO_2 in HEPES and $NaHCO_3$ buffered medium.
The rate of pH_i recovery in HEPES/$NaHCO_3$ buffered medium following acute acid loading of SK-OV-3, MCF-7 and MCF-10A (control) cells under conditions noted in graphs. * = $P < 0.05$; **** = $P < 0.0001$. n=6

5.2.4 Derivation of NAE of cancer cells from HEPES and $NaHCO_3$ buffered medium with altered pH_e and PO_2

NAE of SK-OV-3, MCF-7 and MCF-10A cells was calculated as described by (Roos and Boron, 1981; Hulikova, Vaughan-Jones and Swietach, 2011) (Section 2.11.1.2 and 2.11.1.3). Results are summarised in Figure 5.5. A maximum increase in NAE was observed in MCF-7 cells (under low pH_e & PO_2) followed by SK-OV-3 cells (normal pH_e & PO_2). Among all other conditions tested, low pH_e & PO_2 provided the maximum benefit to MCF-7 cells in promoting their NAE capacity. However, low pH_e significantly ($P < 0.05$) decreased NAE in MCF-7 and in SK-OV-3 cells under normal PO_2 environment, compared to MCF-10A control. MCF-7 cells also underwent a maximum increase in NAE ($P< 0.0001$) at low pH_e & PO_2, compared to normal

control. However, exposure to low pH_e & PO_2 promoted minimal transmembrane acid extrusion in cancer cell lines (summarised in Table 5.2).

	normal pH_e normal PO_2	**low pH_e normal PO_2**	**normal pH_e low PO_2**	**low pH_e low PO_2**
SK-OV-3	3.929 ± 0.078	0.097 ± 0.002	ND	ND
MCF-7	1.639 ± 0.003	0.556 ± 0.01	0.729 ± 0.001	5.326 ± 0.071
MCF-10A ctrl	0.119 ± 0.003	ND	ND	ND

Table 5.2: NAE (mM/min) of cancer cells maintained in altered pH_e and PO_2.
The NAE capacity of SK-OV-3, MCF-7 and MCF-10A cells is represented. The data was obtained from ammonium pre-pulse experiments performed in altered pH_e/PO_2. n = 6

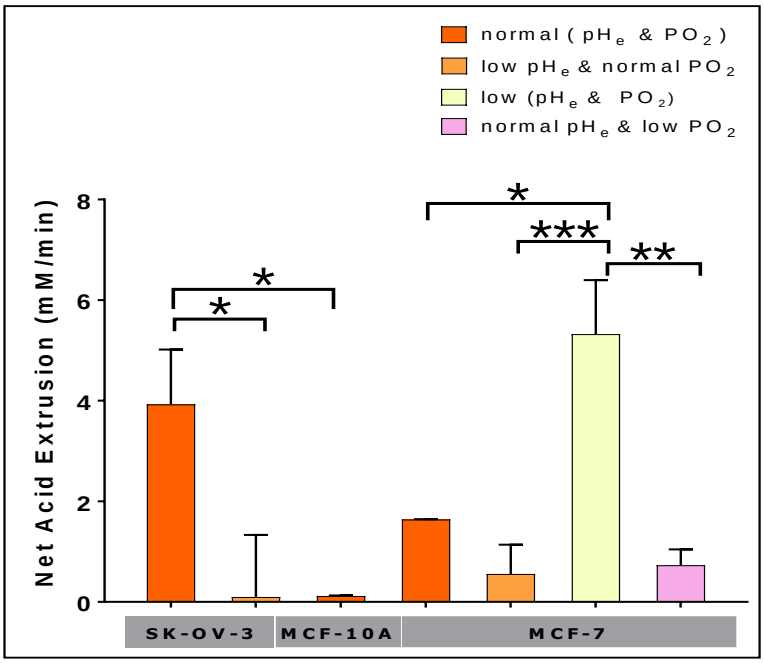

Figure 5.5: NAE of SK-OV-3 and MCF-7 cells in altered pH_e/PO_2.
The NAE in following acute acid loading of SK-OV-3, MCF-7 and MCF-10A cells under conditions are noted in graphs. NAE of MCF-10A in HEPES buffered media was considered as control. * = P< 0.05; ** = P< 0.01; *** = P< 0.001. n = 8.

5.2.5 Mapping the distribution of pH_i oscillations in localised areas within cancer cells

The distribution of protons across the intracellular regions of the target cells was mapped using cSNARF-AM pH-sensing dye (Section 2.11.1.4) to compare areas of high and low pH in steady-state and in response to an acute change in the surrounding pH_e (n = 3). Figure 5.6 shows the raw (A) and processed (B) images of a representative SK-OV-3 cell from a monolayer, recorded in HEPES buffer at normal pH_e & PO_2.

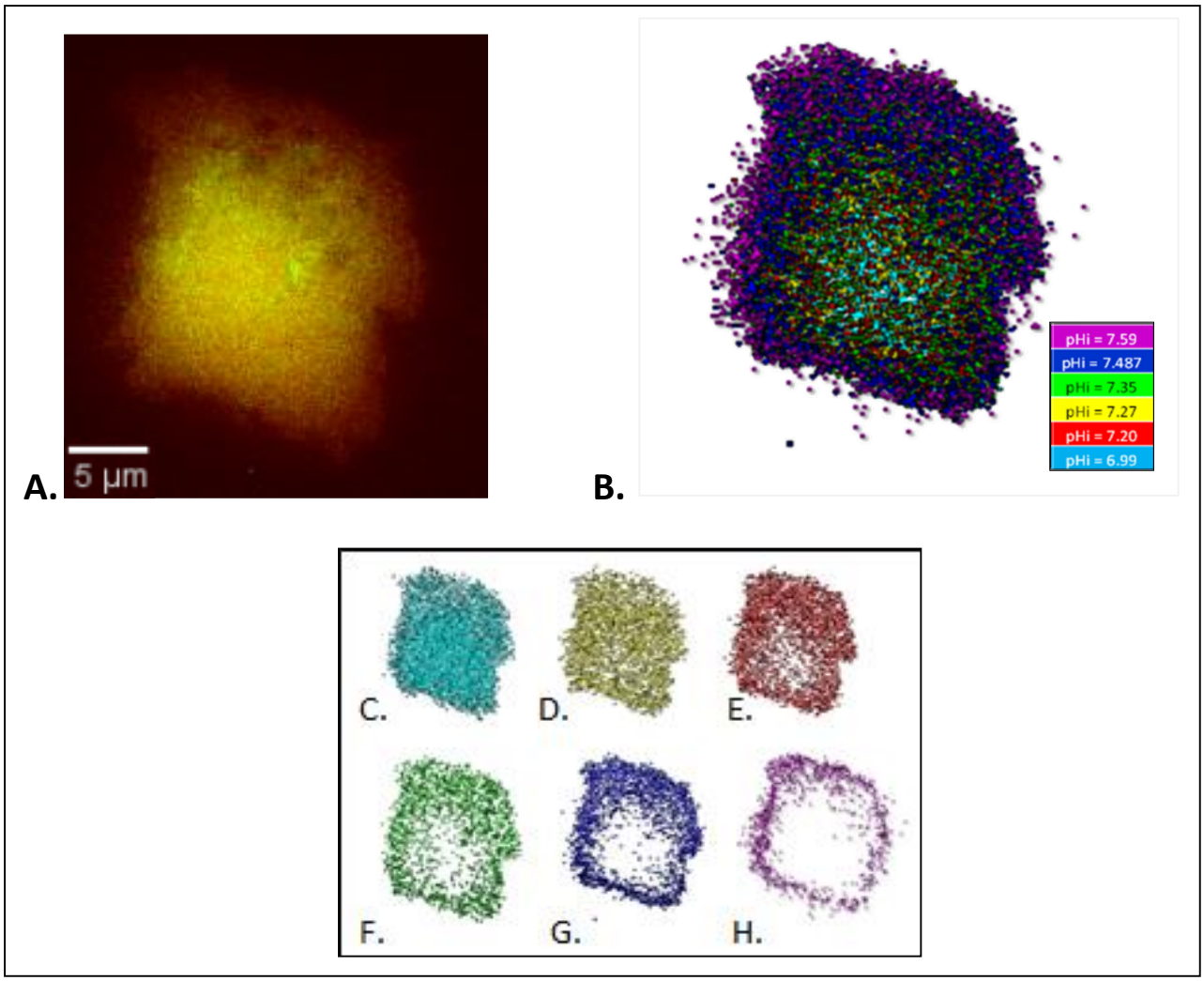

Figure 5.6: Representative processed image of a SK-OV-3 cell cultured in normal pH_e & PO_2. Images were acquired using (A) wide field microscope representing pH_i distribution (B); heat map of pH_i; (C-H) Individual pH_i areas of the composite image.

It was observed that the boundary of this representative cell was depicted by a lower composite value (representing high pH_i values) which corresponds to the regions shown in Figure 5.6 C - H. The complete pH_i heat-map of superimposed pH signal (Figure 5.6 B) shows how the central region of the cell predominantly contains a higher proton concentration.

The ammonium pre-pulse manoeuvre (Section 2.11.1) was also used to determine the pH_i distribution within a cluster of (n = 5; Figure 5.7) SK-OV-3 cells in low pH_e/normal PO_2. The overall pH_i of the cluster is 7.47 as established by the regions

depicted in insets D and E (Figure 5.7). Regions of very high alkaline pH are virtually absent in inset H (Figure 5.7). Pockets of very high proton concentrations are represented by inset C (Figure 5.7). Inset B (Figure 5.7) displays the composite superimposed image of pH_i.

Finally, Figure 5.8A depicts a representative wide field image of signals from the pH sensing dye from the monolayer of non-neoplastic MCF-10A cells. Some cells appear to selectively exhibit very low or very high pH values as computed from the signal differences. The processed image representing the distribution of protons across the cell as in Figure 5.8 B is a composite of superimposed images of signals from each pH_i value ranging from 7.74 to 8.82. The overall pH_i of the cells was recorded to be relatively alkaline (8.41 pH) after dumping the acid loaded by the ammonium pre-pulse.

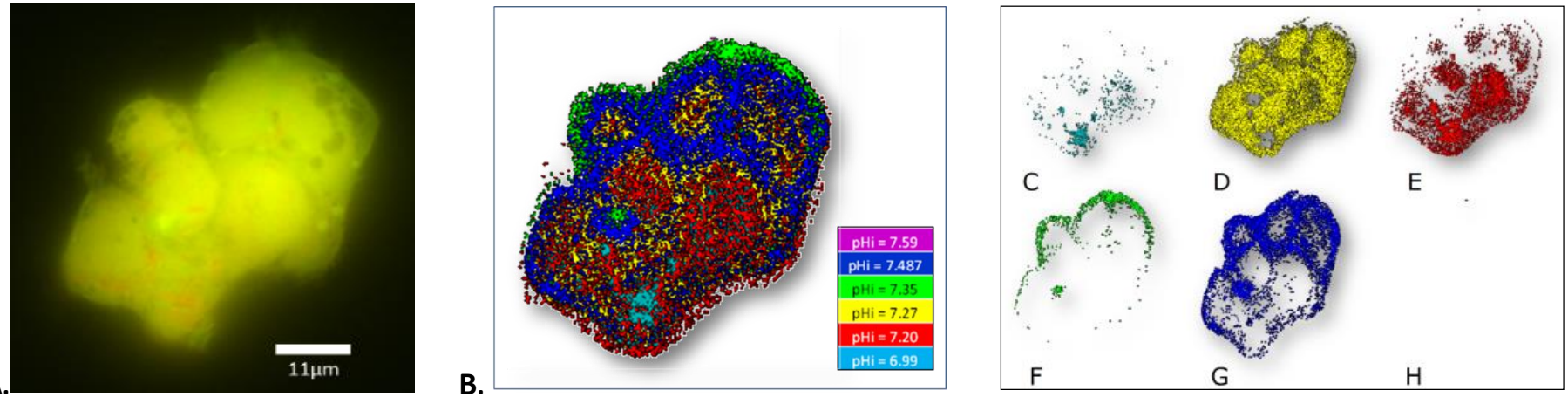

Figure 5.7: Processed image of a cluster of monolayer of SK-OV-3 cells. Cells cultured in low pH_e/normal PO_2, acquired in (A) wide field microscope representing pH_i distribution and mapping. (B) Composite pH_i heatmap. (C-H) Individual pH_i areas of the composite image.

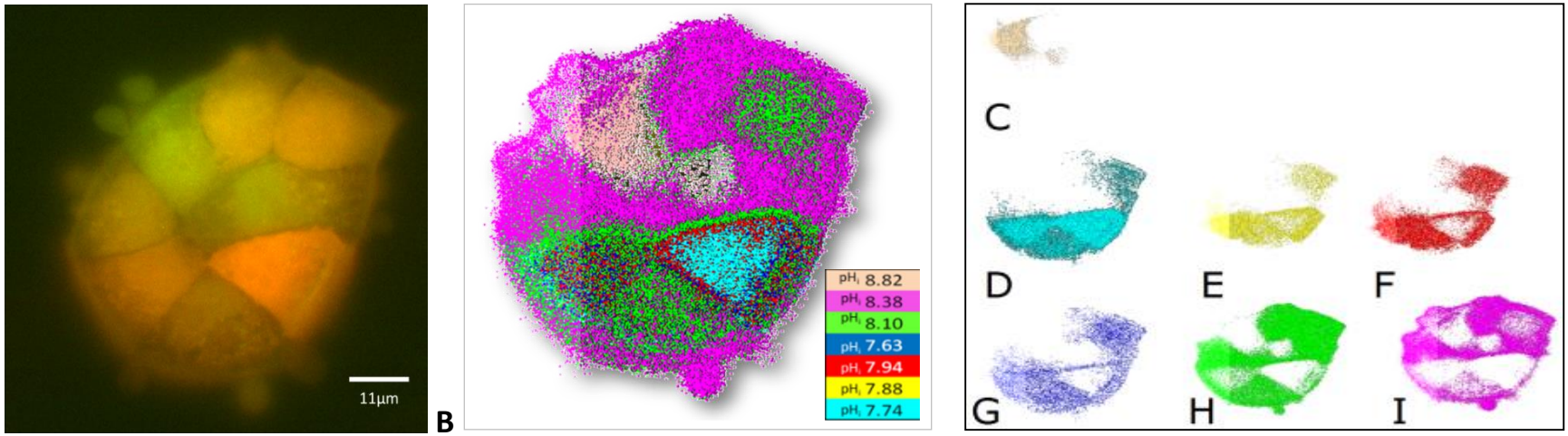

Figure 5.8: Processed image of a cluster of monolayer of MCF-10A cells. Cells cultured in normal pH_e & PO_2 acquired in (A) wide field microscope representing pH_i distribution and mapping. (B) Composite pH_i mapping. (C-H) Individual pH_i areas of the composite image.

5.2.6 Identifying associations between intracellular zones of pH oscillations with the spatial distribution of mitochondria in test cancer cell lines under altered pH_e/PO_2

5.2.6.1 Optimisation of mitochondrial membrane potential sensitive fluorescence dye

The optimisation of MitoTracker Deep Red dye was performed on SK-OV-3 cells as described in (Section 2.10).

The identification of a non-uniform distribution of intracellular protons prompted the requirement for an assessment of the organelles likely to be associated with the pH signals. In Figure 5.9, non-uniform spatial distribution of mitochondria is depicted in MCF-7 cells maintained in normal pH_e & PO_2 using MitoTracker Deep-Red in combination with pH-nanosensor (Section 2.7.2 and 2.10). The mitochondria appear to form a ring around the periphery of the cells, clustered into discrete areas within the cell (Figure 5.9B) that often do not coincide with the way the pH-nanosensor signals span across the cells (Figure 5.9A). The composite image of the pH distribution with unique areas of high and low pH (green fluorescence) against reference dye (orange red fluorescence) shows only a partial association of these areas with signals that show the presence of mitochondria.

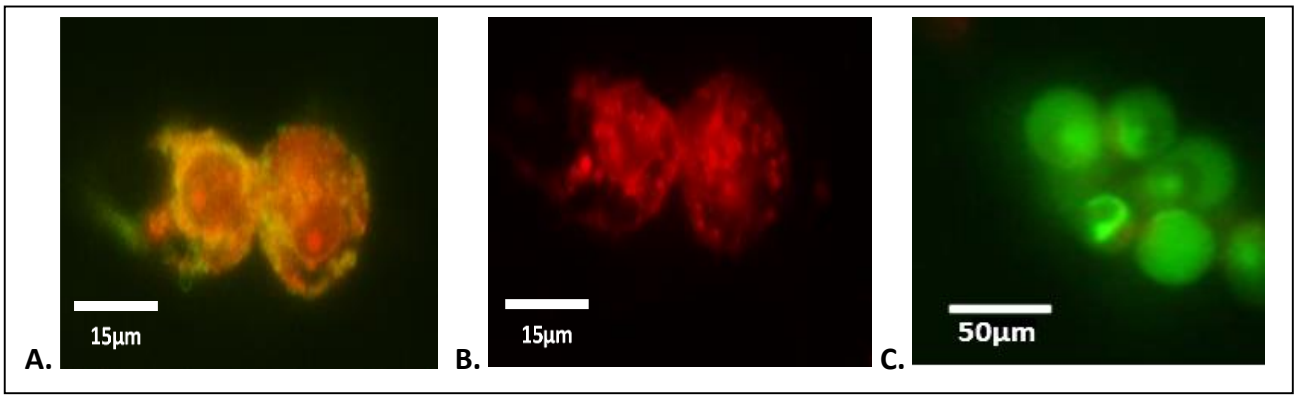

Figure 5.9: Mapping mitochondrial localisation against pH distribution in MCF-7 cells in normal pH_e & PO_2.
[A] pH-nanosensors depicting localised pH pockets in composite image representation in MCF-7 cells. [B] MitoTracker Deep Red dye labelled mitochondria distribution in MCF-7 cells. [C] Control for MitoTracker Deep Red dye - showing absence of mitochondrial labelling in apoptotic (denoted by Caspase 3 as green fluorescence) MCF-7 cells.

Mitochondria in the MCF-7 cells cultured in a low pH_e and normal PO_2, in contrast to the above, appear to be arranged in a cluster around the nucleus forming a much more discrete signal, sparing most of the remaining cytosolic area. The distribution of mitochondria maintained this organisation throughout the entire cell as observed in Z-stack images of MCF-7 cells. When observing along the z-axis of focus (as the plane of focus shifts from the base of the adhered cell through the middle and finally the top of the cell), the close association of the mitochondria with the nucleus was observed. The pH_i distribution does not appear to alter the distribution of the mitochondria under the conditions used (Figure 5.10 B).

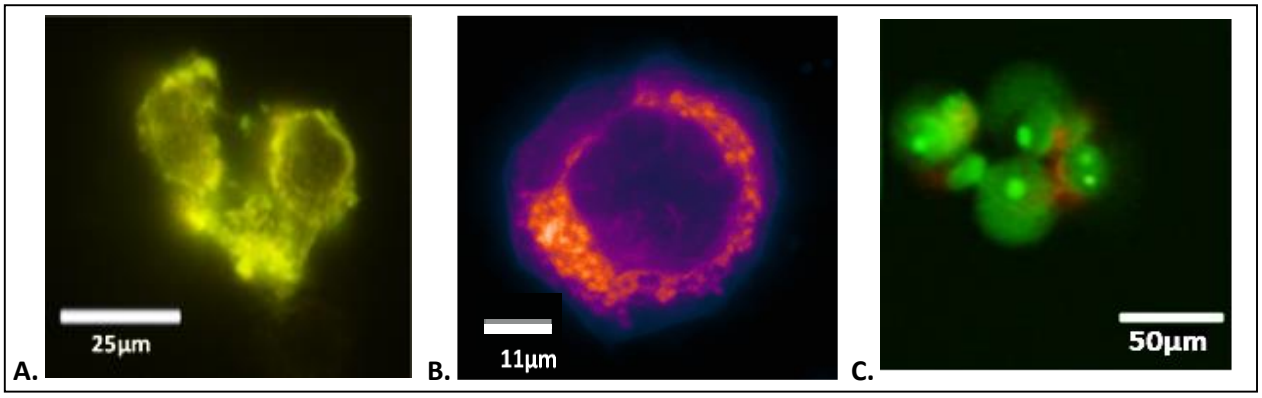

Figure 5.10: Mapping mitochondrial localisation against pH distribution in MCF-7 cells [A] pH_i status of MCF-7 cells. MCF-7 cells with pH-nanosensor maintained in low pH_e medium with normal PO_2. [B] Mitochondria of a representative MCF-7 cell maintained in low pH_e/normal PO_2 is stained with MitoTracker Deep-Red dye. [C] Control for MitoTracker Deep Red dye - showing absence of mitochondrial labelling in apoptotic (denoted by Caspase 3 as green fluorescence) MCF-7 cells.

To corroborate the findings of Mito Tracker, the pH-nanosensors were also used in tandem with the Mito Tracker Deep Red mitochondria staining dye to visualise the localisation of these organelles within the test cells. Figure 5.11A depicts the composite image of SK-OV-3 cells loaded with pH-nanosensor and maintained in low pH_e/normal PO_2. Accumulation of pH-nanosensors was observed across the cytosol with considerably high concentration at the periphery of the cell (Figure 5.11A). In SK-OV-3 cells maintained in low pH_e/normal PO_2 (Figure 5.11A), the distribution of mitochondria did not appear to be perinuclear (Figure 5.11 B) and the Z-stack images revealed a more uniform distribution spanning the cytosol as the plane of focus traversed the cell. These observations helped in tracking the differential distribution of mitochondria in real time while acquiring data on pH_i changes from the live cells loaded with pH sensor dyes.

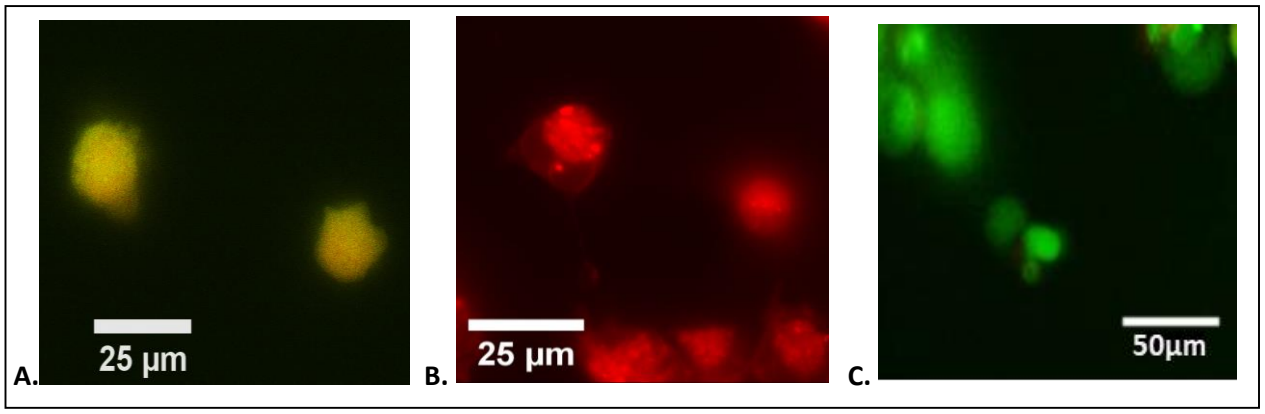

Figure 5.11: Mapping mitochondrial localisation against pH distribution in SK-OV-3 cells.
[A] SK-OV-3 (in low pH_e; normal PO_2) cells stained with cSNARF-AM (pH sensing dye). [B] Mitochondria distribution in SK-OV-3 cells in low pH_e and normal PO_2 stained with Mito Tracker Deep Red in SK-OV-3 cells in low pH_e with normal PO_2. [C] Control for MitoTracker Deep Red dye - showing absence of mitochondrial labelling in apoptotic (denoted by Caspase 3 as green fluorescence) SK-OV-3 cells.

MCF-10A non-neoplastic cells also displayed a mitochondria distribution largely independent of the regions of higher pH_i (Figure 5.12A, B). The concentration of the Mito Tracker dye appeared to produce more fluorescence signals from regions of the cells where the cSNARF-AM dye maintained a yellow-green colour (denoting normal-high pH_i) (Figure 5.12B). These areas of the cells represented balanced signals from the low pH_i (green fluorescence) and the high pH_i (orange-red fluorescence) signals of pH sensing dye.

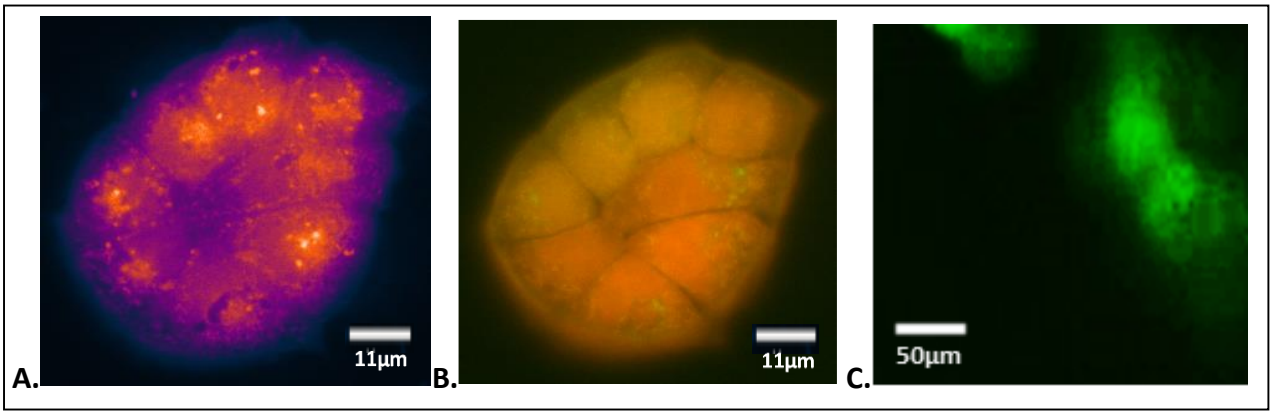

Figure 5.12: Mapping mitochondrial localisation against pH distribution in MCF-10A cells
[A] Mitochondria visualised in MCF-10A cells cultured in normal pH_e & PO_2 loaded with Mito Tracker Deep Red dye. [B] pH_i distribution shown in composite image of MCF-10A cells loaded with cSNARF-AM. [C] Control for MitoTracker Deep Red dye - showing absence of mitochondrial labelling in apoptotic (denoted by Caspase 3 as green fluorescence) MCF-10-A cells.

5.3 Discussion

Acid load extruded by cancer cells is an important cancer hallmark that reveals their need for robust pH_i regulatory systems (Boyer and Tannock, 1992; Hanahan and Weinberg, 2011). These regulatory systems sustain functionality, even in tumour niches that are not adequately perfused (Tannock and Rotin, 1989; Lee and Tannock, 1998). In view of the relationship between pH and cancer cell metabolism, we used live cell imaging and fluorescence methods to determine whether cancer cells have an altered capacity to buffer pH and extrude acid in response to altered pH_e and oxygen tension (other than normal physiological conditions). The study specifically outlines how the aforementioned changes in the microenvironment can also influence the pH_i recovery of acutely acidified cancer cells. Furthermore, we investigated how alterations in the tumour mimicking microenvironment can lead to the development of isolated pockets of high and low pH_i in cancer cells. In addition to earlier reports that associate uniform pH_i to cancer cells (Griffiths, 1991), this study demonstrates how an altered microenvironment can predispose the intrinsic buffering mechanism to a heterogeneous proton distribution within cancer cells. Specifically, it was found that in comparison to normal cells, β_I variation between ovarian and breast cancer cells was influenced by the alterations in acidic pH_e. The extrinsic buffering mechanism had a major influence on the recovery of steady state pH_i from acute acidification of cancer cells under altered microenvironment. Furthermore, the NAE appeared to increase in breast cancer cells under acidic and hypoxic

environment and in ovarian cancer cells under normal pH_e and normal oxygen tension.

It has been demonstrated previously that a change in the acute acid challenge through ammonium pre-pulse manoeuvre alters the pH regulating capacity of mammalian cells (human glomerular cell, colorectal and breast cancer cell lines) (Boyarsky *et al.*, 1988a; Hulikova *et al.*, 2013). The shift in pH_i between the acid loading and acid dumping time points described in Section 5.2.1a and 5.2.1b respectively are consistent with the aforementioned reports, $NaHCO_3$-dependent (intrinsic) or presence of $NaHCO_3$-dependent (extrinsic) buffering (Figure 5.1, 5.2). Following a brief pulse of ammonium (2 to 5 minutes) in principle, the amount of intracellular [NH_3], calculated from the time course traces (Figure 5.1 and 5.2) exceeds the total intracellular [NH_3] as recorded before the APP, indicating the magnitude of equivalent acid loading. Thus, it can be speculated within reason that after long term exposure to a pH_e and PO_2 simulating tumour microenvironment, cancer cells evolve to mobilise acid buffering agents and modulators more efficiently to establish pH homeostasis. We demonstrated that with a drop in the pHe, the cellular response to the same magnitude of acidotic challenge manifests as the test cancer cells' capacity to compensate and handle additional protons and altered oxygen tension differently (Figure 5.1 B, D). This manifestation is subject to factors such as tissue origin and previous exposure of cells to such conditions (Boyer and Tannock, 1992; Do, Ellis and Noireaud, 1996; Kato *et al.*, 2013). The cells dynamic pHi informs us about how microenvironment introduces a set of changes in

metabolism. We can infer that the significant differences in the magnitude of intracellular acidification observed between SK-OV-3 and MCF-7 cells manifest differently to favour cancer survival over their non-tumourigenic counterparts (MCF-10A cells), when the cells' metabolism is challenged (Figure 5.2, 5.3 and 5.5).

In the absence of $NaHCO_3$-dependent pH buffering, the magnitude of response to acute acidic challenge is expected to be significantly larger in cancer cells compared to a non-malignant cell. But the same cancer cell if previously maintained in acidic pH_e, when abruptly exposed to a similar stimulus, elicits a response much smaller in magnitude (although still significantly larger to non-neoplastic or normal counterparts). We suggest that compensatory pH buffering mechanisms are either pre-activated or triggered in these cancer cells. This describes how pH regulation is increasingly sensitive and robust in low pH_e and PO_2 in cancer cells that significantly distance them from adapting metabolic strategies previously employed under physiological conditions.

Thus, time course experiments elucidate that on challenging the pH buffering capacity of the cancer cells, a fast response is promoted independently through the intrinsically active buffering mechanism (Figure 5.1) as also shown by (Boyarsky *et al.*, 1988a, 1988b; Boyer and Tannock, 1992; Goldsmith and Hilton, 1992) under physiological conditions. However, we infer that increased proton availability extracellularly alone, might play a crucial role in significantly augmenting the magnitude of intrinsic buffering response in ovarian and breast cancer cells (Figure 5.1). Thus a fast response to low pH_e can result in possible

revival of pH dependent cellular functions important for tumour growth, that are shown to be potentiated by brief exposures (<6 hours) to acidic pH_e independently (Eagle, 1973; Tannock and Rotin, 1989).

In contrast, a delayed response to acute acidification of cancer cells also indicates that extrinsically active $NaHCO_3$-dependent buffering condition is eventually preferred in re-establishing cellular pH homeostasis (Figure 5.2), functioning not only as a transient buffer to compensate acid extrusion (by facilitating extracellular proton diffusion) but also as a supplier of substrate for acid extrusion via HCO_3^-transporters (Hulikova, Vaughan-Jones and Swietach, 2011).

5.3.1 Measurement of β_I defines pH regulation in cancer cells in altered pH_e/PO_2

The significant difference between the β_I of the cancer cells to that of the non-neoplastic control in normal pH_e can be attributed to the difference in their pH regulating mechanisms that become activated under normal atmospheric oxygen tension. Independent reports suggest increased activity of several pH buffering systems that are unique to tumour microenvironment (eg. NHE_1, MCT and bifunctional CO_2-HCO_3^- system (Fischer *et al*., 2007; Hulikova, Vaughan-Jones and Swietach, 2011; Loo et al., 2012)). These findings set apart the physiological microenvironment and associated pH buffering systems from tumour microenvironments and tumour associated pH buffering systems (that activate under reduced atmospheric oxygen tension).

In addition we discovered that even under similar physiological conditions, the cancer cells appeared to mobilise only a fraction of the pH equivalent species in comparison to the control cells to achieve a significantly larger shift in pH_i in response to an acute acid challenge. Therefore, we infer that the intrinsic acid buffering machinery adapts to subtle changes in the proton distribution when the cancer cells are subjected to microenvironment mimicking tumour specific conditions. Furthermore,, unlike reports published by (Roos and Boron, 1981; Boyer and Tannock, 1992; Goldsmith and Hilton, 1992; Hulikova, Vaughan-Jones and Swietach, 2011; Hulikova *et al.*, 2013), the present study attempts to fill the gap in the understanding of acid buffering potential of different cancer cells by specifically comparing their $\boldsymbol{\beta}_I$ in modified microenvironment with that observed in normal physiological conditions. The exponentially increased $\boldsymbol{\beta}_I$ of breast cancer cells compared to ovarian cancer cell lines (Figure 5.3 A, B) reflects the metabolic advantage of the former to handle acidification.

Interestingly, the change in the pH or oxygen tension of the microenvironment used in combination as four different culture conditions in this study, forces huge fluctuations in the acid buffering capacities of breast cancer cells. In this section the importance of an altered microenvironment on the pH homeostasis of cancer cells is being emphasised. The observed differences in the $\boldsymbol{\beta}_I$ of same cancer cells when maintained in an altered microenvironment (indicating how tumour microenvironment differs from normal interstitium) is being highlighted. In this context it is noteworthy that such fluctuations in the $\boldsymbol{\beta}_I$ of normal mammalian cells, is rarely observed for the cells from the same embryonic origin. The studies

cited show a consistent β_I is observed for cells of similar embryonic origin and hence are rationally maintained in the normal physiological condition. β_I of neuronal cells however, is comparable across estimates made in differing types of mammalian neurons shown by (Curtin, 1986), (Pocock and Richards, 1992) and (Gaillard and Dupont, 1990). For a 0.27 pH unit shift due to a 10mM equivalent drop in acid loading, variation in β_I is observed only in different mammalian cells that ranges from ~4.5 mM/pH - to > 80 mM/pH unit (Boyarsky *et al.*, 1988a; Do, Ellis and Noireaud, 1996). Furthermore, despite both neurons and striated muscle cells in mammals being potentially excitable, significant differences have been recorded between their intrinsic buffering power (Roos and Boron, 1981; Curtin, 1986; Amos and Richards, 1996) under normal pH_e and oxygen tension only. β_I in cancer cells have been shown to range from 0.42 and 3 mM/pH in MDA-MB-435 and MDA-MB-468 respectively to more than 40 mM/pH (Miapaca2, HCT116, MCF-7) in relatively alkaline pH_i (Reshkin *et al*., 2000; Hulikova *et al*., 2013).

In comparison to the published data shown above, we infer that the magnitude of fall in pH_i representing the buffering capacity is greater in cancer cells maintained in tumour microenvironment mimicking conditions. This environment provides them with greater potential to regulate pH such that total metabolic acid generation is at equilibrium with total membrane transport of H^+/H^+ equivalent species (Swietach *et al.*, 2014). Thus, maintaining cancer cells in tumour mimicking environment either directed at metabolic investigation or

pharmacokinetic and pharmacodynamics studies should generate more reliable information.

5.3.2 NAE in cancer cells is influenced by recovery of pH_i in altered microenvironment

In our study, NAE of the test cancer cells was evaluated as a product of the rate of recovery of pH_i with the total β in altered microenvironment (Section 2.11.1). Conventionally the role of these components have been shown either in physiological culture conditions or selectively altered pH_e (Hulikova, Vaughan-Jones and Swietach, 2011; Damaghi, Wojtkowiak and Gillies, 2013; Kato *et al.*, 2013; Swietach *et al.*, 2014). We demonstrated that the constituent components' contribution towards net acid buffering is carried out through two analogous pathways viz., the $NaHCO_3$-independent and the $NaHCO_3$-dependent. The response of both these pathways was observed to vary in altered microenvironment conditions as is evident from the APP experiments conducted either in HEPES buffered or $NaHCO_3$ buffered media. Hence, under altered pH_e/PO_2, the intrinsically acting pathway elucidated the cell's unique response involving $NaHCO_3$-independent flux of protons (all intrinsic pH buffering mechanisms that do not utilise the CO_2-HCO_3^- system). On the other hand, the extrinsic pathway involving $NaHCO_3$-dependent mechanism explains the route involving flux of bicarbonate ion species.

We infer that cancer cells (more importantly, breast cancer cells) are predominantly reliant on reduced oxygen tension (Figure 5.5) to potentiate the transmembrane mobilization of ionic species, required for pH regulation. We

understand that this phenomenon is augmented in the presence of low pH_e microenvironment. Parallel studies have also shown that an effective homeostatic system in cancer cells regulates pH_i by increasing alkalinisation through an increase in the NAE (Hulikova, Vaughan-Jones and Swietach, 2011). Association of allosteric activation of acid extruders with distribution of intracellular protons is attributed with this phenomenon (Aronson, 1985; Swietach *et al.*, 2009). Although extracellular alkalinisation is thought to counteract acid extrusion possibly working as a negative feedback to restrict acid dumping (Hulikova, Vaughan-Jones and Swietach, 2011), we demonstrated that this was observed to be potentiated in breast cancer cell lines under decreased oxygen tension.

Furthermore, conditions specific to tumour microenvironments negatively influence the hallmarks of ovarian cancer cells, pertaining to pH homeostasis and acid extrusion (Figure 5.5). The rate at which the pH_i restoration is achieved also indicates that acidic microenvironment works synergistically with the extrinsic $NaHCO_3$-dependent buffering system in cancer cells (Figure 5.4). We suggest that this property of the microenvironment is generally consistent under reduced oxygen availability. Thus, different cancer cells can be selectively targeted in comparison to their normal counterparts on the basis of their selective preference of either altered pH_e, PO_2 or both. Intrinsically acting pH-regulatory proteins can also be used as potential target sites as more sensitive pH-sensing methods develop.

Furthermore, our key findings also highlighted that cells of a similar tissue origin (MCF-7 cells and MCF-10A cells derived from breast) generated similar levels of pH_i recovery in completely contrasting experimental conditions (Figure 5.4). Interestingly, MCF-7 cancer cells (maintained only in tumour specific conditions) develop the potential to efficiently respond to acute acidification.

Thus substantial drop in pH_e, due to inadequate extracellular buffering or poor diffusive coupling of ionic species, has the potential to inhibit extrusion of acid from cells (Hulikova *et al.*, 2013). Our experiments demonstrate that for cancer cells maintained in a persistent low pH_e, the acid extrusion potential is significantly inhibited when compared to a physiological pH_e and PO_2. The magnitude of pH lowering on acid challenge in breast cancer cell lines (~0.5 pH units) under physiological conditions is lower than that observed in SK-OV-3 cells in our study and human colorectal cancer cells (~1.2 pH units; (Hulikova, Vaughan-Jones and Swietach, 2011)).

It has been shown that MCTs and $NaHCO_3$-dependent buffering mechanisms are insufficient in independently establishing an effective transmembrane proton gradient. As demonstrated in our experiments using a $NaHCO_3$-free medium, the importance of the contribution of multiple intrinsically acting pH regulating mechanisms in cancer pH homeostasis is emphasised. The observation that under normal PO_2, SK-OV-3 cells maintained in low pHe had a decreased rate and extent of acidification following APP, is suggestive of the fact that they harbour and deploy additional intrinsic buffering mechanisms, compared to those in normal pHe. Unlike, SK-OV-3 cells, MCF-7 cells (not known to be hypoxia

resistant) do not exhibit this statistically significant shift in pH_i when pH_e and PO_2 are simultaneously reduced from physiological values. In non-malignant control, MCF-10A cells, only quantifiable data was generated under normal physiological environment implying their tolerance to physiological conditions and susceptibility to any substantial alterations to the pH_e or PO_2 as opposed to cancer cells.

In MCF-10A, during acid loading, Na^+-H^+-Exchanger mediated flux was found to be the dominant constituent of the acid-extrusion component(Hulikova *et al.*, 2013). Acid extrusion by active transport indicates the transfer of proton across membranes at the expense of stored energy. For cells that are already dealing with compromised access to energy resources viz., reduced oxygen availability, reduced perfusion and impeded metabolic processes, active transport of proton/pH entities can prove to be an appreciable load on the energy management of the cells. This can logically force them to generate more energy currency (ATP) with the available resources, as is observed through a shift of metabolism from OXPHOS to aerobic glycolysis or anaerobic glycolysis (Hulikova *et al.*, 2013). This study provides a deeper understanding of NAE and its contribution towards the cancer cell's pH regulatory machinery in dealing with a dynamic pH_e and PO_2. Our data highlights the need to further investigate the dominant components of altered acid extrusion in cancer cells in response to a dynamic microenvironment. Such observations should be made in true hypoxic gradient environments (involving closed hypoxic chamber setups) to elucidate the effects of the switching on and off of different components (by recruiting

pharmacological, and gene silencing methods) of the acid extrusion in cancer cells in order to expose their vulnerability in these scenarios.

5.3.3 Detecting differentially distributed pH_i pockets in cancer cells

The pH_i distribution imaging in SK-OV-3 cells revealed the presence of regions with different pH levels in a pattern reflecting their response to the surrounding pH and oxygen availability. The presence and rearrangement of pockets of high and low pH_i in the cytosol of ovarian cancers indicate their potential role in pH dependent cellular processes. The low pH_i pockets of the cancer cell located away from direct interface with the microenvironment warrant the need for membrane associated processes with lower metabolic activity. The accumulation of protonated cytosolic components radiating inwards and occupying a major area of the cell centrally, also indicates the transiently compromised pH buffering in cancer in the regions of high metabolic activity. This is also helpful in appreciating the potential regions of pH regulation that established a more physiological pH_i. The cells that were cultured in lower pH_e were also mapped for their pH_i distribution. The colour thresholding revealed that majority of the cells in a cluster of monolayers maintained a less acidic to near neutral pH_i in pockets located centrally.

The strict boundary of absolute physiological pH_i was observed in most cells. In non-neoplastic cells, the distribution of protons appears to be very erratic and uneven when the cells were maintained in physiological pH predominantly because the cells although in a monolayer were under differential pH regulation processes.

5.3.4 Association between mitochondrial distribution and pH_i pockets in cancer cells

A similar pattern was also followed when the mitochondria of these cells were imaged along with the distribution of the pH_i. We suggest that limited association exists between zones of proton concentration and mitochondrial distribution, as their respective signals superimposed inadequately. However, large number of mitochondria clustered around the nuclei of SK-OV-3 cells only under low pH_e and atmospheric PO_2, can be explained based on differences in local pH_i. The proton-motive force generated across the inner mitochondrial membrane is mediated by the membrane electron transport chain (ETC) (Matoba *et al.*, 2006). Thus, the inside of the inner membrane is alkaline (Corrado, Scorrano and Campello, 2012; Nagy *et al.*, 2014). The lack of a low pH_e drive could possibly keep the mitochondria aloof from the protonated areas within the cell to restore their internal alkaline environment. The perinuclear localisation of these organelles can be attributed to the altered pH_e that could regulate position, size and trafficking of these dynamic organelles (Corrado, Scorrano and Campello, 2012) . In summary, MCF-7 and SK-OV-3 cells differ from each other in their pH homeostatic and regulatory properties. Tthe overall proton extrusion potential of the two cell lines also uniquely differs from MCF-10A, as changes were brought about in their extracellular environment. In this context, it was evident that the low pH homeostatic threshold of SK-OV-3 cells expose their enhanced vulnerability to small changes in pH_e. Furthermore, while no obvious relationship between mitochondria distribution and high/low pH_i regions was noted, there

are many other cellular factors directing active extravasation, migration and invasion that are known to regulate these properties (Andresen, Jensen and Jorgensen, 2005). In this context we know that re-activation of Akt/mTOR signalling in tumour cells triggers the transport of energetically active, elongated mitochondria to the cortical cytoskeleton of tumour cells (Caino and Altieri, 2015). In turn, these relocated mitochondria actively increase lamellipodia dynamics. Important metastatic events like faster turnover of focal adhesion complexes, more velocity and distance of random cell migration and invasion is increased in tumour cell (Caino and Altieri, 2015). Previous reports also observed mitochondrial re-distribution in the leading edge of cells during persistent migration and enrichment of mitochondrial proteins in invadopodia during active cell invasion (Attanasi*o et al*, 2011; S. P. Desai *et al*, 2013; Caino and Altieri, 2015). More importantly these processes involving tumour cell migration have also been shown to be largely dependent on pH homeostasis (Stock *et al.*, 2005; Damaghi, Wojtkowiak and Gillies, 2013). This has raised questions as to how energy modulating organelle like the mitochondria remain transiently inactive when cells are sedentary and adherent albeit undergoing active pH homeostasis during metabolically exhaustive cellular events. We suggest that increased sensitivity of assays evaluating these phenomena while intervening with the microenvironment might reveal any association between pH regulation and mitochondrial distribution in actively migrating cells.

The limitations of the study largely revolve around the technical issues addressing methodological adaptations used to overcome bias over experimental

conditions. Live cell imaging with widefield fluorescence microscopy was capable of elucidating signals only on individual cell to cell basis. A fluorescence microplate reader setup could incorporate all experimental conditions within reasonable limits allowing us to record collective mean data from monolayers.

There are other players in pH regulation, however, not much is known about pH regulatory proteins that work relatively independent of the $NaHCO_3$ buffering system (Romero, Chang and Mount, 2010; Gorbatenko *et al*., 2014). In this context, although much is known about sodium dependent pH regulation, the interaction between potassium homeostasis and pH regulation is poorly understood. In the following chapter we investigate how potassium homeostasis is associated with pH_i regulation in cancer.

Chapter 6. Role of K^+ and TASK-3 channel in pH homeostasis in cancer cells

6.1 Introduction

A dynamic modification of the intrinsic pH buffering potential is known to be positively influenced by favourable changes in the microenvironment (Chapter 5) (Boyer and Tannock , 1992). Interestingly, among factors that influence buffering potential and pH regulation in cancer cells, K^+ balance across the cell membrane is thought to be of great importance (Adler and Fraley, 1977). A low extracellular K^+ concentration $[K^+]_e$ relative to the intracellular K^+ $[K^+]_i$ is associated with cellular uptake of acid (Grinstein, Cohen and Rothstein, 1984; Grinstein and Dixon, 1989; Balkay *et al.*, 1997). In addition, the ratio of $[K^+]_i$ to $[K^+]_e$ was shown to be directly proportional to the fall in the intracellular to extracellular proton ratio (Adler and Fraley, 1977). Differentiated normal mammalian cells have also been shown to extrude protons in exchange for K^+ to maintain ionic balance (Aronson and Giebisch, 2011). In the microenvironment with depleted levels of K^+, H^+ is shunted from the extracellular compartment into the cell. In contrast during K^+ repletion, cells dump acid into the extracellular compartment (Adler and Fraley, 1977). However, the gap between, a) estimation of the K^+ distribution across cancer cell membranes and b) estimation of dependence of pH on K^+ homeostasis can be bridged using pH associated K^+ ionophore like nigericin (Appendix 4I).

The interaction of pH buffering mechanisms and K^+ homeostasis in the modified (in terms of pH_e and oxygen availability) tumour microenvironment has not been

studied extensively. By experimentally challenging the pH buffering system using the ammonium pre-pulse manoeuvre (Section 2.11.1), one can evaluate interdependence between K^+ distribution and pH regulation in cancer. Studies show that the changes in K^+ concentrations are mediated through transporters or channels that participate in complex cellular functions (Romero *et al.*, 2000; Stock and Schwab, 2009; Gorbatenko *et al.*, 2014). Interestingly, pH sensitive potassium (K^+) channels are known to be expressed in different types of cancers (Williams, Bateman and O'Kelly, 2012; Pardo and Stühmer, 2014) and have been shown to be involved in proliferation, cell cycle kinetics and oncogenic potential in heterologous systems (Sanguinetti *et al.*, 1995; Pardo *et al.*, 1999; Wondergem *et al.*, 2001; Pardo, 2004). Although previous studies have shown that K^+ channels also contribute to pH modulation, not much is known extensively about their role in cancer (Pardo and Stühmer, 2014). Our published findings show that the pH_e sensitive K_2P channel TASK-3, is that it is not only overexpressed in ovarian cancer cells but also has prognostic significance (Innamaa *et al.*, 2013). Owing to the data on overexpression of TASK-3 channels and their functional profile as an oncogenic potassium channel, we sought to determine the dependence of pH regulation on $[K^+]_e$ and in turn investigate the role of the TASK-3 channel in the pH homeostasis of cancer cells in a dynamic microenvironment.

6.1.1 Aims

The aim of this chapter is to deploy the ammonium pre-pulse manoeuvre on SK-OV-3 and MCF-7 cells in HEPES buffered media under altered pH_e/PO_2 in order to:

a) Estimate $[K^+]_I$ using nigericin as the ionophoretic proton exchanger.

b) Generate a time course trace of pH_i recovery from acute acidification in altered $[K^+]_e$.

c) Determine K^+ dependence of pH_i recovery following acute acidification.

d) Generate a time course trace of pH_i recovery from acute acidification in the presence of methanandamide (TASK-3 channel inhibitor).

e) Determine the net acid extrusion (NAE), in the presence of methanandamide.

6.2 Results

In order to study whether regulation of pH_i in the established cancer cell lines SK-OV-3 and MCF-7 is dependent on potassium fluxes, the ammonium pre-pulse technique combined with live-cell imaging and fluorometric measurement respectively was used (Section 2.11.1).

Furthermore, the calibration of the pH-nanosensor probe and pH-sensing dyes used for evaluation of pH_i, was performed before each experiment on SK-OV-3 cells MCF-7 and MCF-10A cells (Section 2.8).

6.2.1 Estimation of $[K^+]_i$ in SKOV and MCF-7 cells

Cell line (pH_e 7.2- 7.42)	Intracellular free K^+ mM)
SK-OV-3	**114 ± 1.21**
MCF-7	**145 ± 4.23**

Table 6.1. Intracellular free potassium ion concentration of cancer cells
$[K^+]_i$ was determined from SK-OV-3 and MCF-7 cells loaded with cSNARF-AM pH sensing dye in the presence of nigericin (Appendix 4I). Displayed data are means ± S.D. values calculated from eight independent repeats.

The present section highlights the observations from experiments to estimate $[K^+]_i$ based on nigericin mediated ionopheretic proton exchange. It was observed that SK-OV-3 and MCF-7 cells when cultured in different concentrations of extracellular $[K^+]_e$, a linear relationship between their pH_e and pH_i was established. The data for SK-OV-3 and MCF-7 cells in Figure 6.1 demonstrates the close yet relatively linear relationship between the known pH_e and observed pH_i in the presence of nigericin. A concentration of 120mM KCl compared to 30mM KCl in media establishes a outwardly decreasing gradient of K^+ efflux across the

cell membrane depending on the $[K^+]_i$ of SK-OV-3 cells. This did not restrict the net movement of protons as observed in Figure 6.1 when the $[K^+]_e$ was reduced from 120mM to 30mM. Substantial changes in the extracellular proton concentration (at 30mM $[K^+]_e$ (solid boxes) or at 120 mM $[K^+]_e$ (open boxes) Figure 6.1) brings about a shift in the pH_i vs. pH_e curve induced by changes in K^+ efflux. For both test cells, the slope for 120 mM $[K^+]_e$ was non-identical and parallel (P value testing the null hypothesis that the lines are identical is < 0.0007) to that for 30 mM $[K^+]_e$.

Inter-relationship between extracellular and intracellular pH values of cancer cells in altered $[K^+]_e$ is represented in Figure 6.1**.** This is depicted by the shift of the linear regression plot curve for 30 mM $[K^+]_e$ to the right of the curve for 120 mM $[K^+]_e$ for the two cancer cell lines. The direction of the shift is the same as in the case of change in potassium level. Thus, the figure also shows that substantial changes in the potassium concentration (at constant K^+ level) of the suspending medium bring about a shift in the pH_i vs. pH_e (Balkay *et al.*, 1997).

It was essential that the two plot lines generated in 120mM and 30nM $[K^+]_e$ be statistically tested to be parallel along the y axis (pH_i). The slopes and intercepts of the regression lines for 120 mM $[K^+]_e$ and 30 mM $[K^+]_e$ were tested by Graphpad Prism 6.0. This was necessary to prove that these two lines are also non-identical/ overlapping due to the shift of the linear regression plot curve for 30 mM $[K^+]_e$ to the right of the curve for 120 mM $[K^+]_e$ for the test cell lines. It is understood that if the slopes are indistinguishable, the lines could be parallel with distinct intercepts. Prism calculates a P value testing the null hypothesis that

the lines are identical. If this P value is low, one can conclude that the lines are not identical (they are distinct but parallel) (Zar, 1984).

In the experiments reported in the thesis we observed very low P value I.e P < 0.0007. Hence the statement the slope for 120 mM $[K^+]_e$ was non-identical and parallel to the 30mM $[K^+]_e$ regression line was included to validate the experiment.

This is depicted by the shift of the linear regression plot curve for 30mM $[K^+]_e$ to the right of the curve for 120mM $[K^+]_e$ for the test cell lines.

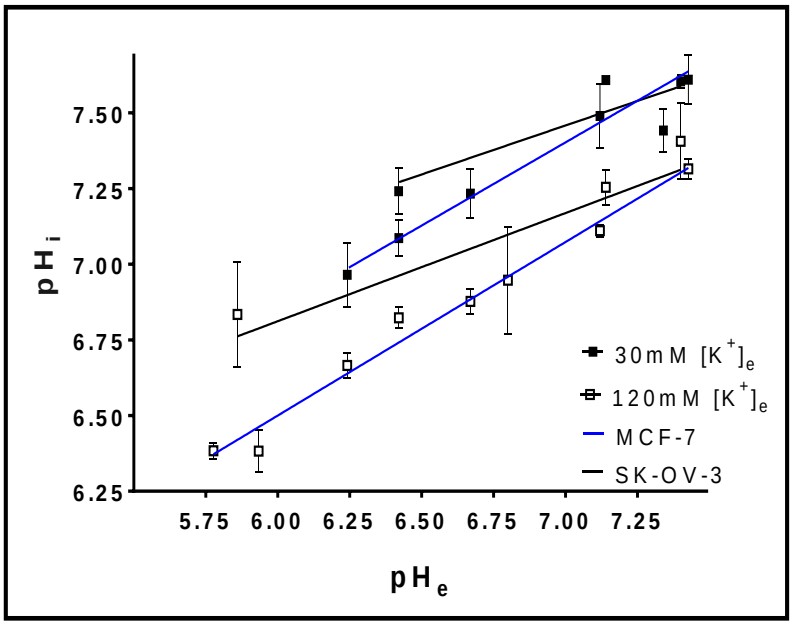

Figure 6.1: Interrelationship between extracellular and intracellular pH values of SK-OV-3 and MCF-7 cells treated with nigericin in altered $[K^+]_e$.
The representative graph to show relative change in pH_i in response to the change in pH_e of SK-OV-3 and MCF-7 cells incubated with 10µM nigericin (3-5 min) in high (120 mM (open box)) and low (30 mM (closed box)) $[K^+]_e$ HEPES buffer (pH_e 7.4) adjusted to different pH values (5-8). The pH of the buffers was adjusted from acidic to alkaline at 37°C; normal PO_2. n=8

6.2.2 Time course of pH_i recovery from ammonium pre-pulse manoeuvre in altered pH_e, PO_2 and $[K^+]_e$ cancer cell

The time course of change in pH_i of SK-OV-3 and MCF-7 cells to achieve steady state pH_i recovery from the ammonium pre-pulse, in increasing $[K^+]_e$ (substituted with equimolar $CsCl_2$ from '*d - i* ' corresponding to 0- 5 mM $[K^+]_e$) is represented [Figure 6.2]. The recovery of MCF-10A cells from ammonium pre-pulse (Section 2.11.1) in increasing concentration of $[K^+]_e$ maintained under normal pH_e and PO_2 were taken as control (solid red line, Figure 6.2). HEPES buffered solution was used to evaluate the contribution of the intrinsic buffering potential of the test cells. In comparison to controls, SK-OV-3 cells subjected to an ammonium pre-pulse were observed to have maximum delayed responses to levels of $[K^+]_e$ below physiological (135 mM) values.

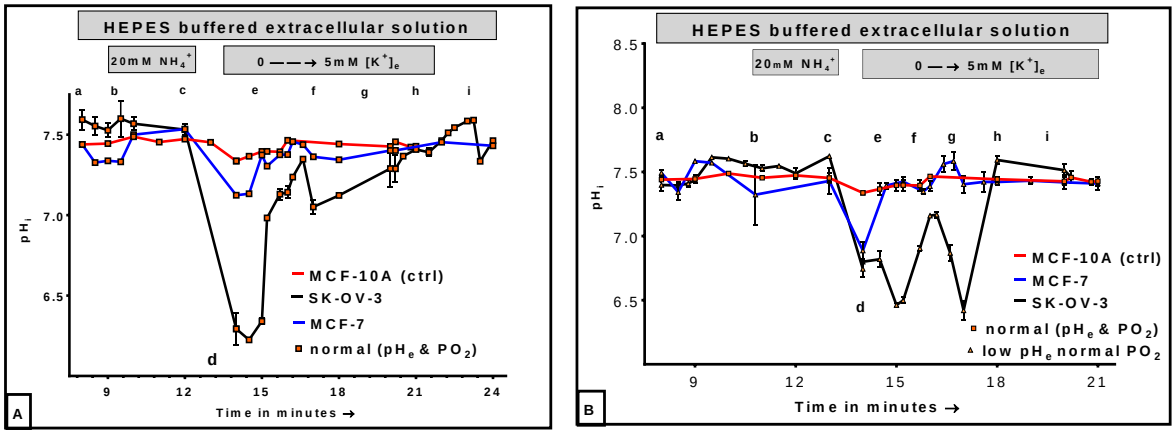

Figure 6.2: pH_i regulation of cancer cells in variable $[K^+]_e$ with altered pH_e/PO_2. Time course of pH_i recovery (to achieve steady state pH_i) of SK-OV-3 and MCF-7 cells in variable $[K^+]_e$ HEPES buffered medium at normal PO_2 and pH_e [A]; at normal PO_2 and low pH_e [B];. Indicated with '*d-i* ' are the pH_i recovery points corresponding to 0-5 mM $[K^+]_e$ when compared between conditions and cell lines as described in the main text. n = 8

6.2.3 Determination of K^+ dependence of pH_i maintenance following acute acidification

The pH_i recovery of the test cells in increasing $[K^+]_e$ (observed in Section 6.2.2) was plotted against the change in $[K^+]_e$ in nonlinear least-squares fit according to the Michaelis-Menten equation (Section 2.11.3.2). The curves in Figure 6.3, depict the change in intracellular alkalinisation with gradual addition of $[K^+]_e$ (to K^+ free HEPES buffer) post NH_4Cl washout. The Michaelis-Menten constant K_m (mM) in Figure 6.3, predicts the $[K^+]_e$ needed to achieve a half-maximum pH_i recovery (from intracellular acidification after ammonium pre-pulse) in the test cell lines maintained in normal/low pH_e and normal PO_2 (Figure 6.3 A). The variation in the K_m is significantly ($P < 0.01$) higher in SK-OV-3 cells compared to MCF-7 cells and normal control in normal as well as low pH_e under normal PO_2 (Figure 6.3 B). The K_m for SK-OV-3 cells maintained in normal pH_e and PO_2 was significantly ($P< 0.01$) higher than that observed in SK-OV-3 cells in low pH_e and under normal PO_2 (Figure 6.3 B).

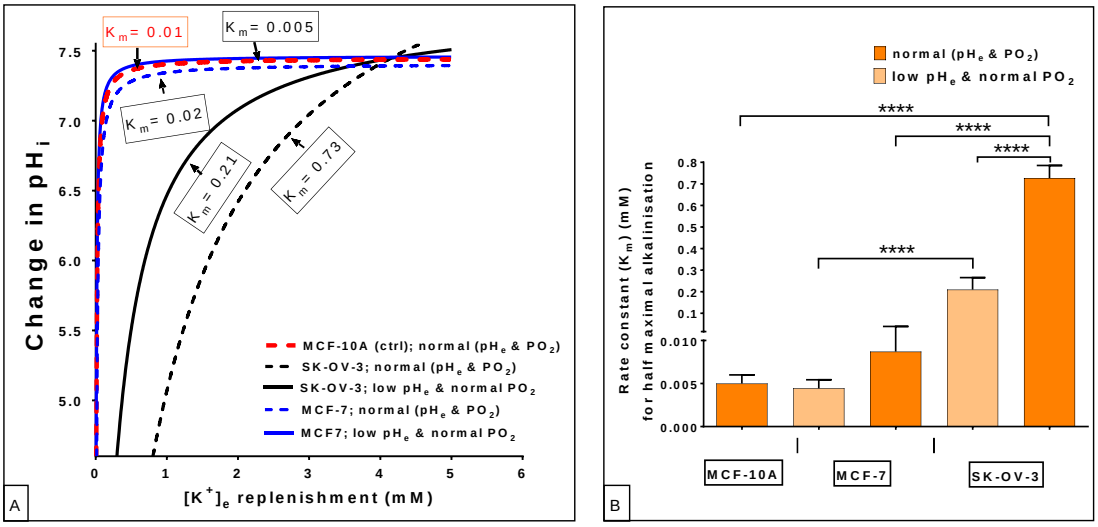

Figure 6.3: Dependence of pH_i recovery (from intracellular acidification) on $[K^+]_e$.[A] Michaelis-Menten constant K_m (mM), predicts the $[K^+]_e$ needed to achieve a half-maximum pH_i recovery (from intracellular acidification after ammonium pre-pulse) in MCF-10A (normal control), SK-OV-3 and MCF-7 cell lines maintained in normal PO_2 and either in normal/low pH_e. [B] The significant variation in the K_m is observed in MCF-10A compared to SK-OV-3 cells in normal pH_e & PO_2. The K_m for SK-OV-3 cells maintained in either normal/low pH_e with PO_2 was significantly higher than that observed in MCF-7 cells in either normal/low pH_e with PO_2 respectively. ****= $P < 0.0001$. n = 8

6.2.4 Time course trace of pH_i recovery ammonium pre-pulse manoeuvre in altered pH_e/PO_2 in the presence of methanandamide (TASK-3 channel inhibitor)

In the presence of the TASK-3 inhibitor methanandamide (3µM), the time course of change in pH_i of SK-OV-3 and MCF-7 cells (to achieve steady state pH_i recovery following acute acid loading from ammonium pre-pulse; Section 2.11.1), is depicted in Figure 6.4 A-D. Methanandamide delayed the pH_i recovery of SK-OV-3 cells in HEPES buffered solution in normal pH_e and normal PO_2 (Figure 6.4 A) compared to normal. However, in low pH_e and normal PO_2, TASK-3 blockade had no effect on the pH_i recovery rate of acidified SK-OV-3 cells following the ammonium pre-pulse, compared to control (Figure 6.4 B). In contrast, in MCF-7 cells, methanandamide potentiated the steady state pH_i recovery from their acute acidification, not only in normal pH_e under both normal (Figure 6.4 A) and

low PO_2 (Figure 6.4 D) but also in low pH_e accompanied with low PO_2 (Figure 6.4 C). Interestingly, irrespective of the pH_e, methanandamide led to recovery of pH_i in acidified MCF-7 cells beyond their baseline steady state levels (Figure 6.4 C & D), when under low PO_2. However, TASK-3 blockade did not provide any change in the pH_i recovery rate in MCF-7 cells in low pH_e under normal PO_2 compared to control (Figure 6.4 B).

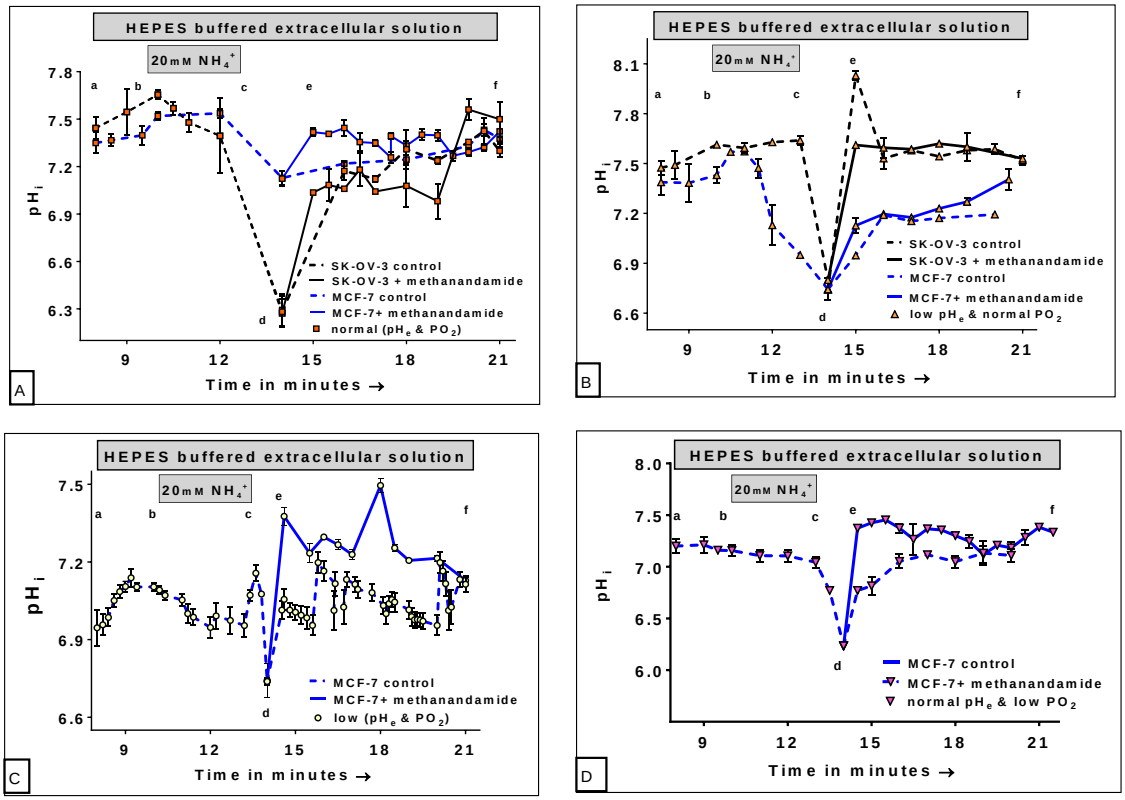

Figure 6.4: TASK-3 effects pH_i regulation following ammonium pre-pulse in SK-OV-3 and MCF-7 cells in altered pH_e. The time course of change in pH_i of SK-OV-3 and MCF-7 cells (to achieve steady state pH_i recovery) in the presence of methanandamide, following ammonium pre-pulse in [A] normal PO_2 and normal pH_e [B] normal PO_2 and low pH_e. pH_i recovery of MCF-7 cells in the presence of methanandamide in [C] low PO_2 and pH_e and [D] low PO_2 and normal pH_e. Indicated with '*d-f* 'are the pH_i recovery points corresponding to 3µM methanandamide mediated inhibition of TASK-3 channel when compared between conditions and cell lines as described in the main text. n = 11

6.2.5 The NAE in cancer cells in the presence of methanandamide

The NAE of SK-OV-3 and MCF-7 cells in the presence or absence of methanandamide was carried out using the β_I and pH_i recovery rate (as per equations described in Section 2.11.1.3 from the time course traces of ammonium pre-pulse manoeuvres depicted in Figure 6.2 and 6.4 respectively. The NAE in the presence of methanandamide in normal pH_e and normal PO_2 for both SK-OV-3 and MCF-7 cells was significantly ($P < 0.0001$) larger compared to that in MCF-10A (no-drug control, as described in Chapter 4) (Figure 6.5A, B).

Interestingly, on simultaneous reduction of both pHe and PO_2 below their normal levels, the NAE of MCF-7 cells in the presence of methanandamide was significantly ($P < 0.0001$) larger compared to that in normal control (Figure 6.5B). Moreover, under normal PO_2, inhibition of TASK-3 channels in SK-OV-3 cells, significantly ($P < 0.05$) increased the NAE only upon increasing pH_e to normal levels (Figure 6.5A).

The NAE in the presence of methanandamide in normal pH_e and PO_2 for both SK-OV-3 and MCF-7 cells was significantly ($P < 0.0001$) larger compared to that in MCF-10A (no-drug control, as described in Chapter 4) (Figure 6.5A, B). Moreover, under normal pH_e/PO_2, inhibition of TASK-3 channels in SK-OV-3 cells by methanandamide, significantly ($P < 0.05$) increased the NAE (Figure 6.5A) compared to their counterparts in low pH_e and normal PO_2. The NAE in the presence of methanandamide in normal pH_e and PO_2 for MCF-7 cells is significantly ($P < 0.0001$) larger than control (Figure 6.5 B).

Finally, we noted that the NAE of MCF-7 cells in the presence of methanandamide in normal as well as low pH_e (while constantly under low PO_2) was significantly larger than that for drug free MCF-7 cells (i.e. without TASK-3 blockade) in normal pH_e and low PO_2 ($P < 0.0001$) as well as in low pH_e and PO_2 ($P < 0.05$) (Figure 6.5 B).

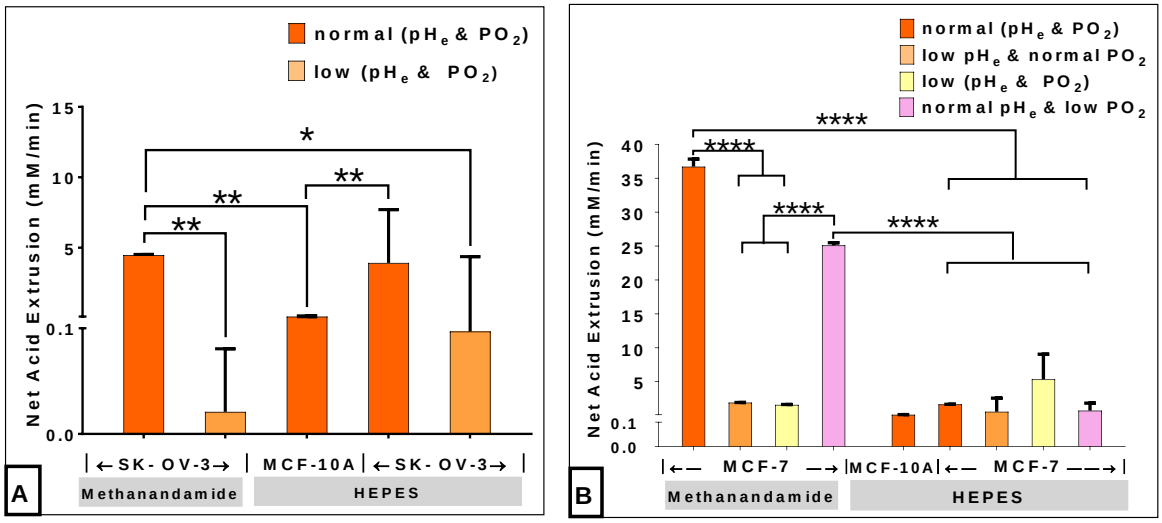

Figure 6.5. Differential effects of methanandamide (TASK-3 inhibitor) on NAE in cancer cells in altered pH_e/PO_2. The NAE in following acute acid loading of SK-OV-3, MCF-7 and MCF-10A (control) in the presence or absence of 3μM methanandamide, under conditions noted in graphs. ** = P < 0.01; ***= P < 0.001; ****= P < 0.0001.n = 8.

6.3 Discussion

6.3.1 Estimation of $[K^+]_i$ in cancer cell lines

The association between potassium fluxes and proton regulation have been investigated in normal tissues as well as tumours focussing on the rise in intracellular Na^+/ K^+ ratio associated with transformation (Davies and Daly, 1984; Kraus and Wolf, 1998). However, relevance of K^+/H^+ ratio and the contribution of the K^+ fluxes that participate in pH equilibria in cancer is poorly understood. In the present study, we recorded that free $[K^+]_i$ in cancer cell lines was close to physiological $[K^+]_i$ values (Thier, 2017) when measured as a function of K^+/H^+ exchange, augmented by the potent potassium ionophore, nigericin. The linear relationship of normal pH_e with equivalent pH_i under the action of nigericin (Figure 6.1) indicate steady equilibration of $[K^+]_e$ (preferably under high $[K^+]_e$). The present study throws light on how $[K^+]_i$ can differ in cancer cells when considering a) high intracellular sodium concentrations found through fluorescence imaging and Na^+ MRI techniques in cancer cells (~500mM) (Cameron *et al.*, 1980; Ouwerkerk, R., Jacobs, M.A., Macura, 2007) and b) studies showing high Na^+/K^+ ratios favouring transformation (Kraus and Wolf, 1998). Based on our findings (Table 6.1 and Figure 6.1), we infer that $[K^+]_i$ potentially oscillates between low and normal values in ovarian and breast cancer cells relative to their proton distribution. It can be argued that that intrinsic pH regulatory mechanisms of proton fluxes across cell membranes that incorporate ion channels (e.g. K^+ ion channels) are predominantly influenced by the differences in the free $[K^+]_i$ in cancer cells (Fenn and Cobb, 1934; Skryma *et al.*, 1997; Sandoz *et al.*, 2009;

Innamaa *et al.*, 2013). In normal and cancer cells, the dependence of pH regulatory mechanism on free Na^+ has been established through the work on amiloride sensitive Na^+/H^+ exchangers (Boyarsky *et al*., 1988b, 1988a; Stüwe *et al*., 2007; Amith and Fliegel, 2013). However, the dependence of pH_i maintenance of cancer cells on the relatively abundant free $[K^+]_I$ has not been explained. We suggest that by investigating how the cancer cells depend on the (tightly controlled) low physiological $[K^+]_e$ to maintain pH_i, the role of free K^+ on pH homeostasis can be understood.

6.3.2 Determination of $[K^+]_e$ dependence of cancer cells to maintain pH_i following acute acidification

Knowledge of the intracellular distribution and concentration of K^+ is also important in understanding the contribution of the K^+ fluxes that participate in steady state pH_i determination in cancer. We demonstrated that significant differences in the $[K^+]_e$ exist between cancer cells and non-tumourigenic counterparts in terms of their potential to maintain pH_i following acute acidification. Furthermore, our observations indicate that acidic pH_e has a negative feedback on this K^+ dependency in the tested ovarian and breast cancer cells. Less than tenfold dependence of breast cancer cells on $[K^+]_e$ for pH_i maintenance compared to ovarian cancer cells, suggests reduced recruitment of K^+ fluxes for intrinsically active pH buffering mechanisms in the former cell line. Since the K^+ dependence has been evaluated as a function of the acid buffering potential of the cancer cells, the K^+ fluxes reflect the their association with pH homeostasis in the test cells. Hence, when the potassium dependence of MCF-7

cells for pH_i maintenance is compared to that of ovarian cancer cells, it is attributable to their individual potentials for proton exchange. Interestingly, we observed that acidic ovarian cancer cells are sensitive at best to less than $^1/_{4^{th}}$ $[K^+]_e$ for their pH_i maintenance in normal pH_e and PO_2 (Figure 6.3B). Although Na^+ and K^+ have contrasting ionic distribution across cell membranes but in terms of ionic dependency on pH_i maintenance, previous studies have shown how progressive addition of extracellular ion (Na^+) to a HEPES buffered solution, can reveal the ionic (Na^+) dependence of the glomerular cells during APP, to manage proton exchange under physiological conditions. Similarly, our study investigated the ionic (K^+) dependence of cancer cells subjected to acute acidic challenge when under the influence of altered pH_e/PO_2. On this basis we were able to understand the functional role of free potassium and potassium channels in cancer progression and pH metabolism (Boyarsky et al., 1988a). We suggest that the potassium dependence of cancer cells to maintain pH can be extrapolated to identify the role of pH_e sensitive membrane potassium channels known to be overexpressed in them (Chapter 3) (Williams, Bateman and O'Kelly, 2012; Pardo and Stühmer, 2014). Thus the role of TASK-3 potassium channel in pH_i recovery of the test cancer cells can be justified by virtue of its oncogenicity, oxygen sensitivity and more importantly extracellular acid sensitivity (Pei *et al.*, 2003; Kim *et al.*, 2009; Ma *et al.*, 2012).

6.3.3 Determination of the role of TASK-3 channel in pH_i recovery from ammonium pre-pulse manoeuvre in altered pH_e, PO_2

The effect of TASK-3 channel inhibition on pH homeostasis can be explained on the basis of our observation that a truncated recovery of steady state pH_i was observed on acute exposure of ovarian and breast cancer cells to channel blockade when maintained in physiological pH_e.

Among other pharmacological and physiological mediators, TASK-3 channels are regulated by cannabinoids such as methanandamide (Hart, Fischer and Ullrich, 2004; Olea-Herrero *et al*, 2009), a non-hydrolysable analogue of the naturally occurring anandamide. Thus, the pharmacological blockade of TASK-3 channels with methanandamide can serve as a useful tool in determining the steady state pH_i recovery of cancer cells in response to a change in pH_e.

However, acid mediated inhibition of acid-sensitive pH regulatory proteins (channels and transporters) in addition to methanandamide further enhanced the pH recovery rate of the tested ovarian cancer cell line in this study. We infer that hypoxia resistant ovarian cancer cells potentially do not utilise TASK-3 associated pH regulation efficiently under physiological pH_e and a normoxic microenvironment. The recovery rate of the cells when in K^+ free medium under similar pH_e can be compared to the enhanced pH recovery rate of ovarian cancer cells from acid mediated inhibition of acid-sensitive pH regulatory proteins (channels and transporters) in addition to the action of methanandamide. Under normal oxygen tension, a substantial drop in pH_e promotes substantial recovery from acute acid dumping in ovarian cancer cells, even with the inhibition of TASK-

3 oncogenic protein. It can be inferred that the short-term effect of TASK-3 blockade is rendered potentially redundant when the pH_e is acidic. The study indicates that a robust pH_i regulation is manifested more effectively under this microenvironment condition (compared to normal pH_e) resulting in quick recovery of steady state pH_i and thus favouring cellular metabolism in these cells. Thus, ovarian cancer cells that exist in acidic environment can predominantly be affected by acid mediated inhibition of acid-sensitive ion channels and transporters. As shown in previous studies the acidic pH_e appears to render additional inhibition of acid-sensitive ion channels like TASK-3 to modulate the effect of methanandamide (Duprat *et al.*, 1997; Bang, Kim and Kim, 2000). As this model partially mimics tumour microenvironment, our findings reveal the dependence of SK-OV-3 cells on acid-sensitive channels like TASK-3 among other compensatory mechanisms in pH homeostasis in normal oxygen tension.

Furthermore, our data shows that when the tissue origin of the cancer cell line was changed to breast tissue, they exhibited different pH_i regulation kinetics after blockade of TASK-3 by methanandamide. The blockade of TASK-3 channels in these cells was associated with high rates of pH_i regulation not only in low pH_e but also low PO_2 unlike in SK-OV-3 cells. Methanandamide is known to significantly reduce resting membrane conductance (Pequignot *et al.*, 2003), however, the dependence of resting membrane conductance on $[K^+]_e$ has been shown to be significantly affected in acidic pH_e by (Strickholm, 1981). We suggest that, loss in membrane conductance associated with TASK-3 channel inhibition in cancer cells facing acute acidotic challenge is manifested as a fast regulation in

pH_i. This is promoted by substantially low pH_e and/or PO_2 in breast cancer cell line. Although factors like channel function and ionic concentration etc. are important in these processes the contribution of low oxygen tension with low pH_e is subjective to cell types. The study indicates the importance of tissue of origin for any cancer type and refers to the response of individual cancer types towards altered microenvironment. In breast cancer cell lines, an environment that more closely resembled the typical tumour microenvironment, enforced a robust pH_i regulation mechanism even when TASK-3 activity was blocked, mobilising significant number of protons across the membrane along the gradient directed outward at a rate that was significantly higher than physiological levels of pH_e and PO_2. These findings emphasise that in the presence of a lower oxygen tension and pH_e, the action of methanandamide on TASK-3 channels activity could be potentiated, as these channels are known to be inhibited by low pH_e (Fenn and Cobb, 1934; Skryma *et al.*, 1997; Sandoz *et al.*, 2009; Innamaa *et al.*, 2013). The consistent drop in pH_i recovery rate of the cancer cells (SK-OV-3 and MCF-7) after drop in the pH_e is observed when assisted by low partial pressure of oxygen. Although this trend is observed in both cell lines after a brief exposure to methanandamide under normal oxygen tension, the slopes of pH_i recovery of MCF-7 cells in pH 6.3 and 7.4 are not significantly different unlike in SK-OV-3 cells. This variation indicates how pH_i rectifying mechanisms might recruit similar pH modulators differently for pH homeostasis. The oxygen sensing property of TASK-3 channels has also been attributed to their inhibitory potential in some studies (Hartness *et al.*, 2001).

Methanandamide at the same dose (3 μM) has also been shown to produce potent blockade of human-TASK-3 channels in transfected HEK-293 (tsa-201) cells (Veale *et al.*, 2007). The importance of TASK-3 channel activity in restoring membrane potential is well documented (Duprat *et al.*, 1997; Pei *et al.*, 2003). The maintenance of membrane potential has its implications in cell proliferation (Yang and Brackenbury, 2013). In electrophysiology experiments conducted by our group we could demonstrate that, even without TASK-3 inhibition at the resting state SK-OV-3 (with very high expression of TASK-3, Chapter 3, (Innamaa *et al.*, 2013)) were more depolarised (membrane potential of~7-to -10mV,(N=7) compared to MCF-7 cells (~ -37 to -42mV, (N=13). This observation exposes the difference in the functional importance of the family of pH sensitive channels like TASK-3 and associated membrane potential changes between different cancer cell types.

Functional roles of TASK-3 channels reveals that inhibition of these channels could potentially prove to impair physiological functions in rapidly dividing cells (Czirjak and Enyedi, 2002). TASK-3 channels have been known to change their permeability to sodium when dealing with cytosolic acidification and exhibit oxygen sensitivity.

Two factors might influence the functional role of TASK-3 channels in cancer cells like SK-OV-3. Firstly, a relatively low copy number variation of *KCNK9* genes and secondly the synthesis and recruitment of exclusively membrane potential associated functional (i.e., K^+ permeable) TASK-3 channels that is attributed to tumorigenicity (Pei *et al.*, 2003).

One of the limitations of the study include the fact that a technical manoeuvre of the $[K^+]_e$ estimation required the use of low Na^+ extracellular solution, while assuming intracellular Na^+ in the test cells to be below 10mM. The high preference of nigericin for K^+ and the use of two different $[K^+]_e$ solutions are aimed at reducing experimental bias for free $[K^+]_I$ estimation. The limitations of the study largely revolve around the technical issues as addressed in Chapter 5 i.e., live cell setup with widefield fluorescence microscopy was capable of elucidating signals only on individual cell to cell basis. Fluorescence microplate reader setup could incorporate all experimental conditions within reasonable limits allowing us to record collective mean data from monolayers. The use of non-pharmacological techniques such as siRNA or shRNA to knock down TASK-3 expression in target cell lines could provide validation of the given data through electrophysiology experiments and thereby by reducing the limitations of the study. The use of transfected cells with overexpression of pH sensitive K^+ channels could also be used to detect minor manifestations of inhibitors or activators of the channels in altered pH_e and PO_2.

In summary, the present study provides insights into the association between pH regulation and K^+ fluxes. Investigation of the functional role of acid-sensitive K^+ channels in pH_i regulation and homeostasis is central to the understanding of proton and K^+ dynamics in cancer cells. Genomic imprinting the oncogenic or pro-oncogenic pH sensitive potassium channel can provide insights into cells with overexpression of these channel proteins (Mu *et al.*, 2003; Ruf *et al.*, 2007). The regulation of expression of these channels is not understood well. Hence

epigenetic profiling of the genes coding for these membrane proteins can potentially reveal the co-regulation of these genes with genes coding for functional proteins involved in cancer progression. Thus, the functional role of target channel proteins can also be investigated by tracing their expression in cancer cells through epigenetic regulation, which would open newer avenues to a better understanding of how these channels are recruited. Finally, this chapter's observations help understand the characterisation of potassium ion channels and transporters are affected by acid fluxes in cancer cells in a dynamic microenvironment.

Chapter 7. General discussion

7.1 General consideration

Proton concentration across biological membranes, their distribution and regulation is central to a complex system of essential biochemical reactions. This study contributes towards the understanding of the mechanisms of pH fluxes that manifest through cellular processes in cancer. We developed in vitro culture models for screening metabolic signatures of cancer cells, not only in altered extracellular pH (pH_e 6.3 and 7.4) but also under varying oxygen tensions (PO_2 of 0.029 atm and 0.21 atm). The study focussed on the interaction between two important components viz., pH_e and PO_2 to mimic the tumour microenvironment. An important outcome of the study is that it contributes to the knowhow of calibration of altered culture media and describes how their manipulation will aid the researcher in customising the culture media mimicking subtle variations in the specific tumour microenvironment to suit the study requirements.

We demonstrated that, ovarian cancer cells exclusively are benefitted by acidification of the hypoxic microenvironment as observed by the increased expression of gene coding for external acid sensitive oncogenic TASK-3 channel. In contrast, the cancer cell lines tested in this study fail to obtain this benefit from low pH_e when the gene expression of other voltage-gated potassium channels are considered. The developed culture models helped us to understand how cancer hallmarks like proliferation and migration are significantly influenced by alterations in pH_e and PO_2. Hence, the study indicates an association between increased expression of oncogenic potassium TASK 3 channels and the

proliferation of ovarian cancer cells. Additionally, the culture models used in this study helped establish the positive influence of acidic pH_e and low PO_2, potentiating the aforementioned association in hypoxia resistant ovarian cancer cells sparing breast cancer cell lines. However, the breast cancer cell lines were found to maintain a better pH homeostasis when compared to the ovarian cancer cells by virtue of having a higher intrinsic buffering capacity in acidic pH_e. But both the ovarian and breast cancer cells possess comparable potential in recruiting the extrinsic buffering mechanism to counter an acute intracellular acidotic challenge that simulates abrupt shift in tumour metabolism.

The study revealed that alterations in K^+ flux under low pH_e & PO_2 indicates the involvement of TASK-3 channels. The behaviour and response of cancer cells to an acidic, low oxygen microenvironment, partially involves the TASK-3 channel. The key findings of this study are pivoted on the culture methodology developed in this study. Further development of these methodologies can prove to be beneficial to investigate the role of these channels in response to the cancer environment and can aid in the development of novel chemotherapeutic strategies and diagnostic tools.

All important physiological processes in health and disease require efficient redistribution of energy derived from cellular metabolism. The regulation of the cellular proton potential is known to play an important role in cellular energetics (Lindner and Raghavan, 2009). Transmembranal flux of protons is thus an indispensible strategy for suitable operation of quintessential cellular events

including cell proliferation and migration in rapidly dividing cells and cancers (Chiche, Brahimi-Horn and Pouyssegur, 2010). Furthermore, the process of transformation leads to the selection of unique malignant phenotypes (Fang, Gillies and Gatenby, 2008) when the cell adapts a reprogrammed metabolic process (Section 1.1) associated with the acidification of the microenvironment (Pavlova and Thompson, 2016).

The metabolic flux of protons in cancer cells is a consequence of this metabolic shift also induced by tumour hypoxic stress, considered as an important hallmark of cancer (Luo, Solimini and Elledge, 2009; Chiche, Brahimi-Horn and Pouyssegur, 2010). In turn, metabolic shift from OXPHOS to glycolysis (Chapter 1; Figure 1.13) in cancer cells, corresponding to ATP generation is primarily promoted by highly expressed cellular and glycolytic enzymes. Hypoxia (through Hypoxia Inducible Factor, HIF-1α) acts as a key factor responsible in inducing the expression of these enzymes (Semenza, 2003; Pouyssegur, Dayan and Mazure, 2006). Hypoxic stress exist as a gradient of oxygen tensions ranging between normal levels (6%), mild hypoxia (0.5 to 3%) and anoxia (0%) (Vaupel, Kallinowski and Okunieff, 1989; Olcina, Lecane and Hammond, 2010). These hypoxic regions are associated with the most aggressive and therapy-resistant fractions of the tumour (Olcina, Lecane and Hammond, 2010). Finally, hypoxic stress works in coordination with cellular systems that are associated with the establishment of a pH gradient across the tumour microenvironment (Harris, 2002; Vaupel, Mayer and Hockel, 2004; Hulikova *et al.*, 2013).

The establishment of an acidic pH_e and its association with a relatively neutral/ alkaline pH_i contributes towards the emerging hallmarks of cancer (Chapter 1) (Griffiths, 1991; Stubbs *et al*., 2000; Gillies, Robey and Gatenby, 2008). A change in pH_e, as low as 0.1 pH unit can interrupt various biological processes ranging from ATP synthesis to protein translation mediated events including cell proliferation and migration (Roos and Boron, 1981; Pouysségur *et al.*, 1984; Chambard and Pouyssegur, 1986; Pouyssegur, Dayan and Mazure, 2006).

This demands a strict and continual buffering of pH across cell membranes to adjust and restore the pH gradient which calls for investigation. Acidosis in cancers modifies the cellular metabolism of a vast array of metabolites by means of pH_i regulatory systems (Fang, Gillies and Gatenby, 2008). These pH_i regulating systems mostly comprise pH regulatory proteins that are abundantly expressed as a result of the abrupt shift in metabolism within malignant cells (Semenza, 2003; Pouyssegur, Dayan and Mazure, 2006). Among several membrane-bound transporters and exchangers (described in Chapter 1) distinct pH-sensitive potassium (K^+) channels (special reference to oncogenic TASK-3 channel) have gained prominence due to their overexpression and predicted involvement in cancer (Chapter 1). The published work from our group has shown how overexpression of this pH_e sensitive potassium channel in epithelial ovarian cancer is associated with significant survival benefit on patients with increased expression (Innamaa *et al.*, 2013). This has generated impetus to further investigate, in this study, the role of K^+ flux and TASK-3 channel's function in

proliferation and pH homeostasis in cancer while considering altered microenvironment as a contributing factor in tumour progression.

In the present study, we investigated how the manipulation of such channel proteins not only affect important cancer hallmarks but also pH regulation and buffering in response to acidotic and oxidative stress. Abiding by the overarching purpose of the study, we investigated theories of intrinsic pH buffering potential by tailoring their culture conditions.

Thus, the relevance of developing special culture models that can be aimed to mimic tumour microenvironment in terms of pH_e and associated PO_2 is well understood through this study (Chapter 3). The functionality and applicability of these culture conditions attained special significance as they had to act in accordance with the metabolic alterations that are observed within tumour microenvironment. We demonstrated that through better control on the regulation of pH_e and PO_2 in the extracellular media, cancer cells can be stimulated in a way akin to their pathological conditions. Moreover, an attempt was made to prove that eliciting both short term and long term responses from cancer cells is ideal when subjected to their native environment in direct comparison to that observed in normal tissues. This strategy proved to be of great importance to allow a better understanding of the underlying biological mechanisms. However, it is well understood that to overcome the technical limitations of this study, targeting multiple levels of hypoxic treatments (like < 0.1% O_2 were carried out in a Bactron chamber (Shel Lab) and at 2% O_2 in a Don

Whitley H35 Hypoxystation) has the potential to better elucidate the contribution of mild and severe hypoxia in cancer metabolism and pH homeostasis.

In support of a potential role of oncogenic TASK-3 channels, we suggest that low pH_e and low PO_2 probably play an important role in the localisation of these proteins on nuclear membrane as also indicated from the scanning depth of the composite z-stack images during confocal microscopy. Although the immunofluorescence experiments provided limited information, the mRNA expression of KCNK17 gene in the test cells when cultured in altered pH_e/PO_2 was not observed to be upregulated even under the influence of tumour microenvironment mimicking condition. Moreover, the relative gene expression profile of these two potassium channels primarily in ovarian cells was consistent with their pH_e sensitivity as demonstrated in Chapter 3. Increased transcription of relevant pH regulatory and oncogenic proteins has been noted to be essential mechanisms that induce a glycolytic shift associated with low PO_2, resulting in acidosis in cancers (Chiche, Brahimi-Horn and Pouyssegur, 2010). The intracellular trafficking of these proteins and associated metabolic modifications can be well appreciated by imaging their localisation in dynamic pH_e and PO_2. The change in the localisation of the pH sensing potassium channels has been shown to be associated with such changes in cancer microenvironment (Mathie *et al*., 2010). This study opened new avenues of research pertaining to the gene expression profile in tumours. The study demonstrated how tissue specific quantifiable variation in gene expression is seen in altered pH_e and PO_2 in

different cancer cells. However, the mechanisms that govern the upregulation or downregulation of these genes in cancer cells can be understood to vary from mutational events to methylation of promotor regions (Yang, Yan and Davidson, 2001; Clark and Melki, 2002; Konduri *et al.*, 2003). The present study can be followed by attempting to answer the question of which molecular processes (e.g. epigenetic markers, secondary messengers and protein complexes) can potentially regulate the expression or switch on/off these genes in tumours (Crociani *et al.*, 2003; Ruf *et al.*, 2007; Enyedi and Czirjak, 2010). However, further studies involving electrophysiological characterisation of membrane potential, genome wide analysis of potential metabolic targets are needed to show specific involvement and functional role of TASK-3 and other pH sensing K^+ channels (TREK2, TASK1 TALK2, TRAAK etc.) in cancer (Kim *et al.*, 1998; Czirjak and Enyedi, 2002).

7.2 Role of pH regulation in important cancer hallmarks

Cellular metabolism and pH regulation play an important role in physiological and pathological processes like embryonic development, wound healing, immune response, inflammation and tumorigenesis. On sensing a substantial increase of pH_i, cancer cells have been shown to proliferate (Chambard and Pouyssegur, 1986) and also transit into a different phase of the cell cycle (Putney and Barber, 2003). Through experimental interventions, we studied the dependence of cell proliferation rate on pH regulation in cancer (Chapter 4). In the present study, we demonstrated that tumour specific culture conditions have the potential to selectively improve the long doubling time of cancer cells (viz., ovarian and

oesophageal cancer cells) compared to conventional culture conditions. Although this observation supports the theory that micrenvironment's interactions are emerging hallmarks of cancer, however it cautions its generalisation incase of all solid tumours. Furthermore, the involvement of pH regulators and pH sensitive membrane proteins including potassium channels have been shown to be quintessential in cancer cell viability and proliferation when a dynamic pH_e and oxygen tension were considered (also shown by (Gillies *et al.*, 1990; S J Reshkin *et al.*, 2000)). Hence, we demonstrated the need for testing this correlation through modifications in culture conditions. The *in vitro* association of pH/PO_2 with cancer cell viability and proliferation can be correlated with in vivo cancer progression. This correlation is inseparably related to their metabolic adaptation and pH/PO_2 dynamics of the microenvironment (Vander Heiden, Cantley and Thompson, 2009; Amith and Fliegel, 2013). In the presented work (Chapter 4), it was demonstrated how pH modulators (with special importance to potassium channels) have a very important role to play in cancer cell proliferation. We demonstrated for the first time that in the presence of acidic pH_e and PO_2, the inhibition of pH sensing TASK-3 channel proteins resulted in significant decrease in cancer cell proliferation and viability of the tested cancer cells except for metastatic breast cancer cells. The study focussed on evaluating viability of the cells exposed to the pharmacological agents (omeprazole, methanandamide and E-4031) not only by assessing their metabolic potential but also by virtue of their pH_i recovery and maintenance. We demonstrated that pH homeostasis in cancer cells is modulated differentially on

targeting H^+ regulatory proteins. Hence through this study we highlighted that the extensive use of the developed culture models can provide experimental assistance to tease out tailored responses through pharmacological inhibition of these modulators in dynamic pH_e and PO_2 microenvironment. We advocate the use of modified culture models in the screening of pH regulatory and pH-sensing proteins to identify potential targets for anti-cancer drugs. A broad spectrum of phenomena associated with pH regulation and metabolism can be simultaneously explained through this approach as demonstrated in our study. The importance of altered pH_e and PO_2 to address an important hallmark of cancer i.e. cell migration, has also been emphasised in this research (Chapter 4). Although the involvement of pH in metastasis was shown in many studies (Martinez-Zaguilan *et al.*, 1996; Klein *et al.*, 2000), our work demonstrated how meticulous dissection of the pH_e and PO_2 components of cancer microenvironment can be used to further understand cancer cell migration and pH homeostasis involved therein. Our observations indicated that hypoxia resistant potential of ovarian cancer cells renders them significant tactical advantage in migratory capabilities when associated with simultaneous acidification of the microenvironment. Interestingly, the maintenance of low pH_i in migrated metastatic breast cancer cells was unanimously significant in response to both low and normal pH_e only when oxygen tension was low. Although our observations could not detect a significantly increased invasive potential of ovarian cancer cells under tumour microenvironment simulating culture conditions, their pH_i restoration was affected markedly. The relevance of

knowing the pH_i of migrated cells as demonstrated in our study holds the key to understand the metabolic modifications in migratory cells. Further investigation aided by elaborate use of modified culture models will help establish an association between cancer migration and pH regulation as compared to the use of only physiological culture models.

7.3 Role of pH buffering in regulating pH_i restoration in cancer cells

An experimental setup to study the *in vitro* pH buffering was also key to this research (Section 2.4.3). Eliciting cellular response to systematic and controlled challenge of the pH regulating systems (Chapter 5) was possible through effective use of the modified media.

Furthermore, this study showed how the pH buffering potential of cancer cells of different tissue origins can respond differently to the magnitude of change in the microenvironment factors. Techniques like live cell imaging was clubbed with physiological experiment (Ammonium pre-pulse manoeuvre) to further understand the role of pH modulation in cancer metabolism (Chapter 5). We demonstrated that intrinsic buffering capacity of ovarian cancer cells increased significantly when switching from normal to low pH_e in a normal PO_2 environment. To the best of our knowledge, we demonstrated for the first time that in metastatic breast adenocarcinoma cells this observation was reversed when pH_e and PO_2 were simultaneously lowered from conditions mimicking normal interstitium. However, the failure of the non-neoplastic breast epithelial cells to withstand acute acid loading in low pH_e is in contrast to their high buffering capacity under physiological pH_e. Through our research, we could

explain how manipulation of the pH and PO_2 component of tumour environment can be effectively used to understand their long term effects on cancer cells.

The present study indicates that breast adenocarcinoma cells chronically thriving under normal pH_e but mild hypoxia can be additionally restricted from extruding accumulated acid extracellularly. This potentiated negative feedback from hypoxia in alkalinised microenvironment can imply unanticipated therapeutic failure of weakly acidic cancer chemotherapeutic agents intended to activate upon ionisation in near neutral pH_i. Interestingly, we propose that this phenomenon can also be weaponised against cancer cells by a double pronged approach. Firstly, Structure Activity Relationship (SAR) of anticancer agents can be manipulated to contain weakly basic functional groups that ensure their selective uptake in normal pH_e and eventual ion-trapping (Ndolo *et al.*, 2012) in acidic pH_i. Secondly, manipulating hypoxic states around tumours can physiologically compell them to drown in the intracellular acid generated from metabolic overactivation.

The present study suggests the existance of centrally localised transiently compromised pH buffering zones in cancer, possibly in the regions of high metabolic activity. This is also helpful in appreciating the potential regions of pH regulation that established a more physiological pH_i.

The data from the experiments that investigated pH buffering were used to understand the potassium dependence of pH_i regulation in cancer (Chapter 6). The relative influence and functional role of external acid-sensing TASK-3 potassium channel through pharmacological blockade in cancer cells was also

demonstrated in this study. The significance of understanding the interrelationship between pH_e/PO_2 with pH-sensing modulators and membrane proteins was emphasised throughout this study. Our data suggested for the first time that manipulation of extracellular potassium can selectively and significantly affect the buffering potential of breast cancer cells in tumour possibly by a positive feedback mechanism. We infer that the relatively lower dependability of ovarian cancer cells towards external potassium is potentiated in alkaline microenvironment (Chapter 6). This implies that the potassium dependent pH homeostasis is probably compensated by alternative salvage mechanisms in ovarian cancer cells that can serve as targets for therapeutic manoeuvre.

The above finding also falls in line with the observation that hypoxia resistant ovarian cancer cells potentially do not utilize TASK-3 potassium channel associated pH regulation efficiently under physiological pH_e and a normoxic microenvironment. It can be inferred that the short-term effect of TASK-3 blockade is rendered potentially redundant in these cells when the pH_e is acidic. In contrast acute TASK-3 inhibition has a major effect in breast adenocarcinoma more dominantly in acidic microenvironment when simultaneously assisted with hypoxic situations. Here it is important to understand that acid mediated inhibition of TASK-3 potassium channel potentiates the action of methanandamide, predominantly in breast adenocarcinoma. Our study clarifies the difference between the effects of long term pharmacological inhibition (Chapter 4) versus the acute inhibition of TASK-3 channels (Chapter 6) in breast and ovarian cancer cells. We demonstrated that extrusion of acutely

accumulated acid in cancers can be selectively mediated by acute TASK-3 channel inhibition, preferably when the pH of surrounding microenvironment is normal irrespective of the oxidative stress in breast cancers more than in ovarian cancer cells. This has therapeutic and diagnostic impications where TASK-3 expression alone should not be considered as indicative of survival criterion for malignant cells.

One of the limitations of the study is that it depends on the chemical ionophore nigericin that can introduce experimental bias for calibration of the pH-sensing dyes when interacting differently with multiple pH-sensitive dyes. The limitations of the study can be the exclusive use of a sensitive live cell setup that can introduce phototoxicity to cells differentially. Transfection models with predominant expression of pH-sensitive potassium channels, cells can serve as models to detect minor manifestations of inhibitors or activators of these channels in altered pH_e and PO_2.

Further limitation of the study is that lack of use of cancer biopsies leaves gap in the knowledge of interaction between modulators of pH_i and pH_e buffering to influence therapeutic strategy designs. Increasing scientific evidence confirms the significance of pH regulation and homeostasis in cancer metabolism (Fais *et al.*, 2007; Le Floch *et al.*, 2011). The potential lack of use of existing cancer chemotherapeutic agents in the study leaves unanswered areas that can reveal striving concepts for therapy, pursuing pH-handling proteins with pharmacological inhibitors, modulators & monoclonal antibodies to increase therapeutic selectivity (also explained by (Fais *et al.*, 2007; Le Floch *et al.*, 2011;

Neri and Supuran, 2011). More effective means (eg. H^+-suicide technique coupled with TASK-3 transfected or knocked down cells) could have been used in this study to compel cancer cells to accumulate protons intracellularly by compromising in vitro acid extrusion (Pouysségur *et al.*, 1984; Rotin *et al.*, 1989; El Hachmane *et al.*, 2014).

Translating such mechanisms into effective in vivo strategies still encounters complex physiological issues concerning intrinsic affinity of ligands or their selectivity to cancer cells (Tannock and Rotin, 1989; Swietach *et al.*, 2014). The seemingly inevitable risk appears to be that of introducing systemic toxicity, an untoward event due to simultaneous blocking of the acid-base modulator proteins in non-neoplastic cells. Multiple molecular targets that jeopardise pH regulatory mechanisms need to be identified. The manipulation of these targets, exclusive to cancer cells, can spare physiological metabolic processes. These targets could not only include cancer specific isoforms of cation-proton exchangers, carboxyl transporters and carbonic anhydrases like NHE-1, hypoxia-induced MCT4 and CAIX but also pH sensitive ion channels with known oncogenic potential (Eg. TASK-3 protein overexpressed in cancer) (Kummola *et al.*, 2005; Chiche *et al.*, 2009; Stock and Schwab, 2009; Vegran *et al.*, 2011). An alternative strategy would involve increasing the efficacy and potency of pharmacological agents by increasing chemical efficacy in tumour microenvironment. This approach should be able to defy the principles of niche engineering in cancer by increasing the bioavailability of therapeutic agents (E.g. bio-activation of prodrugs at low pH_e and/or PO_2, without having to increase its dose or dosage

frequency) (Andresen, Jensen and Jorgensen, 2005; Wu *et al.*, 2006). Another issue with selecting metabolic/pH modulator targets would be to tackle compensatory methods adapted by the cancer cell (Granja *et al.*, 2015). These salvage pathways could bypass interventional severity in mechanisms for acid extrusion by therapeutic agents. Eventually by changing and adapting actively to metabolic alterations during therapy, cancer cells can compensate for the targeted protein. Achievement of positive clinical outcome by blocking pH_i regulation (targeting pH_i modulator) in cancer can face potential challenges and concerns.

Hence therapeutic targets that consider pH_e as an important component along with the above mentioned strategy are gaining steady recognition (Stock and Schwab, 2009; Loo *et al.*, 2012). The theory and rationale supporting acid mediated disease progression has forced the thrust area of cancer research towards pH homeostasis and pH_e modulation to be investigated as a novel and reliable modality for therapy (Fang, Gillies and Gatenby, 2008; Calorini, Peppicelli and Bianchini, 2012). Further investigation should be aimed at discovering novel methods to manoeuvre extracellular proton distribution and manipulate buffering capacity effectively. These methods could act synergistically, potentiate or can even reduce/mitigate the need to target single or multiple non-selective targets for cancer (E.g. membrane bound transporter proteins). A schematic representation of the key findings and implications of this study is depicted in Figure 7.1.

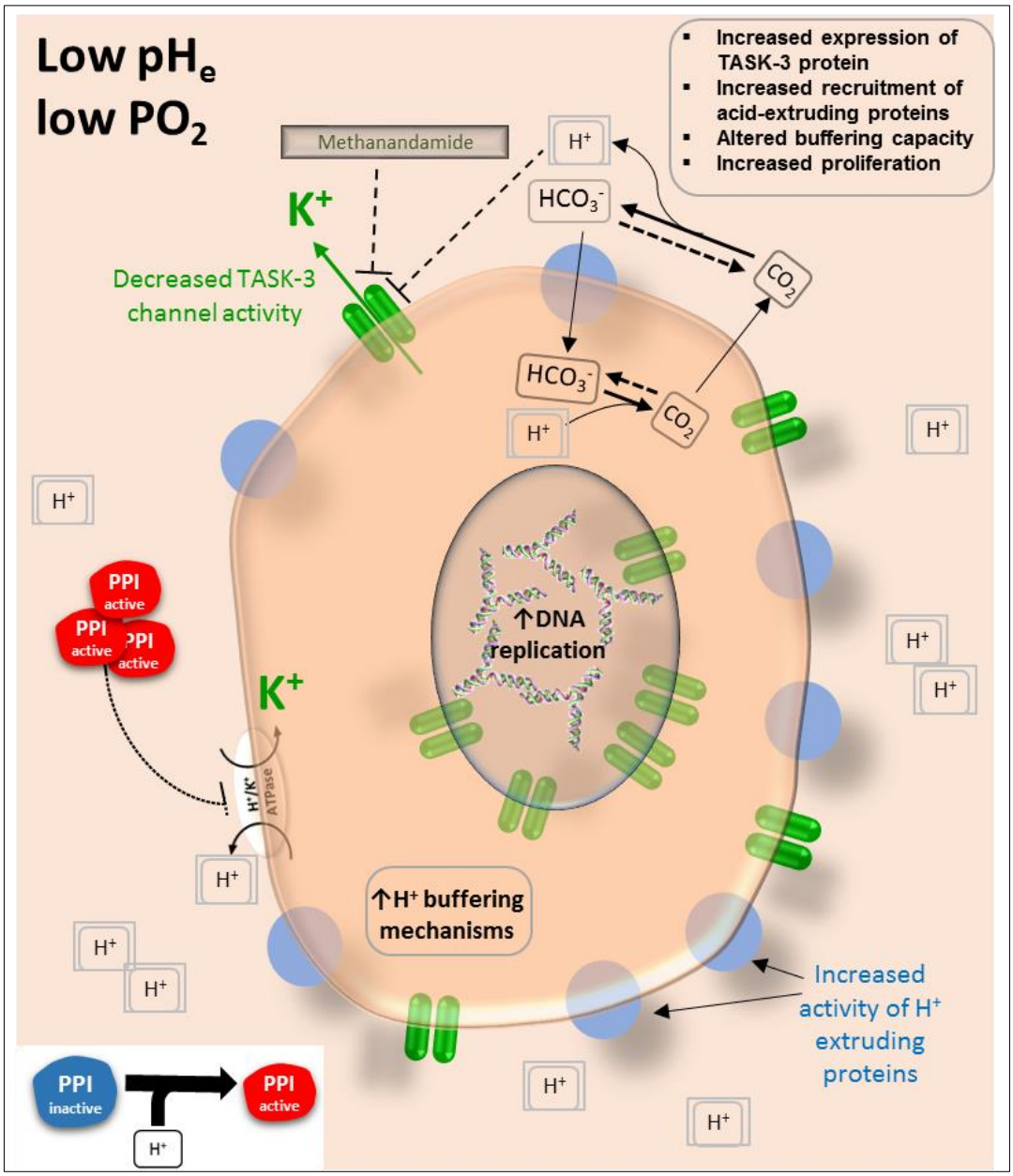

Figure 7.1: Schematic representation of metabolic consequences of altered pH_e and PO_2 in cancer cells. Increased expression of TASK-3 channel protein with nuclear membrane localisation, increased recruitment of acid-extruding proteins and altered buffering capacity which lead to increased proliferation are predominant hallmarks of pH homeostasis in cancer cells in response to low pH_e and low PO_2. Although tumour mimicking microenvironment increases selection of aggressive phenotype in cancer cells, enhanced activation of proton pump inhibitors and inhibition of pH-sensitive K^+ channels is also observed as a consequence of increased proton flux.

7.4 Future research

The knowledge of unique correlation between pH sensitive/regulating membrane proteins with buffering capacity should help identify targets that can overcome selection pressure for cancer over normal cells. The presented work showed the impact of pH_e and PO_2 on cancer cell's response to acid buffering, proliferation, migration and K^+ dependant pH homeostasis through membrane bound K^+ channel. The study also highlighted the differential expression of pH sensitive K^+ channel proteins and genes in cancer cells in response to altered pH_e and PO_2. However, this did not permit the identification of the functional role of pH sensing K^+ channels in contributing towards establishment of membrane potential in response to an altered microenvironment. In an effort to understand the functional behaviour and to characterise these potassium channels in cancer cells under altered pH_e, the inward rectifying pattern of electrophysiological activity can be investigated (Huang and Rane, 1994; Veale *et al.*, 2007; Yang and Brackenbury, 2013). Novel modifications in patch-clamping techniques will help to assess the conductance of these channels through whole cell recording in non-excitable cells (Hopwood and Trapp, 2005; Clarke *et al.*, 2008; El Hachmane *et al.*, 2014). Evaluating their pH regulatory role through single channel recordings (SCR) by recruiting pharmacological inhibitors or through siRNA moderated gene silencing would be of primary focus (Cardone *et al.*, 2008; Lee *et al.*, 2011; Nagelkerke *et al.*, 2013). These studies are also expected to help us understand their functional correlation with other pH regulatory systems through SCR (Cahalan *et al.*, 1985; Rajan *et al.*, 2000; Ashmole *et al.*, 2009).

Furthermore, studies of single perfused cells cannot adequately describe pH regulation in cancer tissue as they do not effectively simulate the multicellular nature and suboptimal perfusion of tumours. Hence it has now been realized that considering cancer biology in just '2 dimensions' (monolayer culture) has serious limitations in

- Assessing the change in the pharmacodynamic effects of inhibitors.

- Evaluating the response of tumour spheroid to alterations in pH_i (Fazeli *et al.*, 2007; Kadletz *et al.*, 2015; Cesarz and Tamama, 2016).

In order to understand the interplay of these limitations in tumour progression, further research is required on the hypoxic and low pH_e models of in vitro three dimensional tumour constructs (spheroid model with cell lines and primary tissue cultures). Thus future research in this line should provide superior amalgamation of the strategies that not only manipulate mobile buffering capacity but also take into consideration pH modulators as targets for novel therapeutic approaches.

7.5 Concluding remarks

In this study, I have shown that a bidirectional interaction between pH homeostasis and pH modulating proteins enable mammalian cells to manage the flux of protons and adapt to their availability in the microenvironment. The presented work highlights that tumours exhibit an everlasting endeavour to dominate the normal cells in its niche. The cancer cells as a result give rise and sustain an uncontrolled pathological process. These pathological processes lead to the development of genetically dominant phenotypes that are capable of manipulating this pH-environment couple. This enables cancer cells to develop strategies- to evade deleterious alterations in cellular and systemic processes and engineer their niche and metastasize. Proton concentration across biological membranes, their distribution and regulation is essential for the functioning of a complex system of essential biochemical reactions. This study contributes towards the understanding of the mechanisms of pH fluxes that manifest through cellular processes in cancer. Further research involving a combination of *in vitro*, translational and computational approaches would be instrumental in developing novel strategies to explore the pH/PO_2 interaction in understanding cancer metabolism.

References

Adler, S. and Fraley, D. S. (1977) Potassium and intracellular pH. *Kidney International*. Elsevier, **11**(6), pp. 433–442.

Aickin, C. C. and Thomas, R. C. (1977) An investigation of the ionic mechanism of intracellular pH regulation in mouse soleus muscle fibres. *The Journal of Physiology*, **273**(1), pp. 295–316.

Alexander, S. P. *et al.* (2017) The concise guide to pharmacology 2017/18: Overview. *British Journal of Pharmacology*, **174 Suppl**, pp. S1–S16.

Alfarouk, K. O. *et al.* (2014) Glycolysis, tumor metabolism, cancer growth and dissemination. A new pH-based etiopathogenic perspective and therapeutic approach to an old cancer question. *Oncoscience*, **1**(12), pp. 777–802.

Aller, M. I. *et al.* (2005) Modifying the subunit composition of TASK channels alters the modulation of a leak conductance in cerebellar granule neurons. *Journal of Neuroscience*, **25**(49), pp. 11455–11467.

Amith, S. R. and Fliegel, L. (2013) Regulation of the Na^+/H^+ Exchanger (NHE1) in Breast Cancer Metastasis. *Cancer Research*, **73**(4), pp. 1259–64.

Amos, B. J. and Richards, C. D. (1996) Intrinsic hydrogen ion buffering in rat CNS neurones maintained in culture. *Experimental Physiology*, **81**(2), pp. 261–271.

Anbalagan, S. *et al.* (2015) In Vitro Radiosensitization of Esophageal Cancer Cells with the Aminopeptidase Inhibitor CHR-2797. *Radiation Research*, **184**(3), pp. 259–65.

Andresen, T. L., Jensen, S. S. and Jorgensen, K. (2005) Advanced strategies in liposomal cancer therapy: problems and prospects of active and tumor specific drug release. *Progress in Lipid Research,* **44**(1), pp. 68–97.

Arcangeli, A. *et al.* (1995) A novel inward-rectifying K^+ current with a cell-cycle dependence governs the resting potential of mammalian neuroblastoma cells. *The Journal of Physiology*, **489**(Pt 2), pp. 455–71.

Arcangeli, A. *et al.* (2009) Targeting ion channels in cancer: a novel frontier in antineoplastic therapy. *Current Medicinal Chemistry*, **16**(1), pp. 66–93.

Arnold, D. L. *et al.* (1990) Proton and phosphorus magnetic resonance spectroscopy of human astrocytomas in vivo. Preliminary observations on tumor grading, *NMR in Biomedicine*, **3**(4), pp. 184–189.

Aronson, P. S. (1985) Kinetic Properties of the Plasma Membrane Na^+-H^+ Exchanger. *The Annual Review of Physiology*, **47**(1), pp. 545–560.

Aronson, P. S. and Giebisch, G. (2011) Effects of pH on potassium: new explanations for old observations. *The Journal of the American Society of Nephrology*, **22**(11), pp. 1981–1989.

Arun Bahl, BS Bahl and Tuli, G. (2005) Acids and Bases, in *Text Book of Physical Chemistry*. 26th edn. S. Chand, pp. 932–975.

Asher, V. *et al.* (2011) The role of Eag and HERG channels in cell proliferation and apoptotic cell death in SK-OV-3 ovarian cancer cell line. *Cancer Cell International*, **11**, p. 6.

Ashmole, I. et al. (2009) 'The response of the tandem pore potassium channel TASK-3 (K(2P)9.1) to voltage: gating at the cytoplasmic mouth', *The Journal of Physiolog*y. **587**(20), pp. 4769–4783.

ATCC® (2017) *ATCC: The Global Bioresource Center*. Available at: https://www.atcc.org/Products/All/CRL-10317.aspx.

ATCC ® (2011) *ANIMAL CELL CULTURE GUIDE tips and techniques for continuous cell lines*, *Animal Cell Culture Basics.* Available at: https://www.atcc.org/~/media/PDFs/Culture Guides/AnimCellCulture_Guide.ashx.

Aylott, J. W. (2003) Optical nanosensors—an enabling technology for intracellular measurements. *The Analyst*, **128**(4), pp. 309–312.

Balkay, L. *et al.* (1997) Flow cytometric determination of intracellular free potassium concentration. *Cytometry*, **28**(1), pp. 42–9.

Bang, H., Kim, Y. and Kim, D. (2000) TASK-3, a New Member of the Tandem Pore K^+ Channel Family. *The Journal of Biological Chemistry*, **275**(13), pp. 17412–17419.

Baronzio, G. *et al.* (2014) Tumor interstitial fluid: proteomic determination as a possible source of biomarkers. *Cancer Genomics and Proteomics*, **11**(5), pp. 225–237.

Bayliss, D. A., Sirois, J. E. and Talley, E. M. (2003) The TASK family: two-pore domain background K^+ channels. *Molecular Interventions*, **3**(4), pp. 205–219.

Berger, T., Saunders, M. E. and Mak, T. W. (2016) Beyond the Oncogene Revolution: Four New Ways to Combat Cancer. *Cold Spring Harbor Symposia on Quantitative Biology*, **81**, pp. 85–92.

Bergman, J. A. *et al.* (1991) Use of the pH-sensitive dye BCECF to study pH regulation in cultured human kidney proximal tubule cells. *The Journal of Tissue Culture Methods*, **13**(3), pp. 205–209.

Besancon, M. et al. (1997) 'Sites of reaction of the gastric H^+/K^+-ATPase with

extracytoplasmic thiol reagents', *The Journal of Biological Chemistry*. **272(**36), pp. 22438–22446.

Bianchi, L. *et al.* (1998) Herg encodes a K^+ current highly conserved in tumors of different histogenesis: a selective advantage for cancer cells? *Cancer Research*, **58**(4), pp. 815–22.

Bischof, G. *et al.* (1996) Effects of extracellular pH on intracellular pH-regulation and growth in a human colon carcinoma cell-line. *Biochimica et Biophysica Acta - Biomembranes*, **1282** (1), pp. 131–139.

Blin, S. *et al.* (2014) Tandem pore domain halothane-inhibited K^+ channel subunits THIK1 and THIK2 assemble and form active channels. *The Journal of Biological Chemistry*, **289**(41), pp. 28202–12.

Blum, R. *et al.* (2005) Ras inhibition in glioblastoma down-regulates hypoxia-inducible factor-1 alpha, causing glycolysis shutdown and cell death, *Cancer Research*, **65**(3), pp. 999–1006.

Bose, P., Dort, J. C. and Brockton, N. T. (2013) Identifying the stromal cell type that contributes to tumor aggressiveness associated with carbonic anhydrase IX. *Cell Cycle*, **12**(16), pp. 2535–6.

Bourguignon, L. Y. *et al.* (2004) CD44 interaction with Na^+-H^+ exchanger (NHE1) creates acidic microenvironments leading to hyaluronidase-2 and cathepsin B activation and breast tumor cell invasion. *The Journal of Biological Chemistry*, **279**(26), pp. 26991–7007.

Boyarsky, G. *et al.* (1988a) pH regulation in single glomerular mesangial cells. I. Acid extrusion in absence and presence of HCO_3^-. *The American Journal of Physiology*, **255**(6 Pt 1), pp. C844-56.

Boyarsky, G. *et al.* (1988b) pH regulation in single glomerular mesangial cells. II. Na^+-dependent and -independent Cl^--HCO_3^- exchangers. *The American Journal of Physiology*, **255**(6 Pt 1), pp. C857-69.

Boyer, M. J. and Tannock, I. F. (1992) Regulation of Intracellular pH in Tumor Cell Lines : Influence of Microenvironmental Conditions. *Cancer Research*, **52**(16), pp. 4441–4447.

Brizel, D. M. *et al.* (2001) Elevated tumor lactate concentrations predict for an increased risk of metastases in head-and-neck cancer. *The International Journal of Radiation Oncology, Biology, Physics*, **51**(2), pp. 349–353.

Busa, W. B. and Nuccitelli, R. (1984) Metabolic regulation via intracellular pH., *The American Journal of Physiology*, **246**(4 Pt 2), pp. R409-38.

Bustin, S. A. *et al.* (2009) The MIQE guidelines: minimum information for publication of quantitative real-time PCR experiments. *Clinical Chemistry*, **55**(4), pp. 611–622.

Bustin, S. A., Li, S. R. and Dorudi, S. (2001) Expression of the Ca^{2+}-activated chloride channel genes CLCA1 and CLCA2 is downregulated in human colorectal cancer. *DNA and Cell Biology*, **20**(6), pp. 331–8.

Cahalan, M. D. *et al.* (1985) A voltage-gated potassium channel in human T lymphocytes. *The Journal of Physiology*, **358**, pp. 197–237.

Caino, M. C. and Altieri, D. C. (2015) 'Cancer cells exploit adaptive mitochondrial dynamics to increase tumor cell invasion', *Cell Cycle*. Taylor & Francis, **14**(20), pp. 3242–3247.

Cairns, R. A., Harris, I. S. and Mak, T. W. (2011) Regulation of cancer cell metabolism. *Nature Reviews Cancer*, **11**(2), pp. 85–95.

Cairns, R. A. and Mak, T. W. (2016) The current state of cancer metabolism, *Nature Reviews Cancer*, **16**(10), pp. 613–614.

Calorini, L., Peppicelli, S. and Bianchini, F. (2012) 'Extracellular acidity as favouring factor of tumor progression and metastatic dissemination', *Experimental Oncology*. **34**(2), pp. 79–84.

Camacho, J. (2006) Ether a go-go potassium channels and cancer, *Cancer Letters*, **233**(1), pp. 1–9.

Cameron, I. L. *et al.* (1980) Intracellular Concentration of Sodium and Other Elements as Related to Mitogenesis and Oncogenesis in Vivo. *Cancer Research*, **40**(5), pp. 1493–1500.

Cardone, R. A. *et al.* (2008) 'HPV16 E7-dependent transformation activates NHE_1 through a PKA-RhoA-induced inhibition of p38alpha', *PLoS One*. **3**(10), p. e3529.

Cesarz, Z. and Tamama, K. (2016) 'Spheroid Culture of Mesenchymal Stem Cells', *Stem cells international*. **201**, p. 9176357

Chakrabarti, A., Ekuta, J. E. and Onaivi, E. S. (1998) Neurobehavioral effects of anandamide and cannabinoid receptor gene expression in mice. *Brain Research Bulletin*, **45**(1), pp. 67–74.

Chambard, J. C. and Pouyssegur, J. (1986) Intracellular pH controls growth factor-induced ribosomal protein S6 phosphorylation and protein synthesis in the G0-G1 transition of fibroblasts. *Experimental Cell Research*, **164**(2), pp. 282–294.

Chao, W. S. *et al.* (2012) 'Selection and validation of endogenous reference genes for qRT-PCR analysis in leafy spurge (Euphorbia esula)', *PloS one*. **7**(8), pp. e42839–e42839.

Chaperon, F. and Thiébot, M. H. (1999) Behavioral effects of cannabinoid agents in animals. *Critical Reviews in Neurobiology*, **13**(3), pp. 243–81.

Chaplin, D. J., Durand, R. E. and Olive, P. L. (1985) Cell selection from a murine tumour using the fluorescent probe Hoechst 33342. *British Journal of Cancer*, **51**(4), pp. 569–572.

Chen, H. *et al.* (2014) Classification of 2-pore domain potassium channels based on rectification under quasi-physiological ionic conditions. *Channels (Austin)*, **8**(6), pp. 503–508.

Chiche, J. *et al.* (2009) 'Hypoxia-inducible carbonic anhydrase IX and XII promote tumor cell growth by counteracting acidosis through the regulation of the intracellular pH', *Cancer Resarch*, **69**(1), pp. 358–68.

Chiche, J., Brahimi-Horn, M. C. and Pouyssegur, J. (2010) Tumour hypoxia induces a metabolic shift causing acidosis: a common feature in cancer. *The Journal of Cellular and Molecular Medicine*, **14**(4), pp. 771–794.

Christ, E. J. (2009) The Warburg Effect and Its Role in Cancer Detection and Therapy. *Columbia University Academic Commons*, pp. 3–4.

Clark, H. A. *et al.* (1998) Subcellular optochemical nanobiosensors: probes encapsulated by biologically localised embedding (PEBBLEs). *Sensors and Actuators B: Chemical*, **51**(1), pp. 12–16.

Clark, H. A., Hoyer, M., Philbert, M. A., *et al.* (1999) Optical Nanosensors for Chemical Analysis inside Single Living Cells. 1. Fabrication, Characterization, and Methods for Intracellular Delivery of PEBBLE Sensors. *Analytical Chemistry*, **71**(21), pp. 4831–4836.

Clark, H. A., Hoyer, M., Parus, S., *et al.* (1999) Optochemical Nanosensors and Subcellular Applications in Living Cells. *Microchimica Acta*, **131**(1–2), pp. 121–128.

Cohen, A. *et al.* (2008) A novel mechanism for human K2P2.1 channel gating. Facilitation of C-type gating by protonation of extracellular histidine residues. *The Journal of Biological Chemistry*, **283**(28), pp. 19448–19455.

Comes, N. *et al.* (2013) The voltage-dependent K^+ channels Kv1.3 and Kv1.5 in human cancer. *Frontiers in Physiology*, **4**, p. 283.

Cooper, S. (2003) Reappraisal of serum starvation, the restriction point, G0, and G1 phase arrest points. *Federation of American Societies for Experimental Biology Journal*, **17**(3), pp. 333–340.

Corrado, M., Scorrano, L. and Campello, S. (2012) Mitochondrial dynamics in cancer and neurodegenerative and neuroinflammatory diseases. *The International Journal of Cell Biology*, **2012**, p. 729290.

Cortes, J. R. *et al.* (2009) Omeprazole inhibits IL-4 and IL-13 signaling signal transducer and activator of transcription 6 activation and reduces lung inflammation in murine asthma. *The Journal of Allergy and Clinical Immunology*, **124**(3), p. 607–10, 610 e1.

Cory, G. (2011) 'Scratch-wound assay.', *Methods in molecular biology (Clifton, N.J.)*. United States, **769**, pp. 25–30.

Corvini, P. F. *et al.* (2000) Intracellular pH determination of pristinamycin-producing Streptomyces pristinaespiralis by image analysis. *Microbiology*, **146 (Pt 1)**, pp. 2671–2678.

Crociani, O. *et al.* (2003) Cell cycle-dependent expression of HERG1 and HERG1B isoforms in tumor cells. *The Journal of Biological Chemistry*, **278**(5), pp. 2947–2955.

Curtin, N. A. (1986) Buffer power and intracellular pH of frog sartorius muscle. *Biophysical Journal*, **50**(5), pp. 837–841.

Czirjak, G. and Enyedi, P. (2002) Formation of functional heterodimers between the TASK-1 and TASK-3 two-pore domain potassium channel subunits. *The Journal of Biological Chemistry*, **277**(7), pp. 5426–5432.

Damaghi, M., Wojtkowiak, J. W. and Gillies, R. J. (2013) pH sensing and regulation in cancer. *Frontiers in Physiology*, **4**, p. 370.

Dang, C. V (2012) Links between metabolism and cancer. *Genes & Development* **26**(9), pp. 877–890.

Davies, R. J. and Daly, J. M. (1984) Potassium depletion and malignant transformation of villous adenomas of the colon and rectum. *Cancer*, **53**(6), pp. 1260–1264.

Desai, A. S. *et al.* (2013) Fluorescent nanosensors for intracellular measurements: synthesis, characterization, calibration, and measurement, *Frontiers in Physiology*, **4**, p. 401.

Desai, S. P. et al. (2013) 'Mitochondrial Localization and the Persistent Migration of Epithelial Cancer cells', *Biophysical Journal*. **104**(9), pp. 2077–2088.

Ding, X. *et al.* (2010) Essential role of TRPC6 channels in G2/M phase transition and development of human glioma., *The Journal of the National Cancer Institute*, **102**(14), pp. 1052–68.

Dixon, K. C. (1937) The pasteur effect and its mechanism. *Biological Reviews*, **12**(4), pp. 431–460.

Do, E., Ellis, D. and Noireaud, J. (1996) Intracellular pH and intrinsic H^+ buffering capacity in normal and hypertrophied right ventricle of ferret heart. *Cardiovascular Research*, **31**(5), pp. 729–738.

Duprat, F. *et al.* (1997) TASK, a human background K^+ channel to sense external pH variations near physiological pH. *European Molecular Biology Organization Journal*, **16**(17), pp. 5464–5471.

Eagle, H. (1973) The effect of environmental pH on the growth of normal and malignant cells. *The Journal of Cellular Physiology*, **82**(1), pp. 1–8.

Elstrom, R. L. *et al.* (2004) Akt stimulates aerobic glycolysis in cancer cells. *Cancer Research*, **64**(11), pp. 3892–3899.

Enyedi, P. and Czirjak, G. (2010) 'Molecular background of leak K^+ currents: two-pore domain potassium channels', Physiological Review, **90**(2), pp. 559–605.

Estrella, V. *et al.* (2013) Acidity generated by the tumor microenvironment drives local invasion. *Cancer Research*, **73**(5), pp. 1524–1535.

Fais, S. *et al.* (2007) Targeting vacuolar H^+-ATPases as a new strategy against cancer. *Cancer Research*, **67**(22), pp. 10627–10630.

Fang, J., Gillies, R. and Gatenby, R. (2008) Fang JS, Gillies RD, Gatenby RA.. Adaptation to hypoxia and acidosis in carcinogenesis and tumor progression, *Seminars in Cancer Biology*, **18**(5), pp. 330–337.

Fazeli, G. R. et al. (2007) 'Reduced DNA damage in tumor spheroids compared to monolayer cultures exposed to ionizing radiation', *Iranian Journal of Radiation Research*, **5**(2), pp. 63–69.

Fenn, W. O. and Cobb, D. M. (1934) 'The potassium equilibrium in muscle', *The Journal of general physiology*, **17**(5), pp. 629–56.

Ferrari, S. *et al.* (2013) Proton pump inhibitor chemosensitization in human osteosarcoma: from the bench to the patients' bed. *The Journal of Translational Medicine*, **11**(268), pp. 1–7.

Fink, M. *et al.* (1998) A neuronal two P domain K^+ channel stimulated by arachidonic acid and polyunsaturated fatty acids. *European Molecular Biology Organization Journal*, **17**(12), pp. 3297–3308.

Fischer, K. *et al.* (2007) Inhibitory effect of tumor cell-derived lactic acid on human T cells. *Blood*, **109**(9), pp. 3812–3819.

Le Floch, R. *et al.* (2011) CD147 subunit of lactate/H^+ symporters MCT1 and hypoxia-inducible MCT4 is critical for energetics and growth of glycolytic tumors. *Proceedings of National Acadademy of Science, U S A*, **108**(40), pp. 16663–16668.

Fraser, S. P. *et al.* (2014) Regulation of voltage-gated sodium channel expression in cancer: hormones, growth factors and auto-regulation. *Philosophical Transactions of the Royal Society of London. Series B, Biological Sciences*, **369**(1638), p. 20130105.

Frigault, M. M. *et al.* (2009) Live-cell microscopy - tips and tools. *The Journal of Cell Science*, **122**(Pt 6), pp. 753–767.

Fukumura, D. *et al.* (2001) Hypoxia and acidosis independently up-regulate vascular endothelial growth factor transcription in brain tumors in vivo. *Cancer Research*, **61**(16), pp. 6020–4.

Gaethje, H. (2007) Advances in Fluorescence Microscopy. *Optik & Photonik*, **2**(2), pp. 56–59.

Gaillard, S. and Dupont, J. L. (1990) Ionic control of intracellular pH in rat cerebellar Purkinje cells maintained in culture. *The Journal of Physiology*, **425**, pp. 71–83.

Ganetzky, B. *et al.* (1999) The eag family of K^+ channels in Drosophila and mammals. *Annals of the New York Academy of Sciences*, **868**, pp. 356–369.

Gerweck, L. E., Gillette, E. L. and Dewey, W. C. (1974) Killing of Chinese hamster cells in vitro by heating under hypoxic or aerobic conditions. *European Journal of Cancer*, **10**(10), pp. 691–693.

Gillies, R. J. *et al.* (1990) Tumorigenic 3T3 cells maintain an alkaline intracellular pH under physiological conditions. *Proceedings of National Academy of Science, U S A*, **87**(19), pp. 7414–7418.

Gillies, R. J., Liu, Z. and Bhujwalla, Z. (1994) 31P-MRS measurements of extracellular pH of tumors using 3-aminopropylphosphonate. *American Journal Physiology*, **267**(1 Pt 1), pp. C195-203.

Gillies R. J., Robey I. and Gatenby, R. A. (2008) Causes and consequences of increased glucose metabolism of cancers. *The Journal of nuclear medicine*, **49 Sup2**, p. 24S–42S.

Girard, C. *et al.* (2001) Genomic and functional characteristics of novel human pancreatic 2P domain K^+ channels. *Biochemical and Biophysical Research Communications*, **282**(1), pp. 249–56.

Glunde, K. *et al.* (2003) Extracellular acidification alters lysosomal trafficking in human breast cancer cells. *Neoplasia*, **5**(6), pp. 533–545.

Goldsmith, D. J. A. and Hilton, P. J. (1992) Relationship between intracellular proton buffering capacity and intracellular pH. *Kidney International*, **41**(1), pp. 43–49.

Goldstein, S. A. N. *et al.* (2005) International Union of Pharmacology. LV. Nomenclature and molecular relationships of two-P potassium channels. *Pharmacological Reviews*, **57**(4), pp. 527–40.

Gorbatenko, A. *et al.* (2014) Regulation and roles of bicarbonate transporters in cancer. *Frontiers in Physiology*, **5**, p. 130.

Gos, M., Miloszewska, J. and Przybyszewska, M. (2009) Epithelial-mesenchymal transition in cancer progression. *Postepy Biochemii*, **55**(2), pp. 121–128.

Graber, M. L. *et al.* (1986) Characteristics of fluoroprobes for measuring intracellular pH. *Analytical Biochemistry*, **156**(1), pp. 202–12.

Granja, S. *et al.* (2015) Glucose Addiction in Cancer Therapy: Advances and Drawbacks. *Current Drug Metabolism,* **16**(3), pp. 221–242.

Griffiths, J. R. *et al.* (1981) 31P-NMR investigation of solid tumours in the living rat. *Bioscience Reports*, **1**(4), pp. 319–325.

Griffiths, J. R. (1991) Are cancer cells acidic?. *British Journal of Cancer*, **64**(3), pp. 425–427.

Grinstein, S., Cohen, S. and Rothstein, A. (1984) Cytoplasmic pH regulation in thymic lymphocytes by an amiloride-sensitive Na^+/H^+ antiport. *The Journal of General Physiology*, **83**(3), pp. 341–69.

Grinstein, S. and Dixon, S. J. (1989) Ion transport, membrane potential, and cytoplasmic pH in lymphocytes: changes during activation. *Physiological Reviews*, **69**(2), pp. 417–81.

Le Guennec, J. Y. *et al.* (2007) Voltage-gated ion channels, new targets in anti-cancer research. *Recent Patents Anticancer Drug Discovery*, **2**(3), pp. 189–202.

Gullino, P. M. *et al.* (1965) Modifications of the acid-base status of the internal milieu of tumors. *The Journal of Naionatl Cancer Institute*, **34**(6), pp. 857–869.

Gullino, P. M. (1966) The internal milieu of tumors. *Progress in Experimental Tumor Research*, **8**, pp. 1–25.

Gullino, P. M., Clark, S. H. and Grantham, F. H. (1964) The Interstitial Fluid of Solid Tumors. *Cancer Research*, **24**, pp. 780–794.

El Hachmane, M.-F. et al. (2014) 'Enhancement of TWIK-related acid-sensitive potassium channel 3 (TASK3) two-pore domain potassium channel activity by

tumor necrosis factor α.', *The Journal of biological chemistry*, **289**(3), pp. 1388–401.

Hammond, E. M. and Giaccia, A. J. (2005) The role of p53 in hypoxia-induced apoptosis. *Biochemical and Biophysical Research Communications*, **331**(3), pp. 718–725.

Hammoudi, N. *et al.* (2011) Metabolic alterations in cancer cells and therapeutic implications. *Chinese Journal of Cancer*, **30**(8), pp. 508–525.

Hanahan, D. and Weinberg, R. A. (2000) The Hallmarks of Cancer. *Cell*, **100**(1), pp. 57–70.

Hanahan, D. and Weinberg, R. A. (2011) Hallmarks of Cancer: The Next Generation. *Cell*, **144**(5), pp. 646–674.

Hansen, S. D. *et al.* (2013) αE-catenin actin-binding domain alters actin filament conformation and regulates binding of nucleation and disassembly factors. *Molecular Biology of the Cell*, **24**(23), pp. 3710–20.

Harris, A. L. (2002) Hypoxia--a key regulatory factor in tumour growth. *Nature Reviews Cancer*, **2**(1), pp. 38–47.

Hart, S., Fischer, O. M. and Ullrich, A. (2004) Cannabinoids induce cancer cell proliferation via tumor necrosis factor alpha-converting enzyme (TACE/ADAM17)-mediated transactivation of the epidermal growth factor receptor. *Cancer Research*, **64**(6), pp. 1943–50.

Hartness, M. E. *et al.* (2001) Combined antisense and pharmacological approaches implicate hTASK as an airway O_2 sensing K^+ channel. *The Journal of Biological Chemistry*, **276**(28), pp. 26499–508.

Hatten, M. E. and Roussel, M. F. (2011) Development and cancer of the cerebellum. *Trends in Neurosciences*, **34**(3), pp. 134–42.

Vander Heiden, M. G., Cantley, L. C. and Thompson, C. B. (2009) Understanding the Warburg effect: the metabolic requirements of cell proliferation. *Science*, **324**(5930), pp. 1029–1033.

Hopwood, S. E. and Trapp, S. (2005) 'TASK-like K^+ channels mediate effects of 5-HT and extracellular pH in rat dorsal vagal neurones in vitro.', *The Journal of physiology*, **568**(Pt 1), pp. 145–54.

Hockel, S. *et al.* (2001) Association between host tissue vascularity and the prognostically relevant tumor vascularity in human cervical cancer. *The International Journal of Oncology*, **19**(4), pp. 827–832.

Honore, E. *et al.* (2002) An intracellular proton sensor commands lipid- and mechano-gating of the K^+ channel TREK-1, *EMBO J*, **21**(12), pp. 2968–2976.

Huang, X. and Jan, L. Y. (2014) Targeting potassium channels in cancer. *The Journal of Cell Biology*, **206**(2), pp. 151–62.

Huber, S. M. (2013) Oncochannels. *Cell Calcium*, **53**(4), pp. 241–255.

Hulikova, A. *et al.* (2013) Regulation of intracellular pH in cancer cell lines under normoxia and hypoxia. *The Journal of Cell Physiology*, **228**(4), pp. 743–752.

Hulikova, A., Vaughan-Jones, R. D. and Swietach, P. (2011) Dual role of CO_2/HCO_3^- buffer in the regulation of intracellular pH of three-dimensional tumor growths. *The Journal of Biological Chemistry*, **286**(16), pp. 13815–13826.

Im, W. B. *et al.* (1985) Omeprazole, a specific inhibitor of gastric (H^+-K^+)-ATPase, is a H^+-activated oxidizing agent of sulfhydryl groups. *Journal of Biological Chemistry*, **260**(8), pp. 4591–4597.

Innamaa, A. *et al.* (2013) Expression and prognostic significance of the oncogenic K2P potassium channel KCNK9 (TASK-3) in ovarian carcinoma. *Anticancer Research*, **33**(4), pp. 1401–1408.

Jain, M. and Wagner, R. (eds) (1980) Introduction to Biological Membranes. New York, *John Wiley and Sons*, p. 195–229.

Jang, M., Kim, S. S. and Lee, J. (2013) Cancer cell metabolism: implications for therapeutic targets. *Experimental & Molecular Medicine*, **45**(10), p. e45.

Juel, C. (2008) Regulation of pH in human skeletal muscle: adaptations to physical activity. *Acta Physiologica*, **193**(1), pp. 17–24.

Kadletz, L. et al. (2015) 'Evaluation of spheroid head and neck squamous cell carcinoma cell models in comparison to monolayer cultures', *Oncology letters*. **10**(3), pp. 1281–1286.

Kalluri, R. and Weinberg, R. A. (2009) The basics of epithelial-mesenchymal transition. *The Journal of Clinical Investigation*, **119**(6), pp. 1420–1428.

Kato, Y. *et al.* (2013) Acidic extracellular microenvironment and cancer. *Cancer Cell International*, **13**(89), pp. 1–8.

Khajah, M. A. *et al.* (2013) Extracellular alkaline pH leads to increased metastatic potential of estrogen receptor silenced endocrine resistant breast cancer cells. *Public Library of Science One*, **8**(10), p. e76327.

Kim, D. *et al.* (1998) Cloning and functional expression of a novel cardiac two-pore background K^+ channel (cTBAK-1). *Circulation Research*, **82**(4), pp. 513–518.

Kim, D. *et al.* (2009) Heteromeric TASK-1/TASK-3 is the major oxygen-sensitive background $K(^+)$ channel in rat carotid body glomus cells. *The Journal of Physiology*, **587**(Pt 12), pp. 2963–2975.

Kim, Y. *et al.* (2001) Localization of TREK-2 K^+ channel domains that regulate channel kinetics and sensitivity to pressure, fatty acids and pHi. *Pflugers Archiv*, **442**(6), pp. 952–960.

Kizaka-Kondoh, S. *et al.* (2003) Tumor hypoxia: a target for selective cancer therapy. *Cancer Science*, **94**(12), pp. 1021–1028.

Klein, M. *et al.* (2000) Polarization of Na^+/H^+ and Cl^-/HCO_3^- exchangers in migrating renal epithelial cells. *The Journal of General Physiology*, **115**(5), pp. 599–608.

Koltai, T. (2016) Cancer: Fundamentals behind pH targeting and the double-edged approach. *OncoTargets and Therapy*, **9**, pp. 6343–6360.

Konduri, S. D. et al. (2003) 'Promoter methylation and silencing of the tissue factor pathway inhibitor-2 (TFPI-2), a gene encoding an inhibitor of matrix metalloproteinases in human glioma cells', *Oncogene*, **22**(29), pp. 4509-4516.

Koztak, L. (2011) Mitochondrial expression of TASK-3 channels in human malignant melanoma cell cultures and their role in cell survival and proliferation. University of Debrecen, pp. 1-20.

Krahling, H. *et al.* (2009) The glycocalyx maintains a cell surface pH nanoenvironment crucial for integrin-mediated migration of human melanoma cells. *Pflugers Archiv*, **458**(6), pp. 1069–83.

Kraus, M. and Wolf, B. (1998) Physicochemical microenvironment as key regulator for tumor microevolution, invasion, and immune response: Targets for endocytotechnological approaches in cancer treatment. *Endocytobiosis and Cell Research*, **12**(3), pp. 133–156.

Kuang, Q., Purhonen, P. and Hebert, H. (2015) Structure of potassium channels. *Cellular and Molecular Life Sciences*, **72**(19), pp. 3677–93.

Kummola, L. et al. (2005) 'Expression of a novel carbonic anhydrase, CA XIII, in normal and neoplastic colorectal mucosa', *BioMed Centra cancer*, **5,** pp. 1-7

Kunz, M. and Ibrahim, S. M. (2003) Molecular responses to hypoxia in tumor cells. *Molecular Cancer*, **2**, p. 23.

Lacroix, A. and Lippman, M. E. (1980) Binding of retinoids to human breast cancer cell lines and their effects on cell growth. *The Journal of Clinical Investigation*, **65**(3), pp. 586–91.

Lagarde, A. E. *et al.* (1988) Effect of mutations affecting Na^+: H^+ antiport activity on tumorigenic potential of hamster lung fibroblasts. *The Journal of Cellular Biochemistry*, **36**(3), pp. 249–260.

Landecker, H. (2009) Seeing things: from microcinematography to live cell imaging. *Nature Methods*, **6**(10), pp. 707–709.

Lang, F. *et al.* (2000) Cell volume in the regulation of cell proliferation and apoptotic cell death. *Cellular Physiology and Biochemistry*, **10**(5–6), pp. 417–28.

Lardner, A. (2001) The effects of extracellular pH on immune function. *The Journal of Leukocyte Biology*, **69**(4), pp. 522–530.

Lastraioli, E., Iorio, J. and Arcangeli, A. (2015) Ion channel expression as promising cancer biomarker. *Biochimica et Biophysica Acta - Biomembranes*, **1848**(10, Part B), pp. 2685–2702.

Lauritzen, G. *et al.* (2010) NBCn1 and NHE1 expression and activity in Delta NErbB2 receptor-expressing MCF-7 breast cancer cells: contributions to pHi regulation and chemotherapy resistance. *Experimental Cell Research*, **316**(15), pp. 2538–53.

Le, Q.-T. and Courter, D. (2008) Clinical biomarkers for hypoxia targeting. *Cancer Metastasis Reviews*, **27**(3), pp. 351–62.

Lee, A. H. and Tannock, I. F. (1998) Heterogeneity of intracellular pH and of mechanisms that regulate intracellular pH in populations of cultured cells. *Cancer Research*, **58**(9), pp. 1901–8.

Lee, G.-H. *et al.* (2011) An acidic pH environment increases cell death and pro-inflammatory cytokine release in osteoblasts: the involvement of BAX inhibitor-1. *The International Journal of Biochemistry & Cell Biology*, **43**(9), pp. 1305–17.

Lee, U. S. and Cui, J. (2010) BK channel activation: structural and functional insights. *Trends in Neurosciences*, **33**(9), pp. 415–23.

Lee, Y.-E. K., Smith, R. and Kopelman, R. (2009) Nanoparticle PEBBLE sensors in live cells and in vivo. *The Annual Review of Analytical Chemistry*, **2**, pp. 57–76.

Lemasters, J. J. *et al.* (1999) Confocal imaging of Ca^{2+}, pH, electrical potential, and membrane permeability in single living cells. *Methods in Enzymology*, **302**, pp. 341–358.

Leonoudakis, D. *et al.* (1998) An open rectifier potassium channel with two pore domains in tandem cloned from rat cerebellum. *The Journal of Neuroscience*, **18**(3), pp. 868–877.

Leontieva, O. V, Demidenko, Z. N. and Blagosklonny, M. V (2014) Contact inhibition and high cell density deactivate the mammalian target of rapamycin pathway, thus suppressing the senescence program. *Proceedings of the National Academy of Sciences, USA*, **111**(24), pp. 8832–8837.

Lesage, F. *et al.* (2000) Human TREK2, a 2P domain mechano-sensitive K^+ channel with multiple regulations by polyunsaturated fatty acids, lysophospholipids, and Gs, Gi, and Gq protein-coupled receptors. *The Journal of Biological Chemistry*, **275**(37), pp. 28398–28405.

Lesage, F. and Barhanin, J. (2011) Molecular physiology of pH-sensitive background K(2P) channels. *Physiology*, **26**(6), pp. 424–437.

Li, J. *et al.* (2013) Ovarian cancer G protein coupled receptor 1 suppresses cell migration of MCF7 breast cancer cells via a Gα12/13-Rho-Rac1 pathway. *The Journal of Molecular Signaling*, **8**(1), p. 6.

Lin, J. (2000) Recent development and applications of optical and fiber-optic pH sensors, *Trends in Analytical Chemistry*, **19**(9), pp. 541–552.

Lin, Y. *et al.* (2011) NHE1 mediates MDA-MB-231 cells invasion through the regulation of MT1-MMP. *Expermental Cell Research*, **317**(14), pp. 2031–40.

Lindner, D. and Raghavan, D. (2009) Intra-tumoural extra-cellular pH: a useful parameter of response to chemotherapy in syngeneic tumour lines *British Journal of Cancer*, **100**(8), pp. 1287–1291.

Litan, A. and Langhans, S. A. (2015) Cancer as a channelopathy: ion channels and pumps in tumor development and progression. *Frontiers in Cellular Neuroscience*, **9**, p. 86.

Liu, C. *et al.* (2005) Protective effects of TASK-3 (KCNK9) and related 2P K channels during cellular stress *Brain Research*, **1031**(2), pp. 164–173.

Lobikin, M. *et al.* (2012) Resting potential, oncogene-induced tumorigenesis, and metastasis: the bioelectric basis of cancer in vivo. *Physical Biology*, **9**(6), p. 65002.

Lodish, H. *et al.* (2000) Electron Transport and Oxidative Phosphorylation, in *Molecular Cell Biology*. 4th edn. W. H. Freeman, pp. 315–325.

Loo, S. Y. *et al.* (2012) NHE1: a promising target for novel anti-cancer therapeutics. *Current Pharmaceutical Design*, **18**(10), pp. 1372–82.

Lu, X. *et al.* (2010) Hypoxia and hypoxia-inducible factors: master regulators of metastasis. *Clinical Cancer Research*, **16**(24), pp. 5928–35.

Luciani, F. *et al.* (2004) Effect of proton pump inhibitor pretreatment on resistance of solid tumors to cytotoxic drugs. *The Journal of National Cancer Institute*, **96**(22), pp. 1702–1713.

Lucien, F. *et al.* (2011) Hypoxia-induced invadopodia formation involves activation of NHE-1 by the p90 ribosomal S6 kinase (p90RSK). *Public Library of Science One*, **6**(12), p. e28851.

Lundgren, K., Holm, C. and Landberg, G. (2007) Hypoxia and breast cancer: prognostic and therapeutic implications. *Cellular and Molecular Life Sciences*, **64**(24), pp. 3233–47.

Luo, J., Solimini, N. L. and Elledge, S. J. (2009) Principles of Cancer Therapy: Oncogene and Non-oncogene Addiction. *Cell*, **136**(5), pp. 823–837.

Ma, L. *et al.* (2012) Acid-sensitive TWIK and TASK two-pore domain potassium channels change ion selectivity and become permeable to sodium in extracellular acidification. *The Journal of Biological Chemistry*, **287**(44), pp. 37145–37153.

Madshus, I. H. (1988) Regulation of intracellular pH in eukaryotic cells. *Biochemical Journal*, **250**(1), pp. 1–8.

Maingret, F. *et al.* (1999) Mechano- or acid stimulation, two interactive modes of activation of the TREK-1 potassium channel. *The Journal of Biological Chemistry*, **274**(38), pp. 26691–26696.

Martinez-Zaguilan, R. *et al.* (1993) Vacuolar-type H^+-ATPases are functionally expressed in plasma membranes of human tumor cells. *The American Journal of Physiology*, **265**(4 Pt 1), pp. C1015-29.

Martinez-Zaguilan, R. *et al.* (1996) Acidic pH enhances the invasive behavior of human melanoma cells. *Clinical & Experimental Metastasis*, **14**(2), pp. 176–186.

Masson, N. and Ratcliffe, P. J. (2014) Hypoxia signaling pathways in cancer metabolism: the importance of co-selecting interconnected physiological pathways. *Cancer & Metabolism*, **2**(1), pp. 3–20.

Mathie, A. *et al.* (2010) Trafficking of neuronal two pore domain potassium channels. *Current Neuropharmacology*, **8**(3), pp. 276–286.

Matoba, S. *et al.* (2006) p53 regulates mitochondrial respiration. *Science*, **312**(5780), pp. 1650–1653.

McCarty, M. F. and Whitaker, J. (2010) Manipulating tumor acidification as a cancer treatment strategy. *Alternative Medicine Review*, **15**(3), pp. 264–272.

McColl, K. E. L. (2006) Acid inhibitory medication and risk of gastric and oesophageal cancer. *Gut*, **55**(11), pp. 1532–3.

McDonagh, C., Burke, C. S. and MacCraith, B. D. (2008) Optical chemical sensors. *Chemical Reviews*, **108**(2), pp. 400–22.

De Milito, A. *et al.* (2010) pH-dependent antitumor activity of proton pump inhibitors against human melanoma is mediated by inhibition of tumor acidity. *The International Journal of Cancer*, **127**(1), pp. 207–219.

Mu, D. *et al.* (2003) Genomic amplification and oncogenic properties of the KCNK9 potassium channel gene. *Cancer Cell*, **3**(3), pp. 297–302.

Mulkey, D. K. *et al.* (2007) TASK channels determine pH sensitivity in select respiratory neurons but do not contribute to central respiratory chemosensitivity. *The Journal of Neuroscience*, **27**(51), pp. 14049–14058.

Nagarajan, A., Malvi, P. and Wajapeyee, N. (2016) Oncogene-directed alterations in cancer cell metabolism. *Trends in Cancer*, **2**(7), pp. 365–377.

Nagelkerke, A. *et al.* (2013) Hypoxia stimulates migration of breast cancer cells via the PERK/ATF4/LAMP3-arm of the unfolded protein response. *Breast Cancer Research*, **15**(1 R2), pp. 1–13.

Nagy, D. *et al.* (2014) Silencing the KCNK9 potassium channel (TASK-3) gene disturbs mitochondrial function, causes mitochondrial depolarization, and induces apoptosis of human melanoma cells. *Archives of Dermatological Research*, **306**(10), pp. 885–902.

Ndolo, R. A. *et al.* (2012) Lysosomotropic properties of weakly basic anticancer agents promote cancer cell selectivity in vitro. *Public Library of Science One*, **7**(11), p. e49366.

Negendank, W. (1984) Ionic distributions and volume maintenance in human lymphocytes. *Physiological Chemistry and Physics and Medical NMR*, **16**(1), pp. 3–20.

Nelson, D. L. and Cox, M. M. (2013) Glycolysis, Gluconeogenesis, and the Pentose Phosphate Pathway, in *Lehninger Principles of Biochemistry*. 6th edn. New York: W.H. Freeman, pp. 243–273.

Neri, D. and Supuran, C. T. (2011) Interfering with pH regulation in tumours as a therapeutic strategy. *Nature reviews. Drug discovery*, **10**(10), pp. 767–77.

Nishimura, H., Zarnowski, M. J. and Simpson, I. A. (1993) Glucose transporter recycling in rat adipose cells. Effects of potassium depletion. *The Journal of Biological Chemistry*, **268**(26), pp. 19246–53.

Nsiah-Sefaa, A. and McKenzie, M. (2016) Combined defects in oxidative phosphorylation and fatty acid β-oxidation in mitochondrial disease. *Bioscience Reports*, **36**(2), pp: e00313.

Ofinran, O. *et al.* (2016) Selection of suitable reference genes for gene expression studies in normal human ovarian tissues, borderline ovarian tumours and ovarian cancer. *Molecular Medicine Reports*, **14**(6), pp. 5725–5731.

Olcina, M., Lecane, P. S. and Hammond, E. M. (2010) Targeting hypoxic cells through the DNA damage response. *Clinical Cancer Research*, **16**(23), pp. 5624–9.

Olea-Herrero, N. *et al.* (2009) Inhibition of human tumour prostate PC-3 cell growth by cannabinoids R(+)-Methanandamide and JWH-015: Involvement of CB2. *British Journal of Cancer*, **101**, pp. 940–950.

Osthus, R. C. *et al.* (2000) Deregulation of glucose transporter 1 and glycolytic gene expression by c-Myc. *The Journal of Biological Chemistry*, **275**(29), pp. 21797–21800.

Ouwerkerk, R., Jacobs, M.A., Macura, K. J. et al (2007) Elevated tissue sodium concentration in malignant breast lesions detected with non-invasive 23Na MRI. *Breast Cancer Research and Treatatment*, **106**(2), pp. 151–160.

Ow, H. *et al.* (2005) Bright and stable core-shell fluorescent silica nanoparticles. *Nano letters*, **5**(1), pp. 113–7.

Ozkan, P. and Mutharasan, R. (2002) A rapid method for measuring intracellular pH using BCECF-AM. *Biochimica et Biophysica Acta*, **1572**(1), pp. 143–148.

Paolacci, A. R. et al. (2009) 'Identification and validation of reference genes for quantitative RT-PCR normalization in wheat', *BioMed Central molecular biology*, **10**(11), pp. 1-27.

Pardo, L. A. *et al.* (1999) Oncogenic potential of EAG K^+ channels. *European Molecular Biology Organization Journal*, **18**(20), pp. 5540–5547.

Pardo, L. A. (2004) Voltage-gated potassium channels in cell proliferation. *Physiology*, **19**(5), pp. 285–92.

Pardo, L. A. and Stühmer, W. (2014) The roles of K^+ channels in cancer. *Nature Reviews Cancer*, **14**(1), pp. 39–48.

Patlolla, J. M. R. *et al.* (2012) Anti-carcinogenic properties of omeprazole against human colon cancer cells and azoxymethane-induced colonic aberrant crypt foci formation in rats. *The International Journal of Oncology*, **40**(1), pp. 170–175.

Pavlova, N. N. and Thompson, C. B. (2016) The Emerging Hallmarks of Cancer Metabolism. *Cell Metabolism*, **23**(1), pp. 27–47.

Pei, L. *et al.* (2003) Oncogenic potential of TASK3 (Kcnk9) depends on K^+ channel function. *Proceedings of National Academy of Scienc,e U S A*, **100**(13), pp. 7803–7807.

Pequignot, J.-M. *et al.* (2003) 2P Domain K^+ Channels: Novel Pharmacological Targets for Volatile eneral Anaesthetics, in Pequignot, J.-M. (ed.)

Chemoreception: From Cellular Signaling to Functional Plasticity. Kluwer Academic/Plenum publishers, pp. 9–24.

Plas, D. R. and Thompson, C. B. (2005) Akt-dependent transformation: there is more to growth than just surviving. *Oncogene*, **24**(50), pp. 7435–7442.

Pocock, G. and Richards, C. D. (1992) Hydrogen Ion Regulation in Rat Cerebellar Granule Cells Studied by Single-Cell Fluorescence Microscopy, *European Journal of Neuroscience*, **4**(2), pp. 136–143.

Porter, A. G. and Janicke, R. U. (1999) Emerging roles of caspase-3 in apoptosis. *Cell Death and Differentiation*, **6**(2), pp. 99–104.

Pouysségur, J. *et al.* (1984) A specific mutation abolishing Na^+/H^+ antiport activity in hamster fibroblasts precludes growth at neutral and acidic pH. *Proceedings of National Academy of Science, U S A*, **81**(15), pp. 4833–4837.

Pouyssegur, J., Dayan, F. and Mazure, N. M. (2006) Hypoxia signalling in cancer and approaches to enforce tumour regression. *Nature*, **441**(7092), pp. 437–443.

Pouyssegur, J., Franchi, A. and Pages, G. (2001) pHi, aerobic glycolysis and vascular endothelial growth factor in tumour growth. *Novartis Foundation Symposium*, **240**, pp. 186–188.

Putney, L. K. and Barber, D. L. (2003) Na^+-H^+ exchange-dependent increase in intracellular pH times G2/M entry and transition. *The Journal of Biological Chemistry*, **278**(45), pp. 44645–9.

Racker, E. (1974) History of the Pasteur effect and its pathobiology. *Molecular and Cellular Biochemistry*, **5**(1–2), pp. 17–23.

Rajan, S. *et al.* (2000) TASK-3, a novel tandem pore domain acid-sensitive K^+ channel. An extracellular histidine as pH sensor. *The Journal of Biological Chemistry*, **275**(22), pp. 16650–16657.

Rathmell, J. C. *et al.* (2003) Akt-directed glucose metabolism can prevent Bax conformation change and promote growth factor-independent survival. *Molecular and Cellular Biology*, **23**(20), pp. 7315–7328.

Ren, J. and Zhang, L. (2011) Effects of ovarian cancer G protein coupled receptor 1 on the proliferation, migration, and adhesion of human ovarian cancer cells. *Chinese Medical Journal*, **124**(9), pp. 1327–32.

Reshkin, S. J. *et al.* (2000) Na^+/H^+ exchanger-dependent intracellular alkalinization is an early event in malignant transformation and plays an essential role in the development of subsequent transformation-associated phenotypes. *Federation of American Societies for Experimental Biology Journal*, **14**(14), pp. 2185–2197.

Reshkin, S. J. *et al.* (2000) Phosphoinositide 3-Kinase Is Involved in the Tumor-specific Activation of Human Breast Cancer Cell Na^+/H^+ Exchange, Motility, and Invasion Induced by Serum Deprivation. *The Journal of Biological Chemistry*, **275**(8), pp. 5361–5369.

Reshkin, S. J., Greco, M. R. and Cardone, R. A. (2014) Role of pHi, and proton transporters in oncogene-driven neoplastic transformation. *Philosophical Transactions of the Royal Society B*, **369**(1638), p. 20130100.

Reyes, R. *et al.* (1998) Cloning and expression of a novel pH-sensitive two pore domain K^+ channel from human kidney. *The Journal of Biological Chemistry*, **273**(47), pp. 30863–9.

Romero, M. F. *et al.* (2000) Cloning and characterization of a Na^+-driven anion exchanger (NDAE1). A new bicarbonate transporter. *The Journal of Biological Chemistry*, **275**(32), pp. 24552–24559.

Romero, M. F., Chang, M.-H. and Mount, D. B. (2010) From Cloning to Structure, Function, and Regulation of Chloride-dependent and Independent Bicarbonate Transporters (BT), in Alvarez-Leefmans, F. J. and Delpire, E. (eds) *Physiology and Pathology of Chloride Transporters and Channels in the Nervous System : From Molecules to Diseases*, pp. 43–79.

Roos, A. and Boron, W. F. (1981) Intracellular pH. *Physiology Review*, **61**(2), pp. 296–434.

Rotin, D. *et al.* (1989) Requirement of the Na^+/H^+ exchanger for tumor growth. *Cancer Research*, **49**(1), pp. 205–211.

Ruan, K., Song, G. and Ouyang, G. (2009) Role of hypoxia in the hallmarks of human cancer. *Journal of Cellular Biochemistry*, **107**(6), pp. 1053–62.

Sandoval, M. *et al.* (2011) Extracellular pH in Restricted Domains as a Gating Signal for Ion Channels Involved in Transepithelial Transport. *Biological and Pharmaceutical Bulletin*, **34**(6), pp. 803–809.

Sandoz, G. *et al.* (2009) Extracellular acidification exerts opposite actions on TREK1 and TREK2 potassium channels via a single conserved histidine residue. *Proceedings of National Acadademy of Science U S A*, **106**(34), pp. 14628–14633.

Sanguinetti, M. C. *et al.* (1995) A mechanistic link between an inherited and an acquired cardiac arrhythmia: HERG encodes the IKr potassium channel. *Cell*, **81**(2), pp. 299–307.

Sano, Y. *et al.* (2003) A novel two-pore domain K^+ channel, TRESK, is localized in the spinal cord. *The Journal of Biological Chemistry*, **278**(30), pp. 27406–12.

Sauvant, C. *et al.* (2008) Acidosis induces multi-drug resistance in rat prostate cancer cells (AT1) in vitro and in vivo by increasing the activity of the p-glycoprotein via activation of p38. *The International Journal of Cancer*, **123**(11), pp. 2532–2542.

Schlichter, L. C. and Khanna, R. (2002) Potassium channels and proliferation of neuroimmune cells. *Research Signpost*, pp. 121–151.

Schmidt, B. L. *et al.* (2010) Mechanism of cancer pain. *Molecular Interventions*, **10**(3), pp. 164–78.

Schonichen, A. *et al.* (2013) Considering protonation as a posttranslational modification regulating protein structure and function. *The Annual Review of Biophysics*, **42**, pp. 289–314.

Schwab, A. *et al.* (2012) Role of ion channels and transporters in cell migration. *Physiological Reviews*, **92**(4), pp. 1865–913.

Semenza, G. L. *et al.* (1994) Transcriptional regulation of genes encoding glycolytic enzymes by hypoxia-inducible factor 1. *The Journal of Biological Chemistry*, **269**(38), pp. 23757–23763.

Semenza, G. L. *et al.* (2001) The metabolism of tumours: 70 years later. *Novartis Foundation Symposium*, **240**, pp. 251–254.

Semenza, G. L. (2003) Targeting HIF-1 for cancer therapy. *Nature Reviews Cancer*, **3**(10), pp. 721–732.

Sennoune, S. R., Luo, D. and Martínez-Zaguilán, R. (2004) Plasmalemmal vacuolar-type H^+-ATPase in cancer biology. *Cell Biochemistry and Biophysics*, **40**(2), pp. 185–206.

Shafee, N. *et al.* (2009) PI3K/Akt activity has variable cell-specific effects on expression of HIF target genes, CA9 and VEGF, in human cancer cell lines. *Cancer Letters*, **282**(1), pp. 109–15.

Shim, H. *et al.* (1997) c-Myc transactivation of LDH-A: implications for tumor metabolism and growth. *Prococeedings of National Acadademy of Science U S A*, **94**(13), pp. 6658–6663.

Skryma, R. N. et al. (1997) 'Potassium conductance in the androgen-sensitive prostate cancer cell line, LNCaP: Involvement in cell proliferation', *The Prostate*, **33**(2), pp. 112–122.

Solaini, G., Sgarbi, G. and Baracca, A. (2011) Oxidative phosphorylation in cancer cells. *Biochimica et Biophysica Acta*, **1807**(6), pp. 534–542.

Solimini, N. L., Luo, J. and Elledge, S. J. (2007) Non-oncogene addiction and the stress phenotype of cancer cells. *Cell*, **130**(6), pp. 986–988.

Sontheimer, H. (2008) An unexpected role for ion channels in brain tumor metastasis. *Experimental Biology and Medicine*, **233**(7), pp. 779–91.

Spriet, L. L. (1991) Phosphofructokinase activity and acidosis during short-term tetanic contractions. *Canadian Journal of Physiology and Pharmacology*, **69**(2), pp. 298–304.

Stock, C. and Schwab, A. (2009) Protons make tumor cells move like clockwork. *Pflügers Archiv*, **458**(5), pp. 981–92.

Strickholm, A. (1981) Ionic permeability of K^+, Na^+, and Cl- in potassium-depolarized nerve. Dependency on pH, cooperative effects, and action of tetrodotoxin. *Biophysical Journal*, **35**(3), pp. 677–697.

Struski, S., Doco-Fenzy, M. and Cornillet-Lefebvre, P. (2002) Compilation of published comparative genomic hybridization studies. *Cancer Genetics and Cytogenetics*, **135**(1), pp. 63–90.

Stubbs, M. *et al.* (2000) Causes and consequences of tumour acidity and implications for treatment. *Molecular Medicine Today*, pp. 15–19.

Stüwe, L. *et al.* (2007) pH dependence of melanoma cell migration: protons extruded by NHE1 dominate protons of the bulk solution. *The Journal of Physiol*, **585**(2), pp. 351–60.

Sun, H. *et al.* (2006) Synthesis and Characterization of Ratiometric, pH Sensing Nanoparticles with Covalently Attached Fluorescent Dyes. *Chemistry of Materials*, **18**(15), pp. 3381–3384.

Sutherland, R. L., Hall, R. E. and Taylor, I. W. (1983) Cell proliferation kinetics of MCF-7 human mammary carcinoma cells in culture and effects of tamoxifen on exponentially growing and plateau-phase cells. *Cancer Research*, **43**(9), pp. 3998–4006.

Suzuki, A. *et al.* (2014) Acidic extracellular pH promotes epithelial mesenchymal transition in Lewis lung carcinoma model. *Cancer Cell International*, **14**(129), pp. 1–11.

Suzuki, T. *et al.* (2007) Recent Advances in Fluorescent Labeling Techniques for Fluorescence Microscopy. *Acta Histochemica et Cytochemica*, **40**(5), pp. 131–137.

Swietach, P. *et al.* (2008) Tumor-associated carbonic anhydrase 9 spatially coordinates intracellular pH in three-dimensional multicellular growths *The Journal of Biological Chemistry*, **283**(29), pp. 20473–83.

Swietach, P. *et al.* (2009) The Role of Carbonic Anhydrase 9 in Regulating Extracellular and Intracellular pH in Three-dimensional Tumor Cell Growths. *The Journal of Biological Chemistry*, **284**(30), pp. 20299–20310.

Swietach, P. *et al.* (2010) New insights into the physiological role of carbonic anhydrase IX in tumour pH regulation. *Oncogene*, **29**(50), pp. 6509–6521.

Swietach, P. *et al.* (2014) The chemistry, physiology and pathology of pH in cancer. *Philosophical Transactions of the Royal Society of London*, **369**(1638), p. 20130099.

Tanaka, S. *et al.* (2003) Direct measurement of acid permeation into rat oesophagus. *Gut*, **52**(6), pp. 775–783.

Tannock, I. (1982) Response of aerobic and hypoxic cells in a solid tumor to adriamycin and cyclophosphamide and interaction of the drugs with radiation. *Cancer Research*, **42**(12), pp. 4921–4926.

Tannock, I. F. and Rotin, D. (1989) Acid pH in tumors and its potential for therapeutic exploitation. *Cancer Research*, **49**(16), pp. 4373–4384.

Tennant, D. A., Durán, R. V. and Gottlieb, E. (2010) Targeting metabolic transformation for cancer therapy. *Nature Reviews Cancer*, **10**(4), pp. 267–277.

Thier, S. O. (2017) Potassium physiology. *The American Journal of Medicine*, **80**(4), pp. 3–7.

Tym, J. E. *et al.* (2016) canSAR: an updated cancer research and drug discovery knowledgebase. *Nucleic Acids Research*, **44**(D1), pp. D938–D943.

Vaupel, P. and Höckel, M. (2002) Tumor hypoxia and therapeutic resistance, in Nowrousian, M. R. (ed.) *Recombinant Human Erythropoietin (rhEPO) in Clinical Oncology: Scientific and Clinical Aspects of Anemia in Cancer*, pp. 127–146.

Vaupel, P., Kallinowski, F. and Okunieff, P. (1989) Blood flow, oxygen and nutrient supply, and metabolic microenvironment of human tumors: a review. *Cancer Research*, **49**(23), pp. 6449–65.

Vaupel, P. and Mayer, A. (2005) Hypoxia and anemia: effects on tumor biology and treatment resistance. *Transfusion Clinique et Biologique*, **12**(1), pp. 5–10.

Vaupel, P., Mayer, A. and Hockel, M. (2004) Tumor hypoxia and malignant progression. *Methods in Enzymology*, **381**, pp. 335–354.

Vaupel, P., Thews, O. and Hoeckel, M. (2001) Treatment resistance of solid tumors: role of hypoxia and anemia. *Medical Oncology*, **18**(4), pp. 243–259.

Veale, E. L. *et al.* (2007) Identification of a region in the TASK3 two pore domain potassium channel that is critical for its blockade by methanandamide. *British Journal of Pharmacology*, **152**(5), pp. 778–786.

Vogt, P. K. (2010) Oncogenes and the revolution in cancer research: homage to Hidesaburo Hanafusa (1929-2009). *Genes & Cancer*, **1**(1), pp. 6–11.

Walenta, S. *et al.* (1997) Correlation of high lactate levels in head and neck tumors with incidence of metastasis. *The American Journal of Pathology*, **150**(2), pp. 409–15.

Wang, R. *et al.* (2011) The transcription factor Myc controls metabolic reprogramming upon T lymphocyte activation. *Immunity*, **35**(6), pp. 871–882.

Warburg, O. (1961) On the facultative anaerobiosis of cancer cells and its use in chemotherapy. *Munchener Medizinische Wochenschrift*, **103**, pp. 2504–2506.

Warburg, O., Wind, F. and Negelein, E. (1927) The metabolism of tumors in the body. *The Journal of General Physiology*, **8**(6), pp. 519–530.

Weinhouse, S. (1976) The Warburg hypothesis fifty years later. Zeitschrift für Krebsforschung und Klinische Onkologie: *Cancer Research and Clinical Oncology*, **87**(2), pp. 115–126.

WHO IARC (2014) 'Press Release N° 224'. Available at : http://www.iarc.fr/en/media-centre/pr/2014/pdfs/pr224_E.pdf

Wike-Hooley, J. L., Haveman, J. and Reinhold, H. S. (1984) The relevance of tumour pH to the treatment of malignant disease. *Radiotherapy and oncology : Journal of the European Society for Therapeutic Radiology and Oncology*, **2**(4), pp. 343–66.

Williams, S., Bateman, A. and O'Kelly, I. (2012) Role of acid-sensitive two-pore domain potassium (K2P) channels in cancer progression, in *Proceedings of The Physiological Society (27)*. Edinburgh, p. PC282.

Williams, S., Bateman, A. and O'Kelly, I. (2013) Altered expression of two-pore domain potassium (K2P) channels in cancer. *Public Library of Science One,* **8**(10), p. e74589.

Wise, D. R. *et al.* (2008) Myc regulates a transcriptional program that stimulates mitochondrial glutaminolysis and leads to glutamine addiction, *Proceedings of National Acadademy of Science, U S A*, **105**(48), pp. 18782–18787.

Wohlhueter, R. M. and Plagemann, P. G. (1981) Hexose transport and phosphorylation by Novikoff rat hepatoma cells as function of extracellular pH. *The Journal of Biological Chemistry*, **256**(2), pp. 869–875.

Wolfbeis, O. S. (2005) *Fiber Optic Chemical Sensors and Biosensors*. *Analytical Chemistry*, **74**(12), pp. 2663-2678.

Wondergem, R. *et al.* (2001) Blocking swelling-activated chloride current inhibits mouse liver cell proliferation. *The Journal of Physiology*, **532**(Pt 3), pp. 661–72.

Wonderlin, W. F. and Strobl, J. S. (1996) Potassium channels, proliferation and G1 progression, *Journal of Membrane Biology*, **154**(2), pp. 91–107.

Wu, W. et al. (2006) 'Targeting cell-impermeable prodrug activation to tumor microenvironment eradicates multiple drug-resistant neoplasms.', *Cancer research*, **66**(2), pp. 970–980.

Xu, L., Fukumura, D. and Jain, R. K. (2002) Acidic extracellular pH induces vascular endothelial growth factor (VEGF) in human glioblastoma cells via ERK1/2 MAPK signaling pathway: mechanism of low pH-induced VEGF. *The Journal of Biological Chemistry*, **277**(13), pp. 11368–74.

Xu, R. H. *et al.* (2005) Synergistic effect of targeting mTOR by rapamycin and depleting ATP by inhibition of glycolysis in lymphoma and leukemia cells. *Leukemia*, **19**(12), pp. 2153–2158.

Xu, Y., Cui, J. and Puett, D. (2014) Cancer Development in Competitive and Hostile Environments, in *Cancer Bioinformatics*,NY: Springer, pp. 205–227.

Xu, Z. *et al.* (2015) PTEN Plays an Important Role in Thrombin-Mediated Lung Cancer Cell Functions. *BioMedical Research International*, **2015**, pp. 1–9.

Yang, M. *et al.* (2006) Expression of and Role for Ovarian Cancer G-protein-coupled Receptor 1 (OGR1) during Osteoclastogenesis. *Journal of Biological Chemistry*, **281**(33), pp. 23598–23605.

Yang, M. and Brackenbury, W. J. (2013) Membrane potential and cancer progression. *Frontiers in Physiology*, **4**(185), pp. 1–10.

Yang, X., Yan, L. and Davidson, N. E. (2001) 'DNA methylation in breast cancer', *Endocrine Related* Cancer, **8** (2) , pp. 115-27.

Zar, H. J. (1984) 'Biostatistical Analysis', in. *Prentice-Hall*, p. 944.

Zatovicova, M. *et al.* (2010) Carbonic anhydrase IX as an anticancer therapy target: preclinical evaluation of internalizing monoclonal antibody directed to catalytic domain. *Current Pharmaceutical Design*, **16**(29), pp. 3255–3263. 257

Zhanping, W. *et al.* (2007) Voltage-gated K^+ channels are associated with cell proliferation and cell cycle of ovarian cancer cell. *Gynecological Oncology*, **104**(2), pp. 455–460.

Zhong, Y. *et al.* (2013) Potassium ion channels in retinal ganglion cells. *Molecular Medicine Reports*, **8**(2), pp. 311–319.

Zhu, A., Lee, D. and Shim, H. (2011) Metabolic PET Imaging in Cancer Detection and Therapy Response. *Seminars in Oncology*, **38**(1), pp. 55–69.

Zimna, A. and Kurpisz, M. (2015) Hypoxia-Inducible Factor-1 in Physiological and Pathophysiological Angiogenesis: Applications and Therapies. *BioMedical Research International*, **2015**, pp. 1–13.

Appendix

Appendix 1I:

Appendix 1I.1

From: Damaghi, Mehdi <Mehdi.Damaghi@moffitt.org>
To: Gillies, Robert; Ujjal Bose
Subject: Re: EXT: Request permission to use article figures in PhD thesis

I don't think there would be a problem if you cite the journal.
Although as Bob said it'd better to double check with the journal policy …

From: "Gillies, Robert"
<Robert.Gillies@moffitt.org<mailto:Robert.Gillies@moffitt.org>>
To: Ujjal Bose
<Ujjal.Bose@nottingham.ac.uk<mailto:Ujjal.Bose@nottingham.ac.uk>>
Cc: mehdi damaghi
<mehdi.damaghi@moffitt.org<mailto:mehdi.damaghi@moffitt.org>>
Subject: Re: EXT: Request permission to use article figures in PhD thesis

I will have t check with the publisher, as I am unfamiliar with their copyright terms. Some allow, some require you to approach the with your request.

[Description: Description: Description: cid:image001.jpg@01C9126A.E408B8E0]

Robert J. Gillies, PhD
Assistant: Rachel.Snayd@moffitt.org<mailto:Rachel.Snayd@moffitt.org>
Moffitt Cancer Center

12902 Magnolia Drive Tampa, FL 33612 | tel: 813-745-8355 | fax: 813-745-8375| email: robert.gillies@moffitt.org<mailto:robert.gillies@moffitt.org>

FRONTIERS COPYRIGHT STATEMENT

© Copyright 2007-2017 Frontiers Media SA. All rights reserved.

All content included on Frontiers websites (including Loop), such as text, graphics, logos, button icons, images, video/audio clips, downloads, data

compilations and software, is the property of the person or entity who or which owned it prior to submission to Frontiers. If not owned by Frontiers it is licensed to Frontiers Media SA ("Frontiers") or its licensees and/or subcontractors.

The copyright in the text of individual articles (including research articles, opinion articles, book reviews, conference proceedings and abstracts) is the property of their respective authors, subject to a general license granted to Frontiers and a Creative Commons CC-BY licence granted to all others, as specified below. The compilation of all content on this site, as well as the design and look and feel of this website are the exclusive property of Frontiers.

All contributions to Frontiers (including Loop) may be copied and re-posted or re-published in accordance with the Creative Commons licence referred to below.

Images and graphics not forming part of user-contributed materials may not be downloaded or copied without Frontiers' explicit and specific permission.

The combination of all content on Frontiers websites, and the look and feel of the Frontiers websites, is the property of Frontiers Media SA.

Articles and other user-contributed materials may be downloaded and reproduced subject to any copyright or other notices.

As an author or contributor you grant permission to others to reproduce your articles, including any graphics and third-party materials supplied by you, in accordance with the Frontiers Terms and Conditions and subject to any copyright notices which you include in connection with such materials. The licence granted to third parties is a Creative Common Attribution ("CC BY") licence. The current version is CC-BY, version 4.0 (http://creativecommons.org/licenses/by/4.0/), and the licence will automatically be updated as and when updated by the Creative Commons organisation.

[Description: Description: Description: cid:image001.jpg@01C9126A.E408B8E0]

Appendix 1I.2

Re: PhD student requests permission to use article figure in thesis draft
Aronson, Peter <peter.aronso
Dear Ujjal,
I am delighted to learn that you found our JASN review to be helpful. I approve your use of figures from the paper with appropriate citation of the source.
Best wishes for success with your studies,
Peter Aronson
-- Section of Nephrology Department of Medicine Yale School of Medicine
1 Gilbert Street,

TAC S-255
P.O. Box 208029
New Haven,
CT 06520-8029
phone: 203-785-4902
fax: 203-785-3756
email: peter.aronson@yale.edu

Appendix 1I.3



Creative Commons License Deed

Attribution 4.0 International (CC BY 4.0)



This is a human-readable summary of (and not a substitute for) the license.

You are free to:

Share — copy and redistribute the material in any medium or format

Adapt — remix, transform, and build upon the material

for any purpose, even commercially.

The licensor cannot revoke these freedoms as long as you follow the license terms.

Under the following terms:

Attribution — You must give appropriate credit, provide a link to the license, and indicate if changes were made. You may do so in any reasonable manner, but not in any way that suggests the licensor endorses you or your use.

No additional restrictions — You may not apply legal terms or technological measures that legally restrict others from doing anything the license permits.

Notices:

You do not have to comply with the license for elements of the material in the public domain or where your use is permitted by an applicable exception or limitation.

No warranties are given. The license may not give you all of the permissions necessary for your intended use. For example, other rights such as publicity, privacy, or moral rights may limit how you use the material.

https://creativecommons.org/licenses/by/4.0/legalcode

Appendix 2I:

At normal atmospheric pressure a 5% CO_2 environment with a partial pressure ($p(CO_2)/PCO_2$) of 38 mm Hg would require 0.15 - 0.22 mM of $NaHCO_3$ will create a pH_e of 7.42-7.8

$$pH = pKa + \log [HCO_3^-]/[CO_2]$$

Sodium bicarbonate when used as a physiological buffer in cell culture applications has two pKa, 6.4 and 10.3.

The pKa for bicarbonate <-> carbonic acid reaction is 6.4.

The pKa for bicarbonate <-> carbonate reaction is 10.3.

At high CO_2 concentration $NaHCO_3$ has a pKa of 6.4 as it favours the reaction delivering carbonic acid in the reaction site

(Physiological pH) $7.42 = 10^{-6.4} + \log [HCO3-]/[CO_2]$

Therefore 76 mm Hg $p(CO_2)$ with 0.37mM of $NaHCO_3$ will create a pHe of 7.42-7.8. Substituting these values into the equation it can be deduced that for every 10 % increase in $p(CO_2)$ to 76 mm Hg, the $NaHCO_3$ concentration gets approximately doubled.

Thus ~ 7.4 g/L $NaHCO_3$ will create a pHe of 7.42-7.8 in 20% CO_2
~ 1 g/L $NaHCO_3$ will create a pHe of 6.34-6.58 in 5% CO_2.

Appendix 2II:

Experimental designing and data collection for establishing medium with altered pH and oxygen concentration. In altering the pH_e, different permutations and combinations of time points, sodium bicarbonate concentrations and medium were tested. Representatives of these experiments are explained through three such plate plans as depicted below.

To understand how potentially time would affect external pH and cellular metabolism plate plan 1 was designed. The results showed that initial exposure of medium to 0.21 atm PO_2 for 12 hours (as would be required during cell adhesion) forced a (pH_e 7.2 – 7.4)neutral to slightly alkaline pH_e. Subsequently on exposure of medium to 0.029 atm PO_2 for 48 hours during incubation followed by re-exposure of the medium to the atmospheric PO_2 for 12 hours the pH_e was reduced (pH_e 6.58 - 6.8) acidic range. Since our earlier experiments showed that culture medium exposed to a 0.21atm PO_2 shifted the pH to slightly alkaline, the above mentioned results helped understand how a temporal effect of exposure to lower PO_2 results in gradual acidification of the pH_e at a sooner than maintaining medium atmospheric PO_2 only.

The results from a parallel wing showed that initial exposure of the medium to 0.029 atm PO_2 for 12 hours forced a slightly acidic pH_e. Subsequently on exposure of medium to 0.21 atm PO_2 for 48 hours followed by re-exposure of the medium to the original conditions for 12 hours the pH_e was reduced to stabilise above neutral to slightly alkaline range.

The results showed how time of exposure along with HEPES would turn out to be extremely critical to be considered to establish and sustain pH_e.

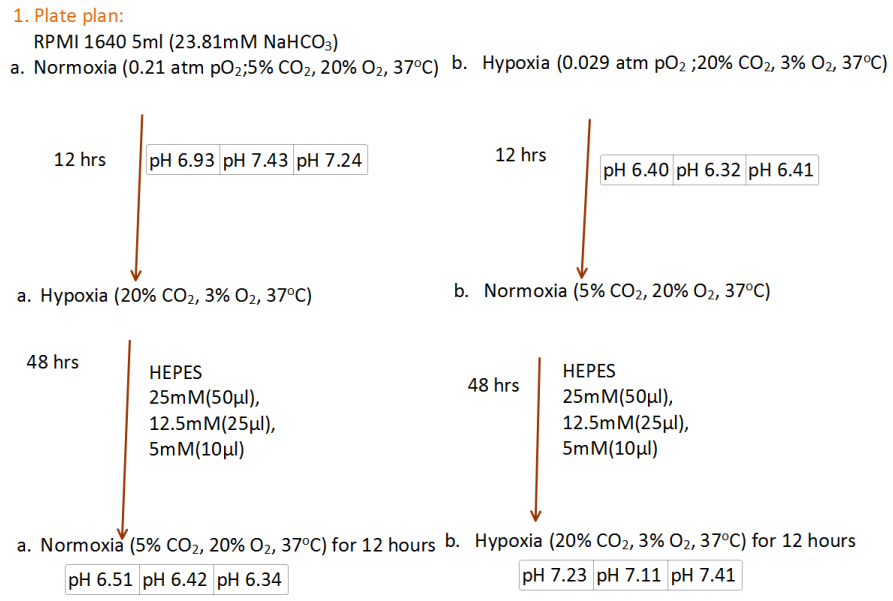

To further understand how a variation in medium composition could potentially affect the pH equilibration a variation in bicarbonate concentration was used according to the pHe range desired. RPMI 1640 (liquid medium with pre added bicarbonate ;for most of the cell lines to be used) and MEM(obtained in powder without bicarbonate added) culture medium were tested for the experiment . In plate plans 2 and three a 48 hour exposure in respective culture

conditions only lowered the pH_e. Although addition of 5 mM HEPES stabilised the pH_e reasonably to be used in cell culture experiments.

2. Plate plan:

a. RPMI 1640 5ml(23.81mM $NaHCO_3$)

b. Normoxia (5% CO_2, 20% O_2, 37°C)

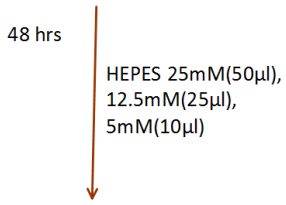

a. Normoxia (5% CO_2, 20% O_2, 37°C) 0 hours

pH 7.23	pH 7.42	pH 7.21

b. Hypoxia (20% CO_2, 3% O_2, 37°C)

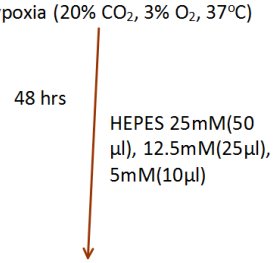

b. Hypoxia (20% CO_2, 3% O_2, 37°C) 0 hours

pH 6.31	pH 6.32	pH 6.52

3. Plate plan:

MEM 5ml 26mM $NaHCO_3$

a. Normoxia (5% CO_2, 20% O_2, 37°C)

pH 6.61	pH 6.82	pH 6.84

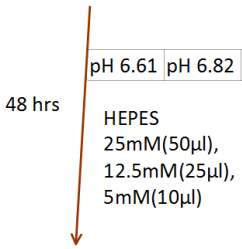

1. MEM 5ml 26mM $NaHCO_3$

a. Hypoxia (20% CO_2, 3% O_2, 37°C)

pH 6.51	pH 6.41	pH 6.201

b. Hypoxia (20% CO_2, 3% O_2, 37°C)

pH 6.20	pH 6.23	pH 6.18

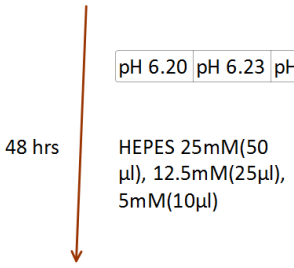

b. Normoxia (5% CO_2, 20% O_2, 37°C)

pH 6.81	pH 6.813	pH 7.014

Appendix 2III:

Introduction to Henry's Constant:
In order to incorporate the bicarbonate buffering component to assist the Henderson Hasselbalch's equation to calculate the concentration of sodium bicarbonate Henry's law is required. To form a completely homogenous mixture a gas undergoes diffusion in a solution when dissolved until equilibrium is reached. An equilibration constant can be derived when representing this state of equilibrium mathematically.
When carbon dioxide gas is passes through a column of water a similar equilibrium is reached between the dissolved and the undissolved gas . At this point further dissolution is not possible under the given conditions and can be represented as:
CO_2 (dissolved) $\leftrightarrow$ CO_2 (undissolved).
This phenomenon of steady state at equilibrium can be explained by the constant (equilibrium constant):
, and can be represented by:
K = partial pressure (CO_2)/Molar concentration (CO_2).
Thus for a column of gas above the solution at equilibrium the concentration of a solute gas is directly proportional to the partial pressure of that gas. In the above equation the equilibrium constant represents this theory. Although constant only under a specified set of conditions, this statement, is known as Henry's law. In our experimental setup when stating the pressure-concentration ratio of the carbon dioxide that is administered and dissolved in the medium in an incubator basis gives the following form of the otherwise empirical formulae for the Henry's law:

Partial Pressure of the Gas (p) = k'c (Equilibrium constant) X Molar Concentration of a Gas

In the above form of the equation, the constant for the equation when at equilibrium, k'c is the Henry's law constant on the molar concentration scale. Hence Henry's law was used to accurately description of the behaviour of carbon dioxide when dissolving in the culture medium under the influence of a buffering system. This value is found to be consistent when concentrations and partial pressures are reasonably low. As partial pressures of the dissolving gas increases, there is also a subsequent increase in concentrations and deviations from Henry's law become apparent. Hence CO_2 which is found to follow this law when dissolved in the culture medium produces what is known as 'Ideal Dilute Solution'. This shift in the equilibrium constant often mimics the deviation of gas laws from their standard values when physical conditions like temperature and pressure are decreased. Hence in a multi gas incubator with20% CO_2 and a high concentration of sodium bicarbonate Henry's law constant will tend to deviate from a calculated pH value.
Close monitoring of the change in pH_e and its stabilisation under a given concentration of sodium bicarbonate and partial pressure of CO_2 was carried out over different time points. This was much necessary as the growth kinetics, population doubling time and the pH buffering capacity of different cell lines also contributed in stabilising the medium pH.
As a metabolism driven buffering mechanism the CO_2-bicarbonate system works by the reversible breakdown of carbonic acid:
$H_2CO_3 \leftrightarrow CO_2$ and HCO_3^-
According the above explanation the concentration of sodium bicarbonate to be used is the product of the partial pressure of CO_2 and the Henry's law constant of CO_2 at 37^oC.

$[H_2CO_3]$= Henrys constant X Partial pressure of CO_2 (PCO_2)
Henrys constant= 0.03 mmol/(L-torr)
Thus according to the Henderson Hasselbalch's equation pH of a solution can be represented as follows:

$$pH = 6.1 + \log [HCO_3^-]/(0.03X\ PCO_2)$$

Since the total bicarbonate in the solution is derived from the total amount of dissolved sodium bicarbonate

$[HCO_3^-]$= $[NaHCO_3]$ mmol/L and

PCO_2= (total pressure in torr) × (volume fraction of CO_2),

Appendix 2IV:

Determination of sodium bicarbonate concentration for selective culture medium preparation pH_e by incorporating Henry's constant. Using the the Henderson Hasselbalch's equation mentioned in Chapter 2; section 2.4 for validation of pH_e model for cell culture the following observations were made.

1.Concentration of [$NaHCO_3$] (mM) required to attain a pH of 7.42 in a culture medium when incubated at 37°C with 5% of ambient CO_2 (PCO_2 = 38 mm of Hg), 95% Air (PO_2 = 159.6 mm of Hg).

pH= 6.1 + log [$NaHCO_3$]/{0.03X (total pressure) × (volume fraction of CO_2)} ……(5)

- 7.46 = 6.1 + log [$NaHCO_3$]/[0.03 X (760 mm of Hg X (5/100)]
- 1.36 = log [$NaHCO_3$]/[0.03 X 38]
- 1.36 = log [$NaHCO_3$]/1.14
- $10^{1.36}$ = [$NaHCO_3$]/1.14
- [$NaHCO_3$] = [($10^{1.36}$)x1.14] mM
- [$NaHCO_3$] = 23.817 mM

Preparation of Complete Growth Medium:

Prepare 10% $NaHCO_3$ solution in MEM as Stock

Add 1 ml of this stock to 49 ml fresh MEM

Substitute 5 ml FBS to prepared MEM

Substitute 0.5 ml Pen/Strep to this MEM

2.Concentration of [$NaHCO_3$] (mM) required to attain a pH of 6.30 in a culture medium when incubated in 37°C with 5% of ambient CO_2 (PCO_2 = 38 mm of Hg), 95% Air can be determined as described above.

Applying equation (5)

- [$NaHCO_3$] = [($10^{0.2}$)x1.14] mM
- [$NaHCO_3$] = 1.805 mM

Preparation of Complete Growth Medium:

Prepare 10% $NaHCO_3$ solution in MEM as Stock

Add 0.05 ml stock to 49.95 ml fresh MEM

Substitute 5 ml FBS to prepared MEM

Substitute 0.5 ml Pen/Strep to this MEM

3. Concentration of [$NaHCO_3^-$] (mM) required to attain a pH of 7.42 in a culture medium when incubated in 37°C with 20% ambient CO_2 (PCO_2 = 152 mm of Hg), 3% Air can be determined as described above.

Using equation (5):

- [$NaHCO_3$] = [$(10^{0.32})$x45.6] mM
- [$NaHCO_3$] = 95.271 mM

Preparation of Complete Growth Medium:

Prepare 10% $NaHCO_3$ solution in MEM as Stock:

Add 4 ml (realistically 10 ml; as Sod Bicarb exhibits pKa 10.2 at higher conc of Carbon Dioxide; enabling pH_e to shoot much higher than 7.42 when 40 ml are used.) stock to 10 ml fresh MEM. Substitute 5 ml FBS to prepared MEM. Substitute 0.5 ml Pen/Strep to this MEM

4. Concentration of [$NaHCO_3$] (mM) required to attain a pH of 6.30 in a culture medium when incubated in 37°C with 20% ambient CO_2 (PCO_2 = 152mm of Hg), 3% Air can be determined as described above.

Using equation (5):

- [$NaHCO_3$] = [$(10^{-0.8})$x45.6] mM
- [$NaHCO_3$] ~= 7.22 mM

Preparation of Complete Growth Medium:

Prepare 10% $NaHCO_3$ solution in MEM as Stock

Add 0.2 ml stock to 47 ml fresh MEM

Substitute 5 ml FBS to prepared MEM

Substitute 0.5 ml Pen/Strep to this MEM

1 atm= 760 torr).

Add 0.2 ml (realistically 0.5 ml; as Sod Bicarb exhibits pKa 10.2 at higher conc of Carbon Dioxide; enabling pH_e to shoot much lower than 6.3 when 0.2 ml are used.) stock to 10 ml fresh MEM. Substitute 5 ml FBS to prepared MEM. Substitute 0.5 ml Pen/Strep to this MEM

Appendix 2V:

pH	Volume (ml)	
	Sodium phosphate dibasic (0.2 M)	Citric acid monohydrate (0.1 M)
2.5	2.16	17.84
3.0	4.08	15.92
3.5	6.04	13.96
4.0	7.72	12.28
4.5	9.00	11.00
5.0	10.28	9.72
5.5	11.36	8.64
6.0	12.84	7.16
6.5	14.20	5.80
7.0	17.44	2.56
7.5	17.98	2.02
8.0	19.53	0.47

Table 2I: Volume of Sodium Phosphate and citric acid required to attain specific pH solutions for calibration of pH-nanosensors.

Appendix 2VI:

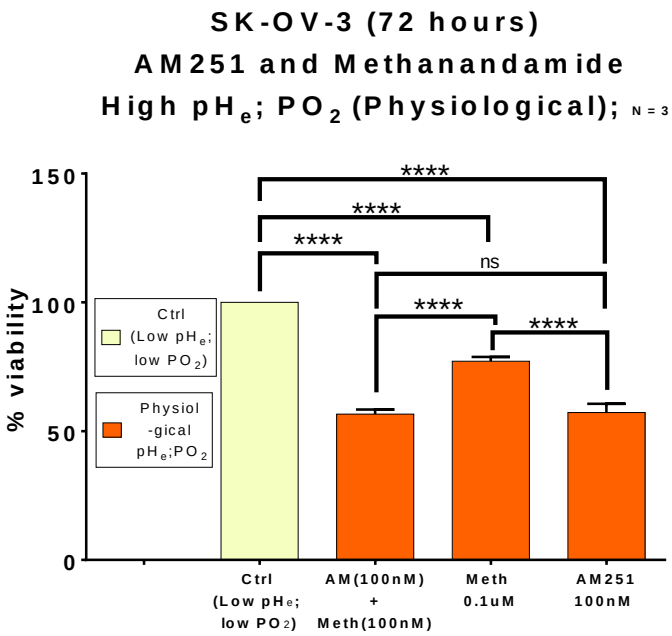

Figure 2VI: Methanandamide at 0.1uM (dose used in my study, inhibitor of TASK-3 and agonist of CB1) in combination with AM-251at 100nM (antagonist of CB1) produces a significantly higher antiproliferative effect than when used alone.
Methanandamide at 0.1uM and AM-251at 100nM combination produce similar antiproliferative effect as AM-251at 100nM alone.
Methanandamide at 0.1uM produces a larger antiproliferative effect in SK-OV-3 cells when acting only through TASK-3 inhibition.

Appendix 2VII:

Seeding density(Cells/200µl)	MCF-7											
	$5x10^3$		$10x10^3$		$25x10^3$		$50x10^3$		$80x10^3$		$100x10^3$	
P_{25}(hr)	1.5 ±0.05	1.5 ±0.05	1.4 ±0.06	1.9 ±0.07	1.3 ±0.05	4.5 ±0.17	7.8 ±0.42	11.6 ±0.56	33.2 ±1.73	36.5 ±1.9	29.4 ±1.63	13.7 ±0.71
P_{50}(hr)	15.3 ±0.32	14.5 ±0.3	16.6 ±0.37	18.9 ±0.40	17.1 ±0.40	44.2 ±0.93	15.8 ±0.93	23.6 ±1.25	66.4 ±3.46	72.9 ±3.95	58.7 ±3.26	27.4 ±1.42
P_{100}(hr)	20.4 ±0.43	19.4 ±0.4	22.1 ±0.49	25.2 ±0.53	22.8 ±0.65	58.9 ±1.52	< 100% increase in cell proliferation					
	Published population doubling time is ~24 hr (Robert L. Sunderland et al. 1983) ~36hr (ATCC®HTB-77)											

Seeding density(Cells/200µl)	OE-19											
	$5x10^3$		$10x10^3$		$25x10^3$		$50x10^3$		$80x10^3$		$100x10^3$	
P_{25}(hr)	25.4 ±0.28	< 0% cell proliferation	10.8 ±0.24	47.2 ±0.20	6.4 ±0.23	22.0 ±0.36	8.7 ±0.47	21.0 ±0.74	39.8 ±2.04	52.3 ±1.90	18.6 ±1.30	27.3 ±1.71
P_{50}(hr)	49.5 ±0.30		41.7 ±0.51	60.7 ±0.14	54.1 ±1.06	57.7 ±0.51	17.7 ±1.05	42.5 ±1.64	79.6 ±4.08	104.6 ±3.81	37.3 ±2.61	54.6 ±3.43
P_{100}(hr)	66.1 ±0.40		55.6 ±0.69	81.0 ±0.18	72.0 ±1.73	76.9 ±0.83	< 100% increase in cell proliferation					
	Published population doubling time is ~50-60 hr (96071721 SIGMA, OE19 Cell Line human)											

Seeding density(Cells/200µl)	SK-OV-3											
	$5x10^3$		$10x10^3$		$25x10^3$		$50x10^3$		$80x10^3$		$100x10^3$	
P_{25}(hr)	2.6 ±0.09	16.9 ±0.31	1.5 ±0.06	1.5 ±0.06	3.0 ±0.1	1.2 ±0.1	6.8 ±0.36	4.5 ±0.24	45.3 ±2.31	33.2 ±1.65	8.3 ±0.44	7.9 ±0.43
P_{50}(hr)	23.9 ±0.49	50.0 ±0.50	18.8 ±0.44	17.6 ±0.40	34.7 ±0.8	14.4 ±0.3	13.9 ±0.80	9.3 ±0.54	90.6 ±4.62	66.4 ±3.30	16.6 ±0.89	15.8 ±0.87
P_{100}(hr)	31.9 ±0.65	66.7 ±0.66	25.1 ±0.59	23.5 ±0.53	46.3 ±1.3	19.1 ±0.5	< 100% increase in cell proliferation					
	Published population doubling time is ~35hr (ATCC®HTB-77); ~48 hr(CLL1135 SIGMA SKOV3 Cells GFP-HER2)											

Figure 2VII. Evaluating association between cell seeding density and proliferation in altered pH_e/PO_2. MCF-7, OE-19 and SK-OV-3 cells under different cell seeding density showed variations in proliferation when subjected to different pH_e/PO_2. P_{25}, P_{50} and P_{100} correspond to $1/4^{th}$, ½ and total time to complete proliferation assays by achieving plateau phase growth rate with different passage numbers.

Appendix 2VIII:

Rationale for selection of imaging platform: Our investigation involved the use of a ratiometric method for determining pH_i in cultured monolayer of cancer and non-neoplastic cells using fluorescence wide-field microscopy or fluorescence multi-well plate scanner used for its technical usefulness to deal with different culture and gassing conditions. Tracking pH_i changes in real-time could be best achieved by live cell imaging by visualising changes in pH sensing fluorophores (Landecker, 2009). The live cell imaging format with hassle free changing of reagents during experiments, minimum time in preparation and processing of samples (unlike Flowcytometry, X-ray diffraction, conventional Spectrofluorometry etc.) enables ease of operation in controlled environment and ability to carry out long-term studies (Grant, R. et.al. 1994).

Selection of pH sensing dye/probe: BCECF-AM is a pH sensing dye with two excitation (490 and 440 nm) and one emission wavelengths (535 nm) wavelengths that were expressed as ratios of intensities that are associated with pH of the cell and its uptake dynamics. The pKa is 6.97 enabling its use for accurately measuring physiological changes in pH_i by appropriately selecting the pH range of solutions for calibration.

In contrast to BCECF-AM, cSNARF®-1-AM undergoes a pH-dependent wave length shift at the emission spectrum. Thus, fluorescence intensities from the dye at two emission wavelengths were also used for ratiometric determinations of pHi with greater accuracy than BCECF-AM. The dye with a pK_a ~7.5 enables accurate measurement of physiological and alkaline changes in pH_i by appropriately selecting the pH range of solutions for calibration. It was used by exciting the dye at a wave length, ranging between 488 nm and 530 nm, while collecting the emitted fluorescence signals at two unique wave lengths, typically spanning between about 580 nm and 640 nm. The dependence of a reference excitation or emission wavelength that is independent of proton dynamics within the cell, accounts for any loss in accuracy in terms of variable dye loading, cell thickness, dye leakage, and detector sensitivity (Bright. G. R. *et al*., 1989).

These dyes were loaded into cells by virtue of their acetoxymethyl ester (AM) moiety and hence do not require an invasive approach. The uptake of inactive lipophilic cSNARF or BCECF esterified with Acetoxymethyl by the cell was verified after 5 minutes, at the higher excitation/emission wavelengths respectively without changing the dye solution during loading. A minimum of 10-20 minutes is allowed for inactive dye passes through the plasma membrane into the cytosol before the nonspecific intracellular esterases cleave the acetoxymethyl ester bonds rendering the dyes active to changes in proton dynamics within the cell. The dye solution is replaced with fresh media after verifying that the ionised form of the dye is trapped and is well retained within the cells.

The pH-nanosensors feature tuneable pK_a to permit the measurement of an extended dynamic range, from pH 4.0 to 7.5 (Roos *et al*., 1981, Wolfbeis, 2002). The Dual fluorophores include fluorescein isothiocyanate dextran (FITC-D) and Oregon Green dextran (OG-D)) and a reference fluorophore (5-(and-6)-carboxytetramethylrhodamine dextran (TAMRA-D)). The entrapment is achieved with a biocompatible polymer matrix (Veeren M. Chauhan, *et al.*, 2011, J. Lin *et al.*, 2000). This leads to easier cellular uptake, retention and viability with the use of these dual-fluorophore pH nanosensors (McDonagh C. *et al.*, 2008)

Appendix 2IX:

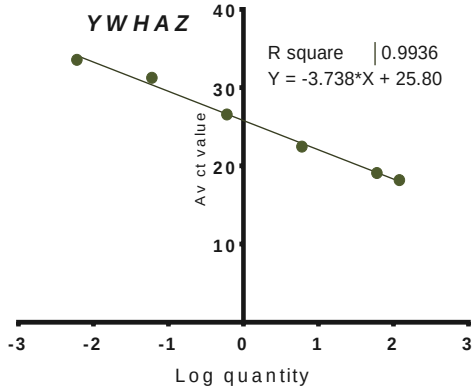

A B

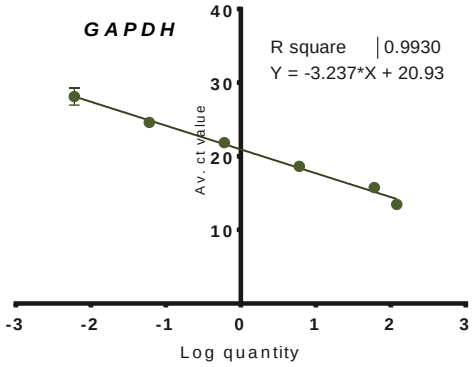

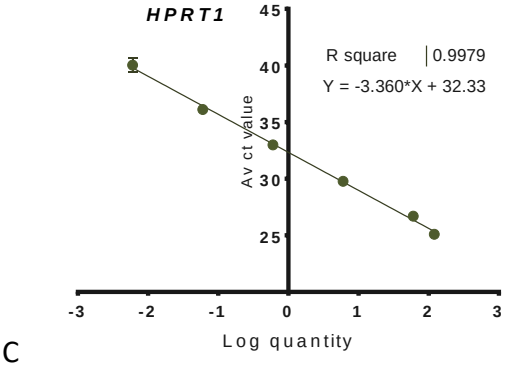

C

D

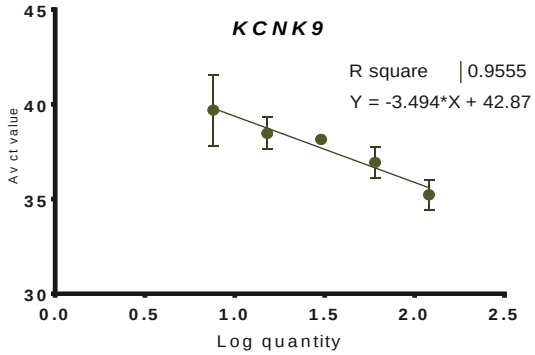

A. Reference gene YWHAZ - Best Reference Gene ; Efficiency 85.15%

B. Reference gene GAPDH - 2nd Best Reference Gene ; Efficiency 103.67%

C. Reference gene HPRT1 ; Efficiency 98.69%

D. TASK-3 - Target Gene ; Efficiency 93.79%

Figure: Effeciency determination of 20X Taqman gene assays. Standard curves for reference genes and TASK-3 in ostoecarcinoma cells showing calculated efficiencies. qPCR was performed using Taqman assays and efficiencies of reference genes and TASK-3 gene were calculated from the standard curve.

Appendix 2X:

2X.1: **Cell culture media and reagents:**

Roswell Park Memorial Institute (RPMI) 1640, Dulbecco's Modified Eagle Medium (DMEM), McCoy's 5A are general purpose media to resuscitate and support the propagation of established cell lines.
Minimum Essential Medium (MEM) with Earl's balanced salts, 2 mM l-glutamine, without NaHCO3 was from SAFC Biosciences (Sigma-Aldrich, Dorset, UK).
Epidermal growth factor (EGF), recombinant human Insulin and cholera toxin were procured from Sigma-Aldrich, Dorset, UK.
Foetal Bovine Serum (FBS), Charcoal stripped horse serum and hydrocortisone was from Sigma, Dorset, UK.
Penicillin/ streptomycin (10000 U/ml and 10 mg/ml respectively) solution, Trypsin/EDTA (0.05%) and Hank's Balanced Salt Solution (HBSS) were also procured from Gibco®, Thermo Fisher, Paisley, UK.
L-Glutamine (BP 381) from Fisher, Loughborough, UK. N-2-Hydroxyethylpiperazine-N-2-Ethane Sulfonic Acid (HEPES) (H3375 SIGMA, Sigma-Aldrich, Dorset, UK) a zwitterion organic chemical buffering agent was used in cell culture media.

2X.2: Cell culture surfaces and plastics:

Cryovials, Tissue culture-treated flasks (T-25 and T-75) and tissue culture-treated flat bottom optics plates (24 and 96 well) were from Corning®, SIGMA, Dorset, UK.
Nunc™ Cell Culture/Petri Dishes (35 mm) from Thermo Scientific Paisley, UK. **MILLICELL®-PCF 12 µm Cell culture plate inserts** (PIXP0 12 50, MILLIPORE, Watford, UK).

2X.3: Pharmacological agents and chemicals used:

Omeprazole Cat no: O104, Sigma-Aldrich, Dorset, UK. **E-4031 dihydrochloride** (1808) and **R-(+)-methanandamide** (1121) from TOCRIS, Bristol, UK.
MTS (3- (4, 5-dimethylthiazol-2-yl)-5- (3-carboxymethoxyphenyl)-2- (4-sulfophenyl)-2-tetrazolium, inner salt) assay in the form of the **CellTiter 96 aqueous non-radioactive cell proliferation assay kit** (Promega, UK) was used for the cell proliferation assays. **Resazurin sodium salt** (R7017 SIGMA0) and **Trypan Blue** (T8154 SIGMA) from Sigma-Aldrich, Dorset, UK.
Dimethyl Sulfoxide (**DMSO**), NaCl, NaOH, KCl, $CsCl_2$, D-Glucose, $NaHPO_4$, Na_2HPO_4, NH_4Cl, $CaCl_2$, $MgCl_2$, $NaHCO_3$, from Sigma Aldrich, Dorset, UK.

2X.4: pH sensing dye/probe:

The 2',7'-Bis-(2-Carboxyethyl)-5-(and-6)-Carboxyfluorescein, Acetoxymethyl Ester (BCECF-AM) and Carboxy seminaphthorhodafluor-1-Acetoxymethyl Ester (cSNARF®-1-AM) pH sensing dyes (C-1271, Thermo Scientific, Paisley, UK). Polyacryllamide pH-nanosensors, a generous gift from Dr Johnathan Aylott and Dr Veeren Chauhan (Faculty of Science, University of Nottingham).

Mitochondrial dyes:
MitoTracker® Deep Red FM- M22426 (abs/em ~644/665nm) and MitoTracker® Red CMXRos - M7512 (abs/em 579⁄599 nm), Molecular Probes™ from Thermofisher Scientific, Paisley, UK(kind

gift by Dr Christopher Gell, Faculty of Medicine & Health Sciences, QMC and University of Nottingham).
JC10 (MAK159**)** and MitoTracker® Red CMXRos (M7512, a kind gift from Dr Nathane Szewczyk, Associate Professor, Faculty of Medicine & Health Sciences, University of Nottingham, UK)

2X.5: Reagents and kits for protein expression assay:

Materials for protein expression assays:
Paraformaldehyde (P6148), BSA (A9418), Igepal (I8896), Goat serum (G9023). Glycine from Fisher, Loughborough, UK. PBS (BR14a) from Oxoid.
Antibodies used:
The primary antibodies for immunofluorescence and Western blot techniques viz., Anti-KCNK9 (KCN-75) Carboxyterminal end and Anti-KCNK17 antibody (ab57259) were obtained from Abcam, Cambridge, UK, Beta-actin was from Sigma and Cytokeratin antibody (MN0821) was from, Dako, Cambridge, UK.
Secondary antibodies like Anti-Rabbit IgG Fluorescein Isothiocyanate (FITC) conjugate, Anti-Mouse IgG FITC (F0257) were from Sigma, UK.

2X.6: Reagents and kits for gene expression assays

RNA extraction reagents:
TRI® reagent (T9424 SIGMA), **Agarose, Ethidium Bromide, Chloroform, Isopropanol, Ethyl Alcohol** from Sigma-Aldrich, Dorset, UK.
Mini-Sub® Cell GT Horizontal Electrophoresis System (1704406), ChemiDoc™ MP System (1708280), Bio-Rad, Hertfordshire, UK.

Reagents and kits for RT-PCR:
High-Capacity cDNA Reverse Transcription Kit - 4368814**, TaqMan® Universal PCR Master Mix** - 4304437 (Applied Biosystems™) and **RNase/DNase free RT-PCR Grade Water** - AM9935, (Ambion™), Thermofisher Scientific, Paisley, UK.
Gene expression assays for qPCR:
The following **gene expression (Taqman®) assays** mixes were procured from Thermofisher Scientific, Paisley, UK.
Reference Genes:
GAPDH (Hs02758991_g1),
YWHAZ (Hs03044281_g1),
HPRT1 (Hs02800695_m1)
ACTB (Hs01060665_g1),
B2M (Hs03044281_g1).
Target Genes:
KCNK9 (Hs00363153_m1),
KCNK17 (Hs00230249_m1),
KCNH1 (Hs00924320_m1),
KCNH2 (Hs04234270_g1).
DNA Engine/Chromo 4 Real time PCR Detector from Bio-Rad, Hertfordshire, UK.

Appendix 3I:

Acid Extrusion calculation (an example): An acid buffering capacity of SK-OV-3 cell was measured in pHe 7.4 and 6.3. The known value of the ammonium $[NH_4^+]_e$ at pH_e 7.4 or 6.3 is 20 mM or 0.02 M. Hence the pOH_e is derived by subtracting the pH from 14 which is 6.6. The pK_b of $[NH_4^+]$ at 37°C is 8.9. Hence the pOH_e can be calculated by the following equation:

$$pOH_e = pK_b + \log[NH_4^+]_e/[NH_3]_e$$

By substituting the respective values of the known parameters the $[NH_3]_e$ can be calculated at the respective pH_e.

$$6.6 = 8.9 + \log([NH_4^+]/0.02$$

$$[NH_3]_e = 3.99M$$

Thus the $[NH_3]$ in the extracellular medium is deduced to be 3.99 M.

When NH_4Cl in the extracellular medium establishes a $[NH_4^+]$ of 20 mM the pH_i of the cell was recorded to be (i.e at 'c')= 7.52. Assuming that at this point

$$[NH_3]_e = [NH_3]_i$$

$[NH_3]_i$ at pH_i 7.52 is 3.99 M

As described above the pOH_i is 6.48. Again by substituting the known values in the following equation the $[NH_4^+]_i$ can be calculated as follows: .

$$pOH_i = pK_b + \log[NH_4^+]_i/[NH_3]_i$$

$$6.76 = 8.9 + \log([NH_4^+]/3.99$$

$$[NH_4^+]_i = 15.23\ mM$$

Hence the $[NH_4^+]_i$ is calculated to be 15.23 mM.

Now after the pulse of NH_4Cl is removed, the concentration of ammonium is reduced to 1 mM. Hence after removing the ammonium from the medium:

Now the pOH_e is derived by subtracting the pH from 14 which is 6.6. The pK_b of $[NH_4^+]$ at 37°C is 8.9. Hence the pOH_e can be calculated by the following same equation but substituting the new value of $[NH_4^+]_e$.

$$pOH_e = pK_b + \log[NH_4^+]_e/[NH_3]_e$$

The $[NH_3]_e$ can be calculated at the respective pH_e.

$6.6 = 8.9 + \log([NH_4^+]) / 0.02$

$[NH_3]_e = 1.995M$

Thus now the $[NH_3]$ in the extracellular medium is reduced to 1.995 M.

When NH_4Cl in the extracellular medium establishes a $[NH_4^+]$ of 20 mM the pH_i of the cell was recorded to be (i.e at 'c')= 6.231. Assuming that at this point once again $[NH_3]_e = [NH_3]_i$

$[NH_3]_i$ at pH_i 6.23 is 1.995 M

As described above the pOH_i is calculated to be 7.683. Again by substituting the known values in the following equation the $[NH_4^+]_i$ can be calculated.

$pOH_i = pK_b + \log[NH_4^+]_i/[NH_3]_i$

$7.683 = 8.9 + \log([NH_4^+]_i)/1.995$

$[NH_4^+]_i = 14.73$ mM

Now the 'Intrinsic buffering capacity', $\boldsymbol{\beta}_I$ of the SK-OV3 cell when maintained at a pH_e of 7.4 and PO_2 of 0.21 atm.

$$\beta_I = \frac{([NH_4^+]_i \text{ at pH } 7.52) - ([NH_4^+]_I \text{ at pH } 6.23)}{6.23 - 7.52}$$

$\beta_I = 0.38$ pH/mM

The above method is used to calculate the β_I of the different cell lines when exposed to acute acid loading at altered pH_e. The figure 3.3.2.2 represents the difference in β_I of the SK-OV-3 cell when maintained at an altered pH_e.

Net acid extrusion capacity of cancer cells:

Net Acid extrusion of SK-OV-3 cells maintained in extracellular medium with altered pH_e

The pH_e independent, HCO_3^- - independent "total" H^+ extrusion flux (J_{tot}) was calculated as:

i. J_{totH} measured in pH_e 6.3, PO_2 0.21 atm- HEPES-buffered solutions.

β_I X Recovery rate in pHe 6.3 in HEPES buffered system

$J_{totH} = 0.8$ mM/pH X 0.5429 pH/min = 0.434 mM/min

i. J_{totN} in the presence of pH_e 7.4, 0.21 atm PO_2/25mM HCO_3^- minus J_{tot}.

β_I X Recovery rate in pHe 7.4 in HEPES buffered system =

J_{totN} = 0.38 mM/pH X 0.2720 pH/min = 0.103 mM/min

HCO_3^--transporter activity (J_{bicarb}) was calculated from

J_H measured in CO_2/HCO_3^- buffered solutions minus J_{tot} measured in HEPES-buffered solutions of different pH_e.

J_H in pH_e 6.3 = β_I X Recovery rate in pHe 6.3 in bicarbonate buffered system.

J_H in pH_e 6.3 = 0.38 mM/pH X 0.04438 = 0.35504 mM/min

J_H in pH_e 7.4 = β_I X Recovery rate in pHe 7.4 in bicarbonate buffered System.

J_H in pH_e 7.4 = 0.38 mM/pH X 0.03724 = 0.01415 mM/min

To derive the approximate net acid extrusion in a particular pH_e:

Net acid extrusion of the cells in pH_e 7.4 (J_{totH} - J_H in pH_e 7.4) is 0.089 mM/min. Net acid extrusion of the cells in pH_e 6.3 (J_{totH} - J_H in pH_e 6.3) is 0.079 mM/min.

Comparing individual values of net acid extrusion would enable us with a better understanding of the contribution of the cancer cells pH regulatory machinery to deal with extracellular pH in the given PO_2.

Appendix 3II:

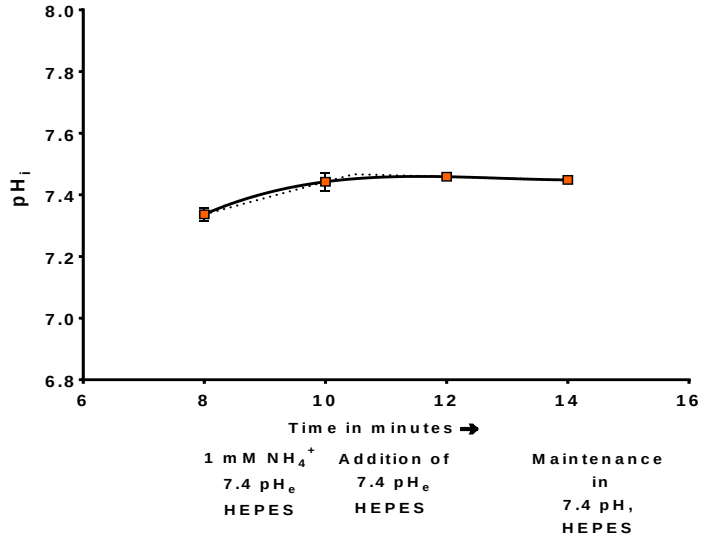

Figure: The pH_i recovery rate in MCF-10A cells when exposed to a pulse of 20 mM ammonium by partially substituting the NaCl in HEPES buffered extracellular medium at 0.21 atm PO_2 7.4 pH_e.

Appendix 4I:

Nigericin is an ionophore mentioned earlier for calibrating pH sensing dyes and selectively increases the permeability of biological membranes and promotesgradientdefined exchange of molecules between the extracellular micronvironment to the intracellular space of cells (Berton C Pressman.1976). Ionophores like nigericin and monensin have unique molecular properties which extend their use for a range of other functions.

Belonging to the class of carboxylic ionophores, nigericin actively carries protons through the lipid bilayer membranes. Owing to the acidic functional group when bound to a proton their movement across the membrane is independent of the direction of the transmembrane potential. This is achieved because after protonation that nigericin molecule does not possess any net charge and hence traverses the cell membrane as an unionised molecule. Interestingly the same Nigericin molecule in its deprotonated form exists as an anion. This anionic nigericin can easily form complexes with other larger positively charged monovalent cations two form zwitter ions that are electrically neutral. Hence larger cations can be transported across the cell membrane (Berton C Pressman.1976). Under these given conditions do lead to an acute and heavy acidification of the intracellular space.

An incredible rate to acid loading is observed in such a scenario. It appears more likely for the proton to have a much greater chance of loaded into the cell than being pushed out. As a result subsequent to their exposure to nigericin, cancer cells exhibit a rapid rate of acidification. This phenomena can be expressed mathematically by taking into account the number of times the nigericin molecule forms transient complexes with a proton that simultaneously gives rise to an event in the extracellular microenvironment as described above. For this probability, L, one can write :

L(complex formed with a proton) = $[H^+]/ ([H^+]+ x[K^+]+ y[Na^+])$.... (I).

The above equation takes into consideration that nigericin can primarily form stable complexes only with H^+, K^+, and Na^+ . These three cations are the primary monovalent ions in the cell that have greater probability to form complexes with nigericin. The expression mentions x and y which represent nigericin's relative binding constants for the potassium and sodium ions. These are also used as multiples of the binding constant for the transported hydrogen ion . At a point in the chemical interaction between the nigericin molecule and proton in both compartments across the cell membrane an equilibria is struck. The chances of forming complexes with protons on either sides of the cell membrane Dynamic equilibrium between proton influx and efflux is attained when the probability of proton complexing is identical on either sides of the membrane.

$([H^+]/ ([H^+]+x[K^+]+ y[Na^+]))_{intracellular} = ([H^+]/ ([H^+]+ x[K^+]+ y[Na^+]))_{extracellular}$.... (II).

The above equation describes the probabilities of cations and protons forming complexes with nigericin at equilibrium across intracellular and extracellular spaces, respectively. The abundance of alkali cations is four fold more compared to the availability of protons in either compartments. From previous observations it can be inferred that hence proton concentration renders significant contribution to the numerical value only to the numerator ([1]Negendank W, 1984,[2] Nishimura H et.al, 1993.)

Thus, Equation 2 reduces to:

$\{[H^+]/ (x[K^+]+ y[Na^+])\}$intracellular $= \{[H^+]/ (a[K^+] + b[Na^+])$)extracellular.... (III).

A shift in the plot of pHi against pHe is observed with a change in extracellular sodium with a constant concentration of potassium. When the reverse experimental conditions are setup this shift although is relatively identical but reduces in magnitude as the change in the K^+ level of the buffer is brought about. Experimentally observed drop of pH by less than a unit was observed large increase in extracellular Na^+ concentration(140 mM) was made a sodium free environment with constant potassium availability of 5 mM. This drop in the pHi/pHe curve was observed only with a minor change of about double fold increase in extracellular potassium with a constant sodium in the solution. This observation show the preference of the ionophore to potassium. A 45 times increased preference of nigericin towards potassium compared to sodium([3]Jain MK ,et.al, 1980).

$x\{[K^+]\}$intracellular >> $y\{[Na^+]\}$intracellular ..... (IV).

This is not observed in the extracellular space as sodium and potassium exist almost in reverse gradients and dynamics. A reduced concentration of sodium(15 mM) was maintained by replacing it with non-permeant

(N-methyl-D-glucamine) NMDG with symmetrical potassium. This would provide a selection benefit of nigericin towards potassium compared to sodium . In the presence of more potassium in the extracellular medium nigericin now will have a higher probability of forming complexes with protons and potassium without interfering much with the sodium. This interaction would potentially contribute towards equilibrium during acid loading.

With the above modifications in place, the equilibrium is maintained with:

$\{[H^+]/[K^+]\}$intracellular = $\{[H^+]/[K^+]\}$extracellular ..... (V).

The above equation simplifies the theory that if the composition of extracellular K^+ is known in a given pH the intracellular potassium concentration can be calculated.

Appendix 4II:

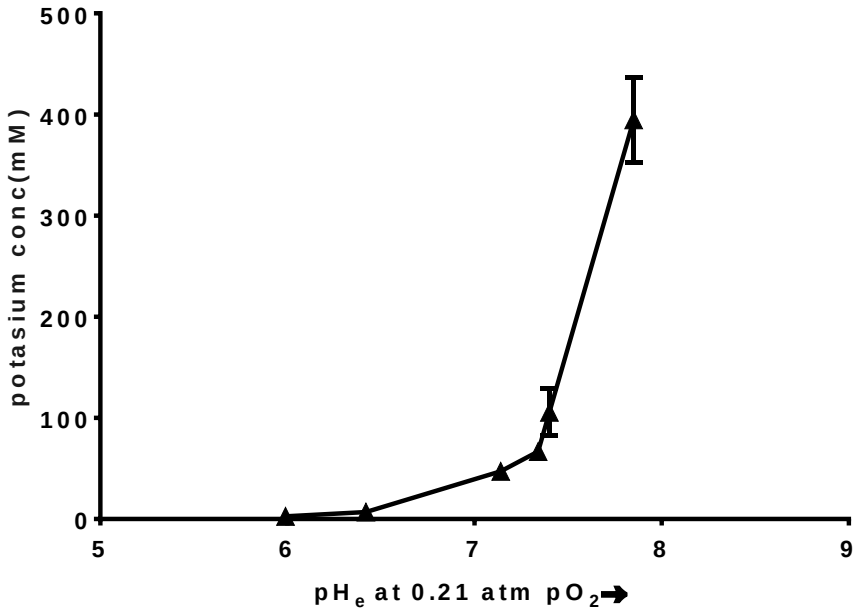

Figure 1$[K^+]_i$ in SKOV-3 cells when the pH_e is changed from acidic to alkaline at 0.21 atm. The rate of K^+ efflux and H^+ influx is defined by a slower in exchange rate at lower pHe ranging from 5.98 mM at pH 6.0 that only increase by less than 100 mM at pH_e 7.0. The dramatic change was observed in the $[K^+]_i$ values for changes in pHe beyond physiological range (7.2- 7.42).

$$([H^+]/ ([H^+] +x[K^+]+ y[Na^+]))_{intracellular} = ([H^+]/ ([H^+]+ x[K^+]+ y[Na^+]))_{extracellular....} \text{ (II)}.$$

The above equation describes the probabilities of cations and protons forming complexes with nigericin at equilibrium across intracellular and extracellular spaces, respectively. The abundance of alkali cations is four fold more compared to the availability of protons and hence it can be inferred that hence proton concentration renders significant contribution to the numerical value only to the numerator (Negendank, 1984; Nishimura, Zarnowski and Simpson, 1993).

Thus, Equation 2 reduces to:

$$\{[H^+]/ (x[K^+]+ y[Na+])\}_{intracellular} = \{[H^+]/ (a[K^+] + b[Na^+]))_{extracellular}.... \text{ (III)}.$$

A 45 times increased preference of nigericin towards potassium compared to sodium (Jain and Wagner, 1980).

$x\{[K^+]\}_{intracellular} >> y\{[Na^+]\}$ intracellular ..... (IV).

A reduced concentration of sodium (15 mM) was maintained by replacing it with non-permeant (N-methyl-D-glucamine) NMDG with symmetrical potassium. (Low Na^+-extracellular salt solution; *125 mM NMDG, 15 mM NaCl, 5 mM KCl, 5.5 mM glucose, 0.1 mM NaH_2PO_4, 0.4 mM $NaHPO_4$, 1 mM $CaCl_2$, 1 mM $MgCl_2$ and 10 mM HEPES*) This would provide a selection benefit of nigericin towards potassium compared to sodium. This interaction would potentially contribute towards equilibrium during acid loading.

With the above modifications in place, the equilibrium is maintained with:

$$\{[H^+]/[K^+]\}_{intracellular} = \{[H^+]/[K^+]\}_{extracellular} \quad \text{..... (V).}$$

The above equation simplifies the theory that if the composition of extracellular K^+ is known in a given pH the intracellular potassium concentration can be calculated. Thus, the presence of nigericin ensures that the pH_i equilibration occurs along the changing pH gradient across the membrane (Goldstein *et al.*, 2005; Lesage and Barhanin, 2011).